OPTIMAL TRANSFERS BETWEEN LIBRATION-POINT ORBITS IN THE ELLIPTIC RESTRICTED THREE-BODY PROBLEM

A Thesis

Submitted to the Faculty

of

Purdue University

by

Lisa Ann Hiday

In Partial Fulfillment of the

Requirements for the Degree

of

Doctor of Philosophy

August 1992

To Atlas—

and to all men
who have borne the weight
of the world on their shoulders.

ACKNOWLEDGEMENTS

The author wishes to recognize her advisor, Professor Kathleen C. Howell, for the suggestion of a most interesting and challenging research topic and for the guidance to bring this investigation to fruition. Gratitude is extended to Professor Robert E. Skelton, Professor Martin J. Corless, and Professor James M. Longuski for their technical suggestions and their reviews of this dissertation. The author also thanks Dr. Jeffrey Layton for provision of the multivariable search routine ADS and for his related technical insights.

This work was funded, in part, by Purdue University (via a Purdue University Fellowship, a David Ross Fellowship, and a Purdue Forever Fellowship), Computer Sciences Corporation, the National Science Foundation (Grant No. MSM-8352281), and the National Aeronautics and Space Administration through the Indiana Space Grant Consortium.

A very special acknowledgement is owed to Paul and Lurilla Hiday for their unbounded parental love, guidance, and support throughout the years. Finally, a heartfelt thanks is expressed to Dr. Robert T. Johnston whose warmth and encouragement have sustained this endeavor.

TABLE OF CONTENTS

Page

LIST OF TABLES vii

LIST OF FIGURES viii

ABSTRACT xv

INTRODUCTION 1

Definition of the Problem 2
Previous Contributions 3
Periodic Orbits in the Restricted Three-Body Problem 3
Lissajous Orbits 5
Optimal Transfers in the Two-Body Problem 6
Transfers in the Three-Body Problem 8
Scope of the Present Work 9

CHAPTER I
THE ELLIPTIC RESTRICTED THREE-BODY PROBLEM 14

Assumptions 14
Coordinate Frames 15
Nondimensionalization 15
Equations of Motion 17
Libration Points 21
State Transition Matrix 25
Approximate Analytic Solutions 27
Numerical Solutions in the Elliptic Restricted Three-Body Problem 38

Page

CHAPTER II
TRANSFERS BETWEEN LIBRATION POINT ORBITS 40

Objective of a Nominal Trajectory 40
Determination of the Initial Halo Orbit 45
Estimation of the Final Halo Orbit 46
Determination of an Approximate Lissajous Transfer 48
Linear Approximation 48
Third-Order Approximation 51
Numerical Integration of the Lissajous Transfer
and the Complete Nominal Trajectory 53
Manual Reduction of the $|\Delta\bar{v}|$ Expenditure 55
Fine-Tuning the Halo Orbits 55
Acceptable Reference Trajectory 62

CHAPTER III
THEORY OF OPTIMAL TRAJECTORIES 66

State and Constraint Equations 66
Extremal Arcs 69
Impulsive Thrusts 74
Primer Differential Equations 79
Weierstrass-Erdmann Corner Conditions 81
Necessary Conditions for an Optimal Trajectory 84
Hamiltonian 84
Adjoint Equation 86

CHAPTER IV
OPTIMIZATION OF NON-OPTIMAL IMPULSIVE TRAJECTORIES 90

Reference and Perturbed Transfer Trajectories 90
Initial Coast 92
Final Coast 102
Dual Coast 110
Additional Impulse 117
Movement of an Interior Impulse 127
Computation of Analytic Gradients 131

Page

CHAPTER V
SUPERIOR TRANSFER OPTIMIZATION APPLICATIONS 135

Optimality of a Nominal Transfer Trajectory 135
Optimal Time-Fixed Superior Transfer Trajectories 137
Optimal Time-Free Superior Transfer Trajectories 159

CHAPTER VI
AN IMPROVED NOMINAL TRANSFER CONSTRUCTION
AND INFERIOR TRANSFER OPTIMIZATION APPLICATIONS 174

A Spiral Method for Target Point Estimation 174
A Differential Corrections Procedure for Impulsive Maneuvers 177
A Continuation Algorithm for Nominal Transfer Construction 180
Optimal Time-Free Inferior Transfer Trajectories 182

DENOUEMENT 218

Summary 218
Conclusions 220
Recommendations 222

REFERENCES 224

VITA 231

LIST OF TABLES

Table		Page
2.1	Timing Conditions for an Estimated TOF on the Lissajous Transfer Trajectory	47
2.2	Timing Conditions for an Analytically Approximated TOF on the Lissajous Transfer Trajectory	54
2.3	Timing Conditions for an Integrated TOF on the Lissajous Transfer Trajectory	56
5.1	Cost on Time-Fixed Superior Transfers to a Variety of Final Halo Orbits	158
5.2	Cost on Time-Free Superior Transfers to a Variety of Final Halo Orbits	173
6.1	Cost on Time-Free Inferior Transfers from a Variety of Initial Halo Orbits	215

LIST OF FIGURES

Figure		Page
1.1	Inertial and Rotating Coordinate Systems	16
1.2	Libration Point Locations in the Rotating Frame	22
1.3	Collinear Libration Point Locations in the Elliptic Restricted Problem	24
1.4	Sun-Earth/Moon Barycenter Primary System	29
1.5	Linear Approximation for a Sample Lissajous Trajectory	36
1.6	Third-Order Analytic Solution for a Sample Lissajous Trajectory	37
1.7	Numerically Integrated Solution for a Sample Lissajous Trajectory	39
2.1	$\underset{\sim}{y}$-$\underset{\sim}{z}$ Projection of the Initial and Final Halo Orbits (Case A)	42
2.2	$\underset{\sim}{x}$-$\underset{\sim}{y}$ Projection of the Initial and Final Halo Orbits (Case A)	43
2.3	$\underset{\sim}{x}$-$\underset{\sim}{z}$ Projection of the Initial and Final Halo Orbits (Case A)	44
2.4	Earth/Moon Barycenter Motion for an Estimated TOF on the Lissajous Transfer Trajectory	47
2.5	Earth/Moon Barycenter Motion for an Analytically Approximated TOF on the Lissajous Transfer Trajectory	54
2.6	Earth/Moon Barycenter Motion for an Integrated TOF on the Lissajous Transfer Trajectory	56
2.7	$\underset{\sim}{y}$-$\underset{\sim}{z}$ Projection of the Two-Impulse Nominal Trajectory (Case A)	57
2.8	$\underset{\sim}{x}$-$\underset{\sim}{y}$ Projection of the Two-Impulse Nominal Trajectory (Case A)	58

Figure Page

2.9 $\underline{x}$-$\underline{z}$ Projection of the Two-Impulse Nominal Trajectory (Case A) 59

2.10 $\underline{y}$-$\underline{z}$ Projection of the Reduced $\Delta\bar{v}$ Trajectory (Case A) 63

2.11 $\underline{x}$-$\underline{y}$ Projection of the Reduced $\Delta\bar{v}$ Trajectory (Case A) 64

2.12 $\underline{x}$-$\underline{z}$ Projection of the Reduced $\Delta\bar{v}$ Trajectory (Case A) 65

3.1 Thrust Magnitude Switching Function for an MT-arc preceded and succeeded by NT-arcs: (a) MT-arc of Finite Duration; (b) Impulsive Thrust; (c) Impulsive Thrust with Cusp 76

3.2 Thrust Magnitude Switching Function for an MT-arc preceded and succeeded by IT-arcs: (a) MT-arc of Finite Duration; (b) Impulsive Thrust; (c) Impulsive Thrust with Cusp 77

4.1 Variations Between Reference and Perturbed Transfer Trajectories 91

4.2 Initial Coast Geometry 93

4.3 Noncontemporaneous and Contemporaneous Velocity Variations at the Instant of the Initial Impulse 97

4.4 Noncontemporaneous and Contemporaneous Position Variations at the Instant of the Initial Impulse 97

4.5 Final Coast Geometry 103

4.6 Noncontemporaneous and Contemporaneous Velocity Variations at the Instant of the Final Impulse 106

4.7 Noncontemporaneous and Contemporaneous Position Variations at the Instant of the Final Impulse 106

4.8 Dual Coast Geometry 111

4.9 Primer Vector Magnitude Time Histories Characteristic of Non-Optimal, Two-Impulse Trajectories Requiring (a) Initial Coast; (b) Early Departure; (c) Final Coast; and, (d) Late Arrival 116

Figure Page

4.10 Two-Impulse Reference and Three-Impulse Perturbed Transfer Trajectories 118

4.11 Additional Impulse Geometry 121

4.12 Two-Step, First-Order, Backward Difference Approximation to the Value of an Arbitrary Function 132

5.1 Primer Magnitude History of Two-Impulse Nominal Transfer (Case A) 136

5.2 Primer Magnitude History of Time-Fixed Three-Impulse Transfer Exhibiting a Cusp (Case A) 138

5.3 Primer Magnitude History of Optimal Time-Fixed Three-Impulse Transfer (Case A) 139

5.4 $\underset{\sim}{y}$-$\underset{\sim}{z}$ Projection of Optimal Time-Fixed Three-Impulse Transfer (Case A) 140

5.5 $\underset{\sim}{x}$-$\underset{\sim}{y}$ Projection of Optimal Time-Fixed Three-Impulse Transfer (Case A) 141

5.6 $\underset{\sim}{x}$-$\underset{\sim}{z}$ Projection of Optimal Time-Fixed Three-Impulse Transfer (Case A) 142

5.7 Adjoint Equation History (Case A) 143

5.8 $\underset{\sim}{y}$-$\underset{\sim}{z}$ Projection of Two-Impulse Nominal Trajectory (Case B) 145

5.9 Primer Magnitude History of Best Time-Fixed Three-Impulse Transfer (Case B) 146

5.10 Primer Magnitude History of Optimal Time-Fixed Four-Impulse Transfer (Case B) 147

5.11 $\underset{\sim}{y}$-$\underset{\sim}{z}$ Projection of Optimal Time-Fixed Four-Impulse Transfer (Case B) 148

5.12 $\underset{\sim}{y}$-$\underset{\sim}{z}$ Projection of Two-Impulse Nominal Trajectory (Case C) 149

5.13 Primer Magnitude History of Best Time-Fixed Three-Impulse Transfer (Case C) 150

5.14 Primer Magnitude History of Optimal Time-Fixed Four-Impulse Transfer (Case C) 151

Figure Page

5.15 $\underset{\sim}{y}$-$\underset{\sim}{z}$ Projection of Optimal Time-Fixed Four-Impulse Transfer (Case C) 152

5.16 $\underset{\sim}{y}$-$\underset{\sim}{z}$ Projection of Two-Impulse Nominal Trajectory (Case D) 153

5.17 Primer Magnitude History of Best Time-Fixed Three-Impulse Transfer (Case D) 154

5.18 $\underset{\sim}{y}$-$\underset{\sim}{z}$ Projection of Best Time-Fixed Three-Impulse Transfer (Case D) 155

5.19 Primer Magnitude History of Optimal Time-Fixed Four-Impulse Transfer (Case D) 156

5.20 $\underset{\sim}{y}$-$\underset{\sim}{z}$ Projection of Optimal Time-Fixed Four-Impulse Transfer (Case D) 157

5.21 Primer Magnitude History of Optimal Time-Free Two-Impulse Transfer (Case A) 162

5.22 $\underset{\sim}{y}$-$\underset{\sim}{z}$ Projection of Optimal Time-Free Two-Impulse Transfer (Case A) 163

5.23 Primer Magnitude History of Best Time-Free Two-Impulse Transfer (Case B) 164

5.24 Primer Magnitude History of Optimal Time-Free Three-Impulse Transfer (Case B) 165

5.25 $\underset{\sim}{y}$-$\underset{\sim}{z}$ Projection of Optimal Time-Free Three-Impulse Transfer (Case B) 166

5.26 Primer Magnitude History of Best Time-Free Two-Impulse Transfer (Case C) 167

5.27 Primer Magnitude History of Best Time-Free Three-Impulse Transfer (Case C) 168

5.28 $\underset{\sim}{y}$-$\underset{\sim}{z}$ Projection of Best Time-Free Three-Impulse Transfer (Case C) 169

5.29 Primer Magnitude History of Best Time-Free Two-Impulse Transfer (Case D) 170

5.30 Primer Magnitude History of Best Time-Free Three-Impulse Transfer (Case D) 171

5.31 $\underset{\sim}{y}$-$\underset{\sim}{z}$ Projection of Best Time-Free Three-Impulse Transfer (Case D) 172

Figure Page

6.1 Spiral of Target Points for a Superior Transfer Between Minimun $\underset{\sim}{z}$-Excursion Points on the Halo Orbits 176

6.2 Spiral of Target Points for an Inferior Transfer Between Maximun $\underset{\sim}{z}$-Excursion Points on the Halo Orbits 176

6.3 $\underset{\sim}{y}$-$\underset{\sim}{z}$ Projection of the Orbit A → Orbit C Nominal Trajectory 183

6.4 $\underset{\sim}{y}$-$\underset{\sim}{z}$ Projection of the Orbit A → Orbit D Nominal Trajectory 184

6.5 $\underset{\sim}{y}$-$\underset{\sim}{z}$ Projection of the Orbit A → Orbit B Nominal Trajectory 185

6.6 $\underset{\sim}{x}$-$\underset{\sim}{y}$ Projection of the Orbit A → Orbit B Nominal Trajectory 186

6.7 $\underset{\sim}{x}$-$\underset{\sim}{z}$ Projection of the Orbit A → Orbit B Nominal Trajectory 187

6.8 $\underset{\sim}{y}$-$\underset{\sim}{z}$ Projection of Two-Impulse Nominal Trajectory (Case E) 191

6.9 Primer Magnitude History of Two-Impulse Nominal Transfer (Case E) 192

6.10 Primer Magnitude History of Best Time-Free Two-Impulse Transfer (Case E) 193

6.11 $\underset{\sim}{y}$-$\underset{\sim}{z}$ Projection of Best Time-Free Two-Impulse Transfer (Case E) 194

6.12 Primer Magnitude History of Best Time-Free Three-Impulse Transfer (Case E) 195

6.13 $\underset{\sim}{y}$-$\underset{\sim}{z}$ Projection of Best Time-Free Three-Impulse Transfer (Case E) 196

6.14 Primer Magnitude History of Best Time-Free Four-Impulse Transfer (Case E) 197

6.15 Primer Magnitude History of Best Time-Free Five-Impulse Transfer (Case E) 198

6.16 $\underset{\sim}{y}$-$\underset{\sim}{z}$ Projection of Two-Impulse Nominal Trajectory (Case F) 199

6.17 Primer Magnitude History of Two-Impulse Nominal Transfer (Case F) 200

Figure Page

6.18 Primer Magnitude History of Best Time-Free Two-Impulse Transfer (Case F) 201

6.19 $\underset{\sim}{y}$-$\underset{\sim}{z}$ Projection of Best Time-Free Two-Impulse Transfer (Case F) 202

6.20 Primer Magnitude History of Best Time-Free Three-Impulse Transfer (Case F) 203

6.21 $\underset{\sim}{y}$-$\underset{\sim}{z}$ Projection of Best Time-Free Three-Impulse Transfer (Case F) 204

6.22 Primer Magnitude History of Best Time-Free Four-Impulse Transfer (Case F) 205

6.23 Primer Magnitude History of Best Time-Free Five-Impulse Transfer (Case F) 206

6.24 $\underset{\sim}{y}$-$\underset{\sim}{z}$ Projection of Two-Impulse Nominal Trajectory (Case G) 207

6.25 Primer Magnitude History of Two-Impulse Nominal Transfer (Case G) 208

6.26 Primer Magnitude History of Best Time-Free Two-Impulse Transfer (Case G) 209

6.27 $\underset{\sim}{y}$-$\underset{\sim}{z}$ Projection of Best Time-Free Two-Impulse Transfer (Case G) 210

6.28 Primer Magnitude History of Best Time-Free Three-Impulse Transfer (Case G) 211

6.29 $\underset{\sim}{y}$-$\underset{\sim}{z}$ Projection of Best Time-Free Three-Impulse Transfer (Case G) 212

6.30 Primer Magnitude History of Best Time-Free Four-Impulse Transfer (Case G) 213

6.31 Primer Magnitude History of Best Time-Free Five-Impulse Transfer (Case G) 214

ABSTRACT

Hiday, Lisa Ann. Ph.D., Purdue University, August 1992. Optimal Transfers Between Libration-Point Orbits in the Elliptic Restricted Three-Body Problem. Major Professor: Kathleen C. Howell.

A strategy is formulated to design optimal impulsive transfers between three-dimensional libration-point orbits in the vicinity of the interior L_1 libration point of the Sun-Earth/Moon barycenter system. Two methods of constructing nominal transfers, for which the fuel cost is to be minimized, are developed; both inferior and superior transfers between two halo orbits are considered. The necessary conditions for an optimal transfer trajectory are stated in terms of the primer vector. The adjoint equation relating reference and perturbed trajectories in this formulation of the elliptic restricted three-body problem is shown to be distinctly different from that obtained in the analysis of trajectories in the two-body problem.

Criteria are established whereby the cost on a nominal transfer can be improved by the addition of an interior impulse or by the implementation of coastal arcs in the initial and final orbits. The necessary conditions for the local optimality of a time-fixed transfer trajectory possessing additional impulses are satisfied by requiring continuity of the Hamiltonian and the derivative of the primer vector at all interior impulses. The optimality of a time-free transfer containing coastal arcs is surmised by examination of the slopes at the endpoints of a plot of the magnitude of the primer vector over the duration of the transfer path. If the initial and final slopes of the primer magnitude are zero, the transfer trajectory is optimal; otherwise, the execution of coasts is warranted. The position and timing of each interior impulse applied to a time-fixed transfer as well as the direction and length of coastal periods implemented on a time-free transfer are specified by the unconstrained minimization of the appropriate variation in cost utilizing a multivariable search technique.

Although optimal solutions in some instances are elusive, the time-fixed and time-free optimization algorithms prove to be very successful in diminishing costs on nominal transfer trajectories. The inclusion of coastal arcs on time-free superior and inferior transfers results in significant modification of the transfer time of flight caused by shifts in departure and arrival locations on the halo orbits.

INTRODUCTION

On November 20, 1978, a spacecraft identified as the International Sun-Earth Explorer-3 (ISEE-3) was inserted into a particular type of three-dimensional periodic trajectory, known as a halo orbit, about the interior Sun-Earth libration point, L_1.[1,2] The scientific objective of ISEE-3 was to conduct a number of particle and field investigations in the interplanetary medium upstream from Earth. From its halo orbit about L_1, ISEE-3 monitored characteristics of the solar wind and other solar-induced phenomena such as solar radio bursts and solar flares about an hour prior to disturbance of the space environment near Earth.[1–3] The stationing of ISEE-3 in a halo orbit marked a milestone in space flight history for ISEE-3 is credited with several achievements previously unrealized. ISEE-3 became:

i) the first artificial libration-point satellite;
ii) the first spacecraft stationed in a halo orbit; and,
iii) the first spacecraft to orbit a point in space rather than a body such as the Sun or Earth.[3]

After spending approximately 3.5 years in its halo orbit, ISEE-3 was retargeted to the Earth's magnetotail and became the first spacecraft to explore the geomagnetic tail between 80 and 237 Earth radii.[4] The decision was then made to radically reconfigure the spacecraft's trajectory in favor of an extended mission to encounter a comet. So, on December 22, 1983, a lunar flyby was employed to hurl the spacecraft, renamed the International Cometary Explorer (ICE), into a heliocentric trajectory; consequently, ICE intercepted the comet Giacobini-Zinner on September 11, 1985 and became the first spacecraft to successfully execute a cometary flyby.[4–6]

The ISEE-3/ICE mission is an excellent example of innovative trajectory concepts tailored to meet specific mission objectives. As space exploration and utilization programs expand, interest in libration-point orbits of various sizes and shapes will continue to increase. Trajectory design studies for scientific missions scheduled for launch in the 1990's have investigated the use of three-dimensional libration-point trajectories

in the vicinity of L_1, the interior libration point of the Sun-Earth/Moon barycenter system. With interest in such orbits increasing, efficient transfers between libration-point orbits may offer more options and greater flexibility in trajectory design. Hence, this research effort is directed toward the formulation of a strategy to design optimal transfers between halo orbits near the L_1 libration point.

Definition of the Problem

The study of the motion of three bodies, each moving under the gravitational influence of the other two, is designated the *three-body problem* in orbital mechanics. All three bodies are assumed to possess spherically symmetric gravity fields such that each body can be modelled as a point mass. If one of the bodies is assumed to have infinitesimal mass, the phraseology *restricted three-body problem* is used. The two bodies of finite mass, termed *primaries*, move on a path determined by their mutual gravitational attraction but unaffected by the third body of infinitesimal mass. The third body is free to travel in all three spatial dimensions. The motion of the primaries is assumed to be either specified or computed simultaneously with the motion of the infinitesimal mass. If the primaries are constrained to move on elliptic paths relative to each other, the terminology *elliptic restricted three-body problem* is customary; however, if the primaries are further confined to circular paths about their center of mass or *barycenter*, the motion of the third body is the subject of the *circular restricted three-body problem.*

Five particular solutions known to exist in the circular problem are located in the plane of motion of the primaries and are called *libration points*. An infinitesimal mass placed at a libration point traces out a circular path about the barycenter with an angular rate equal to that of the primaries. So, a satellite—assumed to be of infinitesimal mass—moving on such an orbit appears stationary when viewed by an observer fixed in a coordinate frame rotating with the primaries about their barycenter. Moreover, because the gravitational force on a satellite as well as the centrifugal force associated with the motion of the rotating frame balance at the libration points, these locations are also *equilibrium points*. Three of the libration points—denoted L_1, L_2, L_3—lie on the line joining the primaries; the other two—denoted L_4, L_5—form equilateral triangles with the primaries in their plane of motion. In addition to the libration points, other solutions in their vicinity are known to exist. One type of three-dimensional orbit

generated in association with each of the three collinear libration points is a periodic solution called a *halo* orbit, the period of which is commensurate with the period of the primary orbit. Additionally, certain quasi-periodic solutions in the neighborhood of the libration points are designated *Lissajous* trajectories, which, in general, do not repeat with every revolution of the primaries.

The ultimate goal of this research is the formulation of a strategy to efficiently design optimal impulsive transfers in the elliptic restricted three-body problem. A preliminary investigation focuses on the design of transfer trajectories that move a spacecraft from an initial halo orbit associated with a collinear libration point to a final halo orbit about the same libration point. Final halo orbits characterized by both larger and smaller out-of-plane amplitudes than the initial halo orbits are considered. An analytic approximation for the transfer path, as well as exact numerical integration of the complete trajectory, is sought. Since the conservation of fuel is highly desirable, exploration of the optimality of a resultant transfer is paramount. Executing multiple impulsive maneuvers and affecting coastal arcs in the initial or final libration-point orbits are two methods of potentially reducing total fuel expenditure that are examined. The transfers obtained are optimal in the sense that the total characteristic velocity exhibits a local minimum. The implementation of additional impulses produces a transfer trajectory upon which the time of flight is fixed. In contrast, the inclusion of a coast in the initial or final libration-point orbit results in a transfer of variable time of flight. The optimization of both time-free and time-fixed transfers between libration-point trajectories in the elliptic problem is pursued.

Previous Contributions

Periodic Orbits in the Restricted Three-Body Problem

Although general, analytic solutions of the restricted three-body problem remain elusive, advances in the understanding of this system's behavior have been based, in large part, on the known particular solution of the circular problem (*i.e.*, the five libration points). That the libration points are commonly identified as *Lagrange points* acknowledges Lagrange for his discovery of these particular solutions in 1772[7,8] and reflects the significance of this contribution to the understanding of the three-body problem. Numerous researchers, among them, Laplace; Liouville; and Jacobi, continue

investigation of the problem of three bodies,[7] but no new periodic solutions are uncovered until Hill[9] publishes his Lunar Theory (1878) in which periodic solutions, including some eccentric and solar perturbations, are obtained. Near the end of the nineteenth century, Poincaré discovers that, when the masses of two of the bodies are small compared to that of the third, an infinite number of initial conditions exist for which periodic motion results, and he develops valuable analytical techniques for solving differential equations, that are employed in the calculation of periodic orbits today.[7] Moreover, Poincaré's non-integrability principle denies availability of generally valid analytical solutions and rejects prediction of the quantitative and qualitative behavior of the three-body problem for any given set of initial conditions.[8] Additionally, Darwin[10] computes a number of periodic orbits in the circular restricted problem utilizing a laborious quadrature method. In the early 1900's, Plummer[11,12] and Moulton[13] catalogue a great variety of periodic orbits, all of which are approximate in nature. Also, whereas all of Plummer's orbits are two-dimensional (*i.e.*, contained in the plane of motion of the primaries), Moulton considers three-dimensional orbits as well.

The search for new periodic orbits continued; however, progress is impeded by the necessity of employing tedious hand calculations and quadrature methods to obtain solutions. Not until the emergence of computers in the mid-twentieth century can numerical studies be conducted efficiently; thus, the advent of computers enables researchers to examine a wide range of exact, numerical solutions. In 1967, Szebehely[14] assembles the body of knowledge pertaining to the restricted three-body problem. Much discussion in this treatise is afforded the circular problem although the fundamentals of the elliptic problem are also presented. Additionally, Szebehely focuses his investigation on two-dimensional orbits in the plane of motion of the primaries and supplies results of numerical analyses of periodic solutions. In the late 1960's, interest piques in the determination of *three*-dimensional periodic orbits in the three-body problem. In analytic approximations that include perturbations due to solar gravity, solar radiation pressure, and an eccentric lunar orbit, Farquhar[15,16] identifies three-dimensional periodic orbits about the translunar libration point (*i.e.*, the libration point in the Earth/Moon primary system that is located on the distant side of the Moon when observed from Earth). Describing this three-dimensional orbit, Farquhar coined the term *halo* due to the orbit's appearance as a halo about the Moon when viewed from Earth. Since Farquhar's initial investigations of these specialized solutions,

additional analytic approximations for halo orbits are published.[17–19] The computation of three-dimensional trajectories is further enhanced by the practicality and efficiency of computer simulations. Since the late 1970's, a few researchers numerically compute a variety of halo orbits from the exact nonlinear equations of motion using differential corrections schemes and catalogue these orbits according to their origin, shape, and stability characteristics.[19–25]

Lissajous Orbits

Following the early work on halo orbits, some researchers devote their efforts to developing analytic approximations for libration-point orbits. In 1973, Heppenheimer,[26] utilizing Lindstedt's method, evolves a third-order theory for the nonlinear out-of-plane motion in the elliptic restricted three-body problem by combining the nonlinear motion in the circular problem (given to third order in terms of Jacobi elliptic functions) with the linear motion in the elliptic problem (using Mathieu's and Hill's equations). Also, Farquhar and Kamel[17], seeking a more accurate approximation for orbits associated with the translunar libration point, develop a third-order solution that includes solar perturbations and eccentric primary motion. In 1975, Richardson and Cary[27] obtained third-order approximate solutions in the vicinity of two of the collinear libration points of the elliptic restricted three-body problem for the Sun-Earth/Moon barycenter system (*i.e.*, Earth and Moon are considered a single body of mass equal to the sum of their individual masses placed at their barycenter). This study treats the eccentricity of the primary orbit and the fourth-body gravitational influence as perturbations to an intermediate solution in the circular three-body problem.

Farquhar and Kamel, as well as Richardson and Cary, demonstrate that the linearized motion near any collinear point consists of a periodic path in the plane of primary motion and an uncoupled periodic out-of-plane path. In general, the two frequencies of oscillation are unequal. However, when the orbits are sufficiently large so that the higher-order terms in the approximation are significant, certain combinations of in-plane and out-of-plane amplitudes exist such that the corresponding frequencies are equal. Periodic three-dimensional solutions having equal in-plane and out-of-plane frequencies are known as *halo* orbits, and such trajectories have periods commensurate with the period of the primary orbit. In the more general event of unequal frequencies, three-dimensional orbits, designated *Lissajous* orbits, arise. Named in honor of Jules

A. Lissajous (1822-1880), these trajectories, some of which are quasi-periodic, exist in the vicinity of each of the libration points. Since Lissajous trajectories do not, in general, repeat with every revolution of the primaries, their periods can be very long. Halo orbits, for which the motion is periodic, are a specialized subset of Lissajous orbits.

The long periods of Lissajous orbits render their computation difficult. However, assuming circular primary motion, Zagouras and Kazantzis[20] are able to locate several periodic orbits, having relatively short periods, about the collinear libration points of the Sun-Jupiter system. These periodic trajectories appear to be unique Lissajous orbits of one-revolution periods. Nevertheless, the vast majority of Lissajous trajectories of practical interest and limited duration should be considered nonperiodic or quasi-periodic at best; thus, the Lissajous orbit's shape, changing slightly with every revolution, evolves gradually. The determination of Lissajous trajectories in the circular restricted three-body problem is advanced by Howell and Pernicka[28,29] who develop a technique to numerically compute bounded, Lissajous orbits of arbitrary, pre-determined length in any primary system. More recently, Pernicka[30] extends this technique to systems modelled by elliptic primary motion, as well as by polynomial representations of ephemeris data which locate the attracting bodies.

Optimal Transfers in the Two-Body Problem

The study of the motion of two bodies, each moving under the gravitational influence of the other, is designated the *two-body problem* in orbital mechanics. Unlike the three-body problem, the motion of two bodies is regarded as a well-understood dynamical system with exact analytic solutions in the form of conic sections. The problem of transferring one of the two bodies (*i.e.*, a satellite) between two points in a given gravitational field such that the minimum amount of fuel is expended has been called the *fundamental navigational problem of astronautics*.[31]

One of the first attempts to solve an optimization problem of this type is made in 1919 by Goddard who recognizes that sending a rocket to high altitude in the most economical manner is a problem in the calculus of variations but gives only an approximate solution.[31] In another early study, the problem of transferring a satellite from one circular orbit to another, coplanar and concentric with the first, is essayed by Hohmann. Assuming rockets of impulsive thrust capability and an inverse-square gravitational field, Hohmann concludes that an elliptical transfer path tangential at its

apses to both circular orbits would realize the greatest fuel economy.[31] The Hohmann transfer is believed to be the minimum fuel trajectory between any two coplanar orbits until 1959 when Hoelker and Silber[32] demonstrate that, for certain ranges of the ratio of inner orbital radius to outer orbital radius, a three-impulse bi-elliptic transfer yields a lower cost than that of the corresponding two-impulse Hohmann transfer.

Throughout the 1950's and 1960's, the search for optimal, impulsive, *time-free* transfers (*i.e.*, transfers on which the time of flight is unspecified) for spacecraft and missiles becomes the focus of numerous research efforts; extensive lists of these contributions are provided in References [31,33-35]. Notable optimization studies of time-free, multiple-impulse trajectories include direct ascent of unconstrained duration by Carstens and Edelbaum;[36] transfers between near-circular orbits by Edelbaum,[37] Marec,[38,39] and Jones;[40] transfers between elliptic orbits by Breakwell,[41,42] Marchal,[43,44] Gobetz *et al.*,[45] and Marec;[46] transfers between hyperbolic orbits by Gobetz,[47] and Marchal;[48] and, finally, specific interplanetary transfers by Marchal,[49] and Gravier *et al.*[50] Additionally, Marchal[51] capsulizes the study of economical time-free transfers in his consideration of the optimal paths between the following types of Keplerian orbits: parabola → arbitrary orbit, arbitrary orbit → parabola, hyperbola → ellipse, and ellipse → hyperbola.

In contradistinction, somewhat fewer results are obtained for the optimal time-fixed case. Formulating the general optimization problem in space navigation as a problem of Mayer in the calculus of variations, Lawden[52] develops the necessary conditions that must be satisfied by the *primer vector* and its derivative on an optimal impulsive trajectory for a satellite moving in an inverse-square gravitational field. The term primer vector is introduced by Lawden to denote a vector comprised of the adjoint variables associated with the velocity. Lawden's necessary conditions are the cornerstone of primer vector theory which seeks to answer: 1) Can the addition of an interior impulse improve the performance of the reference solution? and 2) If an additional impulse is required, where should it be located and how should it be applied? Lawden states that, if the primer magnitude exceeds unity at any instant on a reference trajectory, then this path is non-optimal and its cost can be reduced. In early 1968, Lion and Handelsman[53] extend the utility of the primer vector by considering non-optimal, impulsive trajectories and establishing a criterion whereby the addition of an interior impulse on a time-fixed transfer will improve the performance of the reference solution. Lion and Handelsman also establish criteria in accordance with which a coast in

the initial orbit or a coast in the final orbit accomplishes a decrease in the cost function. The inclusion of either an initial or final coast on a reference solution produces a time-free transfer trajectory.

In an effort to answer the second question, Lion and Handelsman and Jezewski and Rozendaal[54] establish methodologies for locating and orienting the additional impulse such that the greatest reduction in cost is realized; also, utilizing a second order approximation for the cost, Jezewski and Rozendaal determine an estimate for the impulse magnitude. Further developments in the same paper include the application of multiple interior impulses and the generation of an efficient method for computing two-body, fixed-time, multiple-impulse, optimal trajectories. Additionally, Jezewski and Faust[55] examine the imposition of inequality constraints on the control variable. Jezewski[56] coalesces the body of knowledge pertaining to primer vector theory in order to generate completely general, two-body, multiple-impulse, optimal trajectories subject to any set of boundary conditions (open time, initial and terminal constraints, rendezvous, etc.) or inequality constraints (initial, intermediate, and terminal) on both state and control variables. A handful of researchers have employed primer vector theory as it applies to time-fixed trajectories in the two-body problem in order to accomplish specific mission objectives. Prominent contributions include multiple-impulse trajectories between arbitrarily inclined orbit by Jezewski;[57] rendezvous between close circular orbits by Prussing;[58,59] direct ascent rendezvous by Gross and Prussing;[60] rendezvous between circular orbits by Prussing and Chiu;[61] direct ascent interception by Prussing *et al.*;[62] and, finally, rendezvous and interception with path constraints by Taur *et al.*[63] Additionally, Marec[64] provides an exhaustive summary of both time-free and time-fixed optimal trajectories for spacecraft possessing a variety of thrust capabilities.

Transfers in the Three-Body Problem

To date, transfers between two orbits in the three-body problem have been granted a modicum of consideration. First, D'Amario[65] investigates minimum-fuel transfers from a collinear libration point to circular orbits about either the Earth or the Moon. However, since the spacecraft spends little flight time near the libration point, the trajectory is assumed to move quickly between dominant gravity fields. Hence, utilizing a multi-conic technique, D'Amario constructs and optimizes the transfer trajectories in

inertial coordinates associated with the two-body problem. Secondly, Popescu[66,67] and Popescu and Popescu[68,69] perform limited analytic studies of optimal transfers to and from both the collinear and equilateral libration points. The next two independent investigations examine transfers between halo or halo-type orbits, and these studies are distinguished by the method of solution and by the *superior* (small halo → large halo) or *inferior* (large halo → small halo) nature of the transfer. Studying the feasibility of a fuel dumping problem, Pernicka[30] examines superior transfers between two nearly periodic halo orbits about a collinear libration point in the elliptic restricted three-body problem. This investigation utilizes a trial-and-error method to determine a path that approximately connects the specified departure and arrival locations. The optimality of the resultant two-impulse transfer is not explored. Finally, Gómez *et al.*[70] use manifold theory to study a transfer between halo orbits about a collinear libration point in the circular restricted three-body problem. The inferior transfer from a halo orbit characterized by a z-amplitude of 375,000 km to a halo orbit characterized by a z-amplitude of 120,000 km was determined to require 142 m/s.

Scope of the Present Work

Upon commencement of this effort, the determination of transfers between libration-point orbits was limited to the use of a trial-and-error approach which sought an approximate path that connected two specified halo orbits. One of the goals of this investigation is the identification of a more efficient, systematic method to determine a transfer path that closely approximates the departure and arrival locations on the halo orbits; hence, the possibility of the analytic determination of such a transfer is explored. This analytic approximation is utilized as the requisite first guess for the iterative numerical computation of the transfer. The resultant nominal trajectory (initial halo, transfer, final halo) contains two impulsive thrust maneuvers. The first impulse accomplishes the departure from the initial halo orbit, and the second impulse is implemented upon arrival at the final halo orbit in order to match the final orbit's velocity.

Next, since a transfer accomplished with the greatest economy of fuel is always desirable, the magnitudes of the two thrust maneuvers are decreased in order to comply with a self-imposed $|\Delta\bar{v}|$ limitation. Manual reduction of the $|\Delta\bar{v}|$ needed to affect the transfer results in a complete trajectory requiring some adjustment such that the integrity of the original halos is preserved (*i.e.*, so that the integrated halo orbits

correspond more closely to those initially specified). The fine-tuning of the complete reduced-cost trajectory is explored via the following methods: 1) including additional revolutions of the halo orbits; 2) implementing a weighted least squares approach during the numerical, nominal trajectory determination process; and, 3) constraining the endpoints of the halo orbits.

Then, the optimality, in terms of characteristic velocity, of a two-impulse transfer is examined. The possibility of reducing fuel consumption by implementing multiple interior impulsive maneuvers, a coast in the initial halo orbit, or a coast in the final halo orbit is answered by the application of primer vector theory modified to the elliptic restricted three-body problem. The adjoint equation, in terms of rotating coordinates, relating reference and perturbed trajectories in the elliptic restricted three-body problem is shown to be of a distinctly different form from that obtained in the analysis of trajectories in the two-body problem. Also, the necessary conditions for a time-fixed two-impulse transfer trajectory to be optimal are stated in terms of the primer vector. Primer vector theory is then extended to non-optimal impulsive trajectories in order to investigate means of improving the cost of a reference solution.

Criteria are established whereby the implementation of a coast in the initial orbit, a coast in the final orbit, or dual coasts accomplishes a reduction in characteristic velocity. The optimality of a nominal two-impulse transfer can be determined by examining the slope at the endpoints of the plot of the magnitude of the primer vector on the nominal trajectory. If the initial and final slope of the primer magnitude are zero, the transfer trajectory is optimal; otherwise, the execution of coasts is warranted. The magnitudes of the coastal periods are specified by requiring the largest negative variation in the cost function. The optimal time of flight on the time-free transfer and, consequently, the departure and arrival locations on the libration-point orbits are determined by minimizing a function of two variables using a multivariable search method. Since the gradients are known analytically, a minimizing technique that utilizes the gradient components is indicated. One such technique that is successfully employed is the Broydon-Fletcher-Goldfarb-Shanno (BFGS) variable metric method for unconstrained minimization which is available in the Automated Design Synthesis package developed by Vanderplaats.[71]

Additionally, a criterion is established whereby the addition of an interior impulse on a non-optimal, time-fixed, reference trajectory reduces the overall cost. The necessary conditions for the local optimality of a transfer trajectory containing additional

impulses are satisfied by requiring continuity of the Hamiltonian and the derivative of the primer vector at all interior impulses. The determination of the location, orientation, and magnitude of each additional impulse is accomplished by the unconstrained minimization of the cost function using the BFGS multivariable search method. If the transfer between the specified boundary conditions requires K interior impulses to be optimal, then minimization of the total fuel expenditure compels K successive minimizations of a function of four variables.

Note that, since the BFGS method, which is utilized in the optimization of both time-free and time-fixed transfers, employs a gradient technique, the solution for the transfer trajectory converges only to a minimum within the same valley as the reference solution. Hence, the approach outlined herein results in locally optimal multi-impulse transfer trajectories, and other solutions may exist.

The approach and results are presented in the following manner:

CHAPTER I—The elliptic restricted three-body problem is formulated including explanation of simplifying assumptions, specification of the characteristic quantities used in nondimensionalization, derivation of the equations of motion, definition of libration points, and expression of the state transition matrix. Also, a detailed derivation of the approximate analytic solution for Lissajous orbits constructed by Richardson and Cary[27] is provided. This third-order approximation supplies the requisite first-guess utilized in the two-level iteration scheme developed by Howell and Pernicka,[29] which is summarized for the numerical computation of Lissajous orbits in the elliptic restricted three-body problem.

CHAPTER II—The determination of a nominal transfer commences with the specification of the initial halo orbit and estimation of the final halo orbit. Then, the Lissajous trajectory that approximately connects the departure and arrival locations on the halos can be determined first by using a linear approximation, next by employing a third-order approximation, and finally by numerical integration of the transfer trajectory. A consequence of the manual reduction of the fuel consumption necessary to implement the transfer trajectory is the divergence of the integrated halo orbits from those originally specified; therefore, three approaches for restoring the integrity of the halo orbits are explored.

CHAPTER III—Primer vector theory is extended to the elliptic restricted three-body problem and the optimization of a time-fixed transfer with specified terminal positions and velocities is formulated as a problem of Mayer in the calculus of variations. Three extremal arcs are identified and the thrust magnitude switching function over each arc is specified. Henceforth, rocket motors capable of delivering impulsive thrusts are assumed, and the necessary conditions for an impulsive trajectory in the elliptic restricted three-body problem to be optimal are expressed entirely in terms of the primer vector. Additionally, the adjoint equation, which relates the reference and perturbed trajectories, is expressed relative to rotating coordinates and, consequently, possesses a form distinctly different from that generally obtained in the analysis of trajectories in the two-body problem.

CHAPTER IV—If a reference path is non-optimal, a systematic procedure for the reduction of the cost is outlined. First, the implementation of a coast in the initial halo orbit, a coast in the final halo orbit, and dual coasts is examined as means of diminishing the cost on the nominal path. Secondly, the addition of an interior impulse is investigated as a method of achieving greater fuel economy. Thirdly, convergence of both time-free and time-fixed transfer paths to optimal solutions is accomplished utilizing a multivariable search technique, which employs the variable metric method of Broydon-Fletcher-Goldfarb-Shanno, to minimize the variation in cost.

CHAPTER V—The optimization techniques presented in Chapters III and IV are applied to the nominal transfer trajectories constructed utilizing the methodology outlined in Chapter II. Both time-free and time-fixed optimal superior transfers to a variety of final halo orbits are explored. Variances in the times of flight and shifts in the departure and arrival locations on the halo orbits, as the amplitude of the final halo orbit varies, are examined.

CHAPTER VI—An alternative to the nominal transfer construction method presented in Chapter II is developed utilizing a differential corrections routine in conjunction with a continuation algorithm. This improved method of constructing nominal transfer trajectories is employed to determine inferior

transfer paths between halo orbits, and the inclusion of coastal arcs on the halo orbits is explored as a means of reducing the cost on the reference transfers. The resultant optimized inferior transfers are compared to the corresponding superior time-free transfer paths constructed in Chapter V.

CHAPTER I

THE ELLIPTIC RESTRICTED THREE-BODY PROBLEM

The background information contained in this chapter lays the foundation for the theoretical developments in subsequent chapters. First, a detailed description of the elliptic restricted three-body problem that includes all significant assumptions and derivations is presented. Then, the third-order approximate analytic solution, constructed by Richardson and Cary,[27] for the motion of a spacecraft in the vicinity of the collinear libration points L_1 and L_2 is summarized. Finally, the numerical integration of libration-point trajectories is demonstrated utilizing the technique developed by Howell and Pernicka[29] and extended to the computation of Lissajous trajectories in the elliptic restricted three-body problem by Pernicka.[30]

Assumptions

The elliptic restricted three-body problem is a degenerate case of the more general three-body problem in which each of the three bodies of finite mass moves under the influence of the gravitational attraction of the other two. An explicit, closed-form solution of the general three-body problem remains elusive since eighteen integrals of the motion are required to completely determine a solution, and only ten have been discovered to date. However, some simplifying assumptions can be made that reduce the number of degrees of freedom in the problem while attempting to preserve the overall characteristics of the general problem. First, all three bodies are assumed to possess spherically symmetric gravity fields; hence, each body can be modelled as a point mass. Secondly, the *restricted three-body problem* results if one of the bodies is assumed to be of infinitesimal mass such that it does not affect the motion of the other two bodies termed *primaries*. Such an assumption is of practical interest when examining the motion of a moon, spacecraft, or other heavenly body whose mass is much less than the mass of either of the attracting primaries. Thirdly, if the primaries are

constrained to move on coplanar, elliptic orbits about their center of mass or *barycenter*, the problem is designated the *elliptic restricted three-body problem.* Then, the objective is to determine the motion of the infinitesimal mass given the motion of the primaries.

Coordinate Frames

Establishing an accurate geometric model of the elliptic restricted three-body problem is essential to a proper mathematical formulation. Let P_1 and P_2 denote the primaries having finite masses m_1 and m_2, respectively; also, assume $m_1 \geq m_2$ for convenience. Let P_3 denote the infinitesimal mass. Define $\underline{X}$-$\underline{Y}$-$\underline{Z}$ as an inertially fixed coordinate system with origin located at the barycenter B of the primaries [See Figure 1.1]. The $\underline{X}$-$\underline{Y}$ plane coincides with the plane of motion of the primaries, and the $\underline{Z}$-axis completes the right-handed triad. Define a second coordinate system $\underline{x}$-$\underline{y}$-$\underline{z}$ as a rotating frame, also with origin at the barycenter. The $\underline{x}$-axis is parallel to the line joining the primaries and is directed from the barycenter to P_2. Moreover, the $\underline{Z}$ and $\underline{z}$ axes are coincident. Hence, with the $\underline{y}$-axis completing a right-handed coordinate system, the $\underline{x}$-$\underline{y}$ plane describes the plane of motion of P_1 and P_2, and the $\underline{x}$-$\underline{y}$-$\underline{z}$ frame rotates with an angular velocity equal to that of the primary system. Additionally, the inertial frame is defined such that the angle θ between the $\underline{X}$ and $\underline{x}$ axes is zero when the primaries are at periapsis. The elliptic nature of the orbits of the primaries about the barycenter results in a periodically varying distance between P_1 and P_2. That is, the oscillation of P_1 and P_2 along the $\underline{x}$-axis completes one period for each full revolution of the primaries.

Nondimensionalization

A nondimensional formulation of the problem accomplishes both the generalization of results to any primary system and the simplification of subsequent mathematical developments. The three basic quantities of length, mass, and time are each assigned a characteristic value. Choose the characteristic length L^* to be the mean distance between the primaries, and select the characteristic mass M^* to be the sum of the masses of P_1 and P_2. Also, define the characteristic time as $T^* \triangleq \sqrt{L^{*3}/GM^*}$, where G

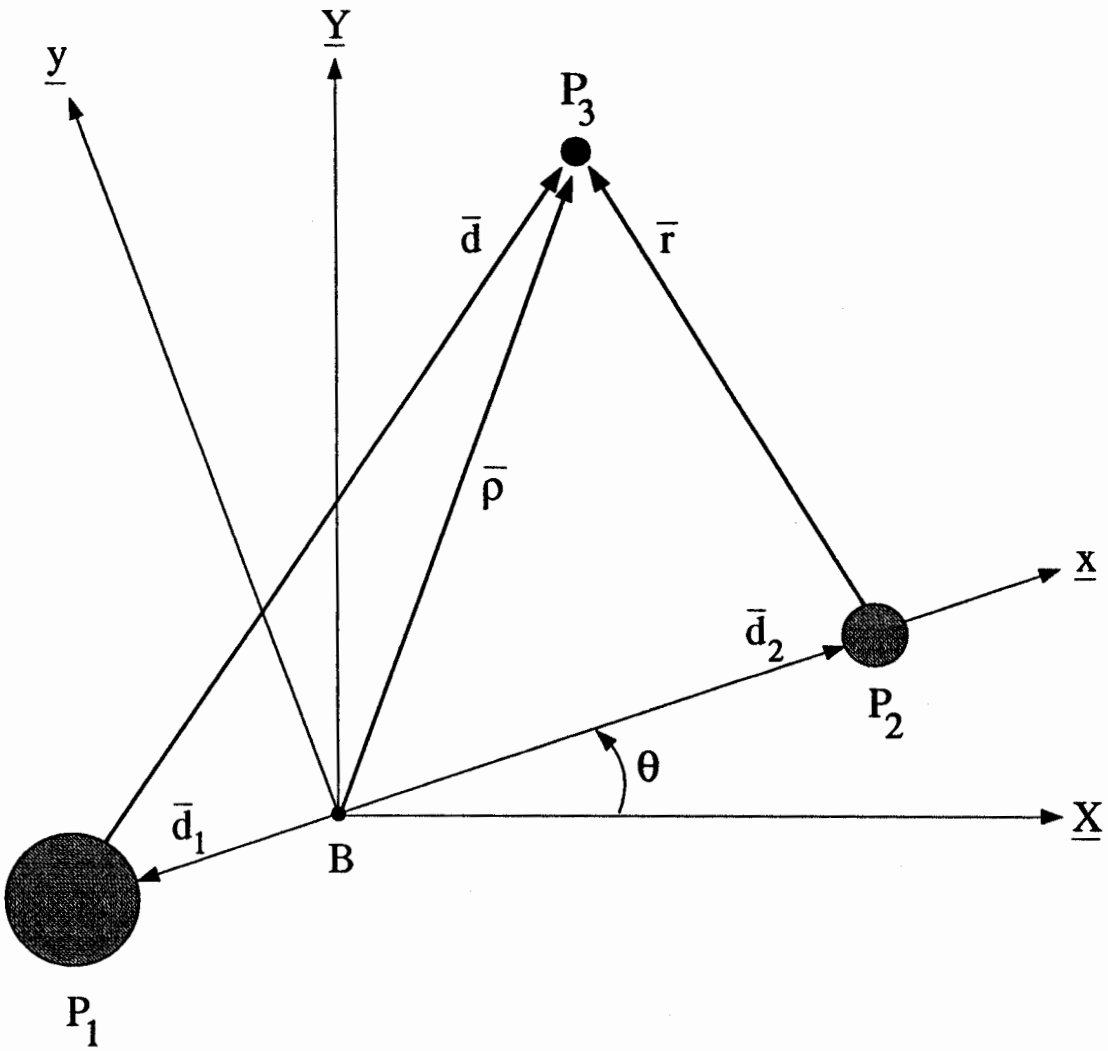

Figure 1.1 Inertial and Rotating Coordinate Systems

is the universal gravitational constant. As a consequence of this definition for T^*, the nondimensional value of G is unity. Similarly, as a result of the definitions for L^* and M^*, respectively, both the nondimensional value of the semi-major axis 'a' of the orbit of the primaries and the nondimensional value of $m_1 + m_2$ are one. From Kepler's equation, the mean motion N of the rotating frame can be expressed as

$$N = \left[\frac{G(m_1 + m_2)}{a^3}\right]^{\frac{1}{2}} . \tag{1.1}$$

Thus, since the nondimensional values of G, a, and $m_1 + m_2$ are unity, N must also have a nondimensional value of one. If the mass-ratio parameter μ is defined as

$$\mu \triangleq \frac{m_2}{(m_1 + m_2)} , \tag{1.2}$$

then the nondimensional masses of the primaries may be written as

$$m_1 = 1 - \mu \tag{1.3a}$$

$$m_2 = \mu . \tag{1.3b}$$

Finally, the eccentricity of the primary orbit is denoted by e, a nondimensional quantity by definition. With these preliminaries, the equations of motion for P_3 can now be derived.

Equations of Motion

The equations of motion for the elliptic restricted three-body problem can be formulated using either vectorial or analytical mechanics. Here, the Newtonian approach is presented. If $\bar{\rho}$ denotes the position of P_3 relative to the barycenter, the total force acting on P_3 is written

$$\Sigma \bar{F} = m_3 \bar{\rho}^{''I} = -\frac{Gm_3 m_1}{d^3}\bar{d} - \frac{Gm_3 m_2}{r^3}\bar{r} , \tag{1.4}$$

where

$$\bar{\rho} = x\hat{i} + y\hat{j} + z\hat{k} . \tag{1.5}$$

Consistent with an assumption stated earlier, equation (1.4) regards P_1 and P_2 as point masses. Primes designate differentiation with respect to dimensional time, and superscript I signifies differentiation with respect to the inertial frame. The positions of P_3

relative to P_1 and to P_2 are represented by the vectors $\bar{d}$ and $\bar{r}$, respectively, as illustrated in Figure 1.1. The unit vectors $\hat{i}$, $\hat{j}$, $\hat{k}$ are directed along the $\underline{x}$, $\underline{y}$, and $\underline{z}$ axes. Utilizing the previously defined characteristic quantities to nondimensionalize equation (1.4) yields

$$\ddot{\bar{\rho}}^{I} = -\frac{(1-\mu)}{d^3}\bar{d} - \frac{\mu}{r^3}\bar{r}, \tag{1.6}$$

where dots designate differentiation with respect to nondimensional time, and $\bar{\rho}$, $\bar{d}$, and $\bar{r}$ now denote nondimensional position vectors.

When written in scalar form, equation (1.6) yields three second order differential equations. The reduction of the left side of (1.6) to scalar form is initiated with the construction of the velocity of P_3 in the inertial frame which is written as

$$\dot{\bar{\rho}}^{I} = \dot{\bar{\rho}}^{F} + {}^{I}\bar{\omega}^{F} \times \bar{\rho}, \tag{1.7}$$

where $\dot{\bar{\rho}}^{F}$ is the velocity of P_3 in the rotating frame, and ${}^{I}\bar{\omega}^{F}$ is the angular velocity of that frame relative to the inertial frame. From Figure 1.1, the angular velocity of the rotating frame relative to the inertial frame is $\dot{\theta}$; moreover, this time-varying angular rate is commonly denoted n. Thus, ${}^{I}\bar{\omega}^{F} = n\hat{k}$. Solution of the two-body problem for the primaries affords the relationship for n, expressed as

$$n = \frac{h}{R^2}, \tag{1.8}$$

where h is the magnitude of the orbital angular momentum of the primaries, and R represents the time-varying distance between the primaries. The dimensional expressions for h and R, arising from the two-body primary analysis, can be written

$$\tilde{h} = \sqrt{G(m_1 + m_2)a(1-e^2)},$$

and

$$\tilde{R} = a(1 - e\cos E),$$

or alternatively expressed in nondimensional form,

$$h = \sqrt{1-e^2}, \tag{1.9}$$

and

$$R = (1 - e\cos E), \tag{1.10}$$

where E is the eccentric anomaly associated with the primary orbit. Substituting equations (1.9) and (1.10) into (1.8) produces the expression for the nondimensional angular rate as

$$n = \frac{\sqrt{1-e^2}}{(1-e\cos E)^2}\,. \tag{1.11}$$

So, performing the required differentiation and vector cross product permits equation (1.7) to be written as

$$\overset{\cdot}{\bar{\rho}}^{I} = (\dot{x} - ny)\hat{i} + (\dot{y} + nx)\hat{j} + \dot{z}\hat{k}\,, \tag{1.12}$$

The acceleration of P_3 is obtained by differentiating (1.7) in the inertial frame with respect to nondimensional time; thus,

$$\overset{\cdot\cdot}{\bar{\rho}}^{I} = \overset{\cdot\cdot}{\bar{\rho}}^{IF} + \bar{\omega}^{I-F} \times \overset{\cdot}{\bar{\rho}}^{I}\,, \tag{1.13}$$

where $\overset{\cdot\cdot}{\bar{\rho}}^{IF}$ denotes differentiation of (1.12) with respect to the rotating frame. Simplifying (1.13),

$$\overset{\cdot\cdot}{\bar{\rho}}^{I} = (\ddot{x} - 2n\dot{y} - \dot{n}y - n^2x)\hat{i} + (\ddot{y} + 2n\dot{x} + \dot{n}x - n^2y)\hat{j} + \ddot{z}\hat{k}\,; \tag{1.14}$$

additionally, $\dot{n}$, obtained by differentiating (1.11), is expressed

$$\dot{n} = -2e\frac{\sqrt{1-e^2}}{(1-e\cos E)^4}\sin E\,. \tag{1.15}$$

Next, the reduction of the right side of (1.6) to scalar form commences by expressing $\bar{d}$ and $\bar{r}$ in terms of $\bar{\rho}$ as

$$\bar{d} = \bar{\rho} - \bar{d}_1 \tag{1.16a}$$

$$\bar{r} = \bar{\rho} - \bar{d}_2\,, \tag{1.16b}$$

where

$$\bar{d}_1 = -\mu R\hat{i} = -\mu(1+\xi)\hat{i} \tag{1.17a}$$

$$\bar{d}_2 = (1-\mu)R\hat{i} = (1-\mu)(1+\xi)\hat{i}\,. \tag{1.17b}$$

The quantity $1+\xi$ is the nondimensional quantity associated with R and, consequently, has the form $1+\xi = 1 - e\cos E$ such that ξ is a measure of the time-varying nature of the nondimensional distance between the primaries. So, substituting equations (1.5) and (1.17) into (1.16) yields

$$\bar{d} = [x + \mu\,(1 + \xi)]\,\hat{i} + y\hat{j} + z\hat{k} \tag{1.18a}$$

$$\bar{r} = [x - (1 - \mu)(1 + \xi)]\,\hat{i} + y\hat{j} + z\hat{k}\,, \tag{1.18b}$$

which are the position vectors from the primaries to P_3 written in terms of rotating coordinates.

Finally, substituting equations (1.14) and (1.18) into (1.6) and decomposing (1.6) into scalar form renders the following three, nondimensional, second order, differential equations of motion:

$$\ddot{x} - 2n\dot{y} - \dot{n}y - n^2x = -\frac{(1-\mu)[x + \mu(1+\xi)]}{d^3} - \frac{\mu[x - (1-\mu)\,(1+\xi)]}{r^3} \tag{1.19a}$$

$$\ddot{y} + 2n\dot{x} + \dot{n}x - n^2y = -\frac{(1-\mu)y}{d^3} - \frac{\mu y}{r^3} \tag{1.19b}$$

$$\ddot{z} = -\frac{(1-\mu)z}{d^3} - \frac{\mu z}{r^3}\,. \tag{1.19c}$$

If a pseudo-potential U is defined as

$$U \triangleq \frac{1}{2}n^2(x^2 + y^2) + \frac{1-\mu}{d} + \frac{\mu}{r}\,, \tag{1.20}$$

then equations (1.19) can be expressed

$$\ddot{x} - 2n\dot{y} = \frac{\partial U}{\partial x} + \dot{n}y \tag{1.21a}$$

$$\ddot{y} + 2n\dot{x} = \frac{\partial U}{\partial y} - \dot{n}x \tag{1.21b}$$

$$\ddot{z} = \frac{\partial U}{\partial z}\,. \tag{1.21c}$$

If eccentricity is specified as zero, the primaries are constrained to move on circular orbits. Setting $e = 0$ in (1.10) results in a constant R with a nondimensional value equal to one; thus, the time-varying quantity denoted by ξ reduces to zero. Additionally, the angular velocity of the rotating frame relative to the inertial frame becomes constant and, from equation (1.11), equal to unity. The motion of P_3 under the gravitational influence of primaries moving on circular paths is designated the *circular restricted three-body problem*, and this system was determined by Jacobi to possess an integral of the motion which renders a constant of integration, *i.e.*,

$$2U - \left[\dot{x}^2 + \dot{y}^2 + \dot{z}^2\right] = \text{constant}\,. \tag{1.22}$$

In addition to reducing the degrees of freedom in the problem, this constant can be utilized for checking the accuracy of the numerical integration in the circular problem.

Libration Points

The equilibrium solutions associated with the differential equations (1.21) are the five particular solutions identified by Lagrange in 1772, and in the circular restricted three-body problem, these five particular solutions are called *libration points*. At each of these locations, the gravitational and centrifugal forces balance; thus, the position of an infinitesimal mass remains stationary relative to the x-y-z rotating frame. So, as viewed in the rotating frame, the libration points are stationary; hence, setting the relative velocity and acceleration at these locations to zero, $\dot{x} = \dot{y} = \dot{z} = \ddot{x} = \ddot{y} = \ddot{z} = 0$. Using this observation in (1.21) and specifying $e = 0$ permits the computation of the five libration point positions via solution of the three equations,

$$\frac{\partial U}{\partial x} = \frac{\partial U}{\partial y} = \frac{\partial U}{\partial z} = 0\,. \tag{1.23}$$

Of the five particular solutions of (1.23), designated as L_i $(i = 1, \cdots, 5)$ and represented in Figure 1.2 for an arbitrary mass ratio, three of the libration points lie on the line joining the primaries. Of these three, L_1 is designated as the point between the primaries; L_2 is positioned on the far side of m_2; and, L_3 is found on the far side of m_1. The two remaining libration points, L_4 and L_5, form equilateral triangles with the primaries in their plane of motion.

In the elliptic restricted three-body problem, however, stationary equilibrium points in the same sense do not exist, for constant values of x, y, and z cannot be found. Nevertheless, the libration points of the circular problem correspond, in the elliptic problem, to five points that oscillate about average values. The two triangular libration points, L_4 and L_5, oscillate periodically on equilateral triangles with sides of length equal to the distance between primaries. The three collinear points oscillate along the x-axis about locales roughly analogous to their positions in the circular problem. The location of the collinear libration points relative to the rotating frame can be determined by assuming the existence of the collinear points in the elliptic problem such that $y = \dot{y} = z = \dot{z} = 0$ and that the ratio of x to R is constant. Equation (1.19b) then

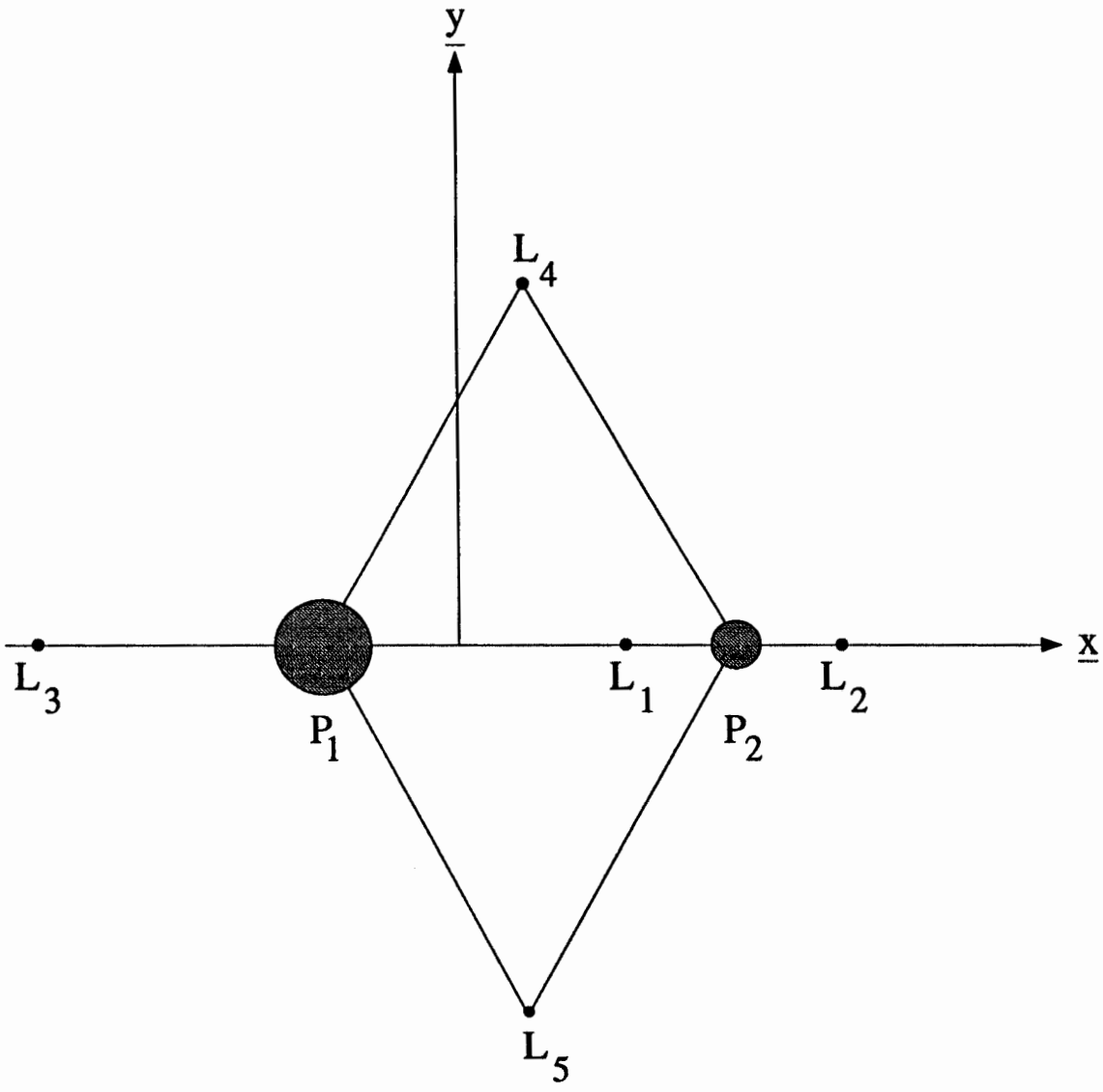

Figure 1.2 Libration Point Locations in the Rotating Frame

simplifies to

$$2n\dot{x} + \dot{n}x = 0\,, \tag{1.24}$$

or solving for $\dot{x}$,

$$\dot{x} = -\frac{\dot{n}}{2n}x\,. \tag{1.25}$$

Substituting (1.11) and (1.15) into (1.25) and recalling that $R = 1 - e\cos E$,

$$\dot{x} = \left[\frac{x}{R}\right]\frac{e\sin E}{R}\,. \tag{1.26}$$

Taking the time derivative of (1.26) produces

$$\ddot{x} = \left[\frac{x}{R}\right]\frac{e(\cos E - e)}{R^3}\,. \tag{1.27}$$

For each of the three ranges of possible collinear-point locations (*i.e.*, between the primaries, on the far side of m_2, or on the far side of m_1), substitution of (1.26), (1.27), and $y = \dot{y} = 0$ into (1.19a) results in a different quintic polynomial in (x/R). Generally calculated numerically, the one real root of each quintic locates the corresponding collinear libration point. If the constant ratio (x/R) is defined as ζ_{L_i} ($i = 1, 2, 3$), then the oscillating location of the collinear point on the x-axis, denoted x_{L_i}, can be expressed

$$x_{L_i} = R\zeta_{L_i} \quad (i = 1, 2, 3)\,. \tag{1.28}$$

Since (x/R) is constant, then the ratio of the nondimensional distance $L_i \rightarrow P_2$ to the length R, denoted as γ_{L_i} ($i = 1, 2$), must also be constant. Analogously, γ_{L_3} designates the constant ratio of the nondimensional distance $L_3 \rightarrow P_1$ to the length R. The relationships between ζ_{L_i} and γ_{L_i} are illustrated in Figure 1.3 and are expressed algebraically as

$$\zeta_{L_1} = 1 - \mu - \gamma_{L_1} \tag{1.29a}$$

$$\zeta_{L_2} = 1 - \mu + \gamma_{L_2} \tag{1.29b}$$

$$\zeta_{L_3} = \mu + \gamma_{L_3}\,. \tag{1.29c}$$

Thus, the instantaneous location of L_i, which is essential to performing coordinate translations between barycenter and libration point, can be computed from (1.29).

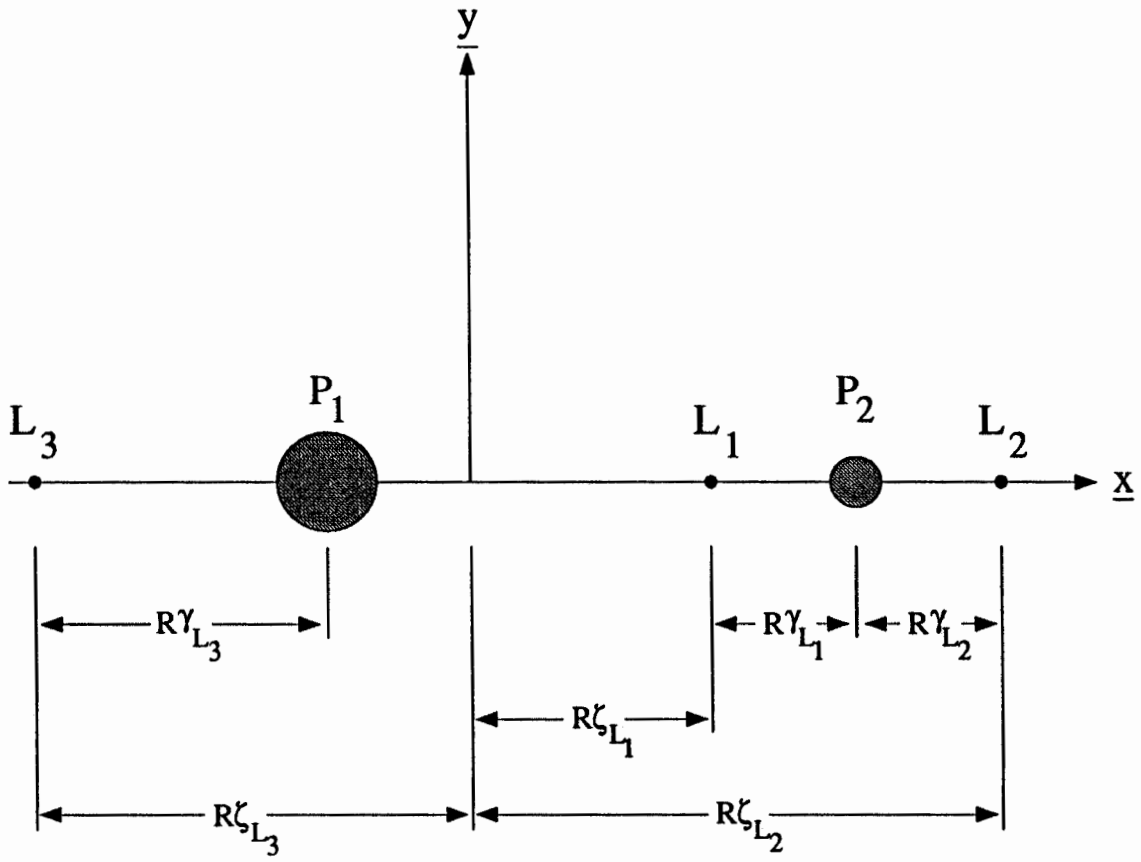

Figure 1.3 Collinear Libration Point Locations in the Elliptic Restricted Problem

State Transition Matrix

Associated with the equations of motion (1.21) is a state transition matrix that is utilized in a differential corrections algorithm to compute nominal orbits. Additionally, knowledge of the state transition matrix is imperative to the calculation of the primer vector employed in the trajectory optimization process. If a six-dimensional state vector is constructed from the position and velocity components of P_3 such that $\bar{x}(t) = [x, y, z, \dot{x}, \dot{y}, \dot{z}]^T$ (superscript T designates transpose), then the linearized vector state variational equation, constructed from equations (1.21) and expressed in terms of a non-constant matrix A(t), is written

$$\delta\dot{\bar{x}}(t) = A(t)\delta\bar{x}(t) \tag{1.30}$$

which has a solution of the form

$$\delta\bar{x}(t) = \Phi(t, t_0)\delta\bar{x}(t_0)\,, \tag{1.31}$$

where the 6x6 state transition matrix, denoted $\Phi(t, t_0)$, is composed of the partial derivatives $\dfrac{\partial\bar{x}(t)}{\partial\bar{x}(t_0)}$ evaluated along the orbit. The differential equation governing $\Phi(t, t_0)$ is

$$\frac{d}{dt}\Phi(t, t_0) = A(t)\,\Phi(t, t_0)\,, \tag{1.32a}$$

with initial condition

$$\Phi(t_0, t_0) = I_6\,, \tag{1.32b}$$

where A(t) is the 6x6 matrix of partial derivatives obtained from the linearized state variational equation (1.30), and I_6 is the 6x6 identity matrix. Partitioned into four 3x3 submatrices, A(t) can be written as

$$A(t) = \begin{bmatrix} 0 & I \\ \Upsilon + \dot{n}\Omega & 2n\Omega \end{bmatrix}, \tag{1.33}$$

where

$0 \triangleq$ Zero Matrix ,

$I \triangleq$ Identity Matrix ,

$$\Omega \triangleq \begin{bmatrix} 0 & 1 & 0 \\ -1 & 0 & 0 \\ 0 & 0 & 0 \end{bmatrix}, \tag{1.34}$$

$$\Upsilon \triangleq \begin{bmatrix} U_{xx} & U_{xy} & U_{xz} \\ U_{yx} & U_{yy} & U_{yz} \\ U_{zx} & U_{zy} & U_{zz} \end{bmatrix}\Bigg|_{\text{trajectory}} . \tag{1.35}$$

Υ is a symmetric matrix containing the second partial derivatives of the pseudo-potential U with respect to x, y, and z evaluated along the trajectory. The components of Υ, calculated from (1.20), are

$$U_{xx} = \frac{\partial^2 U}{\partial x^2} = n^2 - \frac{1-\mu}{d^3} - \frac{\mu}{r^3} + \frac{3(1-\mu)[x+\mu(1+\xi)]^2}{d^5} + \frac{3\mu[x-(1-\mu)(1+\xi)]^2}{r^5} \tag{1.36a}$$

$$U_{xy} = \frac{\partial^2 U}{\partial x \partial y} = \frac{3(1-\mu)[x+\mu(1+\xi)]y}{d^5} + \frac{3\mu[x-(1-\mu)(1+\xi)]y}{r^5} \tag{1.36b}$$

$$U_{xz} = \frac{\partial^2 U}{\partial x \partial z} = \frac{3(1-\mu)[x+\mu(1+\xi)]z}{d^5} + \frac{3\mu[x-(1-\mu)(1+\xi)]z}{r^5} \tag{1.36c}$$

$$U_{yy} = \frac{\partial^2 U}{\partial y^2} = n^2 - \frac{(1-\mu)}{d^3} - \frac{\mu}{r^3} + \frac{3(1-\mu)y^2}{d^5} + \frac{3\mu y^2}{r^5} \tag{1.36d}$$

$$U_{yz} = \frac{\partial^2 U}{\partial y \partial z} = \frac{3(1-\mu)yz}{d^5} + \frac{3\mu yz}{r^5} \tag{1.36e}$$

$$U_{zz} = \frac{\partial^2 U}{\partial z^2} = -\frac{(1-\mu)}{d^3} - \frac{\mu}{r^3} + \frac{3(1-\mu)z^2}{d^5} + \frac{3\mu z^2}{r^5} . \tag{1.36f}$$

Coupling the 36 first order differential equations of (1.32a) with the equations of

motion (1.19) results in the forty-two first-order differential equations which define the dynamic model in the elliptic restricted three-body problem and which must be numerically integrated to produce trajectories.

Approximate Analytic Solutions

As mentioned earlier, no general, closed-form solution of the equations of motion in the elliptic restricted three-body problem has been discovered; hence, a few researchers have devoted efforts to developing approximate, analytic solutions. Plummer[11,12] utilizes Fourier series expansions to create planar periodic solutions near the collinear libration points; whereas, more recently, Heppenheimer,[26] employing Lindstedt's method, evolves a third-order theory for nonlinear out-of-plane motion in the elliptic restricted problem. Farquhar and Kamel[17] apply the method of Lindstedt-Poincaré to develop third-order approximations limited to small amplitude orbits about the translunar libration point (L_2) of the Earth-Moon primary system with solar perturbations inclusive. Finally, Richardson and Cary,[27] using successive approximations and multiple time scales, obtain analytic solutions in the vicinity of the collinear libration points of the restricted three-body problem with eccentric and fourth-body corrections.

In a pedantic sense, analytic approximations provide insight into the general nature of a problem; however, from a practical standpoint, such approximations are essential to the numerical computation of Lissajous orbits. An iterative numerical scheme requires a first guess that is reasonably close to the orbit of interest, and, in most cases, the analytic solutions fulfill this requirement. Due to the ease with which the algorithm is adapted to the elliptic problem and to primary systems of arbitrary mass ratio, Richardson and Cary's approximation is selected for subsequent analytic analyses and for implementation in the numerical technique developed in Reference [30]. The analytic solution obtained by Richardson and Cary is validated, and the following summarizes the development of that third-order approximation.

First, if the Sun and Earth are selected as primaries, then the motion of a spacecraft in this primary system is also influenced, to some extent, by the presence of the Moon. Farquhar[72] concludes that a more accurate solution for the spacecraft's motion in the Sun-Earth primary system is obtained if lunar perturbations are taken into account by considering the Earth and Moon as a single body of mass equal to the sum

of their individual masses placed at their barycenter. Such a configuration of the primaries is designated the Sun-Earth/Moon barycenter primary system, which is represented in Figure 1.4. Richardson and Cary develop their third-order analytic approximation assuming a circular Sun-Earth/Moon barycenter primary system to which eccentric and lunar corrections are applied.

Secondly, to simplify the analysis, a coordinate transformation is performed which translates the origin of the $\underline{x}$-$\underline{y}$-$\underline{z}$ frame to the collinear libration point of interest (L_1 or L_2). Employing equations (1.28) and (1.29) to relate the position coordinates in these two frames,

$$x^L = x^B + R(1 - \mu \mp \gamma_L) \tag{1.37a}$$

$$y^L = y^B \tag{1.37b}$$

$$z^L = y^B \,, \tag{1.37c}$$

where superscript L denotes a quantity relative to the frame with origin at the libration point, superscript B denotes a quantity relative to the frame with origin at the barycenter, and the upper sign of $\mp$ refers to L_1 while the lower sign refers to L_2. In addition, a velocity transformation associated with the origin translation is compulsory. If the derivative of eccentric anomaly is noted to take the form $\dot{E} = (1 - e\,\cos E)^{-1}$, then, from (1.10), the derivative of R is

$$\dot{R} = \frac{e\,\sin E}{(1 - e\,\cos E)} \,, \tag{1.38}$$

and the transformation for velocity components becomes

$$\dot{x}^L = \dot{x}^B + (1 - \mu \mp \gamma_L)\frac{e\,\sin E}{(1 - e\,\cos E)} \tag{1.39a}$$

$$\dot{y}^L = \dot{y}^B \tag{1.39b}$$

$$\dot{z}^L = \dot{z}^B \,. \tag{1.39c}$$

Next, equations (1.37) and (1.39) are used to transform the equations of motion (1.19) to the libration-point-centered coordinate frame, denoted by $\underline{x}$-$\underline{y}$-$\underline{z}$ [See Figure 1.4], and the superscript L will subsequently be omitted. These new equations of motion are expanded in a Taylor series and then truncated to third order. The system parameter chosen to define the order of magnitude is e, the Earth/Moon barycenter orbital eccentricity. The Taylor series expansions are valid only for x, y, and z

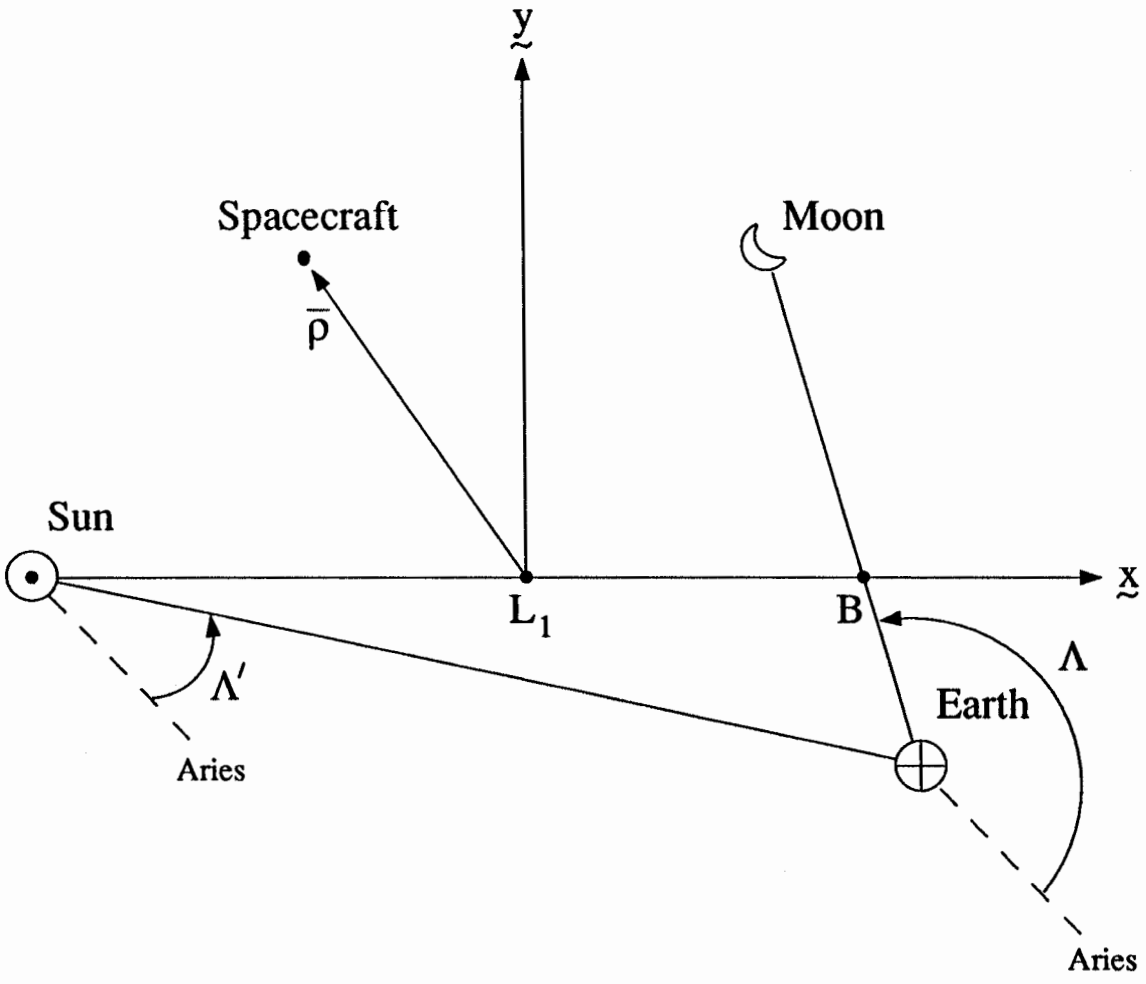

Figure 1.4 Sun-Earth/Moon Barycenter Primary System

satisfying the relations $2x/\gamma_L < 1$, $y/\gamma_L < 1$, and $z/\gamma_L < 1$. Since γ_L is of order e, then x, y, and z must be of order $e^{3/2}$ or higher (*i.e.*, x, y, $z \leq 3.23\text{x}10^5$ km for the Sun-Earth/Moon system). The equations of motion can now be solved via successive approximations by expressing the solution as a sum of a number of terms, each identified by its individual contribution. Assume a solution of the form

$$x = \gamma_L \left[e^{1/2}x^{(1)} + ex^{(2)} + e^{3/2}(x^{(3)} + x^{(3,e)}) + e^2(x^{(4)} + x^{(4,e)} + x^{(4,m)}) \right] \quad (1.40a)$$

$$y = \gamma_L \left[e^{1/2}y^{(1)} + ey^{(2)} + e^{3/2}(y^{(3)} + y^{(3,e)}) + e^2(y^{(4)} + y^{(4,e)} + y^{(4,m)}) \right] \quad (1.40b)$$

$$z = \gamma_L \left[e^{1/2}z^{(1)} + ez^{(2)} + e^{3/2}(z^{(3)} + z^{(3,e)}) + e^2(z^{(4)} + z^{(4,e)} + z^{(4,m)}) \right], \quad (1.40c)$$

where the superscripted numeral designates the order of the contribution, and the superscripted e or m denotes the eccentric or fourth-body corrections, respectively. Despite the appearance of four orders of terms in equations (1.40), that the approximations themselves are truncated at third order becomes obvious when γ_L, which is of order e, is multiplied by the last contribution, $e^2(x^{(4)} + ...)$, and results in a term of order e^3. Hence, the distinction between a third-order contribution and a third-order approximation, for example, is imperative.

The first-order contributions are examined initially. Note that differential equations (1.19) can be transformed using (1.37) and (1.39) such that the new differential equations represent the motion relative to L_i. If the equations of motion relative to the L_i-centered frame are expanded about the libration point, the resultant linear differential equations are

$$\ddot{x}_1 - 2\dot{y}_1 - (1 + 2c)x_1 = 0 \quad (1.41a)$$

$$\ddot{y}_1 + 2\dot{x}_1 + (c - 1)y_1 = 0 \quad (1.41b)$$

$$\ddot{z}_1 + cz_1 = 0, \quad (1.41c)$$

where x_1, y_1, z_1 describe the linearized motion relative to a rotating coordinate system with origin at L_i, and

$$c \triangleq \frac{(1-\mu)}{(1 \mp \gamma_L)^3} + \frac{\mu}{\gamma_L 3}. \quad (1.42)$$

For all possible values of μ, the constant c is greater than one. The variables x_1, y_1, z_1 are related to the first-order contributions in (1.40) by

$$x_1 = \gamma_L e^{1/2} x^{(1)} \tag{1.43a}$$

$$y_1 = \gamma_L e^{1/2} y^{(1)} \tag{1.43b}$$

$$z_1 = \gamma_L e^{1/2} z^{(1)} . \tag{1.43c}$$

From the linearized equations (1.41), the out-of-plane z_1-equation is observed to decouple from the in-plane x_1- and y_1-equations. The general solution of (1.41) can be written as

$$x_1 = A_1 e^{\varepsilon t} + A_2 e^{-\varepsilon t} + A_3 \cos\lambda t + A_4 \sin\lambda t \tag{1.44a}$$

$$y_1 = -k_1 A_1 e^{\varepsilon t} + k_1 A_2 e^{-\varepsilon t} - k_2 A_3 \sin\lambda t + k_2 A_4 \cos\lambda t \tag{1.44b}$$

$$z_1 = B_1 \sin\nu t + B_2 \cos\nu t , \tag{1.44c}$$

where A_1, A_2, A_3, A_4, B_1, B_2 are constants of integration, and k_1, k_2, λ, ν, ε are positive constants. Although the solution of (1.44c) is simple harmonic motion in the $\underset{\sim}{z}$-direction, the existence of exponential growth and decay terms in (1.44a) and (1.44b) render the motion in the $\underset{\sim}{x}$- and $\underset{\sim}{y}$-direction unbounded and non-oscillatory. However, if initial conditions are selected so that $A_1 = A_2 = 0$, bounded, oscillatory (linearized) motion results in all three dimensions. Examining the initial position and velocity conditions from equations (1.44a) and (1.44b) yields

$$x_1(0) = A_1 + A_2 + A_3 \tag{1.45a}$$

$$y_1(0) = -k_1 A_1 + k_1 A_2 + k_2 A_4 \tag{1.45b}$$

$$\dot{x}_1(0) = \varepsilon A_1 - \varepsilon A_2 + \lambda A_4 \tag{1.45c}$$

$$\dot{y}_1(0) = -\varepsilon k_1 A_1 - \varepsilon k_1 A_2 - \lambda k_2 A_3 . \tag{1.45d}$$

Restricting A_1 and A_2 to be zero in (1.45) produces

$$x_1(0) = A_3 \tag{1.46a}$$

$$y_1(0) = k_2 A_4 \tag{1.46b}$$

$$\dot{x}_1(0) = \lambda A_4 \tag{1.46c}$$

$$\dot{y}_1(0) = -\lambda k_2 A_3 . \tag{1.46d}$$

So, once the initial conditions $x_1(0)$ and $y_1(0)$ are selected, the corresponding initial velocities are specified and may not be chosen. If the initial conditions satisfy (1.46), the linear approximation to the motion can be expressed as

$$x_1 = A_3 \cos\lambda t + A_4 \sin\lambda t \tag{1.47a}$$

$$y_1 = -k_2 A_3 \sin\lambda t + k_2 A_4 \cos\lambda t \tag{1.47b}$$

$$z_1 = B_1 \sin\nu t + B_2 \cos\nu t\,; \tag{1.47c}$$

hence, a bounded, oscillatory solution to the linearized equations results. Expressing (1.47) in a more convenient form,

$$x_1 = -A_x \cos(\lambda t + \phi) \tag{1.48a}$$

$$y_1 = kA_x \sin(\lambda t + \phi) \tag{1.48b}$$

$$z_1 = A_z \sin(\nu t + \psi)\,, \tag{1.48c}$$

where λ and ν are linearized frequencies. The frequency λ is the modulus of the imaginary roots of the characteristic equation

$$\tilde{\lambda}^4 + (2 - c)\,\tilde{\lambda}^2 + (1 + 2c)\,(1 - c) = 0\,, \tag{1.49}$$

and ν is determined from

$$\nu^2 = c\,. \tag{1.50}$$

Also, k is a proportionality constant evaluated as

$$k = \frac{1 + 2c + \lambda^2}{2\lambda}\,. \tag{1.51}$$

A_x and A_z, the amplitudes of the in-plane and out-of-plane motion, characterize the size of the orbit; also, the phase angles, ϕ and ψ, are established by the initial conditions. If the frequencies are equal, halo orbits, that have periods commensurate with the period of the primary orbit, are produced; however, the equality of λ and ν can only be realized by the application of specific amplitude constraints involving higher-order terms. The less stringent condition allowing unequal frequencies results in Lissajous trajectories that do not quite repeat at the completion of a revolution.

The method of multiple scales is employed to remove secular terms, ensuing from the successive approximation of the contributions to the solution, so that a bounded, uniformly valid solution results. In conjunction with equations (1.40) which express the solutions in powers of $e^{1/2}$, the time scales are defined as[73]

$$\begin{aligned} T_0 &= t \\ T_1 &= e^{1/2}t \\ T_2 &= et \\ T_3 &= e^{3/2}t \\ T_4 &= e^2t\ . \end{aligned} \tag{1.52}$$

Now, ordinary differentiation can be replaced by partial differentiation with respect to the time scales. The solution form expressed in (1.40) is substituted into the differential equations of motion, and like powers of $e^{1/2}$ are equated. When solving for each order of contribution, the secular terms (which arise when the inhomogeneity of the differential equation contains sinusoidal terms of the same frequency as the homogeneous solution) must be eliminated. Secular term removal is illustrated for the coupled x- and y-equations having the general form

$$D_{00}x - aD_0y - bx = E\ \mathrm{cos}qT_0 + F\ \mathrm{sin}qT_0 \tag{1.53a}$$

$$D_{00}y + aD_0x + cy = G\ \mathrm{cos}qT_0 + H\ \mathrm{sin}qT_0\ , \tag{1.53b}$$

where D denotes partial differentiation with respect to the subscripted time scale; a, b, c are constants; and, E, F, G, H are coefficients of the sinusoidal terms in the inhomogeneity that have frequency q, which is equal to that of the homogeneous solution. The two second-order equations of (1.53) are combined into one fourth-order equation of the form

$$\begin{aligned} D_{0000}x + (c - b + a^2)D_{00}x - bcx = (aHq + cE - Eq^2)\mathrm{cos}qT_0 + \\ (-aGq + cF - Fq^2)\mathrm{sin}qT_0\ . \end{aligned} \tag{1.54}$$

To eliminate the secular terms, the coefficients of the sinusoidal terms must equal zero; hence,

$$aHq + cE - Eq^2 = 0 \tag{1.55a}$$

$$-aGq + cF - Fq^2 = 0\ . \tag{1.55b}$$

Equations (1.55) stipulate conditions on the functional dependence of the parameters A_x, A_z, ϕ, and ψ on the time scales.

Successive solution for the second-, third-, and fourth-order contributions, void of secular terms, can now be accomplished. The expressions for these higher-order terms have the following form:

$$x^{(2)} = \rho_{20} + \rho_{21}\cos 2t_1 + \rho_{22}\cos 2t_2 \tag{1.56a}$$

$$y^{(2)} = \sigma_{21}\sin 2t_1 + \sigma_{22}\sin 2t_2 \tag{1.56b}$$

$$z^{(2)} = \kappa_{21}\sin(t_1 + t_2) + \kappa_{22}\sin(t_2 - t_1) \tag{1.56c}$$

$$x^{(3)} = \rho_{31}\cos 3t_1 + \rho_{32}\cos(t_1 + 2t_2) + \rho_{33}\cos(2t_2 - t_1) \tag{1.57a}$$

$$y^{(3)} = \sigma_{31}\sin 3t_1 + \sigma_{32}\sin(t_1 + 2t_2) + \sigma_{33}\sin(2t_2 - t_1) \tag{1.57b}$$

$$z^{(3)} = \kappa_{31}\sin 3t_2 + \kappa_{32}\sin(2t_1 + t_2) + \kappa_{33}\sin(2t_1 - t_2) \tag{1.57c}$$

$$x^{(3,e)} = q_{31}\cos(M + t_1) + q_{32}(M - t_1) \tag{1.58a}$$

$$y^{(3,e)} = r_{31}\cos(M + t_1) + r_{32}(M - t_1) \tag{1.58b}$$

$$z^{(3,e)} = s_{31}\cos(M + t_2) + s_{32}(M - t_2) \tag{1.58c}$$

$$\begin{aligned} x^{(4)} = {} & \rho_{40} + \rho_{41}\cos 2t_1 + \rho_{42}\cos 2t_2 + \rho_{43}\cos 4t_1 + \rho_{44}\cos 4t_2 \\ & + \rho_{45}\cos 2(t_1 + t_2) + \rho_{46}\cos 2(t_2 - t_1) \end{aligned} \tag{1.59a}$$

$$\begin{aligned} y^{(4)} = {} & \sigma_{41}\sin 2t_1 + \sigma_{42}\sin 2t_2 + \sigma_{43}\sin 4t_1 + \sigma_{44}\sin 4t_2 \\ & + \sigma_{45}\sin 2(t_1 + t_2) + \sigma_{46}\sin 2(t_2 - t_1) \end{aligned} \tag{1.59b}$$

$$\begin{aligned} z^{(4)} = {} & \kappa_{41}\sin(t_1 + t_2) + \kappa_{42}\sin(t_2 - t_1) + \kappa_{43}\sin(t_1 + 3t_2) + \\ & \kappa_{44}\sin(3t_2 - t_1) + \kappa_{45}\sin(3t_1 + t_2) + \kappa_{46}\sin(t_2 - 3t_1) \end{aligned} \tag{1.59c}$$

$$\begin{aligned} x^{(4,e)} = {} & q_{41}\cos M + q_{42}\cos(M + 2t_1) + q_{43}\cos(M - 2t_1) \\ & + q_{44}\cos(M + 2t_2) + q_{45}\cos(M - 2t_2) \end{aligned} \tag{1.60a}$$

$$\begin{aligned} y^{(4,e)} = {} & r_{41}\sin M + r_{42}\sin(M + 2t_1) + r_{43}\sin(M - 2t_1) \\ & + r_{44}\sin(M + 2t_2) + r_{45}\sin(M - 2t_2) \end{aligned} \tag{1.60b}$$

$$\begin{aligned} z^{(4,e)} = {} & s_{41}\sin(M - t_1 + t_2) + s_{42}\sin(M + t_1 - t_2) + \\ & s_{43}\sin(M + t_1 + t_2) + s_{44}\cos(M - t_1 - t_2) \end{aligned} \tag{1.60c}$$

$$x^{(4,m)} = m_{41} + m_{41}\cos 2(\Lambda - \Lambda') \tag{1.61a}$$

$$y^{(4,m)} = n_{41}\sin 2(\Lambda - \Lambda') \tag{1.61b}$$

$$z^{(4,m)} = 0\,, \tag{1.61c}$$

where

$$t_1 = \lambda T_0 + \phi \tag{1.62a}$$

$$t_2 = \nu T_0 + \psi\,. \tag{1.62b}$$

Additionally, M is the mean anomaly of the primary orbit and is expressed in terms of eccentric anomaly as

$$M = E - e\,\sin E\,; \tag{1.63}$$

Λ and Λ' are the lunar and terrestrial mean longitudes; and, the coefficients ρ_{ij}, σ_{ij}, κ_{ij}, q_{ij}, s_{ij}, m_{ij}, and n_{ij} are functions of the input amplitudes, phase angles, and system parameters such as mass ratio μ and semi-major axis a. The lengthy analytic expressions for the coefficients are found in Reference [27].

A sample Lissajous trajectory in the vicinity of the L_1 libration point of the Sun-Earth/Moon barycenter system is computed using only first-order contributions in the analytic approximation. The x and z amplitudes are independently and arbitrarily selected to be $A_x = 160{,}000$ km and $A_z = 450{,}000$ km; additionally, the phase angles are input as $\phi = 180.0°$ and $\psi = 90.0°$. The resultant Lissajous trajectory, which completes approximately twelve revolutions during its nearly six year course, is illustrated in three planar projections in Figure 1.5. The origin of each projection is the L_1 libration point, and the views are arranged in a manner similar to an orthographic projection. The $\underline{x}$-$\underline{z}$ projection in the lower left corner represents the front view. Above the front view, the $\underline{x}$-$\underline{y}$ projection is seen when looking down the $\underline{z}$-axis onto the orbit from above and is, consequently, the top view. Finally, the projection in the lower right corner is the side view observed by peering along the $\underline{x}$-axis from the Earth toward L_1 and the Sun. The motion of the trajectory in the $\underline{x}$-$\underline{y}$ projection is oriented in a clockwise direction; conversely, in the $\underline{x}$-$\underline{z}$ projection, the trajectory proceeds counterclockwise. Also, the direction of motion in the $\underline{y}$-$\underline{z}$ projection originates counterclockwise but switches midway and concludes in a clockwise procession. For comparison, Figure 1.6 illustrates the same trajectory computed utilizing the third-order approximation with eccentric effects inclusive. Notice that, whereas the input amplitudes

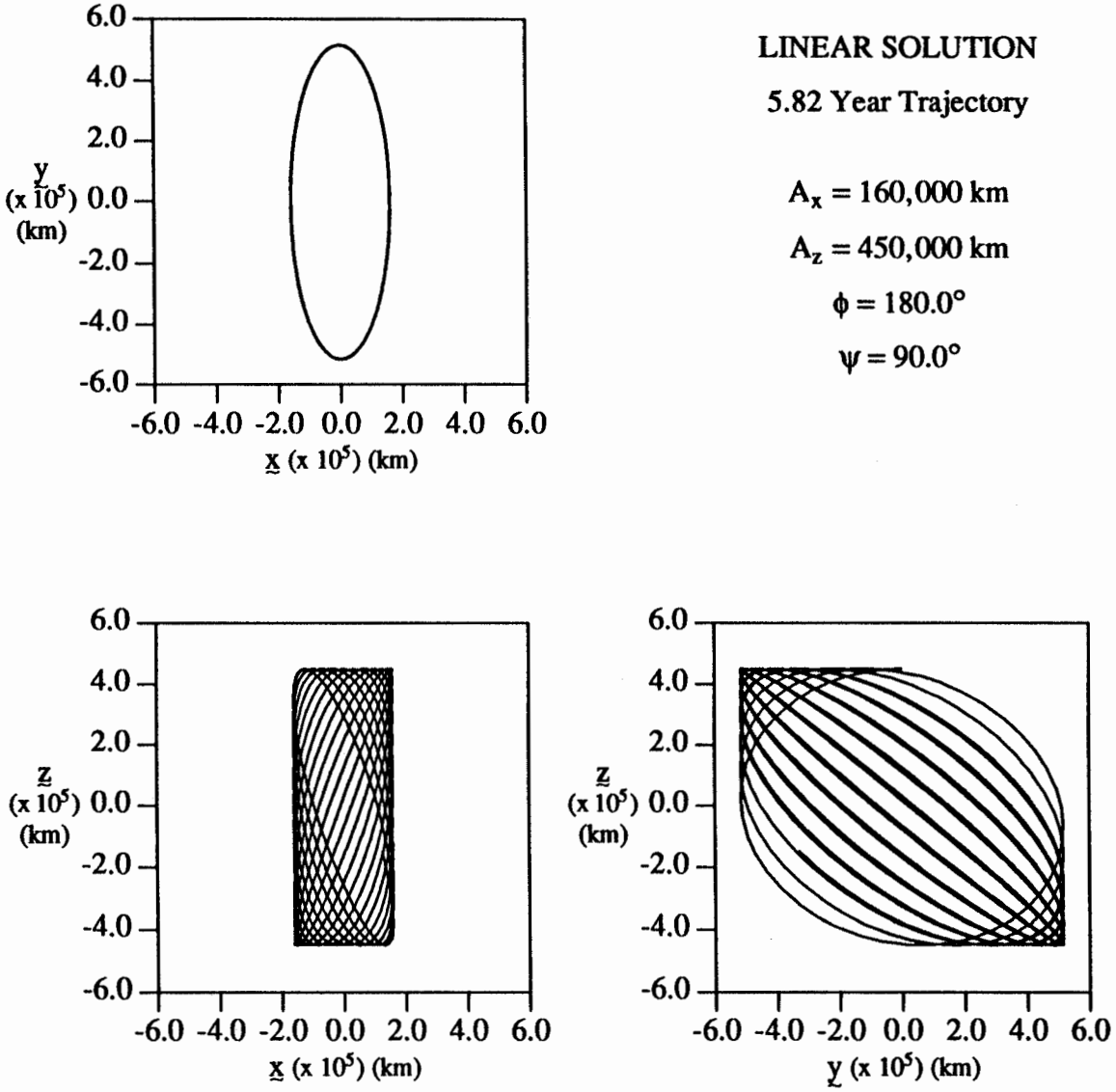

Figure 1.5 Linear Approximation for a Sample Lissajous Trajectory

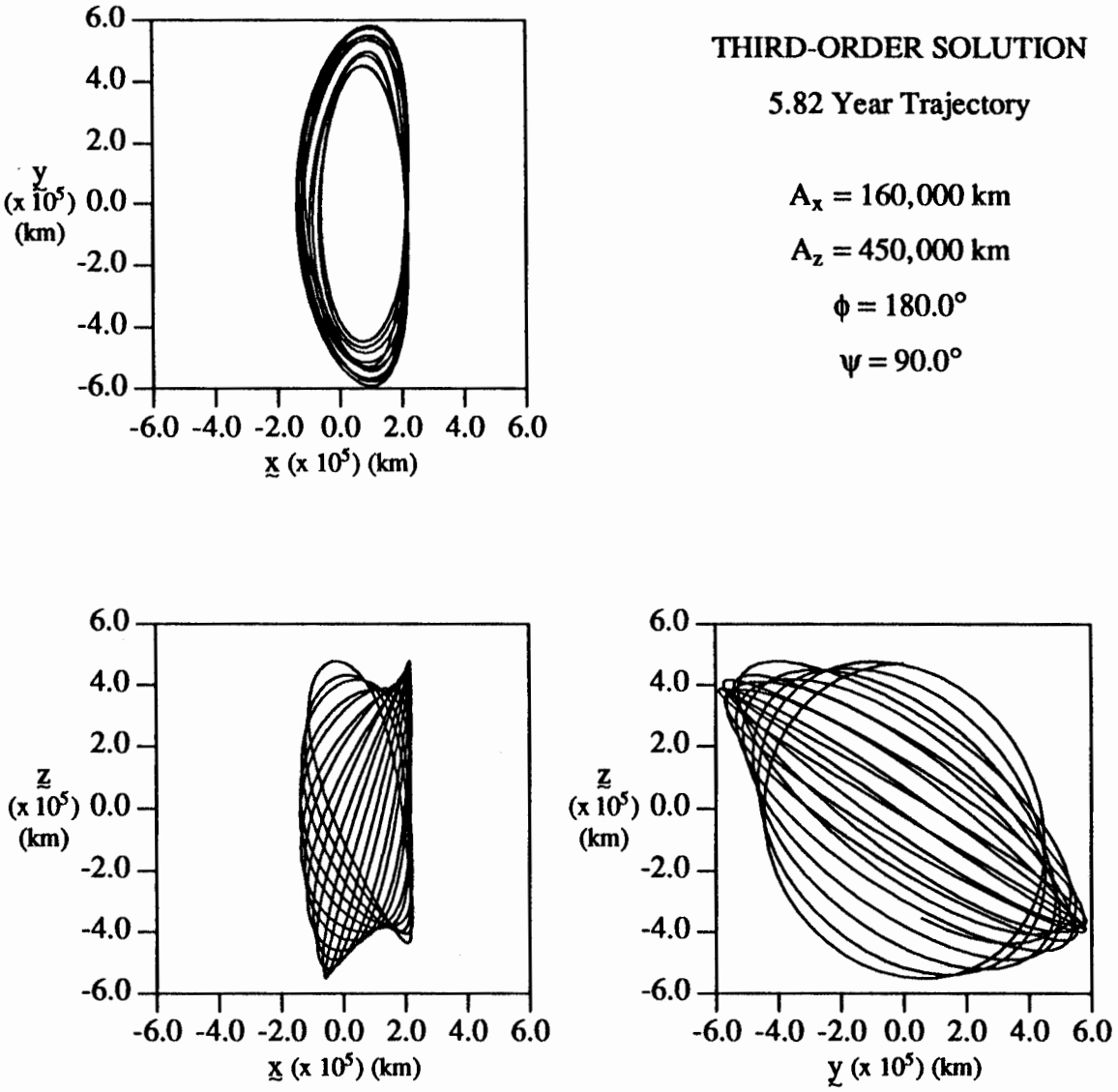

Figure 1.6 Third-Order Analytic Solution for a Sample Lissajous Trajectory

$A_x = 160{,}000$ km and $A_z = 450{,}000$ km provide absolute boundaries on the path in the linear solution, these same inputs supply only rough estimates for the bounds on the path determined from the complete third-order approximation that includes corrections for eccentric primary motion.

Numerical Solutions in the Elliptic Restricted Three-Body Problem

Although providing an excellent starting point, even the third-order approximate analytic solution is inadequate for the computation of Lissajous orbits of multiple revolutions. The unstable nature of Lissajous trajectories, combined with the lack of symmetry conditions for these quasi-periodic solutions, renders lengthy numerical integration difficult. However, one technique developed by Howell and Pernicka[28,29] utilizes a two-level iteration scheme to successfully compute bounded Lissajous trajectories of arbitrary duration assuming circular primary motion in the restricted three-body problem. More recently, Pernicka[30] extends this technique to allow for elliptic primary motion. The first step of this two-level iteration process identifies target points at specified intervals along the trajectory. The third-order analytic approximation provides one means of obtaining an initial estimate for the six-dimensional state (position and velocity) at each target. Trajectory segments between the targets are patched together such that the Lissajous path is continuous in position but contains velocity discontinuities ($\Delta\bar{v}$'s) at the target points. Then, in the second level of the process, the $\Delta\bar{v}$'s are simultaneously reduced by correcting the positions of the targets. When the first level iteration sequence is repeated, the velocity discontinuities are significantly decreased. Both levels of the iteration process employ a differential corrections scheme, and the iteration sequence is repeated until all the $\Delta\bar{v}$'s are diminished to suitably small magnitudes. The resultant path is a numerically integrated Lissajous trajectory continuous in position and velocity. Figure 1.7 illustrates the sample Lissajous trajectory numerically computed utilizing the third-order approximation shown in Figure 1.6 as an initial estimate. Despite the very similar appearances of Figures 1.6 and 1.7, deviations as large as 29,200 km occur at common instants along the trajectories.

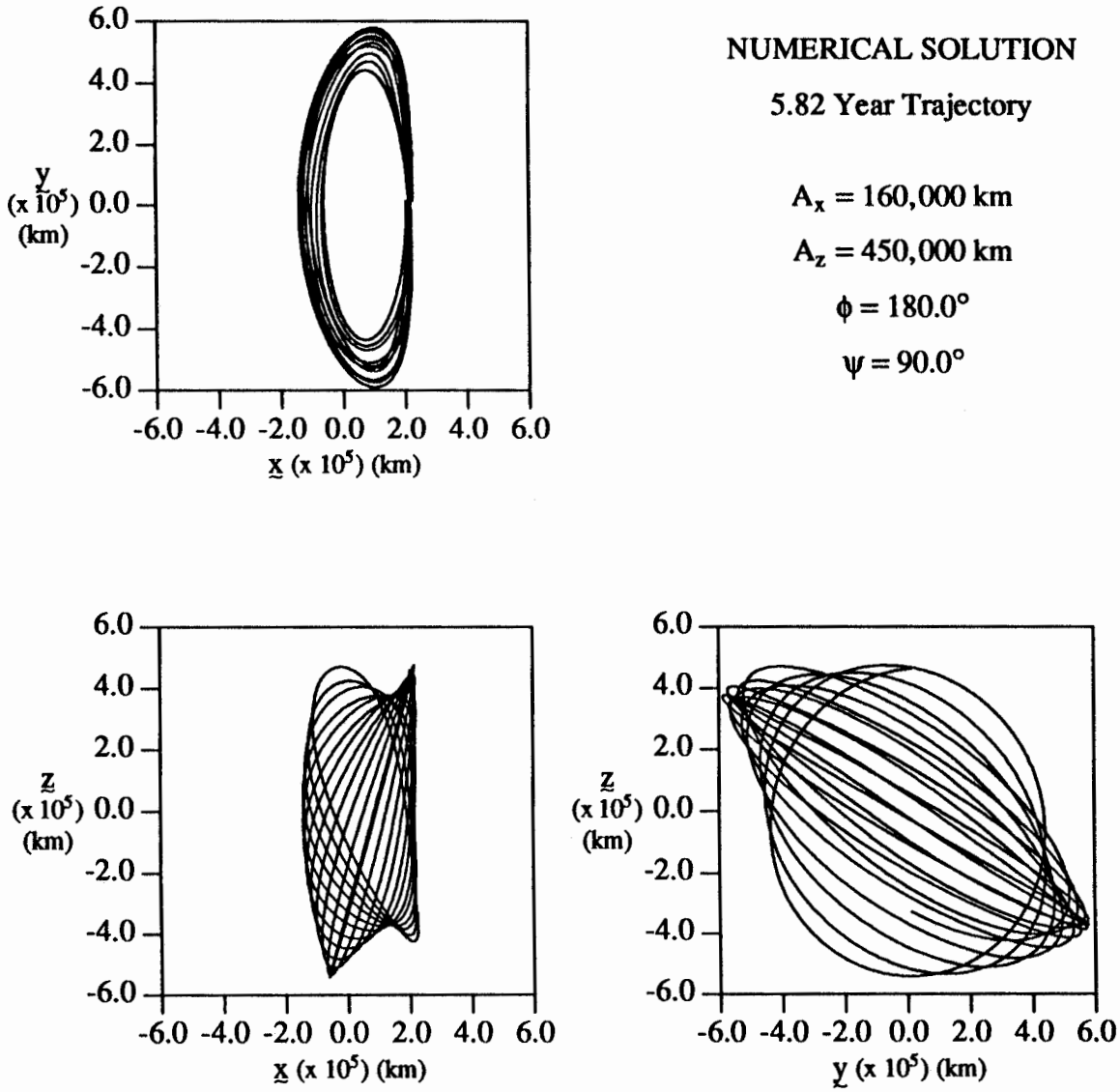

Figure 1.7 Numerically Integrated Solution for a Sample Lissajous Trajectory

CHAPTER II

TRANSFERS BETWEEN LIBRATION-POINT ORBITS

A strategy is presented that outlines the construction of a nominal trajectory which transfers a spacecraft between two specified libration-point orbits. The transfer trajectory that approximately connects the departure and arrival location on the halo orbits is characterized, first, using a linear approximation, then, employing a third-order approximation, and, finally, engaging numerical integration of the exact equations of motion for the infinitesimal mass in the elliptic restricted three-body problem. The resulting nominal trajectory (initial halo, transfer path, final halo) is the reference path whose fuel expenditure is to be diminished. Manual reduction of the nominal fuel consumption effects the divergence of the integrated halo orbits from those originally specified; hence, restoration of the integrity of the halo orbits is undertaken.

Objective of a Nominal Trajectory

The development of a methodology for design of a transfer orbit to move a spacecraft from an initial halo orbit near the L_1 libration point of the Sun-Earth/Moon barycenter system to a second, larger halo orbit is sought. For initial consideration, the spacecraft is assumed to have been originally injected into a halo orbit with a z-amplitude $A_z = 110{,}000$ km. Two $\Delta\bar{v}$ maneuvers, chosen to total approximately 100 m/s, are executed in order to transfer the vehicle to a larger halo orbit with a z-amplitude $A_z = 160{,}000$ km. (These data are consistent with the fuel dumping problem explored in Reference [30].) The transfer of a spacecraft between halo orbits of these prescribed z-amplitudes is designated Case A. For the given z-amplitudes, approximate halo orbits are constructed utilizing Richardson's[18] analytic approximation for periodic orbits about the collinear points. These analytic approximations provide the initial estimates required for the numerical computation of the initial and final halo

orbits in the elliptic restricted three-body problem utilizing the integration technique detailed in Reference [30].

The date of injection into the initial halo orbit at its point of maximum $\underline{z}$-excursion is selected to be August 17. Note that the calendar year for the injection date is not required when assuming elliptic periodic motion for the primaries. Recall that the $\underline{x}$-$\underline{y}$-$\underline{z}$ axes form a rotating coordinate frame with origin located at the oscillating L_1 libration point; then, the $\underline{y}$-$\underline{z}$, $\underline{x}$-$\underline{y}$, and $\underline{x}$-$\underline{z}$ projections of the initial and final halo orbits are illustrated in Figures 2.1-2.3, respectively. Since an analytic approximation lies at the foundation of numerical computation of the libration-point orbits, the resulting integrated halo trajectories are not exactly periodic; rather, they are actually very slowly evolving quasi-periodic Lissajous trajectories. Although these trajectories are not true halo orbits, they render very close approximations and will be defined as halo orbits in this discussion. Also, if total revolutions of the halo orbits were plotted, the orbits would appear to intersect in the $\underline{y}$-$\underline{z}$ projection near the points of minimum and maximum $\underline{y}$-excursion; however, the fact that the final orbit is approximately 5,000 km larger than the initial orbit at these points would not be clear on the scale of Figure 2.1. Departure from the initial halo and arrival at the final halo are arbitrarily chosen to occur near the minimum $\underline{z}$-excursion point of each halo orbit.

The transfer path connecting the departure and arrival states on the halo orbits is actually a portion of a Lissajous trajectory, and a simple approach for determining this transfer is presented in Reference [30]. However, this earlier scheme utilizes a trial-and-error method in order to find a Lissajous path that approximately connects the halo orbits. Amplitudes, phase angles, and times are input into the analytic approximation for Lissajous trajectories (provided in Reference [27]), and these parameters are varied until a path results which nearly passes through the departure and arrival locations. The initial conditions obtained from this approximate, analytic Lissajous transfer are then numerically propagated. This numerical solution for the transfer trajectory, in conjunction with the initial and final halo orbits, yields a continuous orbit containing discrete velocity discontinuities that represent the two $\Delta\bar{v}$ maneuvers necessary to implement the transfer. Simplifying the search for a Lissajous trajectory, that is, identifying a more efficient, systematic approach to determine a transfer path that closely approximates the departure and arrival locations on the halo orbits, is desired; hence, the possibility of the analytic determination of such a Lissajous trajectory is investigated.

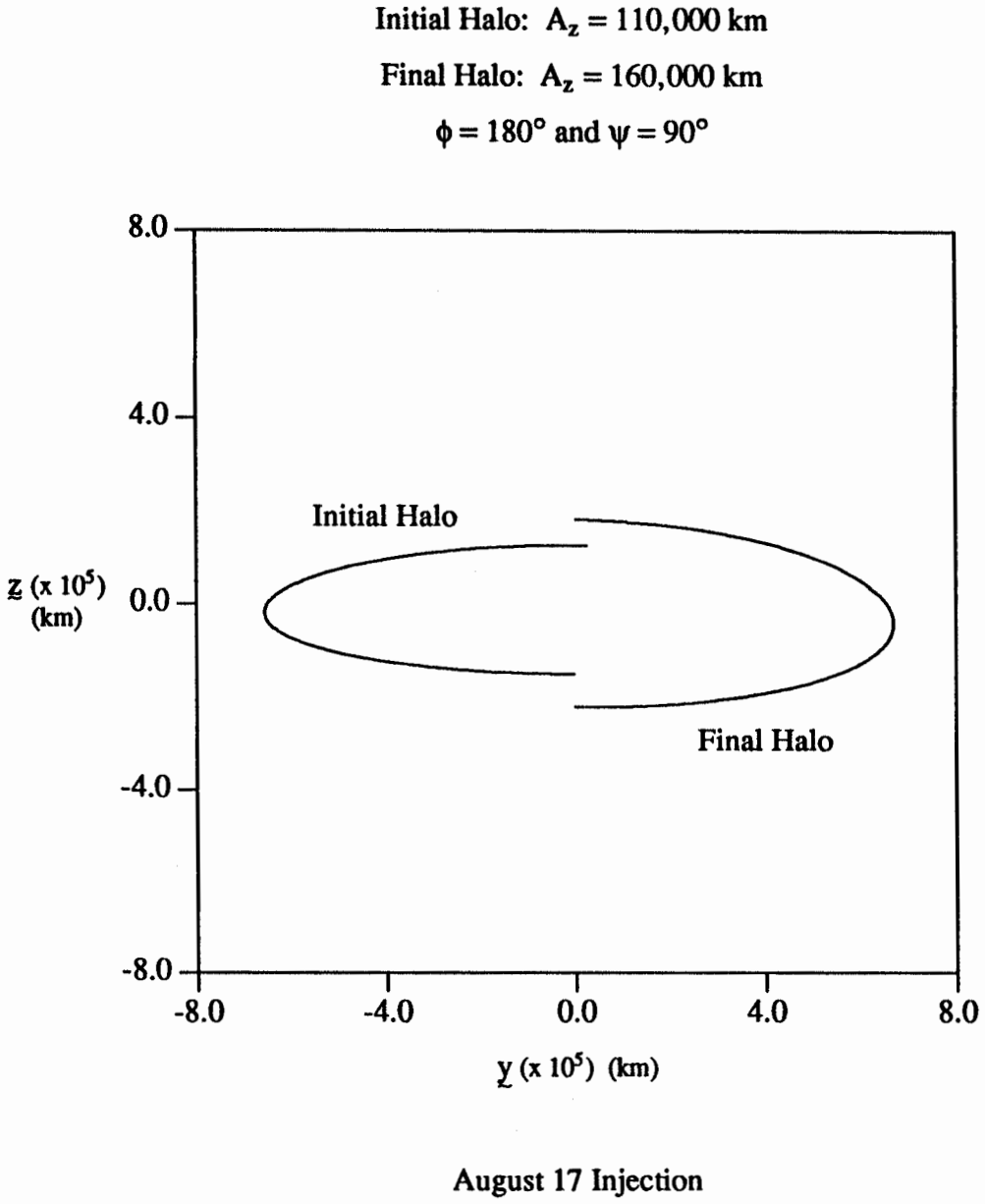

Figure 2.1 y-z Projection of the Initial and Final Halo Orbits (Case A)

Initial Halo: $A_z = 110{,}000$ km

Final Halo: $A_z = 160{,}000$ km

$\phi = 180°$ and $\psi = 90°$

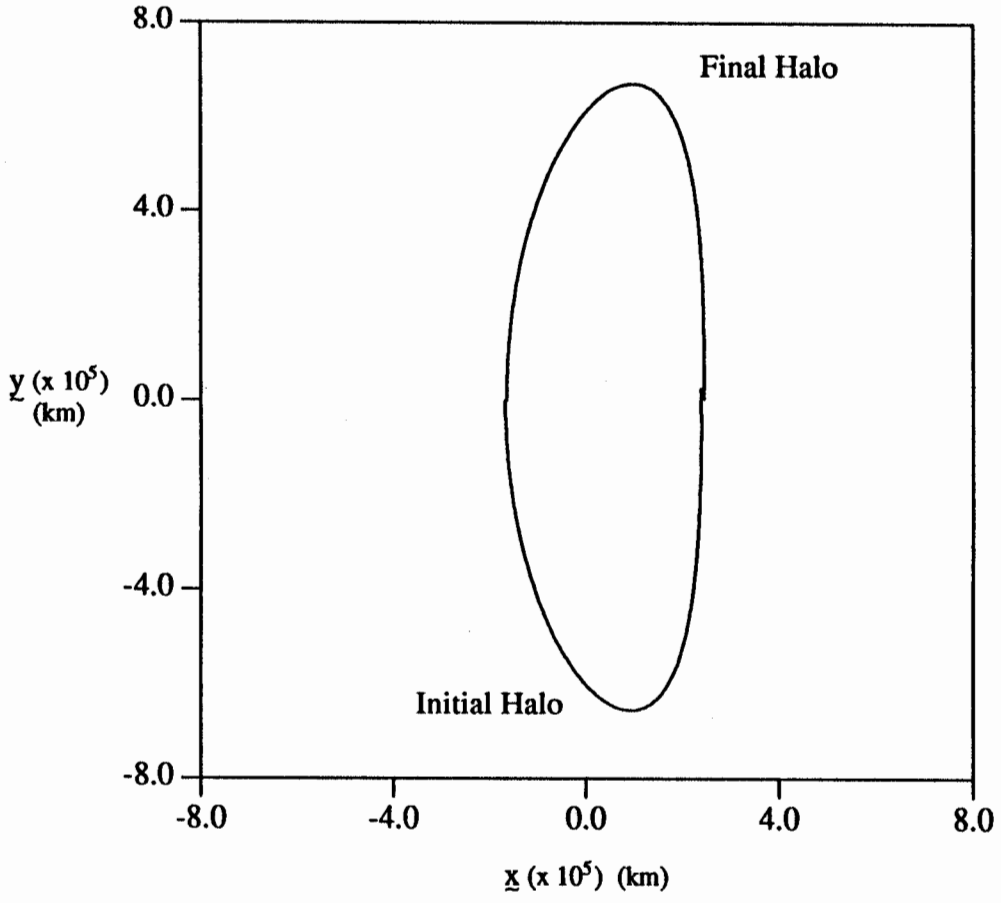

August 17 Injection

Figure 2.2 x-y Projection of the Initial and Final Halo Orbits (Case A)

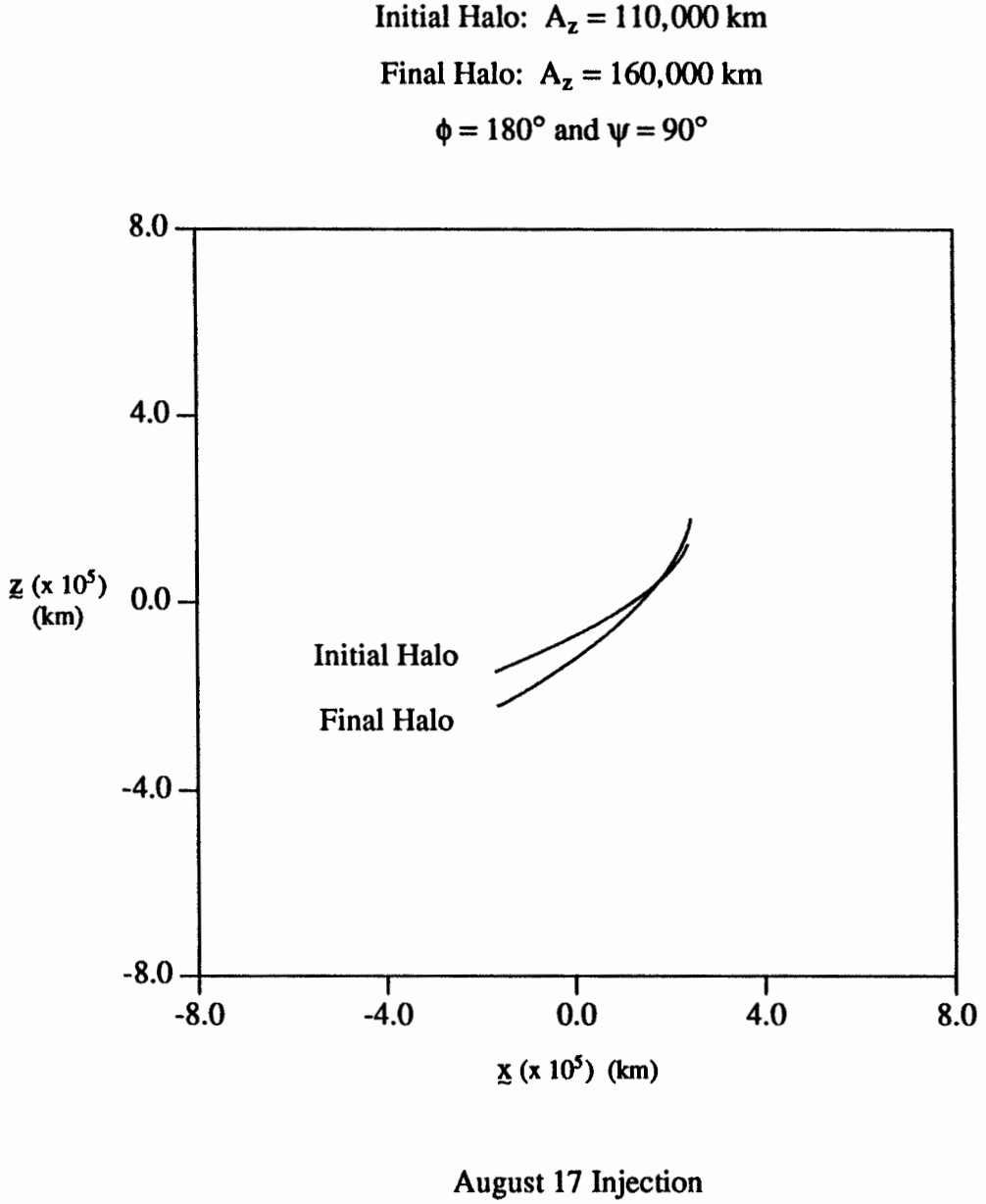

Figure 2.3 x-z Projection of the Initial and Final Halo Orbits

Determination of the Initial Halo Orbit

Numerical determination of a libration-point trajectory requires specification of the parameters that characterize the bounded, oscillatory (linearized) motion. From equations (1.47), these parameters have been identified as A_x and A_z, the in-plane and out-of-plane amplitudes, as well as two phase angles ϕ and ψ. Recall from Chapter 1 that halo orbits, which possess equal in-plane and out-of-plane frequencies (λ and ν), can only be realized by the application of specific amplitude constraints. Thus, choosing the z-amplitude of the initial halo orbit to be $A_z = 110{,}000$ km requires that, in order to obtain a nearly periodic orbit utilizing the third-order analytic approximation developed by Richardson[18], the corresponding y-amplitude is compelled to be $A_y = 664{,}712$ km. In addition, the phase angles

$$\phi = 180^\circ \quad \text{and} \quad \psi = 90^\circ \tag{2.1}$$

are arbitrarily chosen such that the trajectory originates near $y = 0$, with $\underset{\sim}{x}$ and $\underset{\sim}{z}$ near their maximum values. Regardless of the origin of the halo orbit, the phase angles are constrained by the relation[18]

$$\psi = \phi + \frac{n\pi}{2} \; ; \; n = 1, 3 \, . \tag{2.2}$$

The combination of phase angles given in (2.1) renders a halo orbit about L_1 that proceeds in the counterclockwise direction in the $\underset{\sim}{y}$-$\underset{\sim}{z}$ projection and attains its largest $\underset{\sim}{z}$-excursion in the negative $\underset{\sim}{z}$-direction. Consequently, this trajectory belongs to a branch of halo orbits identified as the *southern family*.

Next, the times of initiation and completion of the initial halo orbit must be specified. As the spacecraft moves along its trajectory, let t_s be defined as the time that corresponds to an arbitrary location of the spacecraft relative to the trajectory origin. If t_p is defined as the *time of periapsis passage of the primaries* (*i.e.*, the instant of closest approach of the primaries) relative to the trajectory origin, then the time that has elapsed since the primaries were located at periapsis is

$$\Delta t = t_s - t_p \, . \tag{2.3}$$

So, if the spacecraft is located at the trajectory origin (*i.e.*, $t_s = 0.0$) and if $t_p = 136.5$ days, then $\Delta t = -136.5$ days indicates that the primaries will be at periapsis in 136.5 days. Selecting $t_s = 0.0$ and $t_p = 136.5$ days corresponds to the injection date of August 17. This halo orbit is then numerically integrated for one revolution; however, the minimum $\underset{\sim}{z}$-value occurs after approximately half of a revolution. Recall that departure

from the initial halo orbit is chosen to occur at its minimum $\underline{z}$-excursion which is reached at $t_s = 91.156$ days; thus, the time of periapsis passage corresponding to departure from the initial halo is $\Delta t = (91.156 - 136.5)$ days $= -45.344$ days. If departure from the initial halo is specified as the origin for the transfer trajectory by setting $t_s = 0.0$, then the time of periapsis at departure from the initial halo is given by $t_p = -\Delta t = 45.344$ days. Knowledge of the time of departure from the initial halo renders the corresponding position coordinates as the departure location.

Estimation of the Final Halo Orbit

The choice of a z-amplitude $A_z = 160{,}000$ km for the final halo orbit requires a y-amplitude $A_y = 666{,}677$ km such that a periodic path is produced from the third-order analytic approximation. Also, for convenience, the phase angles are unaltered from those for the initial halo orbit specified in (2.1). Since the time of flight (TOF) on the transfer path is unknown, however, the time of periapsis passage corresponding to injection into the final halo is uncertain. The transfer trajectory is assumed to be a one-rev portion of a Lissajous orbit. Thus, the period of the initial halo, approximated as 180 days, is presumed to proffer an estimate for the time of flight on the transfer. Consequently, upon arrival at the final halo, the time that has elapsed since the primaries were located at periapsis is given by $\Delta t = (180.0 - 45.344)$ days $= 134.656$ days. Again defining the origin of the final halo orbit by setting $t_s = 0.0$, the time of periapsis upon arrival at the final halo is approximated by $t_p = -\Delta t = -134.656$ days. However, integration of the final halo orbit begins with $\underline{z}$ near its maximum value, not at the point of minimum $\underline{z}$-excursion; thus, the final halo must be integrated for one revolution in order to determine the *delay time* $\Delta t_d = 88.722$ days (*i.e.*, one half of the period of the final halo) necessary to reach the minimum $\underline{z}$-value. Then, this delay time is added to the time of periapsis passage corresponding to arrival at the final halo. Beginning integration of the final halo again and utilizing the new time of periapsis $t_p = -45.934$ days, the minimum $\underline{z}$-excursion on the final halo is reached at the estimated $t_p = -134.656$ days, and the location of arrival at the final halo is determined.

For an estimated transfer time of flight of 180 days, the times of periapsis corresponding to integration commencement and orbit commencement and the delay period (if applicable) for each halo orbit are shown in Table 2.1. Also, Table 2.1 illustrates the effect of the uncertainty of the transfer time of flight on the time of periapsis

Table 2.1 Timing Conditions for an Estimated TOF on the Lissajous Transfer Trajectory

Path	Begin Integration t_{p_i} (days)	Delay Period Δt_d (days)	Begin Orbit t_{p_b} (days)	TOF Δt (days)	End Orbit t_{p_f} (days)
Initial Halo	136.5	0.0	136.5	91.156	45.344
Lissajous			45.344	**180.0**	-134.656
Final Halo	-45.934	88.722	-134.656		

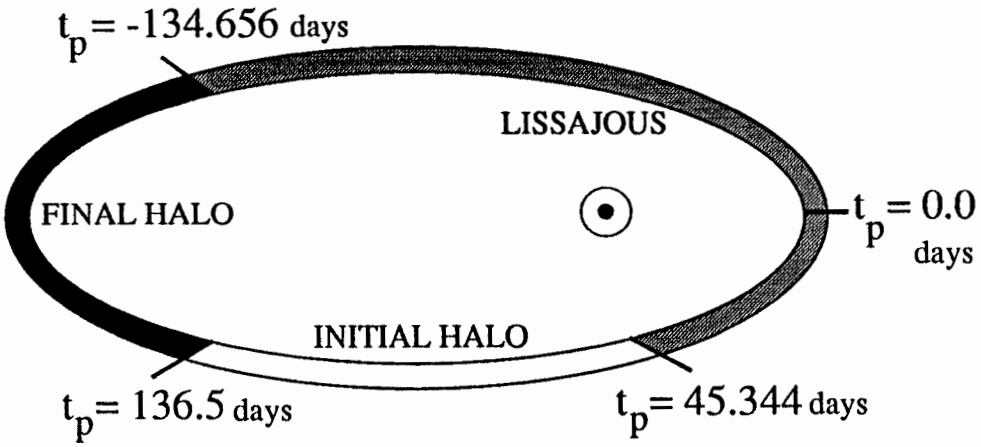

Figure 2.4 Earth/Moon Barycenter Motion for an Estimated TOF on the Lissajous Transfer Trajectory

passage corresponding to injection into the final halo orbit. Additionally, Figure 2.4 depicts the counterclockwise, elliptical motion of the Earth/Moon barycenter about the Sun which is located at a focus of the ellipse. The barycenter is originally located at the $t_p = 136.5$ station and proceeds to the $t_p = 45.344$ station. During this interval, which corresponds to the white segment of the ellipse in Figure 2.4, the spacecraft completes one half of a revolution on the initial halo orbit. Then, as the barycenter passes through periapsis (*i.e.*, $t_p = 0.0$) and moves along the shaded portion of the ellipse to the $t_p = -134.656$ station, the spacecraft executes the transfer between the halo orbits. Finally, the black segment of the barycenter's elliptical path corresponds to the motion of the spacecraft on the final halo orbit.

Determination of an Approximate Lissajous Transfer

With the times and locations of the departure from the initial halo and arrival at the final halo orbit specified, an analytic scheme for determining a Lissajous orbit which will connect these states is developed. Although the time spent on the transfer was previously estimated at 180 days in order to gain an initial approximation for the final halo orbit, this time of flight (despite being influenced by this estimate) is not specified *a priori* in the following development.

Linear Approximation

Given the position coordinates of departure from the initial halo orbit (x_1, y_1, z_1) and the estimated coordinates of arrival at the final halo (x_2, y_2, z_2), the six characteristic parameters $(A_x, A_z, \phi, \psi, t_1, t_2)$ of the Lissajous transfer, which connects these two points, are sought. Use of the linear approximation (1.47) for the motion along the Lissajous orbit, with specified times corresponding to the departure and arrival locations, results in coordinates expressed as

$$\left.\begin{aligned} x_1 &= -A_x\cos(\lambda t_1 + \phi) \\ y_1 &= kA_x\sin(\lambda t_1 + \phi) \\ z_1 &= A_z\sin(\nu t_1 + \psi) \end{aligned}\right\} \text{Departure from Initial Halo} \qquad \begin{aligned} &(2.4) \\ &(2.5) \\ &(2.6) \end{aligned}$$

and

$$\left.\begin{aligned} x_2 &= -A_x\cos(\lambda t_2 + \phi) \\ y_2 &= kA_x\sin(\lambda t_2 + \phi) \\ z_2 &= A_z\sin(\nu t_2 + \psi) \end{aligned}\right\} \text{Arrival at Final Halo}, \qquad \begin{aligned} &(2.7)\\ &(2.8)\\ &(2.9)\end{aligned}$$

where the linearized frequencies, λ and ν, and the proportionality constant, k, are determined from equations (1.48), (1.49), and (1.50), respectively. The six parameters, characteristic of a Lissajous transfer connecting departure and arrival locations, can be obtained from equations (2.4) $\rightarrow$ (2.9).

Combining equations (2.4) and (2.5) and combining equations (2.7) and (2.8), the characteristic x-amplitude is determined from

$$A_x^2 = \frac{y_1^2}{k^2} + x_1^2 , \tag{2.10a}$$

or

$$A_x^2 = \frac{y_2^2}{k^2} + x_2^2 . \tag{2.10b}$$

Expanding the sinusoidal functions in equations (2.4) and (2.5) yields

$$-\frac{x_1}{A_x} = \cos(\lambda t_1 + \phi) = \cos\lambda t_1\cos\phi - \sin\lambda t_1\sin\phi ,$$

and

$$\frac{y_1}{kA_x} = \sin(\lambda t_1 + \phi) = \sin\lambda t_1\cos\phi + \cos\lambda t_1\sin\phi .$$

Forming the ratio

$$-\frac{kx_1}{y_1} = \frac{\cos\phi - \sin\phi\tan\lambda t_1}{\cos\phi\tan\lambda t_1 + \sin\phi} ,$$

and solving for $\tan\lambda t_1$,

$$\tan\lambda t_1 = \frac{y_1 + kx_1\tan\phi}{y_1\tan\phi - kx_1} . \tag{2.11}$$

Similarly, from equations (2.4) and (2.5),

$$\tan\lambda t_2 = \frac{y_2 + kx_2\tan\phi}{y_2\tan\phi - kx_2} . \tag{2.12}$$

So, the times on the Lissajous trajectory corresponding to the instant of departure from

the initial halo orbit and the instant of arrival at the final halo orbit are specified, respectively, as

$$t_1 = \frac{1}{\lambda}\tan^{-1}\left[\frac{y_1 + kx_1\tan\phi}{y_1\tan\phi - kx_1}\right], \tag{2.13}$$

and

$$t_2 = \frac{1}{\lambda}\tan^{-1}\left[\frac{y_2 + kx_2\tan\phi}{y_2\tan\phi - kx_2}\right]. \tag{2.14}$$

Note that the inverse tangent function is double-valued; consequently, the solutions of (2.13) and (2.14) are simply chosen such t_1 and t_2 are positive. Substituting equations (2.11) and (2.12) into the trigonometric identity

$$\tan(\alpha + \beta) = \frac{\tan\alpha - \tan\beta}{1 + \tan\alpha\tan\beta}$$

yields

$$\tan(\lambda t_2 - \lambda t_1) = \frac{\dfrac{y_2 + kx_2\tan\phi}{y_2\tan\phi - kx_2} - \dfrac{y_1 + kx_1\tan\phi}{y_1\tan\phi - kx_1}}{1 + \left[\dfrac{y_2 + kx_2\tan\phi}{y_2\tan\phi - kx_2}\right]\left[\dfrac{y_1 + kx_1\tan\phi}{y_1\tan\phi - kx_1}\right]}.$$

Simplifying the right-hand side,

$$\tan\lambda(t_2 - t_1) = \frac{k(y_1x_2 - x_1y_2)}{y_1y_2 + k^2x_1x_2}.$$

Hence, the time of flight (*i.e.*, TOF $= t_2 - t_1$) on the transfer trajectory is computed as

$$t_2 - t_1 = \frac{1}{\lambda}\tan^{-1}\left[\frac{k(y_1x_2 - x_1y_2)}{y_1y_2 + k^2x_1x_2}\right].$$

Note that the time of flight is specified provided that the initial and final positions are known; however, the arrival position on the final halo is determined using an estimated time of flight. Thus, solution for the arrival position and the time of flight must be obtained iteratively, but two or three iterations are generally sufficient for convergence.

The phase angle, ψ, is determined by expanding the sinusoidal functions in equations (2.6) and (2.9) as follows:

$$z_1 = A_z \sin(\nu t_1 + \psi) = A_z(\sin\nu t_1 \cos\psi + \cos\nu t_1 \sin\psi)$$

$$z_2 = A_z \sin(\nu t_2 + \psi) = A_z(\sin\nu t_2 \cos\psi + \cos\nu t_2 \sin\psi) .$$

Forming the ratio

$$\frac{z_1}{z_2} = \frac{\sin\nu t_1 + \cos\nu t_1 \tan\psi}{\sin\nu t_2 + \cos\nu t_2 \tan\psi} ,$$

and solving for $\tan\psi$, the phase angle may be written as

$$\psi = \tan^{-1}\left[\frac{z_2 \sin\nu t_1 - z_1 \sin\nu t_2}{z_1 \cos\nu t_2 - z_2 \cos\nu t_1}\right] . \tag{2.15}$$

Once again, the solution of (2.15) is double-valued; hence, ψ is selected to be that angle which yields a positive value for the z-amplitude, A_z, which is found from either equation (2.6) or (2.9) to be

$$A_z = \frac{z_1}{\sin(\nu t_1 + \psi)} , \tag{2.16a}$$

or

$$A_z = \frac{z_2}{\sin(\nu t_2 + \psi)} . \tag{2.16b}$$

So, for a chosen phase angle ϕ, the other five parameters (A_x, A_z, ψ, t_1, t_2) that characterize the Lissajous are determined from equations (2.10), (2.16), (2.15), (2.13), and (2.14), respectively. Of importance to note, however, is that this system of equations for the characteristic parameters is over constrained due to the disparity between amplitudes computed from departure conditions and those computed from arrival conditions. That is, equations (2.10a) and (2.10b) will, in general, yield dissimilar values for A_x; analogously, a discrepancy in A_z calculated from equations (2.16a) and (2.16b) will exist. To overcome this difficulty, results from (2.10a,b) and (2.16a,b) are simply averaged to obtain the linear estimates for the x-amplitude and z-amplitude, respectively.

Third-Order Approximation

Next, the six characteristic parameters, arrived at via a linear analysis, become the inputs into the third-order analytic approximation. The six parameters must then be

modified to reflect the more accurate third-order model, and this modification or variation is accomplished with use of a sensitivity matrix. Let $\bar{w} = [x_1, y_1, z_1, x_2, y_2, z_2]^T$ be a 6x1 state vector containing the coordinates of the departure and arrival locations, and let $\bar{p} = [A_y, A_z, \phi, \psi, t_1, t_2]^T$ be a 6x1 vector containing the characteristic parameters on the transfer trajectory. (Note that the y-amplitude parameter is defined as $A_y \triangleq kA_x$.) If δ denotes a variation in a quantity at a specific instant, then the variations in the state and parameter vectors are given as

$$\delta\bar{w} = (\delta x_1, \delta y_1, \delta z_1, \delta x_2, \delta y_2, \delta z_2)^T = \bar{w} - \bar{w}_{guess}$$

$$\delta\bar{p} = (\delta A_y, \delta A_z, \delta\phi, \delta\psi, \delta t_1, \delta t_2)^T = \bar{p} - \bar{p}_{guess} ,$$

where $\bar{p}_{guess}$ and $\bar{w}_{guess}$ are the input and output, respectively, of the third-order approximation. The linear variation in the states can be expressed as

$$\delta\bar{x} = \frac{\partial\bar{w}}{\partial A_y}\delta A_y + \frac{\partial\bar{w}}{\partial A_z}\delta A_z + \frac{\partial\bar{w}}{\partial\phi}\delta\phi + \frac{\partial\bar{w}}{\partial\psi}\delta\psi + \frac{\partial\bar{w}}{\partial t_1}\delta t_1 + \frac{\partial\bar{w}}{\partial t_2}\delta t_2 .$$

Noting that $\frac{\partial w_i}{\partial t_2} = 0$ (i = 1, 2, 3) and $\frac{\partial w_i}{\partial t_1} = 0$ (i = 4, 5, 6), then the linear variational equations can be written in matrix notation as

$$\delta\bar{w} = S\,\delta\bar{p} , \tag{2.17}$$

where

$$S = \begin{bmatrix} \frac{\partial x_1}{\partial A_y} & \frac{\partial x_1}{\partial A_z} & \frac{\partial x_1}{\partial\phi} & \frac{\partial x_1}{\partial\psi} & \frac{\partial x_1}{\partial t_1} & 0 \\ \frac{\partial y_1}{\partial A_y} & \frac{\partial y_1}{\partial A_z} & \frac{\partial y_1}{\partial\phi} & \frac{\partial y_1}{\partial\psi} & \frac{\partial y_1}{\partial t_1} & 0 \\ \frac{\partial z_1}{\partial A_y} & \frac{\partial z_1}{\partial A_z} & \frac{\partial z_1}{\partial\phi} & \frac{\partial z_1}{\partial\psi} & \frac{\partial z_1}{\partial t_1} & 0 \\ \frac{\partial x_2}{\partial A_y} & \frac{\partial x_2}{\partial A_z} & \frac{\partial x_2}{\partial\phi} & \frac{\partial x_2}{\partial\psi} & 0 & \frac{\partial x_2}{\partial t_2} \\ \frac{\partial y_2}{\partial A_y} & \frac{\partial y_2}{\partial A_z} & \frac{\partial y_2}{\partial\phi} & \frac{\partial y_2}{\partial\psi} & 0 & \frac{\partial y_2}{\partial t_2} \\ \frac{\partial z_2}{\partial A_y} & \frac{\partial z_2}{\partial A_z} & \frac{\partial z_2}{\partial\phi} & \frac{\partial z_2}{\partial\psi} & 0 & \frac{\partial z_2}{\partial t_2} \end{bmatrix} .$$

Each component of the sensitivity matrix, S, is easily computed numerically by varying

one parameter at a time in the third-order approximation and recording the subsequent change in the initial and final states. Provided that the sensitivity matrix is non-singular, equation (2.17) can be rewritten to express the linear variation in the characteristic parameters as

$$\delta\bar{p} = S^{-1}\,\delta\bar{w}\,.$$

Ideally, the variations in the six characteristic parameters are calculated until the approximation to the state vector is within a small tolerance of the desired departure and arrival coordinates. However, in reality, convergence to the desired endpoints is rarely achieved. A Lissajous trajectory between two specified endpoints may simply not exist; however, a good approximation for the transfer trajectory is sufficient to proceed with numerical integration.

The above procedure renders an analytic path that essentially connects an initial halo orbit with $A_z = 110{,}000$ km to a final halo orbit with $A_z = 160{,}000$ km. One such Lissajous path is determined to have the following characteristics:

$$\begin{array}{lll} A_y = 665{,}392.7 \text{ km} & \phi = 158.6^\circ & t_1 = 101.0 \text{ days} \\ A_z = 373{,}971.6 \text{ km} & \psi = 142.2^\circ & t_2 = 281.8 \text{ days} \end{array}$$

These parameters then *define* the Lissajous transfer trajectory. For this analytically approximated Lissajous transfer, the times of periapsis passage at integration commencement, orbit commencement, and orbit termination for the initial halo, Lissajous transfer trajectory, and final halo are shown in Table 2.2. The delay periods, representing the amounts of time spent on those portions of the integrated paths which are discarded, are provided for the transfer trajectory and the final orbit. Additionally, Figure 2.5 illustrates the motion of the Earth/Moon barycenter during each segment of the spacecraft's motion given the approximated time of flight on the Lissajous trajectory.

Numerical Integration of the Lissajous Transfer and the Complete Nominal Trajectory

With estimates for the six characteristic parameters of the Lissajous trajectory determined, the transfer can be integrated in the elliptic restricted three-body model utilizing the scheme presented in Reference [30]. Recall that convergence to the specified points is not actually achieved. The endpoints of the transfer are manually chosen as those points for which the z-position coordinate most closely matches that of the departure and arrival locations on the halo orbits; also, the times corresponding to

Table 2.2 Timing Conditions for an Analytically Approximated TOF on the Lissajous Transfer Trajectory

Path	Begin Integration t_{p_i} (days)	Delay Period Δt_d (days)	Begin Orbit t_{p_b} (days)	TOF Δt (days)	End Orbit t_{p_f} (days)
Initial Halo	136.5	0.0	136.5	91.156	45.344
Lissajous	146.344	101.0	45.344	**180.8**	-135.456
Final Halo	-46.734	88.722	-135.456		

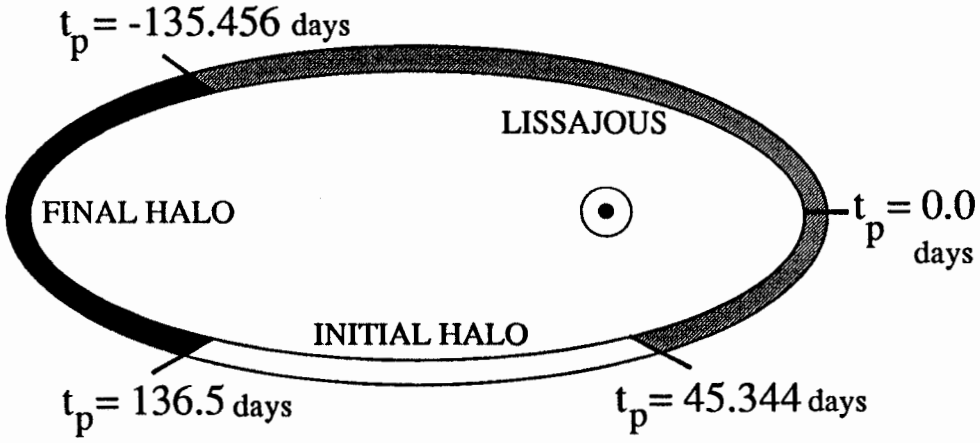

Figure 2.5 Earth/Moon Barycenter Motion for an Analytically Approximated TOF on the Lissajous Transfer Trajectory

these endpoints result in a new, integrated time of flight, TOF = 175.981 days. Since the time necessary to complete the integrated transfer changes substantially from that analytically approximated, the final halo must be re-integrated. Table 2.3 and Figure 2.6 illustrate that integration of the final halo should originate at $t_p = -41.915$ days (instead of at the approximated $t_p = -46.734$ days) in order for the termination of the Lissajous transfer to coincide with the commencement of the final halo orbit.

Once the discrepancies in the times of periapsis at the departure and arrival locations have been minimized, the integrated Lissajous transfer may be patched between the two halo orbits. However, since the endpoints of the Lissajous transfer do not exactly match the corresponding departure and arrival locations on the halo orbits, the terminal target states on the transfer are chosen to be those of the halo orbits while the interior target states on the transfer are specified by the Lissajous trajectory. The resulting complete *nominal* trajectory (initial halo, transfer path, final halo) is continuous in position but contains two velocity discontinuities at the patch points, and the differences in velocity at these points represent the $\Delta\bar{v}$'s necessary to implement the transfer. The magnitudes of these maneuvers are $|\Delta\bar{v}_1| = 99.6378$ m/s and $|\Delta\bar{v}_2| = 98.8208$ m/s. The $\underset{\sim}{y}$-$\underset{\sim}{z}$, $\underset{\sim}{x}$-$\underset{\sim}{y}$, and $\underset{\sim}{x}$-$\underset{\sim}{z}$ projections of this orbit are shown in Figures 2.7-2.9.

Manual Reduction of the $|\Delta\bar{v}|$ Expenditure

Originally, a transfer that could be accomplished with a $|\Delta\bar{v}|$ expenditure of approximately 100 m/s was sought; however, the transfer illustrated in Figures 2.7-2.9 possesses a $|\Delta\bar{v}|$ expenditure of nearly twice that allowed. So, each component of the $\Delta\bar{v}$'s is incrementally reduced manually until $|\Delta\bar{v}_1| = 51.0$ m/s and $|\Delta\bar{v}_2| = 45.3$ m/s. These $\Delta\bar{v}$ maneuvers are chosen to correspond to those determined in Reference [30] using a trial-and-error method. In the process of reducing the $|\Delta\bar{v}|$'s, however, the initial and final halo orbits begin to deviate from the halo orbits originally specified.

Fine-Tuning the Halo Orbits

Once the $|\Delta\bar{v}|$'s are reduced in order to comply with the predetermined (albeit arbitrary) restriction on $|\Delta\bar{v}|$ expenditure of approximately 100 m/s, the initial and final

Table 2.3 Timing Conditions for an Integrated TOF on the Lissajous Transfer Trajectory

Path	Begin Integration t_{p_i} (days)	Delay Period Δt_d (days)	Begin Orbit t_{p_b} (days)	TOF Δt (days)	End Orbit t_{p_f} (days)
Initial Halo	136.5	0.0	136.5	91.156	45.344
Lissajous	148.744	103.442	45.344	**175.981**	-130.637
Final Halo	-41.915	88.722	-130.637		

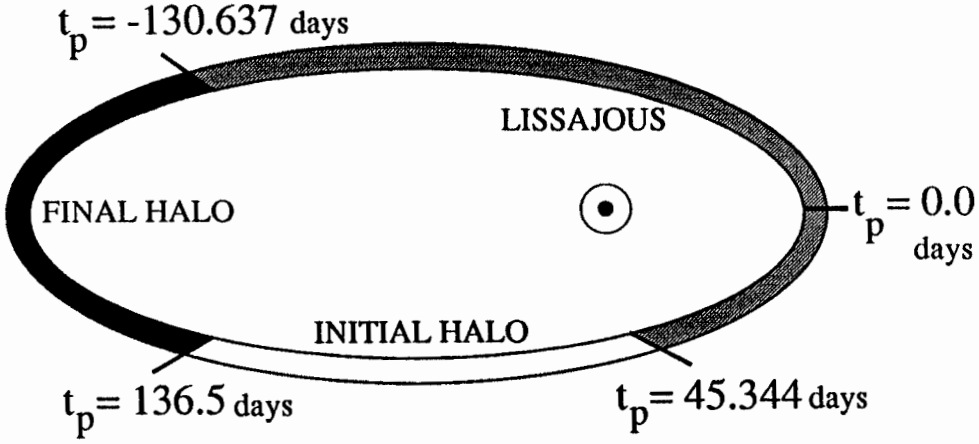

Figure 2.6 Earth/Moon Barycenter Motion for an Integrated TOF on the Lissajous Transfer Trajectory

Initial Halo: $A_z = 110{,}000$ km

Final Halo: $A_z = 160{,}000$ km

Transfer TOF = 175.98 days

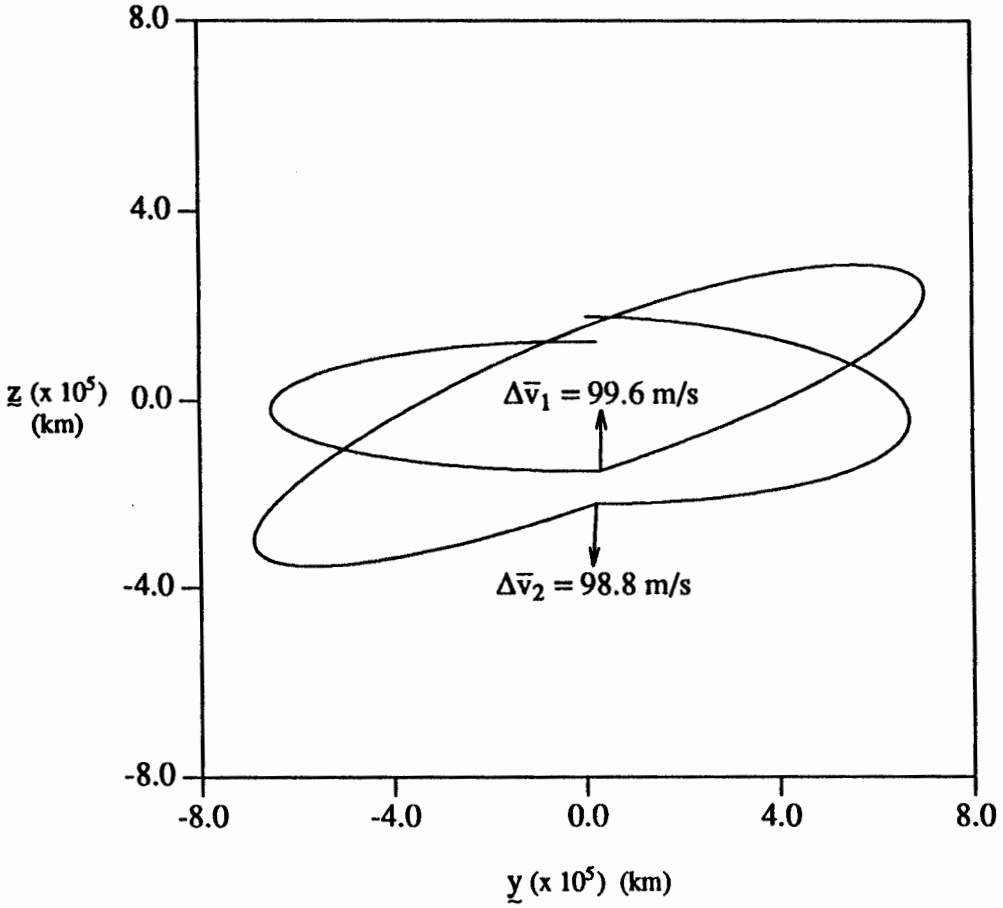

2–Impulse $\Delta\bar{v}$ Expenditure = 198.4 m/s

Figure 2.7 y-z Projection of the Two-Impulse Nominal Trajectory (Case A)

Initial Halo: A_z = 110,000 km

Final Halo: A_z = 160,000 km

Transfer TOF = 175.98 days

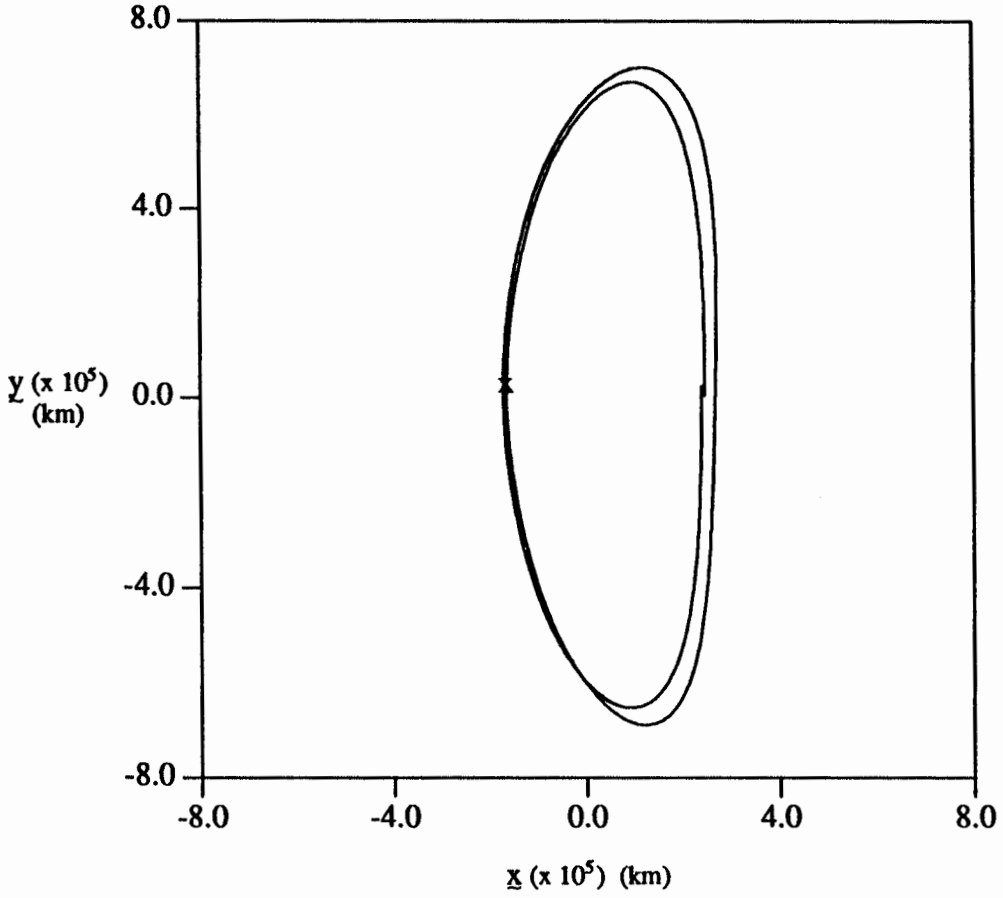

2–Impulse $\Delta\bar{v}$ Expenditure = 198.4 m/s

Figure 2.8 x-y Projection of the Two-Impulse Nominal Trajectory (Case A)

Initial Halo: $A_z = 110{,}000$ km

Final Halo: $A_z = 160{,}000$ km

Transfer TOF = 175.98 days

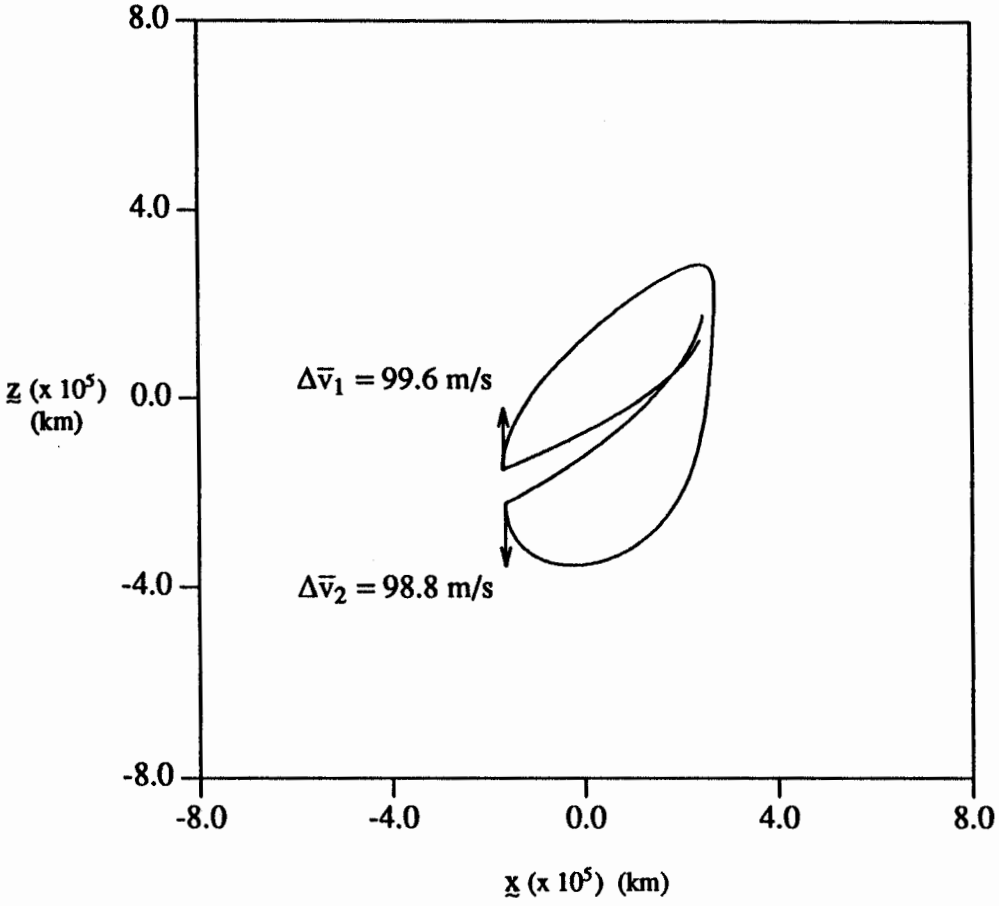

2–Impulse $\Delta\bar{v}$ Expenditure = 198.4 m/s

Figure 2.9 $\underline{x}$-$\underline{z}$ Projection of the Two-Impulse Nominal Trajectory (Case A)

sections of the trajectory then deviate from the initially specified halo orbits. Of course, this result is not surprising since no constraints are placed upon these sections during the convergence process. Hence, alternate ways of producing a complete path are sought in which the integrity of the initial and final halo orbits is preserved without expending more fuel. The following three methods are explored: (1) including additional revolutions of the halo orbits prior to and subsequent to the transfer trajectory; (2) implementing a weighted least squares algorithm in the numerical determination process of the nominal trajectory; and (3) constraining the endpoints of the halo orbits.

First, including additional revolutions of both the initial and final halo orbits is considered. Instead of completing only half of a revolution on the initial halo before transferring onto the Lissajous orbit, $2\frac{1}{2}$ revolutions are completed. Similarly, $2\frac{1}{2}$ revolutions on the final halo are executed as well. By demanding that more time be spent on the halo orbits, but maintaining the one-rev transfer, better convergence of the integrated trajectory to the desired halos is expected. However, by constraining the magnitudes of the $\Delta\bar{v}$ maneuvers to remain the same (*i.e.*, $|\Delta\bar{v}_1| = 51.0$ m/s and $|\Delta\bar{v}_2| = 45.3$ m/s), any potential advantage associated with additional revolutions on the halos is apparently lost. This method does not significantly enhance convergence to the prescribed halo orbits.

Implementation of a weighted least squares method is explored as another means of matching the desired halo orbits. The numerical integration technique developed in Reference [30] utilizes a least squares approach when reducing the velocity discontinuities at the target points along the trajectory, in order to solve the system of equations represented in the form

$$-\Delta\bar{v} = M\,\delta\bar{r}\,,$$

where M is of dimension (3n−3)x(3n+3); $\Delta\bar{v}$ is a column vector containing the 3n−3 velocity discontinuities at the target points; $\delta\bar{r}$ is a column vector of length 3n+3 containing the corrections to the target positions; and n is the number of trajectory segments (*e.g.*, n = 2 or 4 per orbit revolution). A symmetric weighting matrix, Q, which is of dimension (3n+3)x(3n+3), can be chosen such that the target points on the initial and final halo orbits are weighted heavily while the target points on the transfer are allowed more freedom. Such a weighted least squares approach results in the following solution for the corrections to the target positions:

$$\delta\bar{r} = -Q^{-1}M^T\left[MQ^{-1}M^T\right]^{-1}\Delta\bar{v}\,.$$

Denoting Q_1, Q_2, and Q_3 as the scalar weights associated with the initial halo orbit (the first section of the complete trajectory), the transfer trajectory (the second section), and the final halo orbit (the third section), respectively, then a diagonal weighting matrix can be represented as

$$Q = \begin{bmatrix} Q_1 I & 0 & 0 \\ 0 & Q_2 I & 0 \\ 0 & 0 & Q_3 I \end{bmatrix},$$

where I represents an identity matrix of appropriate dimension. Constraining $Q_2 = 1$ and specifying $Q_1 = Q_3 = 100$ results in complete, integrated trajectories with halo orbit sections that more closely approximate the specified halos. The change in the target positions is on the order of 1,000 km closer to the target positions on the desired halo orbits. When the weights on the halos are increased such that $Q_1 = Q_3 = 1000$, again, the integrated halo sections move closer to the desired halos; however, the average change in the target positions decreases substantially. Hence for $Q_1 = Q_3 > 1000$, no significant gains are expected, nor are they achieved.

Finally, constraining the endpoints of the halo orbits is examined. Since the number of columns of M exceeds the number of rows of M by six, six more unknowns than equations exist; thus, a maximum of six constraints may be imposed. Recalling that n is the number of trajectory segments, the change in position vector may be written as

$$\delta\bar{r} = [\delta\bar{r}_0, \delta\bar{r}_1, \cdots, \delta\bar{r}_n]^T .$$

To begin, three constraints which fix the first point of the initial halo are imposed by choosing $\delta\bar{r}_0 = [\delta x_0, \delta y_0, \delta z_0]^T = [0, 0, 0]^T$. The integrated trajectory demonstrates very good correlation to the initial halo orbit; however, the final halo diverges. Then, in addition to fixing the first point of the initial halo, three more constraints are implemented in order to fix the last point of the final halo. By also specifying that $\delta\bar{r}_n = [\delta x_n, \delta y_n, \delta z_n]^T = [0, 0, 0]^T$, both endpoints of the trajectory are constrained to specified values. The resultant, integrated trajectory illustrates very poor correlation to the desired halo orbits. Although the endpoints of the halos match, all other target points on the halo orbits diverge greatly. Applying all six constraints, in effect, removes all degrees of freedom from the system, and any hope of approximating the other target points on the halos is lost; hence, the poor correspondence of the integrated trajectory is not surprising.

Acceptable Reference Trajectory

Since both the weighted least squares approach and the initial halo endpoint constraint method result in good approximations for the desired halo orbits, these two methods are implemented simultaneously. The first point of the initial halo is fixed, but, in order to allow the system some flexibility, the last point of the final halo is unconstrained. Additionally, the weights $Q_1 = Q_3 = 1000$ and $Q_2 = 1$ are chosen so that the transfer trajectory is allowed great freedom while the sections involving the halo orbits are heavily weighted such that their deviations from the desired halo orbits are lessened. The resultant trajectory, illustrated in Figures 2.10-2.12 in the $\underline{y}$-$\underline{z}$, $\underline{x}$-$\underline{y}$, and $\underline{x}$-$\underline{z}$ projections, demonstrates excellent correlation with the initial halo although the final halo section of the integrated trajectory exhibits some deviation in the $\underline{z}$-direction. This trajectory is the two-impulse reduced-fuel-expenditure path that renders the best approximation available to date for the desired two-impulse transfer, given the initial and final halo orbits and a fixed time of flight.

Initial Halo: $A_z = 110{,}000$ km

Final Halo: $A_z = 160{,}000$ km

Transfer TOF = 175.98 days

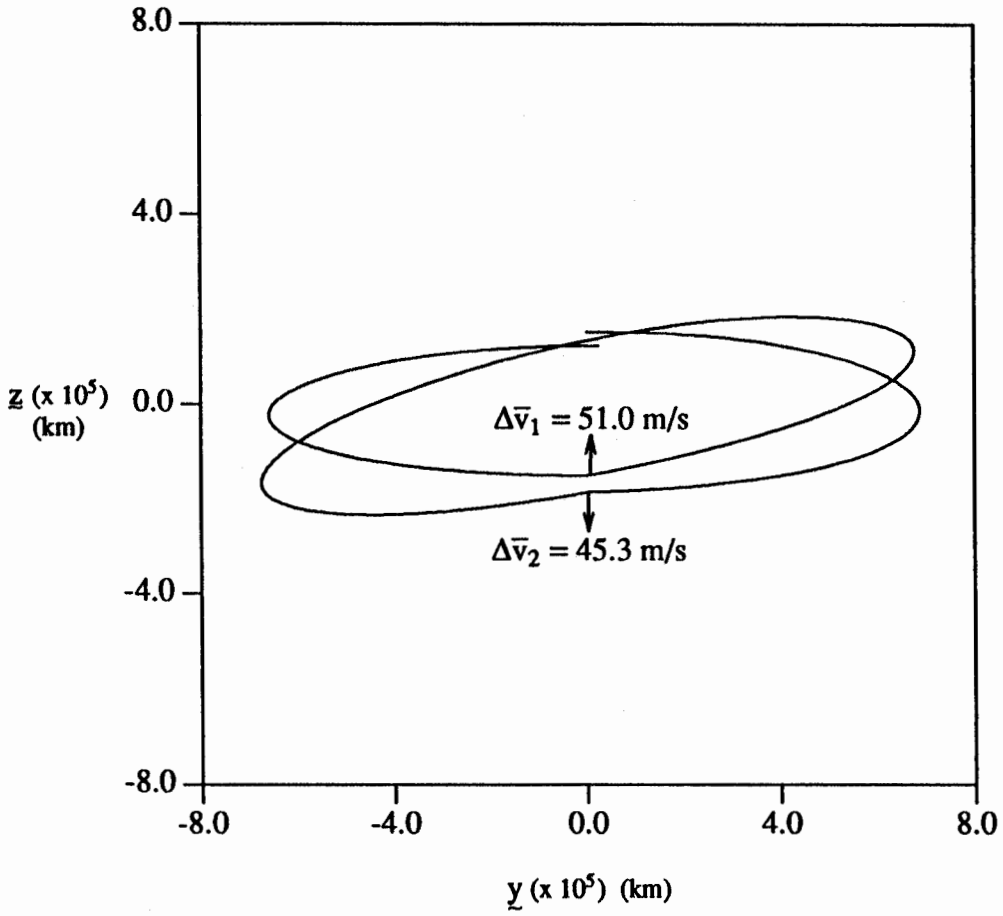

2–Impulse $\Delta\bar{v}$ Expenditure = 96.3 m/s

Figure 2.10 y-z Projection of the Reduced $\Delta\bar{v}$ Trajectory (Case A)

Initial Halo: A_z = 110,000 km

Final Halo: A_z = 160,000 km

Transfer TOF = 175.98 days

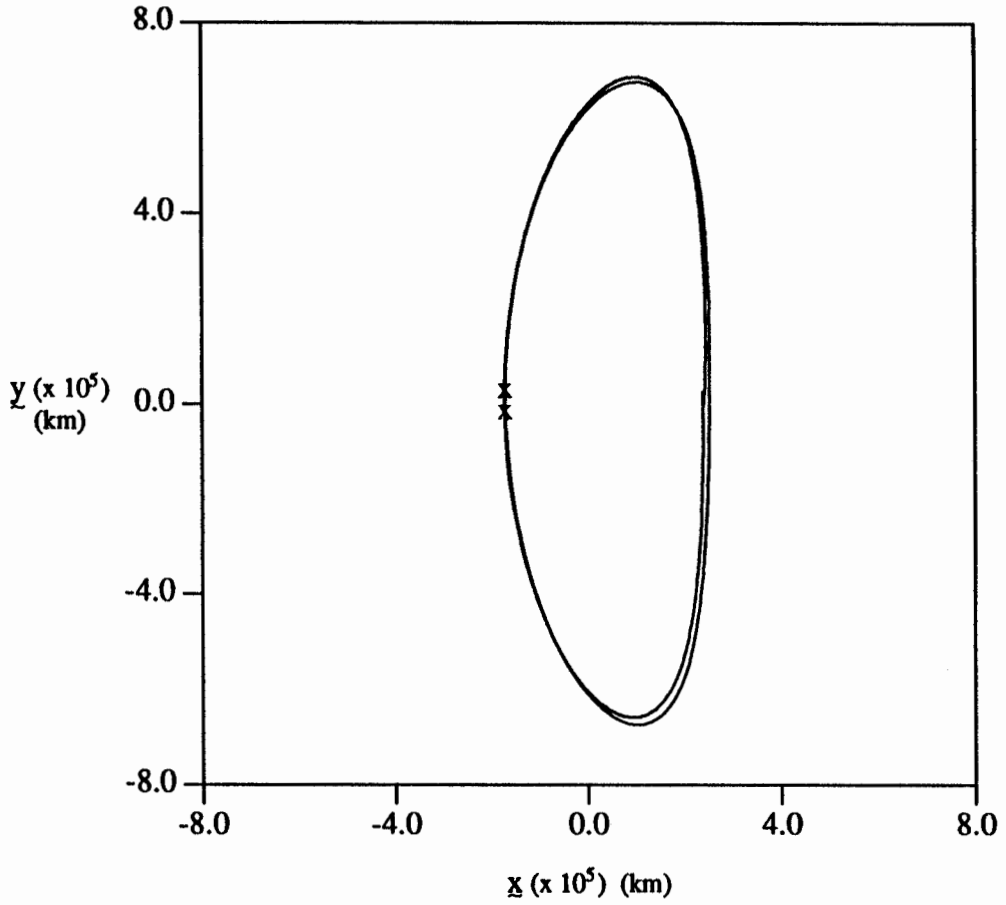

2–Impulse $\Delta\bar{v}$ Expenditure = 96.3 m/s

Figure 2.11 $\underset{\sim}{x}$-$\underset{\sim}{y}$ Projection of the Reduced $\Delta\bar{v}$ Trajectory (Case A)

Initial Halo: $A_z = 110{,}000$ km

Final Halo: $A_z = 160{,}000$ km

Transfer TOF = 175.98 days

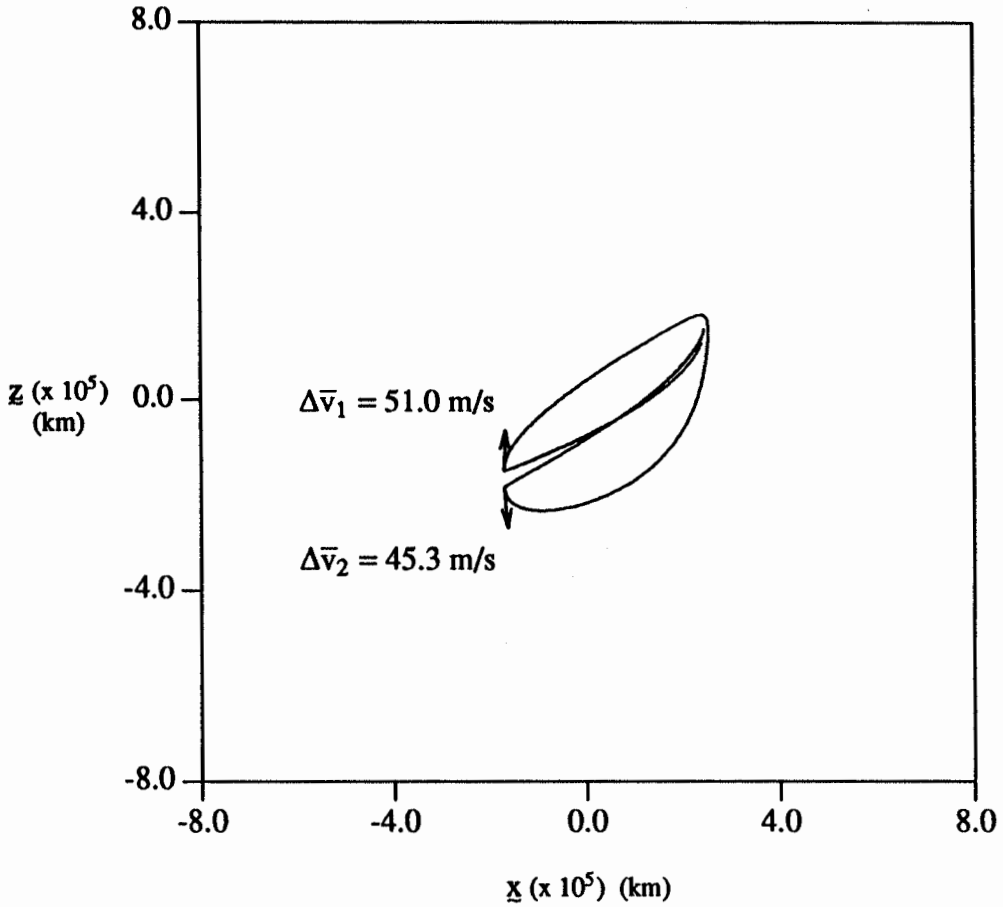

2–Impulse $\Delta\bar{v}$ Expenditure = 96.3 m/s

Figure 2.12 $\underset{\sim}{x}$-$\underset{\sim}{z}$ Projection of the Reduced $\Delta\bar{v}$ Trajectory (Case A)

CHAPTER III

THEORY OF OPTIMAL TRAJECTORIES

Since a transfer accomplished with the greatest economy of fuel is always desirable, a strategy to design optimal transfers efficiently is sought. The problem of optimizing a time-fixed transfer with specified terminal positions and velocities is formulated as a problem of Mayer in the calculus of variations. Three extremal arcs are identified and the thrust magnitude switching function over each arc is specified. Henceforth, impulsive thrusts are assumed, and the necessary conditions for an optimal impulsive trajectory in the elliptic three-body problem are derived. Additionally, a variational expression that relates a reference and a perturbed trajectory is formulated relative to a rotating coordinate system. The subsequent development for the elliptic restricted three-body problem parallels Lawden's[52] treatment of optimal transfers in the two-body problem.

State and Constraint Equations

Let the vectors $\bar{x} = [x, y, z]^T$ and $\bar{v} = [v_x, v_y, v_z]^T$ represent a spacecraft's position relative to the barycenter and inertial velocity, respectively, expressed in rotating coordinates [See Figure 1.1]. Then, the equations of motion (1.21) can be written in first-order form as

$$\dot{\bar{x}} = \bar{v} \tag{3.1a}$$

$$\dot{\bar{v}} = \frac{T}{m}\hat{u}_T + \bar{g}\,, \tag{3.1b}$$

and the conservation of mass can be expressed as

$$\dot{m} = -\frac{T}{c}\,, \tag{3.2}$$

where T is the thrust magnitude, $\hat{u}_T$ is a unit vector in the thrust direction, m is the spacecraft's time-varying mass, c is the effective exhaust velocity, and $\bar{g}$ is given by

$$\bar{g} = \begin{bmatrix} 2nv_y + \dot{n}y + U_x \\ -2nv_x - \dot{n}x + U_y \\ U_z \end{bmatrix}. \tag{3.3}$$

In the formulation of optimal transfers associated with the two-body problem, $\bar{g}$, expressed in inertial coordinates, is simply the gravitational acceleration. However, since a spacecraft's motion in the elliptic restricted three-body problem is more conveniently expressed in terms of rotating coordinates, equation (3.3) contains terms due to the relative motion of the rotating frame with respect to the inertial frame. So, in the elliptic problem, $\bar{g}$, which is expressed in terms of rotating coordinates and which denotes the spacecraft's inertial acceleration when the rocket motors are not operating, will be designated the *coastal acceleration*. Recall that n is the angular velocity associated with the primary motion; also, the quantities U_x, U_y, and U_z are the first partial derivatives of the pseudo-potential U, defined in equation (1.20), with respect to the subscripted position coordinate.

The magnitude of the velocity increment caused by an expenditure of propellant is termed the *characteristic velocity*. Since a two-impulse transfer path is to be optimized such that a minimum amount of fuel is expended, the characteristic velocity can be taken as a measure of the cost of executing the transfer. Hence, the optimization objective becomes the minimization of the cost function J, taken to be the characteristic velocity and expressed as

$$J = c \ln\left[\frac{m_0}{m_f}\right], \tag{3.4}$$

where m_0 and m_f are the initial and final spacecraft mass, respectively.

The rate of propellant expenditure $\dot{m}$ is originally assumed to be limited, so, if $\tilde{T}$ denotes the maximum thrust magnitude allowable (*i.e.*, $\tilde{T} = -c\dot{m}_{max}$), the control function T is subject to the inequality constraints

$$0 \le T \le \tilde{T}. \tag{3.5}$$

In order to transform the constraints (3.5) into equality constraints, a technique promulgated by Valentine[74] is utilized. Another control variable q is introduced such that T

is required to satisfy

$$T(\tilde{T} - T) - q^2 = 0 . \tag{3.6}$$

Since $q^2 \geq 0$, equation (3.6) is equivalent to inequalities (3.5). Also, the thrust direction, specified by $\hat{u}_T$, is constrained to have unit magnitude; hence,

$$|\hat{u}_T| = 1 . \tag{3.7}$$

Thus, state equations (3.1) and (3.2) describe the behavior of the states $[\bar{x}, \bar{v}, m]$ subject to the controls $[\hat{u}_T, T, q]$ where the magnitude and direction of the thrust are further constrained by equations (3.6) and (3.7), respectively.

In order to treat the state equations as differential constraints, Lagrange multipliers, called adjoint variables, are introduced. Define the adjoint vector as $\bar{\lambda}^T \triangleq \left[\bar{\lambda}_x^T, \bar{\lambda}_v^T, \lambda_m\right]$. The vectors $\bar{\lambda}_x$ and $\bar{\lambda}_v$ and the scalar λ_m are the adjoints to the spacecraft's position, velocity, and mass, respectively. Then, the Hamiltonian H can be formulated by the summation of each adjoint variable multiplied by the right-hand side of the corresponding state equation. So, the Hamiltonian takes the form

$$H = \bar{\lambda}_x^T \bar{v} + \bar{\lambda}_v^T \left[\frac{T}{m}\hat{u}_T + \bar{g}\right] - \lambda_m \frac{T}{c} ; \tag{3.8}$$

also, the differential equations for the adjoints, obtained by taking the negative of the partial derivative of the Hamiltonian with respect to the states, are given by

$$\dot{\bar{\lambda}}_x^T = -\frac{\partial H}{\partial \bar{x}} = -\bar{\lambda}_v^T G_x \tag{3.9a}$$

$$\dot{\bar{\lambda}}_v^T = -\frac{\partial H}{\partial \bar{v}} = -\bar{\lambda}_x^T - \bar{\lambda}_v^T G_v \tag{3.9b}$$

$$\dot{\lambda}_m = -\frac{\partial H}{\partial m} = \frac{T}{m^2}\bar{\lambda}_v^T \hat{u}_T . \tag{3.9c}$$

The matrices G_x and G_v are defined by

$$G_x \triangleq \frac{\partial \bar{g}}{\partial \bar{x}} = \Upsilon + \dot{n}\Omega \tag{3.10a}$$

$$G_v \triangleq \frac{\partial \bar{g}}{\partial \bar{v}} = 2n\Omega , \tag{3.10b}$$

and Ω is defined by equation (1.34), and the components of Υ appear in equations (1.36).

Additionally, the Lagrange multipliers σ_1 and σ_2 are introduced in conjunction with the thrust constraints (3.6) and (3.7), respectively. Then, the *Lagrange expression* F, which is defined by the subtraction of the Hamiltonian from the sum of the products of each σ with the corresponding control constraint, can be formulated as

$$F = \sigma_1 \left[T\left(\tilde{T} - T\right) - q^2 \right] + \sigma_2 \left[|\hat{u}_T|^2 - 1 \right] - H . \tag{3.11}$$

where the requirement that $\hat{u}_T$ have unit magnitude is equivalently rewritten to constrain the square of the magnitude to equal one. Expressing $|\hat{u}_T|^2$ as $\hat{u}_T^T \hat{u}_T$ and substituting equation (3.8) into (3.11),

$$\begin{aligned} F = \; & \sigma_1 \left[T\left(\tilde{T} - T\right) - q^2 \right] + \sigma_2 \left[\hat{u}_T^T \hat{u}_T - 1 \right] \\ & - \bar{\lambda}_x^T \bar{v} - \bar{\lambda}_v^T \left(\frac{T}{m} \hat{u}_T + \bar{g} \right) + \lambda_m \frac{T}{c} . \end{aligned} \tag{3.12}$$

The additional requirement, that the first partial derivatives of F with respect to the controls vanish, must be enforced. Taking the partial derivatives of (3.12) with respect to the controls $\hat{u}_T$, T, and q yields

$$\frac{\partial F}{\partial \hat{u}_T} = 0 = 2\sigma_2 \hat{u}_T - \frac{T}{m} \bar{\lambda}_v \tag{3.13a}$$

$$\frac{\partial F}{\partial T} = 0 = \sigma_1 \left(\tilde{T} - 2T \right) - \frac{1}{m} \bar{\lambda}_v^T \hat{u}_T + \frac{1}{c} \lambda_m \tag{3.13b}$$

$$\frac{\partial F}{\partial q} = 0 = -2\sigma_1 q . \tag{3.13c}$$

Equations (3.9) coupled with (3.13) form the set of necessary conditions which the states, controls, and Lagrange multipliers ($\bar{\lambda}_x$, $\bar{\lambda}_v$, λ_m, σ_1, and σ_2) must satisfy such that the cost function assumes a stationary value.[52]

Extremal Arcs

Solutions for the states and controls that satisfy equations (3.9) and (3.13) are termed *extremals*, for these solutions render the cost function an extremum (or stationary value).[75] Notice that equation (3.13c) requires that either σ_1, q, or both should

vanish. If $q = 0$, then, in accordance with equation (3.6), either $T = 0$ or $T = \tilde{T}$. If $\sigma_1 = 0$, the thrust magnitude may assume intermediate values. Thus, the optimal trajectory may be comprised of the following three types of arcs:

i) Null Thrust Arcs (NT-arcs),
ii) Intermediate Thrust Arcs (IT-arcs),
iii) Maximum Thrust Arcs (MT-arcs).

Provided that σ_2 and T are both non-zero, equation (3.13a) indicates that $\hat{u}_T$ and $\bar{\lambda}_v$ must be parallel. Let the adjoint vector to the velocity be termed the *primer vector* and, hereafter, be denoted by $\bar{p}$ (*i.e.*, $\bar{p} = \bar{\lambda}_v$). Then, the thrust direction is always parallel to the primer. [The re-assignment of the components of the velocity adjoint to the moniker primer vector is not an arbitrary (whimsical) decision; rather, as will become evident in the subsequent development, this distinctive vector plays a significant role in facilitating the understanding of optimal trajectories.] If $T = 0$, the motor is not operating, and the components of $\hat{u}_T$ are indeterminate; additionally, if $\sigma_2 = 0$, the primer vanishes.

Pontryagin's Maximum Principle states that the Hamiltonian should be maximized over the choice of control variables in order to minimize the cost function.[75] Therefore, the necessary condition that H assumes its maximum value at every point on the optimal trajectory can be expressed as

$$H^* \geq H, \tag{3.14}$$

where H^* denotes the Hamiltonian on the optimal path. If a state vector is defined such that $\bar{s}^T \triangleq [\bar{x}^T, \bar{v}^T, m]$, then, utilizing (3.8), equation (3.14) can be written as[52]

$$\bar{\lambda}^{*T} \dot{\bar{s}}^* \geq \bar{\lambda}^{*T} \dot{\bar{s}}, \tag{3.15}$$

where $\bar{\lambda}^*$ and $\dot{\bar{s}}^*$ refer to the minimal cost trajectory, and $\dot{\bar{s}}$ is any set of state derivatives obtained from substituting the optimal values of the states $\bar{s}^*$ and any set of controls consistent with the constraints (3.6) and (3.7) into state equations (3.1) and (3.2). Equation (3.15) is known as the *Weierstrass necessary condition*. Substituting (3.1) and (3.2) into (3.15), utilizing the definition of the primer, and simplifying,

$$\left[\frac{1}{m}\bar{p}^{*T}\hat{u}_T^* - \frac{1}{c}\lambda_m^*\right]T^* \geq \left[\frac{1}{m}\bar{p}^{*T}\hat{u}_T - \frac{1}{c}\lambda_m^*\right]T, \tag{3.16}$$

where superscript * denotes the value that a quantity assumes on the minimal cost

trajectory. Hence, at every point on the optimal trajectory, condition (3.16) must be valid for all possible values of $\hat{u}_T$ and T satisfying constraints (3.6) and (3.7).

Over an NT-arc, $T^* = 0$, and inequality (3.16) reduces to

$$\frac{1}{c}\lambda_m^* \geq \frac{1}{m}\bar{p}^{*T}\hat{u}_T . \tag{3.17}$$

Imposing the greatest restriction on the above necessary condition, the upper bound on the right side of (3.17) is sought. The maximum value of the quantity $\bar{p}^{*T}\hat{u}_T$ is obtained when $\hat{u}_T$ is aligned with the primer vector; consequently, this maximum value is just the magnitude of the primer. Hence, the Weierstrass necessary condition on an NT-arc simplifies to

$$\lambda_m^* \geq \frac{cp^*}{m} , \tag{3.18}$$

where p^* denotes the magnitude of the primer vector.

Over an MT-arc, $T^* = \tilde{T}$, and inequality (3.16) becomes

$$\left[\frac{1}{m}\bar{p}^{*T}\hat{u}_T^* - \frac{1}{c}\lambda_m^*\right]\tilde{T} \geq \left[\frac{1}{m}\bar{p}^{*T}\hat{u}_T - \frac{1}{c}\lambda_m^*\right]T . \tag{3.19}$$

Taking $T = \tilde{T}$ in order to maximize the right side of (3.19) requires that

$$\bar{p}^{*T}\hat{u}_T^* \geq \bar{p}^{*T}\hat{u}_T . \tag{3.20}$$

Additionally, if $\hat{u}_T = \hat{u}_T^*$ is taken to determine an upper bound on the right side of (3.19), then

$$\left[\frac{1}{m}\bar{p}^{*T}\hat{u}_T^* - \frac{1}{c}\lambda_m^*\right]\tilde{T} \geq \left[\frac{1}{m}\bar{p}^{*T}\hat{u}_T^* - \frac{1}{c}\lambda_m^*\right]T ; \tag{3.21}$$

moreover, since $T \leq \tilde{T}$, the quantity in parentheses in (3.21) must be positive in order for this necessary condition to be satisfied; thus,

$$\lambda_m^* \leq \frac{c}{m}\bar{p}^{*T}\hat{u}_T^* . \tag{3.22}$$

Conditions (3.20) and (3.22) are sufficient to ensure the validity of necessary condition (3.16). Equation (3.20) will be satisfied for all $\hat{u}_T$ if and only if $\bar{p}^{*T}\hat{u}_T^*$ assumes its maximum value; hence, in agreement with the earlier result for the NT-arc, $\bar{p}^*$ and $\hat{u}_T^*$ must be aligned. Utilizing the result that the primer and thrust directions are parallel reduces equation (3.22) to

$$\lambda_m^* \le \frac{cp^*}{m} . \tag{3.23}$$

Over an IT-arc, T can assume values either greater or less than the optimal thrust magnitude $\tilde{T}$. Taking $\hat{u}_T = \hat{u}_T^*$ in condition (3.16) makes clear that the inequality

$$\left[\frac{1}{m}\bar{p}^{*T}\hat{u}_T^* - \frac{1}{c}\lambda_m^*\right]T^* \ge \left[\frac{1}{m}\bar{p}^{*T}\hat{u}_T^* - \frac{1}{c}\lambda_m^*\right]T$$

cannot be valid for all permissible T; however, equality is possible provided

$$\lambda_m^* = \frac{c}{m}\bar{p}^{*T}\hat{u}_T^* . \tag{3.24}$$

Substituting the value for λ_m^* from equation (3.24) into condition (3.16) and rearranging further requires that

$$\lambda_m^* \ge \frac{c}{m}\bar{p}^{*T}\hat{u}_T , \tag{3.25}$$

for all permissible values of $\hat{u}_T$. An upper bound on the right side of (3.25) is obtained when primer and thrust directions are identical; consequently, necessary condition (3.25) becomes

$$\lambda_m^* \ge \frac{cp^*}{m} . \tag{3.26}$$

Note, however, that equation (3.24) implies that

$$\lambda_m^* \le \frac{cp^*}{m} , \tag{3.27}$$

where equality occurs only when the primer and thrust directions are aligned. Hence, in order for both (3.26) and (3.27) to be valid,

$$\lambda_m^* = \frac{cp^*}{m} , \tag{3.28}$$

and the thrust must be parallel to the primer vector.

Consideration of the necessary condition (3.15) on each of the three extremal arcs is concluded; hence, the superscript * will henceforth be dropped, and the subsequent states, controls, and Lagrange multipliers are assumed to be evaluated on the optimal trajectory. The results obtained from the Weierstrass necessary condition can be summarized as follows:

1. Whenever the thruster is operative and $p \neq 0$, the thrust must act in the direction and sense of the primer vector.
2. If the function S is defined as

$$S \triangleq \frac{cp}{m} - \lambda_m , \tag{3.29}$$

then

$$S \leq 0 \text{ over an NT-arc;}$$
$$S \geq 0 \text{ over an MT-arc;}$$
$$S = 0 \text{ over an IT-arc.}$$

Additionally, at a point where the primer vanishes, the direction of the primer reverses; consequently, the thrust components will be discontinuous, and the thrust direction will also reverse. Because the function S delineates between the amount of thrust on extremal arcs, S is identified as the *thrust magnitude switching function.*

Next, the adjoint λ_m can be eliminated from consideration by expressing it in terms of the thrust magnitude switching function and by employing equations (3.9c), (3.2), and (3.13b). Differentiating equation (3.29) and solving for the derivative of the adjoint,

$$\dot{\lambda}_m = \frac{c}{m}\dot{p} - \frac{cp}{m^2}\dot{m} - \dot{S} . \tag{3.30}$$

Substituting (3.30) into (3.9c) produces

$$\frac{c}{m}\dot{p} - \frac{cp}{m^2}\dot{m} - \dot{S} = \frac{T}{m^2}p ,$$

and utilizing the conservation of mass expression (3.2) renders

$$\dot{S} = \frac{c}{m}\dot{p} - \frac{cp}{m^2}\left[-\frac{T}{c}\right] - \frac{T}{m^2}p ,$$

which reduces to

$$\dot{S} = \frac{c}{m}\dot{p} . \tag{3.31}$$

Also, substituting (3.29) into (3.13b),

$$0 = \sigma_1\left[\tilde{T} - 2T\right] - \frac{p}{m} + \frac{1}{c}\left[\frac{cp}{m} - S\right] . \tag{3.32}$$

Simplifying and rearranging (3.32),

$$S = c\sigma_1 \left[\tilde{T} - 2T\right] . \tag{3.33}$$

Hence, the constraints on the Lagrange multipliers λ_m, and σ_1 have been replaced by the specification of the switching function and its derivative according to equations (3.31) and (3.33). On NT- and MT-arcs, equation (3.33) serves only to determine the value of σ_1. Since the spacecraft mass is constant on an NT-arc, equation (3.31) is integrable to yield

$$S = \frac{c}{m} p + \text{constant} . \tag{3.34}$$

Recall that on an IT-arc, $\sigma_1 = 0$; therefore, from (3.33), $S = 0$. In order for the switching function to remain zero throughout the duration of the IT-arc, the derivative of the switching function must also be identically zero. Accordingly, equation (3.31) implies that

$$\dot{p} = 0 \text{ or } p = \text{constant} . \tag{3.35}$$

Specification of the thrust magnitude switching function on the three types of extremal arcs can be summarized as:

i) On an NT-arc, S is negative and is determined by (3.34).
ii) On an MT-arc, S is positive and is determined by (3.31).
iii) On an IT-arc, S is zero and the primer magnitude is constant.

Impulsive Thrusts

Consider the optimization of a transfer, on a mission of long duration, that employs conventional propulsion (*i.e.*, high thrust acceleration level and low specific impulse) [See Reference 64]. On such a transfer, the duration of an arc of maximum thrust is always small compared to the total time of transit between the terminal points of the mission. Then, the motion of the spacecraft on an MT-arc can, for the purpose of calculating an optimal trajectory, often be neglected; therefore, this MT-arc can be replaced by an impulsive thrust of negligible duration serving to change only the vehicle's velocity and to leave unaffected the vehicle's position.[52] An impulsive thrust, which is equivalent to the idealization of a rocket motor possessing unbounded thrust capacity, can be modelled by allowing $\tilde{T} \to \infty$. If the thrust magnitude is regarded as being infinite, the results of the previous section simplify.

Consider an MT-arc which is preceded and succeeded by NT-arcs. As determined in the previous section, the MT-arc is characterized by $S \geq 0$, and the NT-arcs are characterized by $S \leq 0$, so the graph of the thrust magnitude switching function has the form illustrated in Figure 3.1a. If the duration of the MT-arc is decreased and the magnitude of the thrust is increased, in the limit as $\tilde{T} \rightarrow \infty$, the MT-arc approaches an impulsive thrust, and the graph of S appears as shown in Figure 3.1b. At the instant of application of an impulsive thrust, denoted as $t = t_i$, the shape of Figure 3.1b necessarily implies that

$$S = \dot{S} = 0 \tag{3.36}$$

and that the switching function is a maximum. If either or both of the NT-arcs are replaced by IT-arcs over which $S = 0$, the graphs of the switching function are modified [See Figures 3.2a and 3.2b], but the conclusion (3.36) is unaltered. So, for the case of impulsive thrust maneuvers, $T = 0$ when $S < 0$, and the impulses occur at those instants when the S curve is tangent to $S = 0$. However, since the above argument does not preclude the existence of a cusp at $t = t_i$ [See Figures 3.1c and 3.2c], a more rigorous proof of (3.36) will be undertaken but is delayed until the discussion on corner conditions.

Next, consider an NT-arc that joins two impulsive thrusts. Let P denote the magnitude of the primer vector at the instant of one of the impulsive maneuvers. If equation (3.34), which is valid over the entirety of the arc, is evaluated at one terminus of the arc and since $S = 0$ at such a point, then

$$S = 0 = \frac{c}{m}P + \text{constant}\,.$$

So, the value of the constant is determined to equal $-\frac{c}{m}P$, and

$$S = \frac{c}{m}(p - P) \tag{3.37}$$

is valid over the NT-arc. From (3.37), the magnitude of the primer vector must equal P at the other terminus of the NT-arc as well. Hence, if an optimal trajectory is composed of NT-arcs separated by impulsive maneuvers, then $p = P$ at every application of an impulsive thrust, and equation (3.37) is valid over each NT-arc. If one or both of the impulsive maneuvers is replaced by an IT-arc, the previous argument is unaffected. Over an IT-arc, the switching function vanishes and the primer magnitude is constant; therefore, an IT-arc on an optimal trajectory behaves exactly like an impulsive thrust.

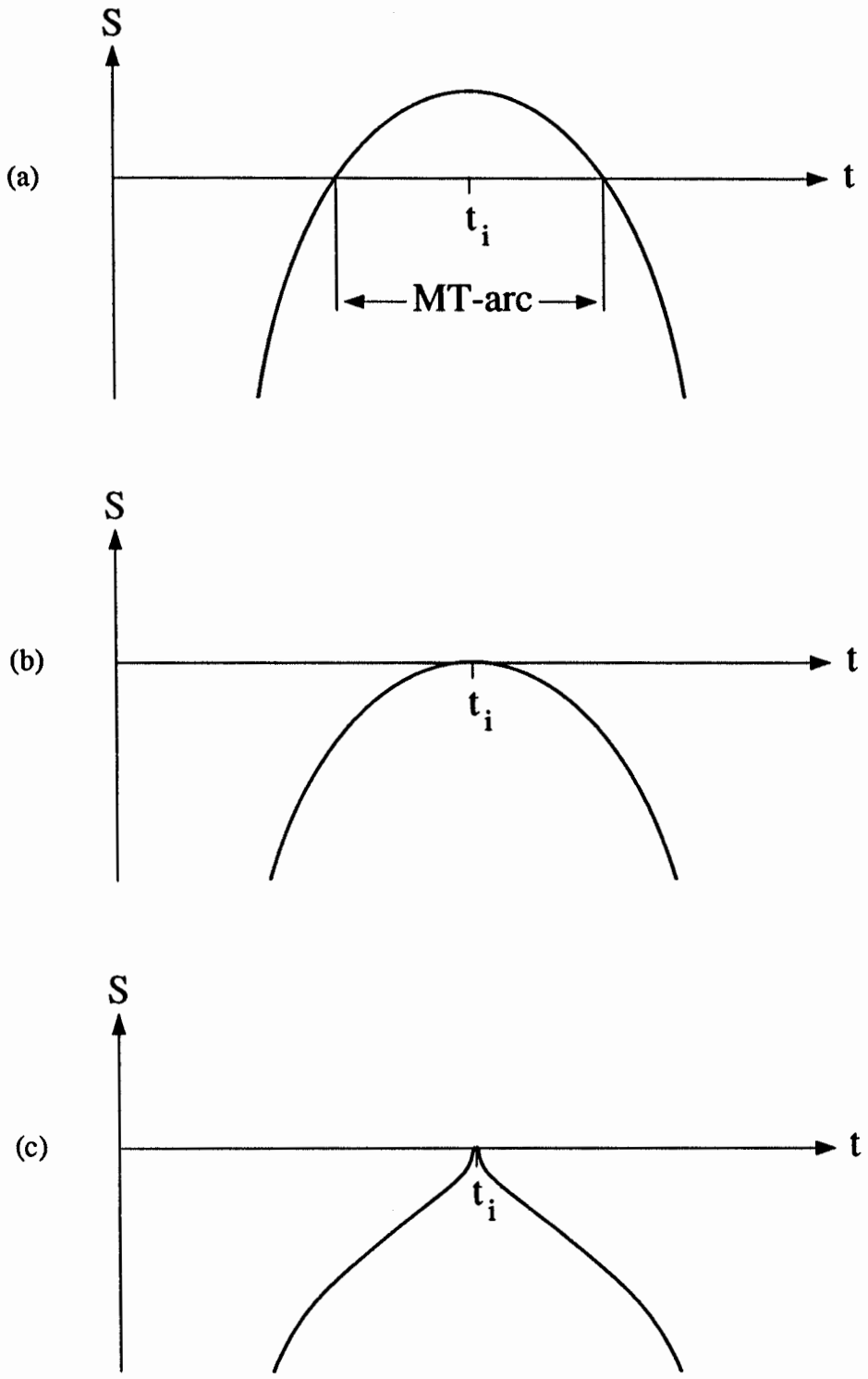

Figure 3.1 Switching Function of NT-Arcs Preceding and Succeeding an (a) MT-Arc, (b) Impulsive Thrust, and (c) Impulsive Thrust with a Cusp

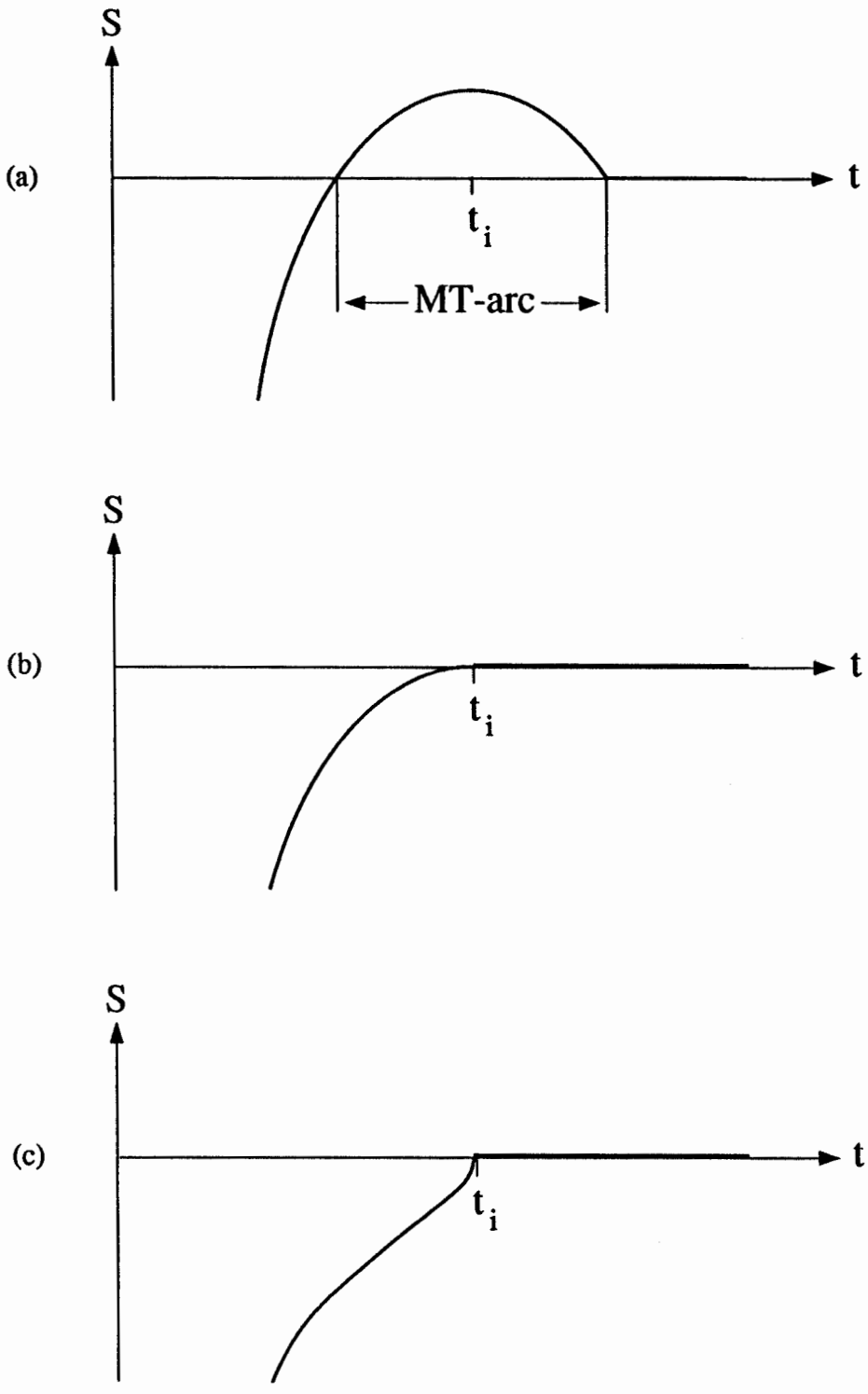

Figure 3.2 Switching Function of an NT-Arc Preceding and an IT-Arc Succeeding an (a) MT-Arc, (b) Impulsive Thrust, and (c) Impulsive Thrust with a Cusp

Consequently, at all impulsive maneuvers and over all IT-arcs $p = P$; also, over all NT-arcs $p \leq P$.

Consider the boundary conditions on an optimal trajectory. Assume that the initial and final positions and velocities, the initial and final times, and the initial mass are specified. Use of the transversality condition[64,75] enables the specification of the missing boundary condition for the final mass as

$$\lambda_m(t_f) = -\frac{\partial J}{\partial m_f}, \tag{3.38}$$

and, if the characteristic velocity is taken as a measure of the cost of executing the transfer, the partial derivative of equation (3.4) with respect to m_f can be evaluated to yield

$$\lambda_m(t_f) = \frac{c}{m_f}. \tag{3.39}$$

Evaluating the switching function given in equation (3.29) at the final time, t_f, and applying equation (3.39) render

$$S(t_f) = \frac{c}{m_f}(p_f - 1). \tag{3.40}$$

Assume that impulsive thrusts are permitted. Then, if the final arc of the trajectory under consideration is an NT-arc, equation (3.37), valid over the duration of this arc, can be evaluated at $t = t_f$ to produce

$$S(t_f) = \frac{c}{m_f}(p_f - P). \tag{3.41}$$

A comparison of equations (3.40) and (3.41) tenders the result that

$$P = 1 \tag{3.42}$$

such that condition (3.40) is satisfied. If the final arc is an IT-arc, then $S = 0$ and $p = P$; thus, condition (3.40) becomes

$$0 = \frac{c}{m_f}(P - 1), \tag{3.43}$$

which can only be satisfied provided $P = 1$. Hence, the magnitude of the primer must not exceed unity on any NT-arc, and, whenever the thruster is operative, the primer vector has unit magnitude and is aligned in the thrust direction.

Primer Differential Equations

Next, the differential equations for the primer vector are developed. The adjoint differential equations (3.9) can be rewritten in terms of the primer vector as

$$\dot{\bar{\lambda}}_x^T = -\bar{p}^T G_x \tag{3.44a}$$

$$\dot{\bar{p}}^T = -\bar{\lambda}_x^T - \bar{p}^T G_v \tag{3.44b}$$

$$\dot{\lambda}_m = \frac{T}{m^2} p \,. \tag{3.44c}$$

Differentiating (3.44b),

$$\ddot{\bar{p}}^T = -\dot{\bar{\lambda}}_x^T - \dot{\bar{p}}^T G_v - \bar{p}^T \dot{G}_v \,;$$

substituting in (3.44a),

$$\ddot{\bar{p}}^T = \bar{p}^T G_x - \dot{\bar{p}}^T G_v - \bar{p}^T \dot{G}_v \,;$$

and, simplifying,

$$\ddot{\bar{p}}^T = \bar{p}^T \left[G_x - \dot{G}_v \right] - \dot{\bar{p}}^T G_v \,. \tag{3.45}$$

Transposing equation (3.45),

$$\ddot{\bar{p}} = \left[G_x - \dot{G}_v \right]^T \bar{p} - G_v^T \dot{\bar{p}} \,. \tag{3.46}$$

Equations (3.10) and the expressions for Y and Ω given in Chapter 1 can be utilized to evaluate the matrix expression $(G_x - \dot{G}_v)^T$. First,

$$G_x - \dot{G}_v = \begin{bmatrix} U_{xx} & U_{xy} + \dot{n} & U_{xz} \\ U_{xy} - \dot{n} & U_{yy} & U_{yz} \\ U_{xz} & U_{yz} & U_{zz} \end{bmatrix} - \begin{bmatrix} 0 & 2\dot{n} & 0 \\ -2\dot{n} & 0 & 0 \\ 0 & 0 & 0 \end{bmatrix} .$$

$$G_x - \dot{G}_v = \begin{bmatrix} U_{xx} & U_{xy} - \dot{n} & U_{xz} \\ U_{xy} + \dot{n} & U_{yy} & U_{yz} \\ U_{xz} & U_{yz} & U_{zz} \end{bmatrix} . \tag{3.47}$$

Then, transposing (3.47),

$$\left[G_x - \dot{G}_v\right]^T = \begin{bmatrix} U_{xx} & U_{xy} + \dot{n} & U_{xz} \\ U_{xy} - \dot{n} & U_{yy} & U_{yz} \\ U_{xz} & U_{yz} & U_{zz} \end{bmatrix}. \tag{3.48}$$

However, the matrix in equation (3.48) is equivalent to the matrix G_x; thus,

$$\left[G_x - \dot{G}_v\right]^T = G_x . \tag{3.49}$$

Also, notice that

$$-G_v^T = \begin{bmatrix} 0 & 2n & 0 \\ -2n & 0 & 0 \\ 0 & 0 & 0 \end{bmatrix} = G_v . \tag{3.50}$$

Substituting equations (3.49) and (3.50) into (3.46) simplifies the second order differential equation for the primer vector to

$$\ddot{\bar{p}} = G_x \bar{p} + G_v \dot{\bar{p}} . \tag{3.51}$$

In contrast to Lawden's development of the primer differential equation associated with transfers in the two-body problem for which the matrix G_v is identically zero, the second derivative of the primer vector does, in fact, depend upon its first derivative in the elliptic restricted three-body formulation. One particularly convenient aspect of the primer vector is the fact that simultaneous integration of (3.51), in conjunction with the previously identified forty-two differential equations defining the dynamic model for the spacecraft's motion, is not necessary.

Note the similarity of equations (1.21) and (3.51) (*i.e.*, equations (1.21) can be written in second order form as $\ddot{\bar{x}} = G_x \bar{x} + G_v \dot{\bar{x}}$). Hence, if the initial conditions for the primer vector and its derivative are known, the solution for $\bar{p}$, in terms of the state transition matrix in (1.31), is

$$\begin{bmatrix} \bar{p}(t) \\ \dot{\bar{p}}(t) \end{bmatrix} = \begin{bmatrix} \phi_{11}(t,t_0) & \phi_{12}(t,t_0) \\ \phi_{21}(t,t_0) & \phi_{22}(t,t_0) \end{bmatrix} \begin{bmatrix} \bar{p}(t_0) \\ \dot{\bar{p}}(t_0) \end{bmatrix}, \tag{3.52}$$

where the state transition matrix is partitioned into four 3x3 submatrices. So, the initial conditions for the primer vector and its derivative must be determined. As demonstrated earlier, at the endpoints of the trajectory, the primer has unit magnitude and is aligned with the velocity increment; hence, the boundary conditions on the primer are

$$\bar{p}(t_0) = \frac{\Delta\bar{v}_0}{|\Delta\bar{v}_0|} \tag{3.53a}$$

$$\bar{p}(t_f) = \frac{\Delta\bar{v}_f}{|\Delta\bar{v}_f|}\,, \tag{3.53b}$$

where $\Delta\bar{v}_0$ and $\Delta\bar{v}_f$ are the terminal impulsive maneuvers connected by an NT-arc. If matrix equation (3.52) is evaluated at $t = t_f$ and if the submatrix $\phi_{12}(t_f, t_o)$ is assumed to be nonsingular, the first equation of (3.52) can be rearranged to yield

$$\dot{\bar{p}}(t_0) = \phi_{12}^{-1}(t_f, t_0)\left[\bar{p}(t_f) - \phi_{11}(t_f, t_0)\,\bar{p}(t_0)\right]. \tag{3.54}$$

Thus, with the initial conditions for the primer vector and its derivative specified by equations (3.53a) and (3.54), the solution for the primer is given by (3.52).

Weierstrass-Erdmann Corner Conditions

If some or all of the states jump (or experience a discontinuity) as a result of an instantaneous change in the control variables (*i.e.*, an impulse), a *corner* is said to exist in the terminology of the calculus of variations. In order for a corner to exist in an optimal solution, the *Weierstrass-Erdmann corner conditions* must be satisfied.

The first condition stipulates that the adjoint variables must be continuous at a corner. If $-$ and $+$ denote the evaluation of a quantity prior to and subsequent to a corner, respectively, then

$$\bar{\lambda}_x^- = \bar{\lambda}_x^+ \tag{3.55a}$$

$$\bar{\lambda}_v^- = \bar{\lambda}_v^+ \text{ or } \bar{p}^- = \bar{p}^+ \tag{3.55b}$$

$$\lambda_m^- = \lambda_m^+\,. \tag{3.55c}$$

An outcome of the first Weierstrass-Erdmann corner condition is the requirement that the derivative of the primer vector must also be continuous at a corner since, from the second adjoint equation (3.44b)

$$\dot{\bar{p}}^T = -\bar{\lambda}_x^T - \bar{p}^T G_v\,,$$

the derivative of the primer vector is expressed solely in terms of continuous adjoint variables and the continuous matrix G_v (which is a function of n and is determined by the primary motion). Hence,

$$\dot{\bar{p}}^{-} = \dot{\bar{p}}^{+} ; \tag{3.56}$$

additionally, from equation (3.31), the derivative of the thrust magnitude switching function must also be continuous at a corner.

The second corner condition demands that the Hamiltonian also be continuous at a corner. Thus,

$$H^{-} = H^{+} . \tag{3.57}$$

The Hamiltonian expressed in equation (3.8) can be rewritten in terms of the primer vector as

$$H = \bar{p}^{T}\bar{g} - \left[\dot{\bar{p}}^{T} + \bar{p}^{T}G_v\right]\bar{v} + \left[\frac{cp}{m} - \lambda_m\right]\frac{T}{c} , \tag{3.58}$$

where equation (3.44b) was used to replace the vector $\bar{\lambda}_x$. If T is discontinuous at a corner, then the Hamiltonian at this point can be continuous only if

$$\frac{cp}{m} - \lambda_m = 0 ,$$

or

$$S = 0 .$$

Thus, at a corner the Hamiltonian simplifies to

$$H = \bar{p}^{T}\left[\bar{g} - G_v\bar{v}\right] - \dot{\bar{p}}^{T}\bar{v} . \tag{3.59}$$

Evaluating the Hamiltonian on each side of a corner and enforcing continuity,

$$H^{+} - H^{-} = 0$$

$$\left[\bar{p}^{T}\left[\bar{g} - G_v\bar{v}\right] - \dot{\bar{p}}^{T}\bar{v}\right]^{+} - \left[\bar{p}^{T}\left[\bar{g} - G_v\bar{v}\right] - \dot{\bar{p}}^{T}\bar{v}\right]^{-} = 0 .$$

Re-grouping terms,

$$\bar{p}^{T}\left[\left[\bar{g} - G_v\bar{v}\right]^{+} - \left[\bar{g} - G_v\bar{v}\right]^{-}\right] - \dot{\bar{p}}^{T}\left[\bar{v}^{+} - \bar{v}^{-}\right] = 0 . \tag{3.60}$$

Employing equations (3.3) and (3.10b) to evaluate the quantity $\bar{g} - G_v\bar{v}$,

$$\bar{g} - G_v \bar{v} = \begin{bmatrix} 2nv_y + \dot{n}y + U_x \\ -2nv_x - \dot{n}x + U_y \\ U_z \end{bmatrix} - \begin{bmatrix} 0 & 2n & 0 \\ -2n & 0 & 0 \\ 0 & 0 & 0 \end{bmatrix} \begin{bmatrix} v_x \\ v_y \\ v_z \end{bmatrix}.$$

Simplifying,

$$\bar{g} - G_v \bar{v} = \begin{bmatrix} \dot{n}y + U_x \\ -\dot{n}x + U_y \\ U_z \end{bmatrix}. \tag{3.61}$$

Since the partial derivatives of the pseudo-potential, the position coordinates, and $\dot{n}$ are all continuous at a corner, the quantity $\bar{g} - G_v \bar{v}$ must also be continuous at a corner, and the first term in equation (3.60) vanishes; thus,

$$H^+ - H^- = 0 = \dot{\bar{p}}^T \Delta \bar{v}, \tag{3.62}$$

where $\Delta \bar{v}$ is the velocity discontinuity at the corner. Since the primer vector is a unit vector aligned with the velocity increment at the instant of an impulsive maneuver (*i.e.*, at a corner), then

$$\dot{\bar{p}}^T \bar{p} = 0. \tag{3.63}$$

Thus, as a consequence of the second corner condition, equation (3.63) demands that the scalar product of the derivative of the primer vector and the primer vector itself must be zero at a corner. Since the magnitude of the primer vector has been previously determined to equal unity at the instant of an impulsive maneuver, the derivative of the magnitude of the primer vector must be equal to zero at a corner in order for (3.63) to be valid. Moreover, from equation (3.31), the derivative of the switching function must also vanish at a corner.

Recall from the argument presented in the section on impulsive thrusts that the switching function and its derivative were inferred to be zero at the instant of an impulsive maneuver and that the appearance of cusps was dismissed. An outgrowth of the Weierstrass-Erdmann corner conditions is the proof that $S = 0$, $\dot{S} = 0$, and $\dot{S}$ is continuous at a corner between two arcs. Hence, equation (3.36) has been proved rigorously and the existence of cusps on an optimal trajectory can be eliminated from consideration.

Necessary Conditions for an Optimal Trajectory

Now, the necessary conditions for an optimal impulsive transfer in the elliptic restricted three-body problem have been developed and can be expressed entirely in terms of the primer vector as:

1. The primer vector satisfies $\ddot{\bar{p}} = G_x \bar{p} + G_v \dot{\bar{p}}$; additionally, it must be continuous and have a continuous first derivative.
2. The magnitude of the primer vector is less than or equal to one during the transfer with impulses occurring at those instants for which $p = 1$.
3. At an impulse time, the primer vector is a unit vector aligned in the optimal thrust direction.
4. At all interior impulses (not at the initial or final times), $\dot{p} = 0$, and the derivative of the primer vector and the primer itself must be orthogonal (*i.e.*, $\dot{\bar{p}}^T \bar{p} = 0$) as a consequence of the continuity of the Hamiltonian at a corner.

With the exception of the inclusion of the matrix G_v in the differential equation for the primer vector, these four necessary conditions are identical to those that Lawden developed for optimal transfer trajectories in the two-body problem. Despite this similarity, the preceding derivations of the necessary conditions for optimal transfers in this formulation of the elliptic restricted three-body problem are substantively different from the corresponding derivations for the two-body problem. The application of primer vector theory to the elliptic restricted three-body problem is an extension—a generalization—that includes Lawden's problem as a special case.

Hamiltonian

When the Hamiltonian of a system is constant, as it is for the two-body and circular three-body problems in orbital mechanics, the system possesses an integral of the motion. The constancy of the Hamiltonian can facilitate theoretical developments as well as provide a check on the accuracy of numerical computations. The Hamiltonian for the elliptic restricted three-body problem is investigated below.

Rearranging the expression for the Hamiltonian on an NT-arc provided in (3.59),

$$H = \bar{p}^T \bar{g} - \left(\dot{\bar{p}}^T + \bar{p}^T G_v \right) \bar{v} . \tag{3.64}$$

The derivative of (3.64) with respect to time yields

$$\dot{H} = \dot{\bar{p}}^T \bar{g} + \bar{p}^T \dot{\bar{g}} - \left[\ddot{\bar{p}}^T + \dot{\bar{p}}^T G_v + \bar{p}^T \dot{G}_v \right] \bar{v} - \left[\dot{\bar{p}}^T + \bar{p}^T G_v \right] \dot{\bar{v}} . \tag{3.65}$$

Evaluating (3.1b) on an NT-arc yields $\dot{\bar{v}} = \bar{g}$ which is substituted into equation (3.65) to produce

$$\dot{H} = \dot{\bar{p}}^T \bar{g} + \bar{p}^T \dot{\bar{g}} - \left[\ddot{\bar{p}}^T + \dot{\bar{p}}^T G_v + \bar{p}^T \dot{G}_v \right] \bar{v} - \dot{\bar{p}}^T \bar{g} - \bar{p}^T G_v \bar{g} . \tag{3.66}$$

Substituting the expression for $\ddot{\bar{p}}^T$ from equation (3.45) into (3.66),

$$\dot{H} = \bar{p}^T \dot{\bar{g}} - \left[\bar{p}^T (G_x - \dot{G}_v) - \dot{\bar{p}}^T G_v + \dot{\bar{p}}^T G_v + \bar{p}^T \dot{G}_v \right] \bar{v} - \bar{p}^T G_v \bar{g} , \tag{3.67}$$

and simplifying,

$$\dot{H} = \bar{p}^T \dot{\bar{g}} - \bar{p}^T G_x \bar{v} - \bar{p}^T G_v \bar{g} . \tag{3.68}$$

Using the chain rule to differentiate $\bar{g}$,

$$\dot{\bar{g}} = \frac{\partial \bar{g}}{\partial \bar{x}} \dot{\bar{x}} + \frac{\partial \bar{g}}{\partial \bar{v}} \dot{\bar{v}} + \frac{\partial \bar{g}}{\partial t} . \tag{3.69}$$

However, utilizing the definitions of G_x and G_v in equations (3.10) and recalling that $\dot{\bar{x}} = \bar{v}$ and $\dot{\bar{v}} = \bar{g}$, equation (3.69) can be rewritten as

$$\dot{\bar{g}} = G_x \bar{v} + G_v \bar{g} + \frac{\partial \bar{g}}{\partial t} . \tag{3.70}$$

Substituting (3.70) into (3.68) renders

$$\dot{H} = \bar{p}^T \left[G_x \bar{v} + G_v \bar{g} + \frac{\partial \bar{g}}{\partial t} \right] - \bar{p}^T G_x \bar{v} - \bar{p}^T G_v \bar{g} ; \tag{3.71}$$

thus,

$$\dot{H} = \bar{p}^T \frac{\partial \bar{g}}{\partial t} . \tag{3.72}$$

The dependence of $\bar{g}$ on time is masked by the functional dependence of $\bar{g}$ on the quantities n and ξ which are themselves dependent on E which, in turn, is explicitly dependent on time. Therefore, $\frac{\partial \bar{g}}{\partial t} \neq 0$. Hence, the elliptic restricted three-body problem does not possess an integral of the motion, and the Hamiltonian is not constant.

In order to compute the derivative of the Hamiltonian, the quantity $\frac{\partial \bar{g}}{\partial t}$, obtained by taking the partial derivative of (3.3) with respect to time, is determined to be

$$\frac{\partial \bar{g}}{\partial t} = \begin{bmatrix} 2\dot{n}v_y + \ddot{n}y + U_{xt} \\ -2\dot{n}v_x - \ddot{n}x + U_{yt} \\ U_{zt} \end{bmatrix}. \tag{3.73}$$

The quantities U_{xt}, U_{yt}, and U_{zt}, calculated from equation (1.20), are

$$U_{xt} = 2n\dot{n}x + \mu(1-\mu)\dot{\xi}\left\{\frac{3[x+\mu(1+\xi)]^2}{d^5} - \frac{1}{d^3} - \frac{3[x-(1-\mu)(1+\xi)]^2}{r^5} + \frac{1}{r^3}\right\} \tag{3.74a}$$

$$U_{yt} = 2n\dot{n}y + 3\mu(1-\mu)y\dot{\xi}\left\{\frac{[x+\mu(1+\xi)]}{d^5} - \frac{[x-(1-\mu)(1+\xi)]}{r^5}\right\} \tag{3.74b}$$

$$U_{zt} = 3\mu(1-\mu)z\dot{\xi}\left\{\frac{[x+\mu(1+\xi)]}{d^5} - \frac{[x-(1-\mu)(1+\xi)]}{r^5}\right\}. \tag{3.74c}$$

Recall, from the primary motion analysis in Chapter 1, that ξ is a measure of the time-varying nature of the nondimensional distance between the primaries and is determined as

$$\xi = -e\cos E,$$

and

$$\dot{\xi} = \frac{e\sin E}{(1-e\cos E)},$$

where E is the eccentric anomaly associated with the primary orbit, and the derivative of E has the form $\dot{E} = (1-e\cos E)^{-1}$.

Adjoint Equation

In contrast to the two-body and circular restricted three-body problems for which the Hamiltonian is an integral of the motion, in the elliptic three-body problem, the expression for $\dot{H}$ in (3.72) is non-vanishing; therefore, H is not constant. The extension of primer vector theory to the elliptic restricted three-body problem is complicated by the non-constancy of the Hamiltonian. However, despite the time-varying nature of the Hamiltonian, a useful *variational* expression can be rendered constant by considering contemporaneous variations between a perturbed and a reference trajectory.

Let Γ represent a reference trajectory that satisfies a given set of boundary conditions, and let Γ' represent a trajectory that satisfies the same boundary conditions but that has been perturbed slightly from the reference. Additionally, let a prime denote a quantity evaluated on the perturbed trajectory Γ'. If $[\bar{x}, \bar{v}]$ and $[\bar{x}', \bar{v}']$ denote the state vectors on Γ and Γ', respectively, and if δ symbolizes a *contemporaneous variation*, then the differences between the states on the perturbed and reference trajectories are

$$\delta\bar{x}(t) = \bar{x}'(t) - \bar{x}(t)$$

$$\delta\bar{v}(t) = \bar{v}'(t) - \bar{v}(t) .$$

The equations of motion of a spacecraft on an NT-arc, obtained by setting $T = 0$ in equations (3.1), can be written

$$\dot{\bar{x}} = \bar{v} \tag{3.75a}$$

$$\dot{\bar{v}} = \bar{g} . \tag{3.75b}$$

If Γ and Γ' are sufficiently close such that a linear analysis is justified, then the contemporaneous variation in velocity on the NT-arc can be expressed as

$$\delta\dot{\bar{x}} = \dot{\bar{x}}' - \dot{\bar{x}} = \delta\bar{v} ; \tag{3.76}$$

similarly, the contemporaneous variation in acceleration is

$$\delta\dot{\bar{v}} = \dot{\bar{v}}' - \dot{\bar{v}} = \delta\bar{g} = \frac{\partial\bar{g}}{\partial\bar{x}}\delta\bar{x} + \frac{\partial\bar{g}}{\partial\bar{v}}\delta\bar{v} . \tag{3.77}$$

Substituting definitions (3.10) into (3.77),

$$\delta\dot{\bar{v}} = G_x\delta\bar{x} + G_v\delta\bar{v} . \tag{3.78}$$

The state variational equations (3.76) and (3.78) can be arranged in the matrix form,

$$\begin{bmatrix} \delta\dot{\bar{x}} \\ \delta\dot{\bar{v}} \end{bmatrix} = \begin{bmatrix} 0 & I \\ G_x & G_v \end{bmatrix} \begin{bmatrix} \delta\bar{x} \\ \delta\bar{v} \end{bmatrix} , \tag{3.79}$$

which has a solution, in terms of the partitioned state transition matrix of equation (1.30), of the form

$$\begin{bmatrix} \delta\bar{x}(t) \\ \delta\bar{v}(t) \end{bmatrix} = \begin{bmatrix} \phi_{11}(t,\tau) & \phi_{12}(t,\tau) \\ \phi_{21}(t,\tau) & \phi_{22}(t,\tau) \end{bmatrix} \begin{bmatrix} \delta\bar{x}(\tau) \\ \delta\bar{v}(\tau) \end{bmatrix} . \tag{3.80}$$

In addition, the variational equation (3.79) can be expressed in second order form as,

$$\ddot{\delta\bar{x}} = \dot{\delta\bar{v}} = G_x \delta\bar{x} + G_v \delta\bar{v} . \tag{3.81}$$

Recall that the second order differential equation for the primer vector is written as

$$\ddot{\bar{p}} = G_x \bar{p} + G_v \dot{\bar{p}} .$$

Additionally, an equivalent expression for the matrix G_x was provided in equation (3.49) which can be transposed to produce

$$G_x - \dot{G}_v = G_x^T ,$$

or

$$G_x = G_x^T + \dot{G}_v . \tag{3.82}$$

However, from differentiating (3.50),

$$\dot{G}_v = -\dot{G}_v^T ; \tag{3.83}$$

hence, substituting equation (3.83) into (3.82),

$$G_x = G_x^T - \dot{G}_v^T . \tag{3.84}$$

Substituting (3.84) and (3.50) into (3.51),

$$\ddot{\bar{p}} = \left[G_x^T - \dot{G}_v^T\right]\bar{p} - G_v^T \dot{\bar{p}} . \tag{3.85}$$

Pre-multiplying equation (3.81) by $\bar{p}^T$ and equation (3.85) by $\delta\bar{x}^T$ and subtracting,

$$\bar{p}^T \ddot{\delta\bar{x}} - \delta\bar{x}^T \ddot{\bar{p}} = \bar{p}^T G_x \delta\bar{x} + \bar{p}^T G_v \delta\bar{v} - \delta\bar{x}^T G_x^T \bar{p} + \delta\bar{x}^T \dot{G}_v^T \bar{p} + \delta\bar{x}^T G_v^T \dot{\bar{p}} . \tag{3.86}$$

Cancelling the first and third terms on the right side simplifies (3.86) to

$$\bar{p}^T \ddot{\delta\bar{x}} - \delta\bar{x}^T \ddot{\bar{p}} - \delta\bar{x}^T G_v^T \dot{\bar{p}} - \delta\bar{x}^T \dot{G}_v^T \bar{p} - \bar{p}^T G_v \delta\bar{v} = 0 . \tag{3.87}$$

Adding and subtracting the quantity $\dot{\bar{p}}^T \delta\bar{v}$,

$$\bar{p}^T \ddot{\delta\bar{x}} + \dot{\bar{p}}^T \delta\bar{v} - \delta\bar{x}^T \ddot{\bar{p}} - \dot{\bar{p}}^T \delta\bar{v} - \delta\bar{x}^T G_v^T \dot{\bar{p}} - \delta\bar{x}^T \dot{G}_v^T \bar{p} - \bar{p}^T G_v \delta\bar{v} = 0 . \tag{3.88}$$

Recalling that $\dot{\delta\bar{x}} = \delta\bar{v}$ and $\ddot{\delta\bar{x}} = \dot{\delta\bar{v}}$ and transposing the third, fifth, and sixth terms in equation (3.88) yield

$$\left[\bar{p}^T \dot{\delta\bar{v}} + \dot{\bar{p}}^T \delta\bar{v}\right] - \left[\ddot{\bar{p}}^T \delta\bar{x} + \dot{\bar{p}}^T \dot{\delta\bar{x}}\right] - \left[\dot{\bar{p}}^T G_v \delta\bar{x} + \bar{p}^T \dot{G}_v \delta\bar{x} + \bar{p}^T G_v \dot{\delta\bar{x}}\right] = 0 . \tag{3.89}$$

The left side of (3.89) is an exact differential; hence,

$$\frac{d}{dt}\left[\bar{p}^T\delta\bar{v} - \dot{\bar{p}}^T\delta\bar{x} - \bar{p}^T G_v \delta\bar{x}\right] = 0\,, \tag{3.90}$$

which can be integrated to yield

$$\bar{p}^T\delta\bar{v} - \left[\dot{\bar{p}}^T + \bar{p}^T G_v\right]\delta\bar{x} = \text{constant}\,. \tag{3.91}$$

Equation (3.91) is called the *adjoint equation* and is used extensively in subsequent derivations.

CHAPTER IV

OPTIMIZATION OF NON-OPTIMAL IMPULSIVE TRAJECTORIES

If a transfer path does not comply with the conditions stipulated for an optimal trajectory, then ways of improving the non-optimal path are sought. First, the inclusion of a coastal arc in the initial orbit, a coastal arc in the final orbit, or dual coasts is explored as a means of diminishing the cost associated with a nominal trajectory. Then, the addition of an interior impulse is investigated as a method of reducing the overall fuel expenditure. Both time-free and time-fixed transfers resulting from the application of coasts and additional impulses, respectively, are examined. The convergence of these transfer paths to optimal solutions is accomplished utilizing a multivariable search technique that employs knowledge of the cost gradients. The following development for the elliptic restricted three-body problem parallels Lion and Handelsman's[53] extension of primer vector theory to non-optimal trajectories in the two-body problem.

Reference and Perturbed Transfer Trajectories

Let Γ represent a two-impulse reference transfer trajectory from the point $\bar{x}_0$ at $t = t_0$ on orbit A to the point $\bar{x}_f$ at $t = t_f$ on orbit B. Γ may be a complete trajectory or a two-impulse segment of a multi-impulse trajectory. Assume that a neighboring trajectory exists which maintains the same terminal points as Γ but accomplishes the transfer with greater fuel economy. Designate this perturbed transfer trajectory as Γ' [See Figure 4.1]. Let the symbol d represent a *noncontemporaneous variation* in a quantity, and denote a quantity on the perturbed trajectory with a prime. So, a noncontemporaneous variation in position is given by

$$d\bar{x} = \bar{x}'(t + dt) - \bar{x}(t) .$$

Recall that the symbol δ represents a contemporaneous variation such that the

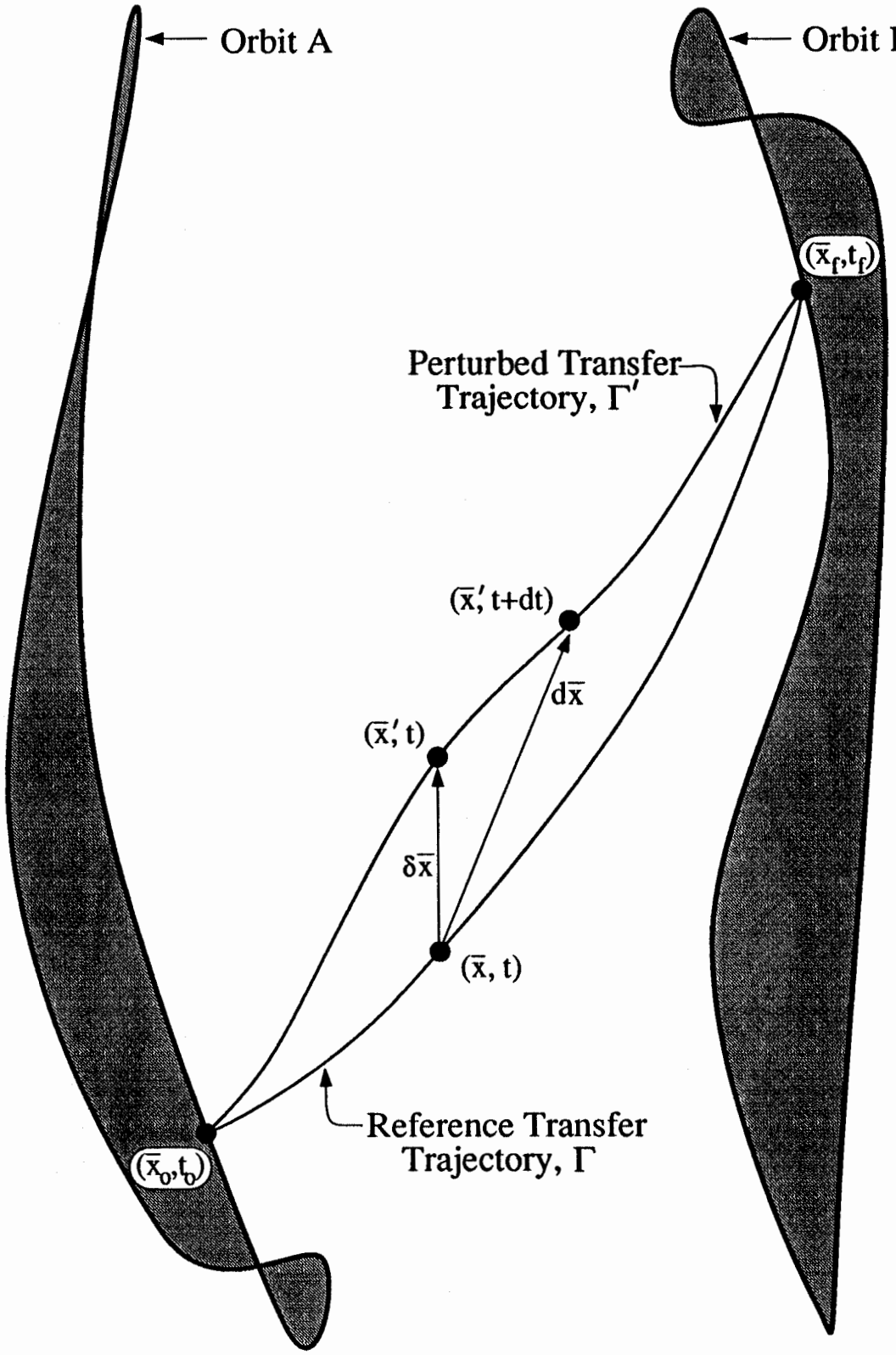

Figure 4.1 Variations Between Reference and Perturbed Transfer Trajectories

relationship between $d\bar{x}$ and $\delta\bar{x}$, to first order, is

$$d\bar{x} = \delta\bar{x} + \dot{\bar{x}}\, dt\,,$$

where

$$\delta\bar{x} = \bar{x}'(t) - \bar{x}(t)\,.$$

A variety of perturbations will subsequently be attributed to Γ' in an effort to reduce the fuel expenditure on the reference trajectory. For each set of traits characterizing the perturbed transfer trajectory, the conditions under which Γ' can be realized are developed.

Initial Coast

To test the efficacy of an initial coast to reduce cost, the reference two-impulse trajectory is compared with a neighboring two-impulse perturbed trajectory Γ' that has been allowed to coast ($dt_0 > 0$) in the initial orbit A [See Figure 4.2]. Although the subsequent theoretical developments are independent of the sign of the coastal period, dt_0 is taken to be positive for illustrative purposes. The criterion for the implementation of an initial coast is developed by considering the variation in the costs on the two trajectories, Γ and Γ'. The cost function, which was previously specified in equation (3.4) to be the characteristic velocity, can be equivalently expressed as the sum of the magnitudes of the impulsive maneuvers; thus,

$$J = \sum_k |\Delta\bar{v}_k|\,. \tag{4.1}$$

On Γ, impulses are applied at t_0 and t_f; whereas, Γ' remains in orbit A until some later time $t_0 + dt_0$ such that the impulses on Γ' are applied at $t_o + dt_0$ and t_f. Both trajectories reach the terminal state $\bar{x}_f$ on orbit B at t_f. From Figure 4.2 the costs on Γ and Γ', respectively, are

$$J_\Gamma = |\bar{v}_0 - \bar{v}_A| + |\bar{v}_B - \bar{v}_f| \tag{4.2a}$$

$$J_{\Gamma'} = |\bar{v}_0' - \bar{v}_A'| + |\bar{v}_B - \bar{v}_f'|\,. \tag{4.2b}$$

Employing the definitions of contemporaneous and noncontemporaneous variations, equation (4.2b) can be rewritten as

$$J_{\Gamma'} = |(\bar{v}_0 + d\bar{v}_{0^+}) - (\bar{v}_A + d\bar{v}_{0^-})| + |\bar{v}_B - (\bar{v}_f + \delta\bar{v}_{f^-})|\,,$$

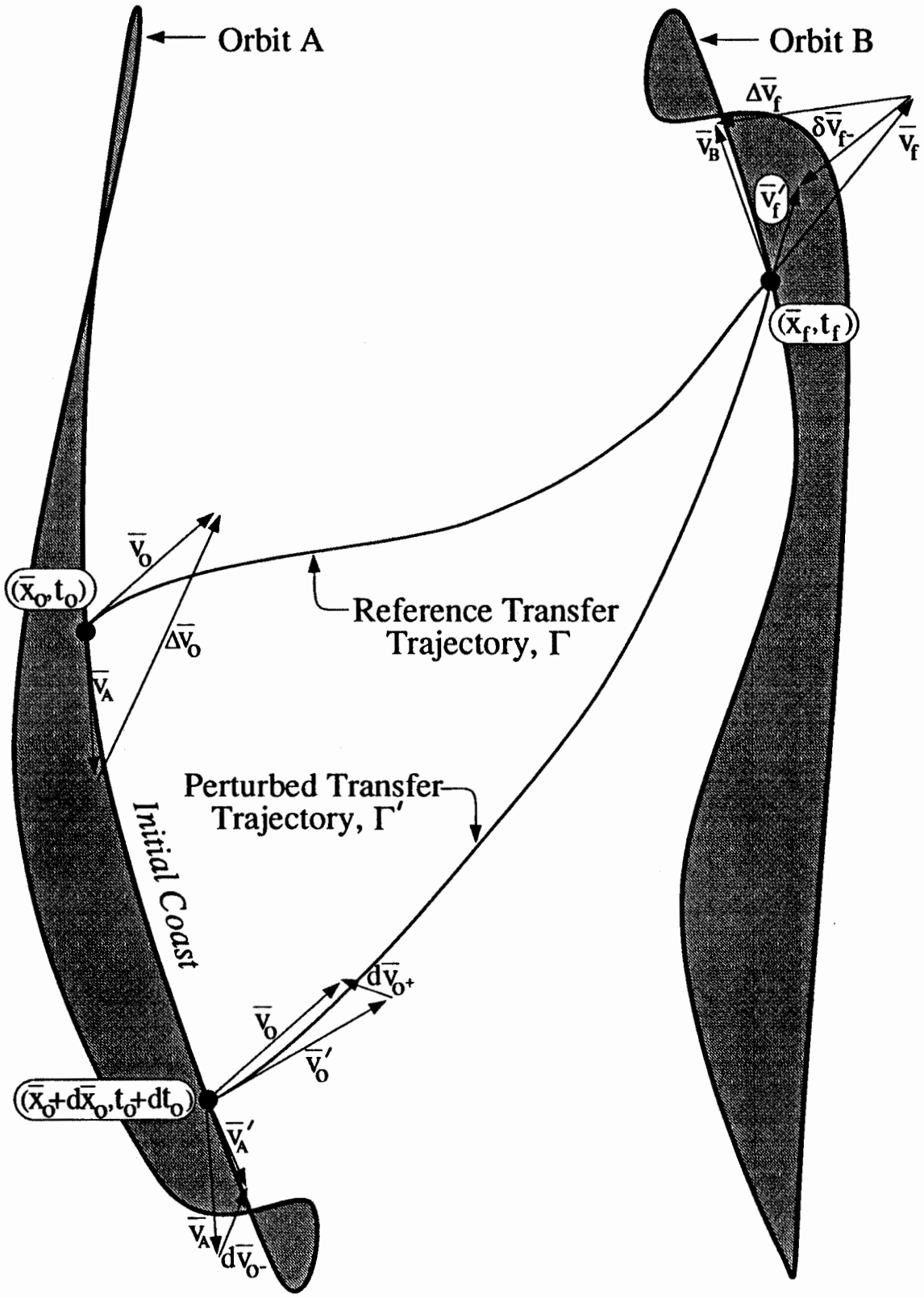

Figure 4.2 Initial Coast Geometry

where subscripts – and + represent the one-sided evaluation of the corresponding quantity immediately before and immediately after, respectively, the specified terminal impulse. Rearranging the equation above,

$$J_{\Gamma'} = |(\bar{v}_0 - \bar{v}_A) + (d\bar{v}_{0^+} - d\bar{v}_{0^-})| + |(\bar{v}_B - \bar{v}_f) - \delta\bar{v}_{f^-}| \ . \tag{4.3}$$

Therefore, the variation in cost, determined by subtracting (4.2a) from (4.3), is

$$\begin{aligned} \delta J = \ & |(\bar{v}_0 - \bar{v}_A) + (d\bar{v}_{0^+} - d\bar{v}_{0^-})| \ - \ |\bar{v}_0 - \bar{v}_A| \\ & + |(\bar{v}_B - \bar{v}_f) - \delta\bar{v}_{f^-}| \ - \ |\bar{v}_B - \bar{v}_f| \ . \end{aligned} \tag{4.4}$$

The quantity δJ represents the difference between the cost on the reference trajectory and the cost on a perturbed trajectory that has been allowed to coast in orbit A before executing the impulsive maneuver that commences the transfer. The expression for the variation in cost given in (4.4) will be simplified substantially in order to determine whether δJ can be made negative; whereby, implementation of an initial coast would lower fuel expenditure.

Note that equation (4.4) contains expressions that represent the differences between the magnitudes of the impulsive maneuvers on the perturbed trajectory and those on the reference trajectory; namely, these expressions are

$$|(\bar{v}_0 - \bar{v}_A) + (d\bar{v}_{0^+} - d\bar{v}_{0^-})| - |\bar{v}_0 - \bar{v}_A| \tag{4.5a}$$

$$|(\bar{v}_B - \bar{v}_f) - \delta\bar{v}_{f^-}| - |\bar{v}_B - \bar{v}_f| \ . \tag{4.5b}$$

Therefore, digress temporarily and consider the difference between the magnitudes of an arbitrary vector $\bar{x}$ on a perturbed and a reference path.[56] Let the scalar value df represent this difference, so

$$df = |\bar{x} \pm \delta\bar{x}| - |\bar{x}|$$

$$df = \left[(\bar{x} \pm \delta\bar{x})^T(\bar{x} \pm \delta\bar{x})\right]^{\frac{1}{2}} - \left[\bar{x}^T\bar{x}\right]^{\frac{1}{2}}$$

$$df = \left[\bar{x}^T\bar{x}\right]^{\frac{1}{2}}\left\{\left[\frac{(\bar{x} \pm \delta\bar{x})^T(\bar{x} \pm \delta\bar{x})}{\bar{x}^T\bar{x}}\right]^{\frac{1}{2}} - 1\right\}$$

$$df = |\bar{x}| \left\{ \left[\frac{\bar{x}^T \bar{x}}{|\bar{x}|^2} \pm \frac{2\delta\bar{x}^T \bar{x}}{|\bar{x}|^2} + \frac{\delta\bar{x}^T \delta\bar{x}}{|\bar{x}|^2} \right]^{\frac{1}{2}} - 1 \right\}.$$

Neglecting second and higher order terms in the small perturbation quantity $\delta\bar{x}$,

$$df = |\bar{x}| \left\{ \left[1 \pm \frac{2\delta\bar{x}^T \bar{x}}{|\bar{x}|^2} + \cdots \right]^{\frac{1}{2}} - 1 \right\}.$$

Utilizing a binomial expansion to simplify,

$$df = |\bar{x}| \left\{ 1 \pm \frac{1}{2} \frac{2\delta\bar{x}^T \bar{x}}{|\bar{x}|^2} + \cdots - 1 \right\}.$$

Truncate df in order to retain only the first order terms in $\delta\bar{x}$; hence,

$$df \approx \pm \frac{\delta\bar{x}^T \bar{x}}{|\bar{x}|}. \tag{4.6}$$

Thus, expressions (4.5) can be written, to first order, as

$$|(\bar{v}_0 - \bar{v}_A) + (d\bar{v}_{0^+} - d\bar{v}_{0^-})| - |\bar{v}_0 - \bar{v}_A| = \frac{(\bar{v}_0 - \bar{v}_A)^T}{|\bar{v}_0 - \bar{v}_A|} (d\bar{v}_{0^+} - d\bar{v}_{0^-}) \tag{4.7a}$$

$$|(\bar{v}_B - \bar{v}_f) - \delta\bar{v}_{f^-}| - |\bar{v}_B - \bar{v}_f| = -\frac{(\bar{v}_B - \bar{v}_f)^T}{|\bar{v}_B - \bar{v}_f|} \delta\bar{v}_{f^-}. \tag{4.7b}$$

With the differences between the magnitudes of the initial and final impulses on the perturbed and the reference trajectories approximated to first order, return to the relationship for the difference in the costs on Γ and Γ'.

Substituting the first order expressions (4.7) into the variation in cost equation (4.4) yields

$$\delta J = \frac{(\bar{v}_0 - \bar{v}_A)^T}{|\bar{v}_0 - \bar{v}_A|} (d\bar{v}_{0^+} - d\bar{v}_{0^-}) - \frac{(\bar{v}_B - \bar{v}_f)^T}{|\bar{v}_B - \bar{v}_f|} \delta\bar{v}_{f^-}. \tag{4.8}$$

Recall that, at the endpoints of the reference trajectory, the primer vector is defined to be a unit vector in the direction of the terminal impulsive maneuver; therefore,

$$\bar{p}_0 = \frac{(\bar{v}_0 - \bar{v}_A)}{|\bar{v}_0 - \bar{v}_A|} \tag{4.9a}$$

$$\bar{p}_f = \frac{(\bar{v}_B - \bar{v}_f)}{|\bar{v}_B - \bar{v}_f|} . \tag{4.9b}$$

Substituting the expressions in (4.9) into (4.8),

$$\delta J = \bar{p}_0^T (d\bar{v}_{0^+} - d\bar{v}_{0^-}) - \bar{p}_f^T \delta\bar{v}_{f^-} , \tag{4.10}$$

and the variation in cost is expressed in terms of the primer vector at the initial and final states on the reference trajectory Γ.

Next, the utility of the adjoint equation, as it pertains to a perturbed trajectory that has been allowed to coast initially, is investigated. Recall that the adjoint equation (3.91),

$$\bar{p}^T \delta\bar{v} - \left[\dot{\bar{p}}^T + \bar{p}^T G_v\right]\delta\bar{x} = \text{constant} ,$$

was previously determined to be a contemporaneous variational expression that is valid everywhere on a coastal arc of a perturbed trajectory. Note that Γ' is comprised of only one coastal arc that originates at $t = t_{0^+}$ and terminates at $t = t_{f^-}$. That the entirety of Γ' can be considered a coastal arc should not be confused with the initial coast on orbit A. This initial coast on the perturbed trajectory is accounted for by the noncontemporaneous variation in time, dt_0. So, evaluating the variational relationship (3.91) over the duration of Γ',

$$@\ t = t_{0^+}, \qquad \bar{p}_0^T \delta\bar{v}_{0^+} - \left[\dot{\bar{p}}_0^T + \bar{p}_0^T G_{v_0}\right]\delta\bar{x}_{0^+} = C \tag{4.11a}$$

$$@\ t = t_{f^-}, \qquad \bar{p}_f^T \delta\bar{v}_{f^-} - \left[\dot{\bar{p}}_f^T + \bar{p}_f^T G_{v_f}\right]\delta\bar{x}_{f^-} = C , \tag{4.11b}$$

where C denotes the constant on the entirety of Γ'. Equating constants and noting that, since both the reference and perturbed trajectories reach the terminal state $\bar{x}_f$ on orbit B at t_f, $\delta\bar{x}_{f^-}$ must equal zero,

$$\bar{p}_0^T \delta\bar{v}_{0^+} - \left[\dot{\bar{p}}_0^T + \bar{p}_0^T G_{v_0}\right]\delta\bar{x}_{0^+} = \bar{p}_f^T \delta\bar{v}_{f^-} . \tag{4.12}$$

Additionally, the first-order relationships between the noncontemporaneous and contemporaneous variations in velocity immediately before and after the initial impulse at $t = t_0$ [See Figure 4.3] are written as

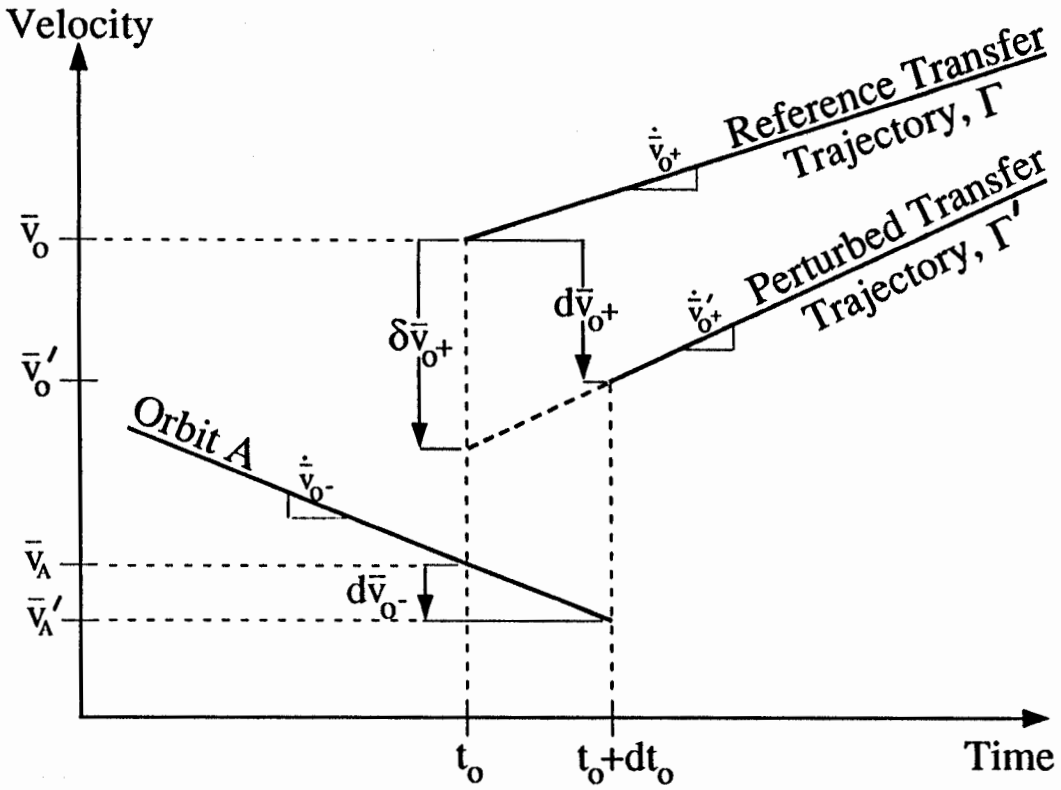

Figure 4.3 Contemporaneous and Noncontemporaneous Velocity Variations at the Instant of the Initial Impulse

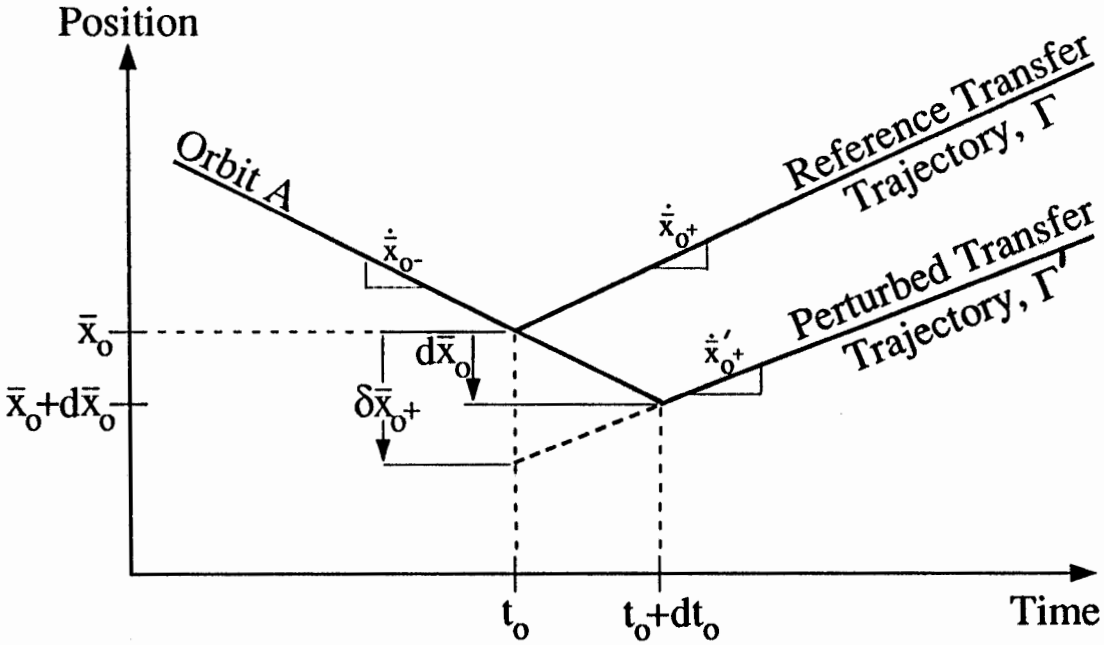

Figure 4.4 Contemporaneous and Noncontemporaneous Position Variations at the Instant of the Initial Impulse

$$d\bar{v}_{0^-} = \delta\bar{v}_{0^-} + \dot{\bar{v}}_{0^-} dt_0 \tag{4.13a}$$

$$d\bar{v}_{0^+} = \delta\bar{v}_{0^+} + \dot{\bar{v}}'_{0^+} dt_0 \,, \tag{4.13b}$$

where $\dot{\bar{v}}_{0^-}$ is the acceleration on orbit A prior to the the initial impulse on Γ', and $\dot{\bar{v}}'_{0^+}$ is the acceleration on Γ' after the initial impulse; however, to first order, the acceleration after the initial impulse can be calculated on the reference trajectory (*i.e.*, $\dot{\bar{v}}'_{0^+} \approx \dot{\bar{v}}_{0^+}$).[54] Also, since the velocity on both the reference and perturbed trajectories prior to $t = t_0$ is equivalent to the velocity associated with orbit A, $\delta\bar{v}_{0^-} = 0$. Hence, equations (4.13) can be rewritten to yield

$$d\bar{v}_{0^-} = \dot{\bar{v}}_{0^-} dt_0 \tag{4.14a}$$

$$d\bar{v}_{0^+} = \delta\bar{v}_{0^+} + \dot{\bar{v}}_{0^+} dt_0 \,. \tag{4.14b}$$

So, the adjoint equation, evaluated over the duration of Γ', as well as the expressions for the velocity variations at $t = t_0$ can be utilized in the simplification of the expression for δJ.

Return now to equation (4.10), the first order expression for the variation in cost,

$$\delta J = \bar{p}_0^T (d\bar{v}_{0^+} - d\bar{v}_{0^-}) - \bar{p}_f^T \delta\bar{v}_{f^-} \,.$$

Substituting equations (4.12) and (4.14) into (4.10),

$$\delta J = \bar{p}_0^T \left[\left(\delta\bar{v}_{0^+} + \dot{\bar{v}}_{0^+} dt_0 \right) - \dot{\bar{v}}_{0^-} dt_0 \right] - \left[\bar{p}_0^T \delta\bar{v}_{0^+} - \left(\dot{\bar{p}}_0^T + \bar{p}_0^T G_{v_0} \right) \delta\bar{x}_{0^+} \right] ,$$

or simplifying,

$$\delta J = \bar{p}_0^T \left(\dot{\bar{v}}_{0^+} - \dot{\bar{v}}_{0^-} \right) dt_0 + \left(\dot{\bar{p}}_0^T + \bar{p}_0^T G_{v_0} \right) \delta\bar{x}_{0^+} \,. \tag{4.15}$$

Writing the contemporaneous variation in position at $t = t_{0^+}$ in terms of the noncontemporaneous variation [See Figure 4.4],

$$\delta\bar{x}_{0^+} = d\bar{x}_0 - \dot{\bar{x}}'_{0^+} dt_0 = d\bar{x}_0 - \bar{v}'_0 \, dt_0 \,,$$

and calculating the velocity on the reference trajectory instead of the perturbed trajectory (*i.e.*, $\bar{v}'_0 \approx \bar{v}_0$ to first order),

$$\delta\bar{x}_{0^+} = d\bar{x}_0 - \bar{v}_0 dt_0 \,. \tag{4.16}$$

Recall that the coastal acceleration has previously been denoted by the symbol $\bar{g}$, so $\dot{\bar{v}}_{0^-}$ which is the acceleration on orbit A immediately prior to the initial impulse can be

represented by the vector $\bar{g}_A$. Similarly, $\dot{\bar{v}}_{0^+}$, the acceleration on Γ immediately subsequent to the impulse at $t = t_0$, can be denoted by the vector $\bar{g}_0$. Making this notational change and substituting (4.16) into (4.15),

$$\delta J = \bar{p}_0^T(\bar{g}_0 - \bar{g}_A)dt_0 + \left[\dot{\bar{p}}_0^T + \bar{p}_0^T G_{v_0}\right](d\bar{x}_0 - \bar{v}_0 dt_0) ,$$

and regrouping terms,

$$\delta J = \bar{p}_0^T(\bar{g}_0 - \bar{g}_A - G_{v_0}\bar{v}_0)dt_0 + \dot{\bar{p}}_0^T(d\bar{x}_0 - \bar{v}_0 dt_0) + \bar{p}_0^T G_{v_0} d\bar{x}_0 . \qquad (4.17)$$

Notice that (4.17) contains the difference in acceleration across the initial impulse (*i.e.*, $\bar{g}_0 - \bar{g}_A$). In contradistinction to the two-body problem, the acceleration vector in this formulation of the elliptic restricted three-body problem is a function of velocity [See equation (3.3)]; hence, acceleration is discontinuous across the impulse, and the quantity $\bar{g}_0 - \bar{g}_A$ is nonzero. So, the accelerations at the initial impulse must be examined in order to further simplify the expression for δJ. Additionally, unlike the two-body problem, the matrix G_v is comprised of non-zero elements. Consequently, the entire parenthetical coefficient of dt_0 in equation (4.17) is evaluated for convenience.

From the definitions of $\bar{g}$ and G_v, given in equations (3.3) and (3.10b), respectively,

$$\begin{aligned}\bar{g}_0 - \bar{g}_A - G_{v_0}\bar{v}_0 = &\left[\begin{matrix} 2nv_y + \dot{n}y + U_x \\ -2nv_x - \dot{n}x + U_y \\ U_z \end{matrix}\right]\Bigg|_{t_{0^+}} - \left[\begin{matrix} 2nv_y + \dot{n}y + U_x \\ -2nv_x - \dot{n}x + U_y \\ U_z \end{matrix}\right]\Bigg|_{t_{0^-}} \\ &- \left[\begin{matrix} 0 & 2n & 0 \\ -2n & 0 & 0 \\ 0 & 0 & 0 \end{matrix}\right]\left[\begin{matrix} v_x \\ v_y \\ v_z \end{matrix}\right]\Bigg|_{t_{0^+}} .\end{aligned} \qquad (4.18)$$

Since U_x, U_y, and U_z are all strictly functions of position (which is required to be continuous) and the quantities n, $\dot{n}$, and ξ (which are determined from the two-body problem analysis of the primary motion and are also continuous functions), these partial derivatives of the pseudo-potential U must be continuous across the impulse at $t = t_0$. Consequently, equation (4.18) simplifies to,

$$\bar{g}_0 - \bar{g}_A - G_{v_0}\bar{v}_0 = \begin{bmatrix} 2nv_{y_{0^+}} - 2nv_{y_{0^-}} \\ -2nv_{x_{0^+}} + 2nv_{x_{0^-}} \\ 0 \end{bmatrix} - \begin{bmatrix} 2nv_{y_{0^+}} \\ -2nv_{x_{0^+}} \\ 0 \end{bmatrix} = \begin{bmatrix} -2nv_{y_{0^-}} \\ 2nv_{x_{0^-}} \\ 0 \end{bmatrix}. \tag{4.19}$$

Note, also, that

$$-G_{v_0}\bar{v}_A = -\begin{bmatrix} 0 & 2n & 0 \\ -2n & 0 & 0 \\ 0 & 0 & 0 \end{bmatrix}\begin{bmatrix} v_x \\ v_y \\ v_z \end{bmatrix}\Bigg|_{t_{0^-}} = \begin{bmatrix} -2nv_{y_{0^-}} \\ 2nv_{x_{0^-}} \\ 0 \end{bmatrix}.$$

Thus, equation (4.19) can be expressed as

$$\bar{g}_0 - \bar{g}_A - G_{v_0}\bar{v}_0 = -G_{v_0}\bar{v}_A \,. \tag{4.20}$$

Substituting (4.20) into equation (4.17),

$$\delta J = -\bar{p}_0^T G_{v_0}\bar{v}_A dt_0 + \dot{\bar{p}}_0^T(d\bar{x}_0 - \bar{v}_0 dt_0) + \bar{p}_0^T G_{v_0} d\bar{x}_0 \,,$$

or, equivalently,

$$\delta J = \dot{\bar{p}}_0^T(d\bar{x}_0 - \bar{v}_0 dt_0) + \bar{p}_0^T G_{v_0}(d\bar{x}_0 - \bar{v}_A dt_0) \,. \tag{4.21}$$

Expressing the noncontemporaneous variation in position at $t = t_{0^-}$ in terms of the contemporaneous variation,

$$d\bar{x}_0 = \delta\bar{x}_{0^-} + \dot{\bar{x}}_{0^-} dt_0 \,;$$

however, since the reference and perturbed trajectories coincide initially (*i.e.*, at $t = t_{0^-}$) on orbit A [See Figure 4.4], $\delta\bar{x}_{0^-}$ must equal zero and $\dot{\bar{x}}_{0^-}$ can be denoted $\bar{v}_A$. Hence,

$$d\bar{x}_0 = \bar{v}_A dt_0 \,; \tag{4.22}$$

the last term in equation (4.21) is zero; and, the variation in the cost reduces to

$$\delta J = \dot{\bar{p}}_0^T d\bar{x}_0 - \left[\dot{\bar{p}}_0^T \bar{v}_0\right] dt_0 \,. \tag{4.23}$$

Equation (4.23) represents, to first order, the difference in cost between two neighboring trajectories whose initial positions differ by $d\bar{x}_0$ and initial times differ by dt_0. Because it is the analog of the transversality condition of the calculus of variations, equation (4.23) is called the *initial coast transversality condition.* However, (4.23) has wider applicability since neither trajectory need be an optimum. Condition (4.23) is identical to that developed by Lion and Handelsman in their work associated with

transfer trajectories in the two-body problem. Despite this similarity, however, the derivation of (4.23) is distinguished from that provided by Lion and Handelsman by an adjoint equation of a distinctly different form and by the discontinuity of the acceleration at an impulsive maneuver in the elliptic restricted three-body problem.

Now that the variation in cost between a reference trajectory and a perturbed trajectory, that has been allowed to coast in the initial orbit A, has been determined, the criterion for the inclusion of such an initial coast, in an effort to reduce fuel expenditure, can be developed. That the noncontemporaneous variation in the position of the initial impulse can be expressed solely in terms of the velocity on orbit A and the coastal period was established by equation (4.22). So, making use of this knowledge by substituting (4.22) into the expression for the variation in cost,

$$\delta J = \dot{\bar{p}}_0^T \bar{v}_A dt_0 - \dot{\bar{p}}_0^T \bar{v}_0 dt_0 ,$$

or, simply,

$$\delta J = -\dot{\bar{p}}_0^T (\bar{v}_0 - \bar{v}_A) dt_0 . \tag{4.24}$$

Since the coastal period is assumed to be positive (*i.e.*, $dt_0 > 0$), then δJ will be negative if and only if

$$\dot{\bar{p}}_0^T (\bar{v}_0 - \bar{v}_A) > 0 . \tag{4.25}$$

Recall from equation (4.9a) that $\bar{p}_0$ is parallel to $(\bar{v}_0 - \bar{v}_A)$; hence, inequality (4.25) can be expressed as

$$\dot{\bar{p}}_0^T \bar{p}_0 > 0 . \tag{4.26}$$

Additionally, note that the scalar product of an arbitrary vector and its tangent vector (*i.e.*, the derivative of the arbitrary vector) can be expressed simply as the product of the vector's magnitude and rate of change of this magnitude, or, specifically in terms of the primer vector,

$$\dot{\bar{p}}^T \bar{p} = \frac{dp}{dt} p , \tag{4.27}$$

where p denotes the magnitude of the primer vector and $\frac{dp}{dt}$ denotes the slope of the magnitude of the primer vector at any instant in time. If (4.27) is evaluated at $t = t_0$, and since the primer vector magnitude is defined to be unity at the instant of the initial impulse, inequality (4.26) simplifies to

$$\frac{dp_0}{dt} > 0 , \tag{4.28}$$

where $\frac{dp_0}{dt}$ symbolizes the slope of the primer vector magnitude at the instant of the initial impulse. So, from (4.28), a reduction in cost can be achieved if the slope of a plot of the magnitude of the primer vector is positive at $t = t_0$. Hence, if the primer magnitude exceeds unity immediately after the initial impulse, an initial coast would lower the cost on the perturbed trajectory.

Final Coast

Next, in a method analogous to the examination of the cost effectiveness of an initial coast, the efficacy of a final coast to reduce cost is investigated. The variation in cost between the reference two-impulse trajectory and a neighboring two-impulse trajectory that has been allowed to coast ($dt_f < 0$) in the final orbit B [See Figure 4.5] is examined in order to evaluate the effect of a final coast. Again, the sign of the final coastal period does not impact the subsequent theoretical developments; however, dt_f is chosen to be negative for the purpose of illustration. The impulses on Γ are still applied at t_0 and t_f; however, on Γ', the impulses are applied at t_0 and $t_f + dt_f$ such that the final coast in orbit B has duration $-dt_f$. Both trajectories have initial states corresponding to $\bar{x}_0$ on orbit A at t_0. Unaltered from that given in equation (4.2a), the cost on Γ, restated here, is

$$J_\Gamma = |\bar{v}_0 - \bar{v}_A| + |\bar{v}_B - \bar{v}_f| . \tag{4.29a}$$

From Figure 4.5, the cost on Γ' is determined to be

$$J_{\Gamma'} = |\bar{v}_0' - \bar{v}_A| + |\bar{v}_B' - \bar{v}_f'| . \tag{4.29b}$$

Employing the definitions of contemporaneous and noncontemporaneous variations, equation (4.29b) can be rewritten as

$$J_{\Gamma'} = |(\bar{v}_0 + \delta\bar{v}_{0^+}) - \bar{v}_A| + |(\bar{v}_B + d\bar{v}_{f^+}) - (\bar{v}_f + d\bar{v}_{f^-})| .$$

Rearranging the equation above,

$$J_{\Gamma'} = |(\bar{v}_0 - \bar{v}_A) + \delta\bar{v}_{0^+}| + |(\bar{v}_B - \bar{v}_f) + (d\bar{v}_{f^+} - d\bar{v}_{f^-})| . \tag{4.30}$$

Thus, the variation in cost, determined by subtracting (4.29a) from (4.30), is

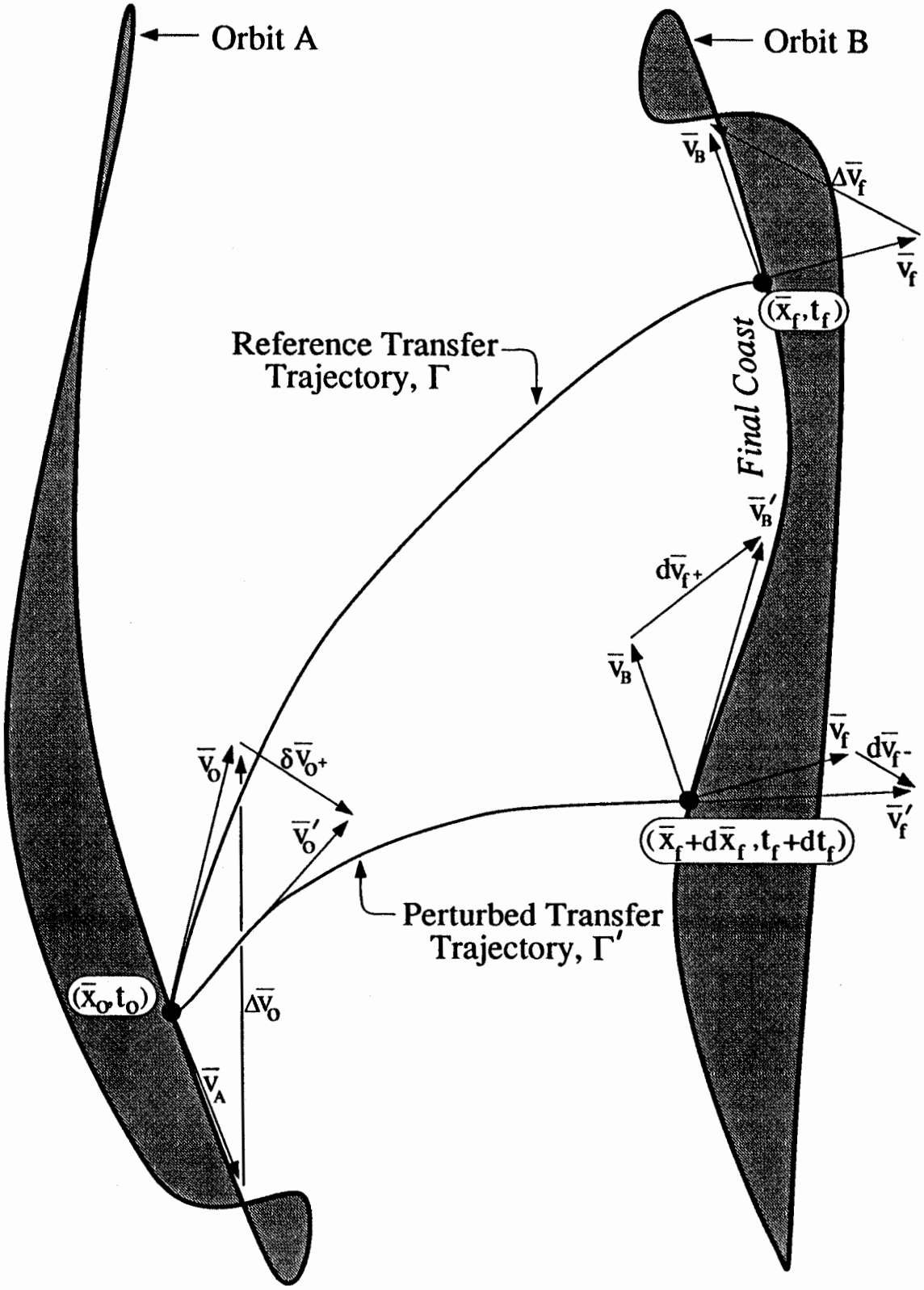

Figure 4.5 Final Coast Geometry

$$\begin{aligned}\delta J = & \quad |(\bar{v}_0 - \bar{v}_A) + \delta\bar{v}_{0^+}| - |\bar{v}_0 - \bar{v}_A| \\ & + |(\bar{v}_B - \bar{v}_f) + (d\bar{v}_{f^+} - d\bar{v}_{f^-})| - |\bar{v}_B - \bar{v}_f| \quad .\end{aligned} \tag{4.31}$$

In this instance, the quantity δJ represents the difference between the cost on the reference trajectory and the cost on a perturbed trajectory that has been allowed to coast in orbit B after executing the final impulsive maneuver on the transfer. The expression for the variation in cost given in (4.31) will be simplified substantially in order to determine whether δJ can be made negative; whereby, implementation of a final coast would lower fuel expenditure.

Note that equation (4.31) contains expressions that represent the differences between the magnitudes of the impulsive maneuvers on the perturbed trajectory and those on the reference trajectory; thus, utilizing equation (4.6) in order to simplify these differences to first order,

$$|(\bar{v}_0 - \bar{v}_A) + \delta\bar{v}_{0^+}| - |\bar{v}_0 - \bar{v}_A| = \frac{(\bar{v}_0 - \bar{v}_A)^T}{|\bar{v}_0 - \bar{v}_A|}\delta\bar{v}_{0^+}$$

$$|(\bar{v}_B - \bar{v}_f) + (d\bar{v}_{f^+} - d\bar{v}_{f^-})| - |\bar{v}_B - \bar{v}_f| = \frac{(\bar{v}_B - \bar{v}_f)^T}{|\bar{v}_B - \bar{v}_f|}(d\bar{v}_{f^+} - d\bar{v}_{f^-}) .$$

Substituting the above expressions into (4.31),

$$\delta J = \frac{(\bar{v}_0 - \bar{v}_A)^T}{|\bar{v}_0 - \bar{v}_A|}\delta\bar{v}_{0^+} + \frac{(\bar{v}_B - \bar{v}_f)^T}{|\bar{v}_B - \bar{v}_f|}(d\bar{v}_{f^+} - d\bar{v}_{f^-}) . \tag{4.32}$$

Recall that the primer vector at the endpoints of the reference trajectory was specified in (4.9). So, substituting the expressions in (4.9) into (4.32),

$$\delta J = \bar{p}_0^T \delta\bar{v}_{0^+} + \bar{p}_f^T (d\bar{v}_{f^+} - d\bar{v}_{f^-}) , \tag{4.33}$$

and the variation in cost is expressed in terms of the primer vector at the initial and final states on the reference trajectory Γ.

Next, the utility of the adjoint equation, as it pertains to a perturbed trajectory that has been allowed to execute a final coast, is investigated. Note that Γ' is comprised of only one coastal arc that originates at $t = t_{0^+}$ and terminates at $t = t_{f^-}$. That the entirety of Γ' can be considered a coastal arc should not be confused with the final coast on orbit B. This final coast on the perturbed trajectory is accounted for by the noncontemporaneous variation in time, dt_f. So, evaluating the variational relationship (3.91) over

the duration of Γ',

$$@\ t = t_{0^+}, \qquad \bar{p}_0^T \delta\bar{v}_{0^+} - \left[\dot{\bar{p}}_0^T + \bar{p}_0^T G_{v_0}\right]\delta\bar{x}_{0^+} = C \tag{4.34a}$$

$$@\ t = t_{f^-}, \qquad \bar{p}_f^T \delta\bar{v}_{f^-} - \left[\dot{\bar{p}}_f^T + \bar{p}_f^T G_{v_f}\right]\delta\bar{x}_{f^-} = C\,, \tag{4.34b}$$

where C denotes the constant on the entirety of Γ'. Equating constants and noting that, since both the reference and perturbed trajectories commence from the same terminal state $\bar{x}_0$ on orbit A at t_0, $\delta\bar{x}_{0^+}$ must equal zero,

$$\bar{p}_0^T \delta\bar{v}_{0^+} = \bar{p}_f^T \delta\bar{v}_{f^-} - \left[\dot{\bar{p}}_f^T + \bar{p}_f^T G_{v_f}\right]\delta\bar{x}_{f^-}\,. \tag{4.35}$$

Also, the first-order relationships between the noncontemporaneous and contemporaneous variations in velocity immediately before and after the initial impulse at $t = t_f$ [See Figure 4.6] are expressed as

$$d\bar{v}_{f^-} = \delta\bar{v}_{f^-} + \dot{\bar{v}}'_{f^-} dt_f \tag{4.36a}$$

$$d\bar{v}_{f^+} = \delta\bar{v}_{f^+} + \dot{\bar{v}}_{f^+} dt_f\,, \tag{4.36b}$$

where $\dot{\bar{v}}'_{f^-}$ is the acceleration on Γ' prior to the final impulse, and $\dot{\bar{v}}_{f^+}$ is the acceleration on orbit B subsequent to the final impulse; however, to first order, the acceleration prior to the final impulse can be calculated on the reference trajectory (*i.e.*, $\dot{\bar{v}}'_{f^-} \approx \dot{\bar{v}}_{f^-}$).[54] Additionally, since the velocity on both the reference and perturbed trajectories subsequent to $t = t_f$ is equivalent to the velocity associated with orbit B, $\delta\bar{v}_{f^+} = 0$. Thus, equations (4.36) can be rewritten to yield

$$d\bar{v}_{f^-} = \delta\bar{v}_{f^-} + \dot{\bar{v}}_{f^-} dt_f \tag{4.37a}$$

$$d\bar{v}_{f^+} = \dot{\bar{v}}_{f^+} dt_f\,. \tag{4.37b}$$

So, the adjoint equation, evaluated over the duration of Γ', as well as the expressions for the velocity variations at $t = t_f$ can be used to simplify the expression for δJ.

Returning to equation (4.33), the first order expression for the variation in cost,

$$\delta J = \bar{p}_0^T \delta\bar{v}_{0^+} + \bar{p}_f^T (d\bar{v}_{f^+} - d\bar{v}_{f^-})\,.$$

Substituting equations (4.35) and (4.37) into (4.33),

$$\delta J = \left[\bar{p}_f^T \delta\bar{v}_{f^-} - \left[\dot{\bar{p}}_f^T + \bar{p}_f^T G_{v_f}\right]\delta\bar{x}_{f^-}\right] + \bar{p}_f^T \left[\dot{\bar{v}}_{f^+} dt_f - \left[\delta\bar{v}_{f^-} + \dot{\bar{v}}_{f^-} dt_f\right]\right],$$

or simplifying,

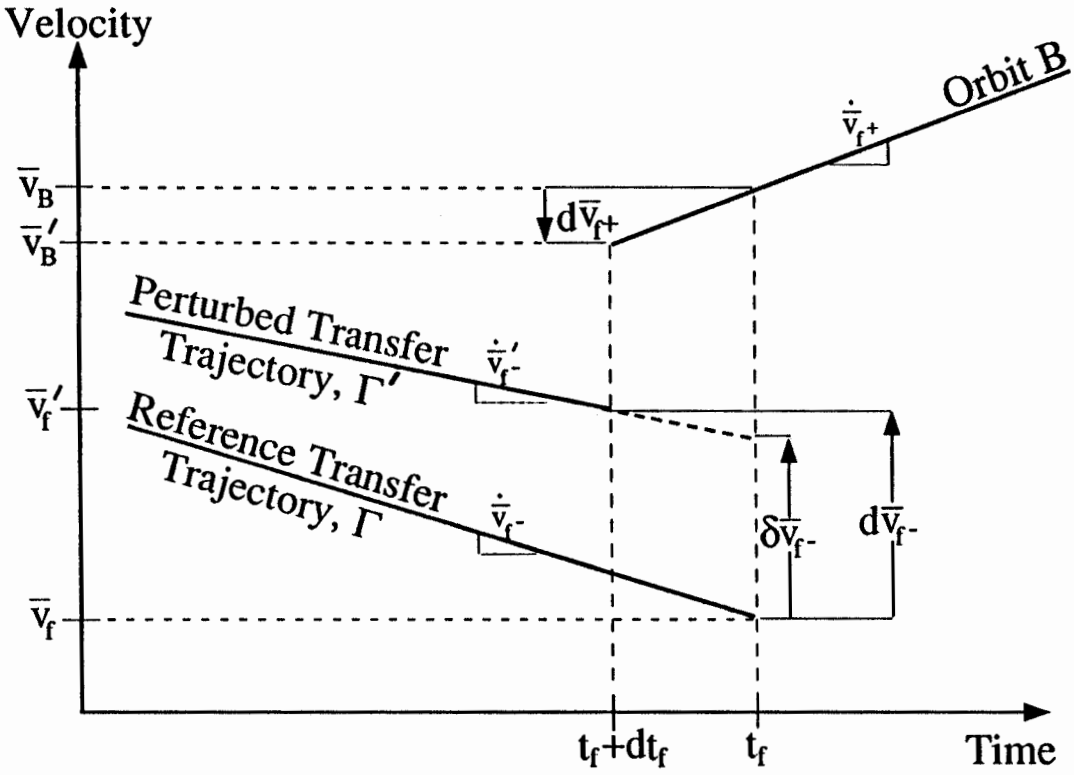

Figure 4.6 Contemporaneous and Noncontemporaneous Velocity Variations at the Instant of the Final Impulse

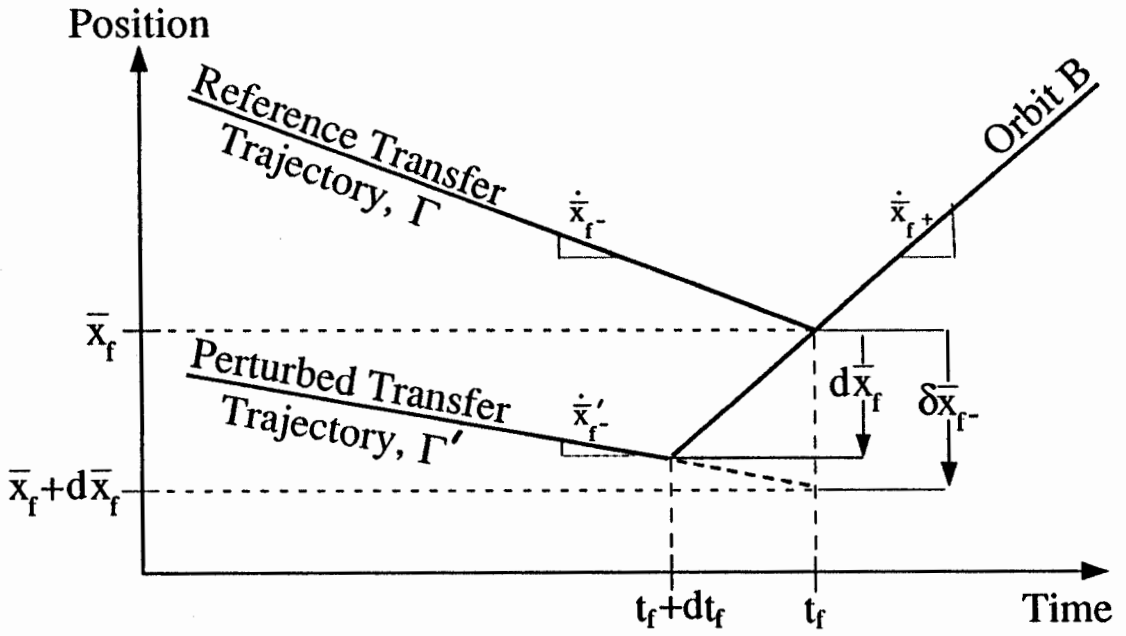

Figure 4.7 Contemporaneous and Noncontemporaneous Position Variations at the Instant of the Final Impulse

$$\delta J = \bar{p}_f^T \left[\dot{\bar{v}}_{f^+} - \dot{\bar{v}}_{f^-} \right] dt_f - \left[\dot{\bar{p}}_f^T + \bar{p}_f^T G_{v_f} \right] \delta \bar{x}_{f^-} \,. \tag{4.38}$$

Expressing the contemporaneous variation in position at $t = t_{f^-}$ in terms of the noncontemporaneous variation [See Figure 4.7],

$$\delta \bar{x}_{f^-} = d\bar{x}_f - \dot{\bar{x}}_{f^-}' dt_f = d\bar{x}_f - \bar{v}_f' \, dt_f \,,$$

and computing the velocity on the reference trajectory instead of the perturbed trajectory (*i.e.*, $\bar{v}_f' \approx \bar{v}_f$ to first order),

$$\delta \bar{x}_{f^-} = d\bar{x}_f - \bar{v}_f dt_f \,. \tag{4.39}$$

Recall that the coastal acceleration is denoted by $\bar{g}$, so $\dot{\bar{v}}_{f^+}$ which is the acceleration on orbit B immediately subsequent to the final impulse can be represented by the vector $\bar{g}_B$. Similarly, $\dot{\bar{v}}_{f^-}$, the acceleration on Γ immediately prior to the impulse at $t = t_f$, can be denoted by the vector $\bar{g}_f$. Implementing this notational change and substituting (4.39) into (4.38),

$$\delta J = \bar{p}_f^T (\bar{g}_B - \bar{g}_f) dt_f - \left[\dot{\bar{p}}_f^T + \bar{p}_f^T G_{v_f} \right] (d\bar{x}_f - \bar{v}_f dt_f) \,,$$

and regrouping terms,

$$\delta J = \bar{p}_f^T (\bar{g}_B - \bar{g}_f + G_{v_f} \bar{v}_f) dt_f - \dot{\bar{p}}_f^T (d\bar{x}_f - \bar{v}_f dt_f) - \bar{p}_f^T G_{v_f} d\bar{x}_f \,. \tag{4.40}$$

Notice that (4.40) contains the difference in acceleration across the final impulse (*i.e.*, $\bar{g}_B - \bar{g}_f$). Again, since the acceleration vector in the elliptic restricted three-body problem is a function of velocity, acceleration is discontinuous across the impulse, and the quantity $\bar{g}_B - \bar{g}_f$ is nonzero. Thus, examination of the accelerations at the final impulse is warranted in order to further simplify the expression for δJ.

Due to the existence of G_v in this elliptic restricted three-body formulation, the entire parenthetical coefficient of dt_f in equation (4.40) is evaluated for convenience. So, from the definitions of $\bar{g}$ and G_v, given in equations (3.3) and (3.10b), respectively,

$$\bar{g}_B - \bar{g}_f + G_{v_f}\bar{v}_f = \begin{bmatrix} 2nv_y + \dot{n}y + U_x \\ -2nv_x - \dot{n}x + U_y \\ U_z \end{bmatrix}\Bigg|_{t_f} - \begin{bmatrix} 2nv_y + \dot{n}y + U_x \\ -2nv_x - \dot{n}x + U_y \\ U_z \end{bmatrix}\Bigg|_{t_f} + \begin{bmatrix} 0 & 2n & 0 \\ -2n & 0 & 0 \\ 0 & 0 & 0 \end{bmatrix}\begin{bmatrix} v_x \\ v_y \\ v_z \end{bmatrix}\Bigg|_{t_f} . \tag{4.41}$$

Consistent with the discussion of an initial coast in the previous section, the partial derivatives U_x, U_y, and U_z must be continuous across the impulse at $t = t_f$. Consequently, equation (4.41) simplifies to,

$$\bar{g}_B - \bar{g}_f + G_{v_f}\bar{v}_f = \begin{bmatrix} 2nv_{y_{f^+}} - 2nv_{y_{f^-}} \\ -2nv_{x_{f^+}} + 2nv_{x_{f^-}} \\ 0 \end{bmatrix} + \begin{bmatrix} 2nv_{y_{f^-}} \\ -2nv_{x_{f^-}} \\ 0 \end{bmatrix} = \begin{bmatrix} 2nv_{y_{f^+}} \\ -2nv_{x_{f^+}} \\ 0 \end{bmatrix} . \tag{4.42}$$

Equation (4.42) corresponds to (4.19) for an initial coast. Also, note that

$$G_{v_f}\bar{v}_B = \begin{bmatrix} 0 & 2n & 0 \\ -2n & 0 & 0 \\ 0 & 0 & 0 \end{bmatrix}\begin{bmatrix} v_x \\ v_y \\ v_z \end{bmatrix}\Bigg|_{t_{f^+}} = \begin{bmatrix} 2nv_{y_{f^+}} \\ -2nv_{x_{f^+}} \\ 0 \end{bmatrix} .$$

So, equation (4.42) can be expressed as

$$\bar{g}_B - \bar{g}_f + G_{v_f}\bar{v}_f = G_{v_f}\bar{v}_B . \tag{4.43}$$

Substituting (4.43) into equation (4.40),

$$\delta J = \bar{p}_f^T G_{v_f}\bar{v}_B dt_f - \dot{\bar{p}}_f^T (d\bar{x}_f - \bar{v}_f dt_f) - \bar{p}_f^T G_{v_f} d\bar{x}_f ;$$

alternatively,

$$\delta J = \bar{p}_f^T G_{v_f}(\bar{v}_B dt_f - d\bar{x}_f) - \dot{\bar{p}}_f^T (d\bar{x}_f - \bar{v}_f dt_f) . \tag{4.44}$$

Writing the noncontemporaneous variation in position at $t = t_{f^+}$ in terms of the contemporaneous variation,

$$d\bar{x}_f = \delta\bar{x}_{f^+} + \dot{\bar{x}}_{f^+} dt_f ;$$

however, because the reference and perturbed trajectories are coincident on orbit B at the final instant (*i.e.*, at $t = t_{f^+}$) [See Figure 4.7], $\delta\bar{x}_{f^+}$ must equal zero and $\dot{\bar{x}}_{f^+}$ can be denoted $\bar{v}_B$. Thus,

$$d\bar{x}_f = \bar{v}_B dt_f \; ; \tag{4.45}$$

the first term in equation (4.44) is zero; and, the variation in the cost simplifies to

$$\delta J = -\dot{\bar{p}}_f^T d\bar{x}_f + \left[\dot{\bar{p}}_f^T \bar{v}_f\right] dt_f \; . \tag{4.46}$$

Equation (4.46) represents, to first order, the difference in cost between two neighboring trajectories whose final positions differ by $d\bar{x}_f$ and final times differ by dt_f. Because it is the analog of the transversality condition of the calculus of variations, equation (4.46) is called the *final coast transversality condition.* However, similar to equation (4.23) for an initial coast, (4.46) has wider applicability since neither trajectory need be an optimum. Once again, in spite of very different derivations, condition (4.46) is identical to the final coast transversality condition established by Lion and Handelsman for transfers in the two-body problem.

With the variation in cost between a reference trajectory and a perturbed trajectory, that has been allowed to coast in the final orbit B, determined, the criterion for the inclusion of such a final coast, in an effort to diminish fuel expenditure, can be developed. In a manner analogous to the initial coast analysis of the previous section, the noncontemporaneous variation in the position of the final impulse can be expressed solely in terms of the velocity on orbit B and the coastal period. So, the variation in cost can be expressed as

$$\delta J = -\dot{\bar{p}}_f^T (\bar{v}_B - \bar{v}_f) dt_f \; . \tag{4.47}$$

Because the coastal period is assumed to be negative (*i.e.*, $dt_f < 0$), δJ will be negative if and only if

$$\dot{\bar{p}}_f^T (\bar{v}_B - \bar{v}_f) < 0 \; . \tag{4.48}$$

Recall from equation (4.9b) that $\bar{p}_f$ is parallel to $(\bar{v}_B - \bar{v}_f)$; thus,

$$\dot{\bar{p}}_f^T \bar{p}_f < 0 \; . \tag{4.49}$$

Note that the determination of the scalar product of the primer vector and its derivative was addressed previously and was found to be

$$\dot{\bar{p}}^T \bar{p} = \frac{dp}{dt} p \; .$$

Evaluating (4.27) at $t = t_f$ and recalling that the primer vector magnitude is defined to be unity at the instant of the final impulse simplifies inequality (4.49) to

$$\frac{dp_f}{dt} < 0 , \tag{4.50}$$

where $\frac{dp_f}{dt}$ denotes the slope of the primer vector magnitude at the instant of the final impulse. If the slope of a plot of the magnitude of the primer vector is negative at $t = t_f$, then, from (4.50), the cost can be reduced. Consequently, a final coast would lower the characteristic velocity on the perturbed trajectory if the primer magnitude exceeds unity immediately prior to the final impulse.

Dual Coast

If a reference two-impulse trajectory is non-optimal, then the coincident application of both an initial and a final coast is explored as a means of reducing the total fuel expenditure. This dual coast procedure results in a two-impulse transfer whose terminal points have been moved in time and, consequently, in position. Therefore, execution and optimization of a dual coast transfer yields the optimal *time-free* two-impulse transfer trajectory between variable endpoints. Again, let Γ represent the reference two-impulse trajectory with impulses applied at t_0 and t_f, and let Γ' denote a neighboring two-impulse trajectory that has been allowed to coast in both the initial orbit A and the final orbit B. The impulses on Γ' are applied at $t_0 + dt_0$ and $t_f + dt_f$ where dt_0 and dt_f can be either positive or negative [See Figure 4.8]. Although Figure 4.8 depicts an *initial coast* ($dt_0 > 0$) and a *final coast* ($dt_f < 0$), the subsequent theoretical development is not restrictive of the sign of the coastal period. If $dt_0 < 0$, the spacecraft executes an *early departure* from orbit A; additionally, if $dt_f > 0$, the spacecraft performs a *late arrival* on orbit B. For a given reference transfer trajectory, minimum fuel considerations render the optimal choices for signs corresponding to the coastal periods.

The difference in cost between the reference trajectory and the dual coast trajectory can be inferred from the independently-calculated cost variations for the initial coast and for the final coast trajectories of the preceding sections. Recall that the initial and final coast transversality conditions are developed without restriction on the sign of the coastal periods. So, the variation in cost between Γ and Γ' can be represented as

$$\delta J = \delta J \text{ (Initial Coast)} + \delta J \text{ (Final Coast)} , \tag{4.51}$$

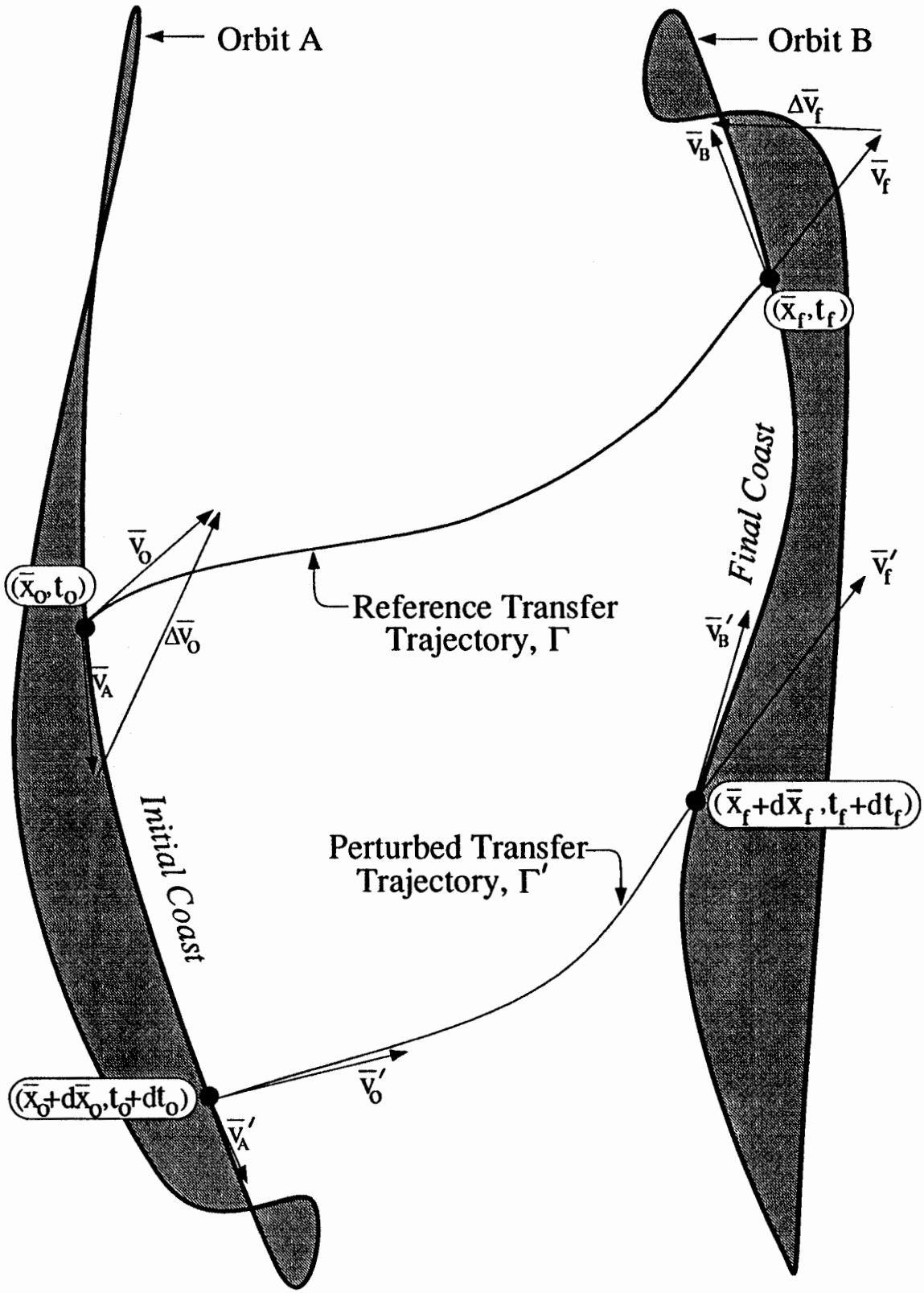

Figure 4.8 Dual Coast Geometry

and, substituting the initial coast and final coast transversality conditions (4.23) and (4.46) into (4.51),

$$\delta J = \dot{\bar{p}}_0^T d\bar{x}_0 - \left[\dot{\bar{p}}_0^T \bar{v}_0\right] dt_0 - \dot{\bar{p}}_f^T d\bar{x}_f + \left[\dot{\bar{p}}_f^T \bar{v}_f\right] dt_f \,. \tag{4.52}$$

Moreover, equation (4.52) is termed the *dual coast transversality condition.* Alternatively, substituting equations (4.24) and (4.47), which utilize expression of the noncontemporaneous variations in the positions of the terminal points in terms of orbital velocities and coastal periods, into (4.51),

$$\delta J = -\dot{\bar{p}}_0^T \Delta\bar{v}_0 dt_0 - \dot{\bar{p}}_f^T \Delta\bar{v}_f dt_f \,, \tag{4.53}$$

where

$$\Delta\bar{v}_0 = \bar{v}_0 - \bar{v}_A \tag{4.54a}$$

$$\Delta\bar{v}_f = \bar{v}_B - \bar{v}_f \tag{4.54b}$$

represent the terminal velocity impulses. Then, recall from equations (3.53) that

$$\bar{p}_0 = \frac{\Delta\bar{v}_0}{|\Delta\bar{v}_0|} \tag{4.55a}$$

$$\bar{p}_f = \frac{\Delta\bar{v}_f}{|\Delta\bar{v}_f|} \,; \tag{4.55b}$$

hence, rearranging (4.55),

$$\Delta\bar{v}_0 = \bar{p}_0 |\Delta\bar{v}_0| \tag{4.56a}$$

$$\Delta\bar{v}_f = \bar{p}_f |\Delta\bar{v}_f| \,. \tag{4.56b}$$

Replacing the velocity increments in (4.53) with equations (4.56),

$$\delta J = -\dot{\bar{p}}_0^T \bar{p}_0 |\Delta\bar{v}_0| dt_0 - \dot{\bar{p}}_f^T \bar{p}_f |\Delta\bar{v}_f| dt_f \,. \tag{4.57}$$

Recall from equation (4.27) that the scalar product of the primer vector and its derivative can be expressed as the product of the primer magnitude and the rate of change of this magnitude. So, evaluating (4.27) at the endpoints of the transfer trajectory and substituting into (4.57),

$$\delta J = -\dot{p}_0 p_0 |\Delta\bar{v}_0| dt_0 - \dot{p}_f p_f |\Delta\bar{v}_f| dt_f \,, \tag{4.58}$$

where p_0 and p_f denote the magnitude of the primer vector and $\dot{p}_0$ and $\dot{p}_f$ denote the slope of the magnitude of the primer vector at the initial and final impulses,

respectively. Since the primer vector is defined to have unit magnitude at the terminal points,

$$p_0 = p_f = 1 ;$$

consequently, equation (4.58) simplifies to

$$\delta J = - \dot{p}_0 \, | \Delta \bar{v}_0 | \, dt_0 - \dot{p}_f \, | \Delta \bar{v}_f | \, dt_f . \tag{4.59}$$

So, equation (4.59) represents, to first order, the variation in cost between the reference two-impulse trajectory and the perturbed, time-free two-impulse trajectory.

In order for a neighboring dual coast two-impulse trajectory with a lower cost than Γ to exist, the variation in cost must be made negative. From (4.59), a negative δJ requires that

$$- \dot{p}_0 \, | \Delta \bar{v}_0 | \, dt_0 - \dot{p}_f \, | \Delta \bar{v}_f | \, dt_f < 0 ,$$

or

$$- \dot{p}_0 \, | \Delta \bar{v}_0 | \, dt_0 < \dot{p}_f \, | \Delta \bar{v}_f | \, dt_f . \tag{4.60}$$

If inequality (4.60) is valid, then Γ' represents an improvement in cost, in terms of $\Delta \bar{v}$ expenditure, over Γ. Whether criterion (4.60) is met is dependent upon the sign associated with each coastal period and the slope of the primer magnitude at the terminal points. For all combinations of initial and final slope of the primer magnitude of the reference trajectory, condition (4.60) renders the relationship between the magnitudes of the coastal periods necessary for optimality. Also, the signs of the coastal periods are determined by compelling equation (4.59) to yield the largest negative variation in cost resulting in the greatest decrease in the fuel expenditure. The following four cases are representative of all possible combinations of initial and final slope of the primer magnitude:

CASE 1—Initial Slope Positive & Final Slope Negative ($\dot{p}_0 > 0$, $\dot{p}_f < 0$)

From (4.60),

$$- \| \dot{p}_0 \| \, | \Delta \bar{v}_0 | \, dt_0 < - \| \dot{p}_f \| \, | \Delta \bar{v}_f | \, dt_f ,$$

or

$$dt_0 > \frac{\| \dot{p}_f \| \, | \Delta \bar{v}_f |}{\| \dot{p}_0 \| \, | \Delta \bar{v}_0 |} dt_f .$$

From (4.59),

$$\delta J = -\left\|\dot{p}_0\right\| |\Delta\bar{v}_0| \, dt_0 + \left\|\dot{p}_f\right\| |\Delta\bar{v}_f| \, dt_f \, .$$

Therefore, the largest decrease in cost is attained if
$dt_0 > 0$ and $dt_f < 0 \rightarrow$ Initial Coast/Final Coast.

CASE 2—Initial Slope Positive & Final Slope Positive ($\dot{p}_0 > 0$, $\dot{p}_f > 0$)

From (4.60),

$$-\left\|\dot{p}_0\right\| |\Delta\bar{v}_0| \, dt_0 < \left\|\dot{p}_f\right\| |\Delta\bar{v}_f| \, dt_f \, ,$$

or

$$dt_0 > -\frac{\left\|\dot{p}_f\right\| |\Delta\bar{v}_f|}{\left\|\dot{p}_0\right\| |\Delta\bar{v}_0|} dt_f \, .$$

From (4.59),

$$\delta J = -\left\|\dot{p}_0\right\| |\Delta\bar{v}_0| \, dt_0 - \left\|\dot{p}_f\right\| |\Delta\bar{v}_f| \, dt_f \, .$$

Therefore, the largest decrease in cost is attained if
$dt_0 > 0$ and $dt_f > 0 \rightarrow$ Initial Coast/Late Arrival.

CASE 3—Initial Slope Negative & Final Slope Negative ($\dot{p}_0 < 0$, $\dot{p}_f < 0$)

From (4.60),

$$\left\|\dot{p}_0\right\| |\Delta\bar{v}_0| \, dt_0 < -\left\|\dot{p}_f\right\| |\Delta\bar{v}_f| \, dt_f \, ,$$

or

$$dt_0 < -\frac{\left\|\dot{p}_f\right\| |\Delta\bar{v}_f|}{\left\|\dot{p}_0\right\| |\Delta\bar{v}_0|} dt_f \, .$$

From (4.59),

$$\delta J = \left\|\dot{p}_0\right\| |\Delta\bar{v}_0| \, dt_0 + \left\|\dot{p}_f\right\| |\Delta\bar{v}_f| \, dt_f \, .$$

Therefore, the largest decrease in cost is attained if
$dt_0 < 0$ and $dt_f < 0 \rightarrow$ Early Departure/Final Coast.

CASE 4—Initial Slope Negative & Final Slope Positive ($\dot{p}_0 < 0$, $\dot{p}_f > 0$)

From (4.60),

$$\| \dot{p}_0 \| \, | \Delta \bar{v}_0 | \, dt_0 < \| \dot{p}_f \| \, | \Delta \bar{v}_f | \, dt_f \, ,$$

or

$$dt_0 < \frac{\| \dot{p}_f \| \, | \Delta \bar{v}_f |}{\| \dot{p}_0 \| \, | \Delta \bar{v}_0 |} dt_f \, .$$

From (4.59),

$$\delta J = \| \dot{p}_0 \| \, | \Delta \bar{v}_0 | \, dt_0 - \| \dot{p}_f \| \, | \Delta \bar{v}_f | \, dt_f \, .$$

Therefore, the largest decrease in cost is attained if
$dt_0 < 0$ and $dt_f > 0 \rightarrow$ Early Departure/Late Arrival.

The symbol $\| \, \|$ represents the absolute value of a scalar variable; whereas, the symbol $| \, |$ is reserved for the magnitude of a vector quantity. Figure 4.9 illustrates primer vector magnitude time histories depicting positive and negative initial and final primer slopes. The four possible combinations of initial and final slope conditions are representative of cases 1-4 which are encountered in the time-free optimization of a two-impulse transfer trajectory.

Note that equation (4.59) can be written in the form

$$\delta J = \nabla J \cdot d\bar{z} \, ,$$

where

$$\nabla J = \begin{bmatrix} - \dot{p}_0 \, | \Delta \bar{v}_0 | \\ - \dot{p}_f \, | \Delta \bar{v}_f | \end{bmatrix} , \tag{4.61}$$

and $\bar{z}$ is a vector comprised of the times of the initial and final impulsive maneuvers. Thus, the problem of determining an optimal trajectory becomes one of minimizing $J(\bar{z})$ by a multivariable search method. Since the gradients are known analytically in terms of the initial and final impulses and the derivative of the primer vector at the terminal points of the reference trajectory, a minimizing technique that utilizes the gradient components is indicated. One such technique that has been employed is the Broydon-Fletcher-Goldfarb-Shanno (BFGS) variable metric method for unconstrained

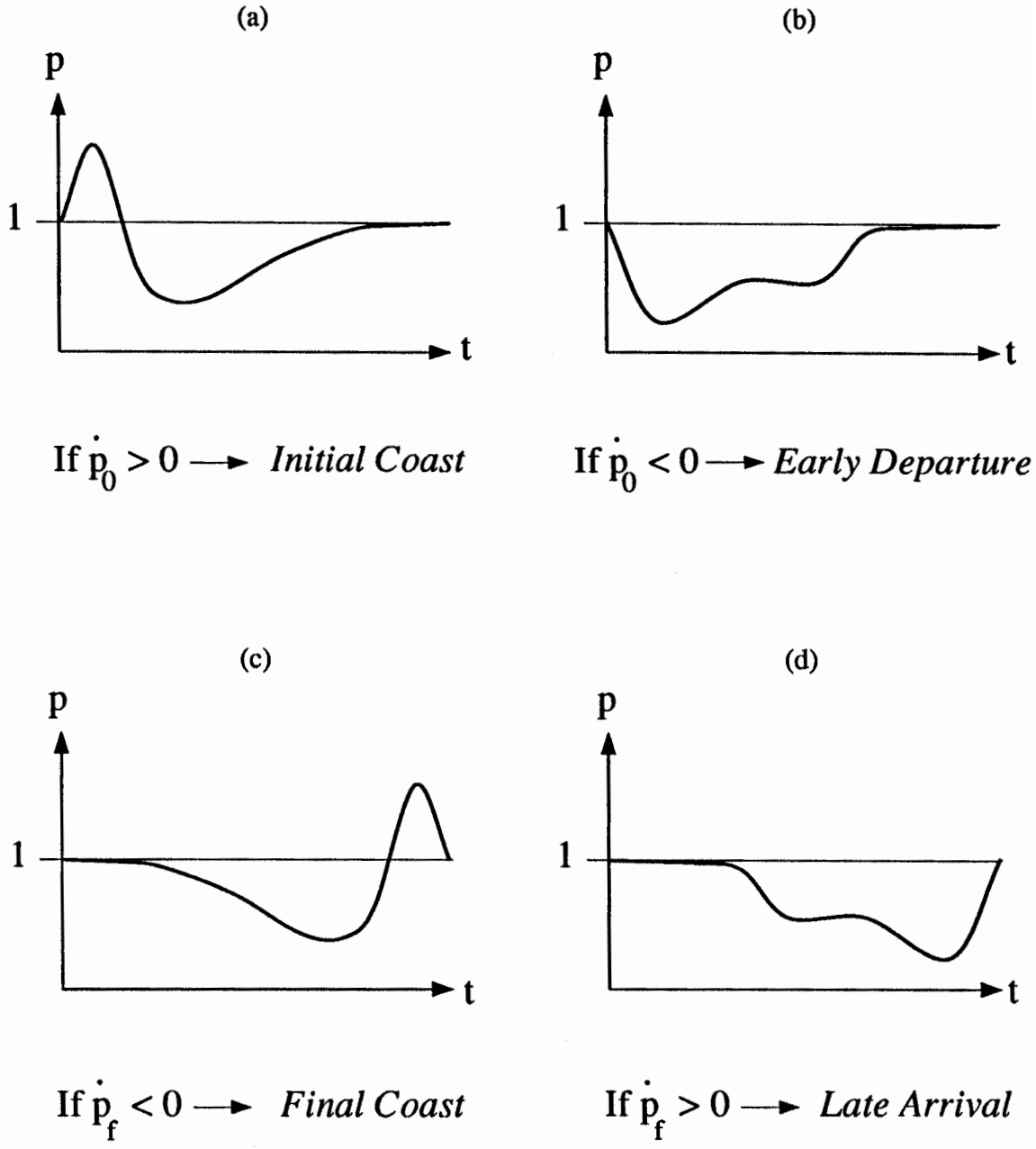

Figure 4.9 Primer Magnitude Time Histories Characteristic of Non-Optimal, Two-Impulse Trajectories Requiring (a) Initial Coast; (b) Early Departure; (c) Final Coast; and, (d) Late Arrival

minimization which is available in the Automated Design Synthesis (ADS) package developed by Vanderplaats.[71] A discussion of the numerical computation of the analytic gradients is delayed until the last section on this chapter.

Once the coastal periods that minimize the cost function are determined, the time of flight on the transfer trajectory is established and subsequently unmodified. The primer magnitude plot of the resultant transfer should display terminal points of zero slope. Additionally, if the primer magnitude, with the exception of the endpoints, lies entirely below unity, this two-impulse time-free transfer is optimal. However, should the primer magnitude exceed unity at any instant, then additional measures must be explored in order to further reduce the cost.

Additional Impulse

In order to investigate the effect of an additional impulse on the total cost needed to execute a desired transfer, a two-impulse trajectory is compared to a neighboring trajectory to which an interior impulse has been added. Recall that Γ represents a two-impulse trajectory from $\bar{x}_0$ at $t = t_0$ to $\bar{x}_f$ at $t = t_f$. Also, assume that Γ passes through a midpoint $\bar{x}_m$ at $t = t_m$. Let Γ' denote a neighboring three-impulse (perturbed) trajectory with the same terminal conditions as Γ; however, Γ' passes through the point $\bar{x}'_m$ at $t = t_m$ [See Figure 4.10].

Since Γ and Γ' have the same terminal points, $\delta\bar{x}_0 = \delta\bar{x}_f = 0$. The change in the velocities at the endpoints are chosen such that Γ' passes through $\bar{x}_m + \delta\bar{x}_m$ at $t = t_m$. The position vector on Γ' is obtained by expanding the position vector in a Taylor series about $\bar{x}$ (the position vector on the reference trajectory, Γ). Consider the first segment of Γ' (denoted Γ'_1) which originates at $(\bar{x}_0, t_0)$ and terminates at $(\bar{x}'_m, t_m)$. The Taylor series expansion, evaluated at $t = t_m$, for the position vector on Γ'_1 can be expressed as

$$\bar{x}'(t_m) - \bar{x}(t_m) = \delta\bar{x}_m = \frac{\partial\bar{x}(t_m)}{\partial\bar{x}_0}\delta\bar{x}_0 + \frac{\partial\bar{x}(t_m)}{\partial\bar{v}_0}\delta\bar{v}_0 + \bar{\chi}_0 , \qquad (4.62)$$

where $\bar{\chi}_0$ denotes a vector containing second and higher order terms. Recall that $\delta\bar{x}_0 = 0$ on the first segment of Γ'; therefore, (4.62) can be rearranged to yield

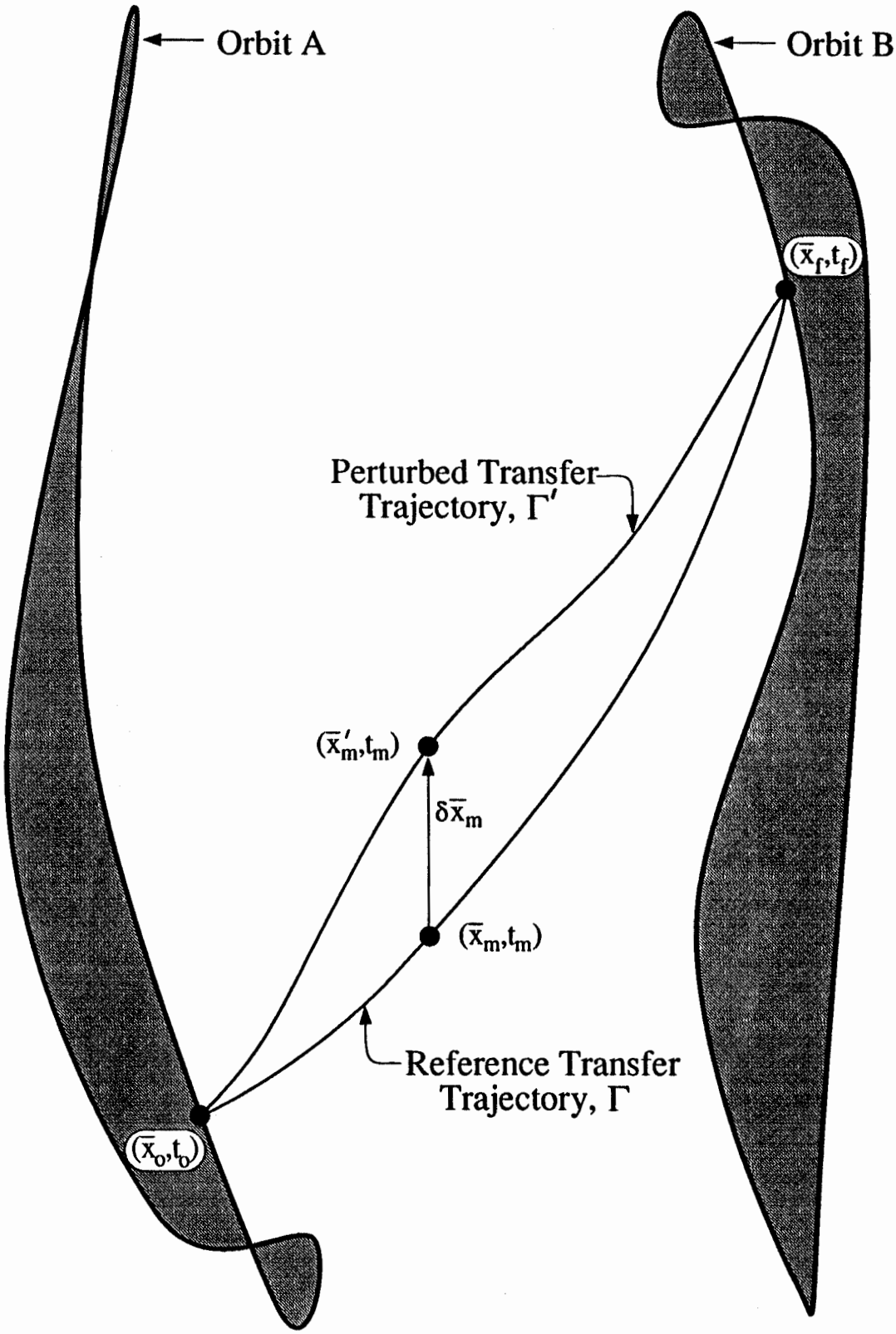

Figure 4.10 Two-Impulse Reference and Three-Impulse Perturbed Transfer Trajectories

$$\delta\bar{v}_0 = \left[\frac{\partial\bar{x}(t_m)}{\partial\bar{v}_0}\right]^{-1}\delta\bar{x}_m - \left[\frac{\partial\bar{x}(t_m)}{\partial\bar{v}_0}\right]^{-1}\bar{\chi}_0 \,. \tag{4.63}$$

The second term on the right side of (4.63) is a term of order higher than first order; hence, this term will subsequently be neglected. Thus, to first order, the contemporaneous variation in velocity at $t = t_0$ is

$$\delta\bar{v}_0 = \left[\frac{\partial\bar{x}_m}{\partial\bar{v}_0}\right]^{-1}\delta\bar{x}_m \,. \tag{4.64}$$

Next, consider the second segment of Γ' (denoted Γ_2') which originates at $(\bar{x}_m', t_m)$ and terminates at $(\bar{x}_f, t_f)$. The Taylor series expansion, evaluated at $t = t_m$, for the position vector on Γ_2' can be expressed as

$$\bar{x}'(t_m) - \bar{x}(t_m) = \delta\bar{x}_m = \frac{\partial\bar{x}(t_m)}{\partial\bar{x}_f}\delta\bar{x}_f + \frac{\partial\bar{x}(t_m)}{\partial\bar{v}_f}\delta\bar{v}_f + \bar{\chi}_f \,, \tag{4.65}$$

where $\bar{\chi}_f$ denotes a vector containing second and higher order terms. Again, recall that $\delta\bar{x}_f = 0$ on the second segment of Γ'; therefore, equation (4.65) is rearranged so that, to first order, the contemporaneous variations in velocity at $t = t_f$ is

$$\delta\bar{v}_f = \left[\frac{\partial\bar{x}_m}{\partial\bar{v}_f}\right]^{-1}\delta\bar{x}_m \,. \tag{4.66}$$

The partial derivatives in (4.64) and (4.66) can be determined by evaluating equation (3.80) from $t_0 \rightarrow t_m$ and from $t_f \rightarrow t_m$, respectively, and by utilizing the fact that $\delta\bar{x}_0 = \delta\bar{x}_f = 0$; thus, equations (4.64) and (4.66) simplify to

$$\delta\bar{v}_0 = \phi_{12}^{-1}(t_m, t_0)\,\delta\bar{x}_m \tag{4.67a}$$

$$\delta\bar{v}_f = \phi_{12}^{-1}(t_m, t_f)\,\delta\bar{x}_m \,, \tag{4.67b}$$

where ϕ_{12} is a submatrix of the partitioned state transition matrix. So, Γ' exists provided equations (4.67) are satisfied; hence, a sufficient condition for the existence of a neighboring three-impulse trajectory is that $\phi_{12}(t_m, t_0)$ and $\phi_{12}(t_m, t_f)$ are nonsingular.

Suppose that Γ, the two-impulse reference trajectory, is a transfer from orbit A to orbit B formed by applying velocity impulses $\Delta\bar{v}_0$ at $t = t_0$ and $\Delta\bar{v}_f$ at $t = t_f$. Since the

perturbed three-impulse transfer trajectory Γ' contains an intermediate (interior) velocity impulse, the velocities on Γ' differ from those on Γ; therefore, terminal velocity perturbations ($\delta\bar{v}_0$ at $t = t_0$ and $\delta\bar{v}_f$ at $t = t_f$) exist. From Figure 4.11, which illustrates the velocities on the reference and perturbed trajectories, the costs on Γ and Γ' can be written

$$J_\Gamma = |\Delta\bar{v}_0| + |\Delta\bar{v}_f| \,, \tag{4.68a}$$

and

$$J_{\Gamma'} = |\Delta\bar{v}_0 + \delta\bar{v}_0| + |\bar{v}'_{m^+} - \bar{v}'_{m^-}| + |\Delta\bar{v}_f - \delta\bar{v}_f| \,, \tag{4.68b}$$

where subscripts m^- and m^+ denote quantities evaluated immediately before and immediately after, respectively, the intermediate impulse occurring at $t = t_m$. The expression for the intermediate impulse on Γ' can be written in an alternate form. Note that the contemporaneous variations in velocity just prior to and subsequent to the impulse at $t = t_m$ are

$$\delta\bar{v}_{m^+} = \bar{v}'_{m^+} - \bar{v}_{m^+} \tag{4.69a}$$

$$\delta\bar{v}_{m^-} = \bar{v}'_{m^-} - \bar{v}_{m^-} \,. \tag{4.69b}$$

Subtracting (4.69b) from (4.69a),

$$\delta\bar{v}_{m^+} - \delta\bar{v}_{m^-} = \bar{v}'_{m^+} - \bar{v}'_{m^-} - (\bar{v}_{m^+} - \bar{v}_{m^-}) \,. \tag{4.70}$$

The quantity in parentheses in equation (4.70) is the difference in the velocity at $t = t_m$ on Γ, and, since no impulse occurs on the reference trajectory at this instant, this term must equal zero. Therefore, equation (4.70) is rearranged to yield the velocity increment of the intermediate impulse,

$$\bar{v}'_{m^+} - \bar{v}'_{m^-} = \delta\bar{v}_{m^+} - \delta\bar{v}_{m^-} \,. \tag{4.71}$$

Substituting (4.71) into (4.68b),

$$J_{\Gamma'} = |\Delta\bar{v}_0 + \delta\bar{v}_0| + |\delta\bar{v}_{m^+} - \delta\bar{v}_{m^-}| + |\Delta\bar{v}_f - \delta\bar{v}_f| \,. \tag{4.72}$$

So, the difference in cost, $J_{\Gamma'} - J_\Gamma$, is

$$\begin{aligned} \delta J = \; & |\Delta\bar{v}_0 + \delta\bar{v}_0| - |\Delta\bar{v}_0| + |\delta\bar{v}_{m^+} - \delta\bar{v}_{m^-}| + \\ & |\Delta\bar{v}_f - \delta\bar{v}_f| - |\Delta\bar{v}_f| \end{aligned} \,. \tag{4.73}$$

The variation in cost, denoted δJ, represents the difference between the cost on the reference trajectory and the cost on a perturbed trajectory that contains an interior

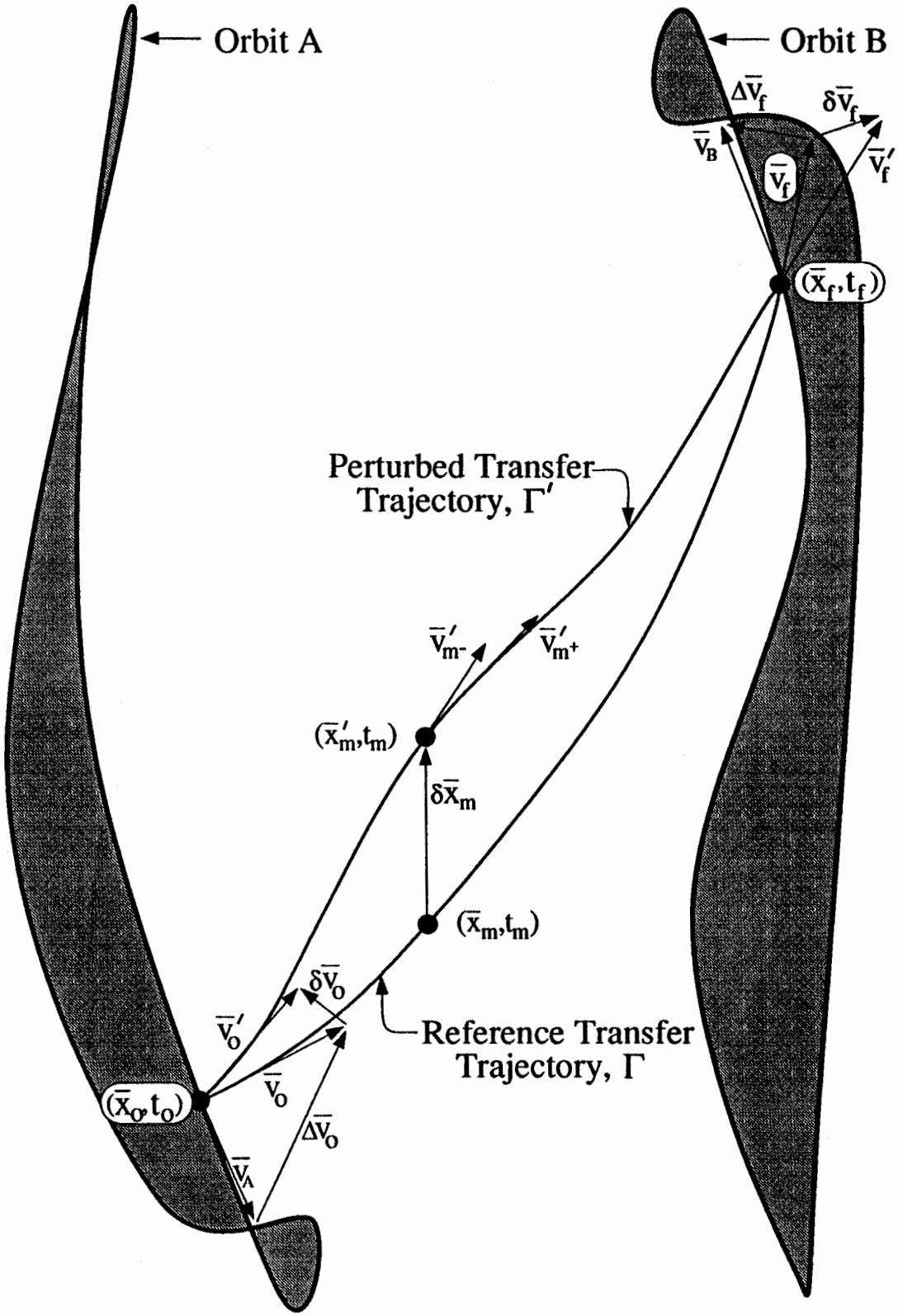

Figure 4.11 Additional Impulse Geometry

impulse. The expression for δJ given in (4.73) will subsequently be simplified in order to examine the feasibility of implementing an additional impulse such that the overall fuel expenditure is reduced.

Note that equation (4.73) contains expressions that represent the differences between the magnitudes of impulsive maneuvers on the perturbed and reference trajectories; thus, utilizing equation (4.6) in order to simplify these differences to first order,

$$|\Delta\bar{v}_0 + \delta\bar{v}_0| - |\Delta\bar{v}_0| = \frac{\Delta\bar{v}_0^T}{|\Delta\bar{v}_0|}\delta\bar{v}_0 \tag{4.74a}$$

$$|\Delta\bar{v}_f - \delta\bar{v}_f| - |\Delta\bar{v}_f| = -\frac{\Delta\bar{v}_f^T}{|\Delta\bar{v}_f|}\delta\bar{v}_f \,. \tag{4.74b}$$

Substituting equations (4.74) into (4.73),

$$\delta J = \frac{\Delta\bar{v}_0^T}{|\Delta\bar{v}_0|}\delta\bar{v}_0 + |\delta\bar{v}_{m^+} - \delta\bar{v}_{m^-}| - \frac{\Delta\bar{v}_f^T}{|\Delta\bar{v}_f|}\delta\bar{v}_f \,. \tag{4.75}$$

Recall that at the endpoints of a trajectory the primer vector is defined to have unit magnitude and to be aligned with the velocity increment; hence, the conditions at the endpoints of the reference transfer trajectory were specified in equations (3.53) and can be substituted into (4.75) to yield

$$\delta J = \bar{p}_0^T\delta\bar{v}_0 + |\delta\bar{v}_{m^+} - \delta\bar{v}_{m^-}| - \bar{p}_f^T\delta\bar{v}_f \,. \tag{4.76}$$

Additionally, the adjoint equation from (3.91),

$$\bar{p}^T\delta\bar{v} - \left[\dot{\bar{p}}^T + \bar{p}^T G_v\right]\delta\bar{x} = \text{constant} \,,$$

was previously determined to be valid everywhere on a coastal arc of a perturbed trajectory. In equation (3.91), $\bar{p}$ and $\dot{\bar{p}}$ are computed on the reference trajectory Γ; whereas, $\delta\bar{x}$ and $\delta\bar{v}$ are the position and velocity variations, respectively, of the perturbed trajectory from the reference trajectory. So, evaluate (3.91) on the two coastal arcs of Γ'.

First, on Γ_1':

$$@\ t = t_0, \qquad \bar{p}_0^T\delta\bar{v}_0 - \left[\dot{\bar{p}}_0^T + \bar{p}_0^T G_{v_0}\right]\delta\bar{x}_0 = C_1 \tag{4.77a}$$

$$@\ t = t_{m^-}, \quad \bar{p}_{m^-}^T\delta\bar{v}_{m^-} - \left[\dot{\bar{p}}_{m^-}^T + \bar{p}_{m^-}^T G_{v_{m^-}}\right]\delta\bar{x}_{m^-} = C_1 \,, \tag{4.77b}$$

where C_1 denotes the constant on coastal arc Γ_1'. Recalling that $\delta\bar{x}_0 = 0$ and equating the constants,

$$\bar{p}_0^T \delta\bar{v}_0 = \bar{p}_{m^-}^T \delta\bar{v}_{m^-} - \left[\dot{\bar{p}}_{m^-}^T + \bar{p}_{m^-}^T G_{v_{m^-}}\right]\delta\bar{x}_{m^-} . \tag{4.78}$$

Secondly, on Γ_2':

$$@\ t = t_{m^+}, \quad \bar{p}_{m^+}^T \delta\bar{v}_{m^+} - \left[\dot{\bar{p}}_{m^+}^T + \bar{p}_{m^+}^T G_{v_{m^+}}\right]\delta\bar{x}_{m^+} = C_2 \tag{4.79a}$$

$$@\ t = t_f, \quad \bar{p}_f^T \delta\bar{v}_f - \left[\dot{\bar{p}}_f^T + \bar{p}_f^T G_{v_f}\right]\delta\bar{x}_f = C_2 , \tag{4.79b}$$

where C_2 denotes the constant on coastal arc Γ_2'. Recalling that $\delta\bar{x}_f = 0$ and equating the constants,

$$\bar{p}_f^T \delta\bar{v}_f = \bar{p}_{m^+}^T \delta\bar{v}_{m^+} - \left[\dot{\bar{p}}_{m^+}^T + \bar{p}_{m^+}^T G_{v_{m^+}}\right]\delta\bar{x}_{m^+} . \tag{4.80}$$

Subtracting equation (4.80) from (4.78),

$$\begin{aligned} \bar{p}_0^T \delta\bar{v}_0 - \bar{p}_f^T \delta\bar{v}_f = \ & \bar{p}_{m^-}^T \delta\bar{v}_{m^-} - \left[\dot{\bar{p}}_{m^-}^T + \bar{p}_{m^-}^T G_{v_{m^-}}\right]\delta\bar{x}_{m^-} - \\ & \bar{p}_{m^+}^T \delta\bar{v}_{m^+} + \left[\dot{\bar{p}}_{m^+}^T + \bar{p}_{m^+}^T G_{v_{m^+}}\right]\delta\bar{x}_{m^+} \quad . \end{aligned} \tag{4.81}$$

As noted previously, the primer vector and its derivative are calculated on the reference trajectory Γ, which is a coastal arc (*i.e.*, no impulses exist interior to the terminal impulses at $\bar{x} = \bar{x}_0$ and $\bar{x} = \bar{x}_f$); thus, $\bar{p}$ and $\dot{\bar{p}}$ are continuous. So,

$$\bar{p}_{m^-} = \bar{p}_{m^+} \ \text{ and } \ \dot{\bar{p}}_{m^-} = \dot{\bar{p}}_{m^+} . \tag{4.82}$$

Additionally, since matrix G_v, which is computed on the reference trajectory, is solely a function of n (the angular velocity associated with the two-body problem defining the primary motion—a continuous function), G_v must be continuous; hence,

$$G_{v_{m^-}} = G_{v_{m^+}} . \tag{4.83}$$

In light of equations (4.82) and (4.83), the superscripts + and – can be dropped from the subscripts on the quantities $\bar{p}_m$, $\dot{\bar{p}}_m$, and G_{v_m}. Then, rearranging equation (4.81),

$$\bar{p}_0^T \delta\bar{v}_0 - \bar{p}_f^T \delta\bar{v}_f = \bar{p}_m^T(\delta\bar{v}_{m^-} - \delta\bar{v}_{m^+}) + \left[\dot{\bar{p}}_m^T + \bar{p}_m^T G_{v_m}\right](\delta\bar{x}_{m^+} - \delta\bar{x}_{m^-}) . \tag{4.84}$$

Note that, despite the allowance for a discontinuity in velocity at $t = t_m$, the perturbed trajectory is still required to be continuous in position at this instant (*i.e.*, $\delta\bar{x}_{m^+} = \delta\bar{x}_{m^-}$);

thus, the last term in the equation above must equal zero, and (4.84) simplifies to

$$\bar{p}_0^T \delta\bar{v}_0 - \bar{p}_f^T \delta\bar{v}_f = \bar{p}_m^T (\delta\bar{v}_{m^-} - \delta\bar{v}_{m^+}) . \tag{4.85}$$

Substituting (4.85) into (4.76) renders an expression for the variation in cost which, to first order, can be written as

$$\delta J = -\bar{p}_m^T (\delta\bar{v}_{m^+} - \delta\bar{v}_{m^-}) + |\delta\bar{v}_{m^+} - \delta\bar{v}_{m^-}| . \tag{4.86}$$

Equation (4.86) expresses δJ solely in terms of the primer vector at the interior impulse and the intermediate velocity increment itself.

Now that the variation in cost between Γ and Γ' has been determined, the criterion for the inclusion of an intermediate impulse on a transfer trajectory in order to reduce the cost can be developed. If δJ can be made negative, then Γ' represents an improvement in cost over Γ. Let κ denote the magnitude of the intermediate impulse, and let $\hat{\eta}$ denote a unit vector in the direction of the impulse such that

$$(\delta\bar{v}_{m^+} - \delta\bar{v}_{m^-}) = \kappa\hat{\eta} ;$$

then the variation in cost (4.86) can be expressed as

$$\delta J = \kappa(1 - \bar{p}_m^T \hat{\eta}) . \tag{4.87}$$

Illustrating that only if the magnitude of the primer vector at $t = t_m$ is greater than unity can $\delta J < 0$, equation (4.87) constitutes an alternate proof of the necessary conditions for Γ to be optimal. If the magnitude of the primer vector is greater than one at any time, then there exists a three-impulse trajectory that has a lower cost than the reference two-impulse trajectory. Additionally, the greatest improvement in cost, to first order, can be realized by applying the intermediate impulse at the instant that the primer magnitude attains its maximum (*i.e.*, $\dot{\bar{p}} = 0$) and in the direction of the primer vector. However, the position on Γ' at $t = t_m$ as well as the magnitude of the interior impulse are yet to be determined.

If the state transition matrix is evaluated from $t_0 \rightarrow t_{m^-}$ and from $t_f \rightarrow t_{m^+}$ and if $\delta\bar{x}_0 = \delta\bar{x}_f = 0$, the following relations are obtained from equation (3.80):

$$\delta\bar{x}_{m^-} = \phi_{12}(t_m, t_0)\delta\bar{v}_0 \tag{4.88a}$$

$$\delta\bar{v}_{m^-} = \phi_{22}(t_m, t_0)\delta\bar{v}_0 , \tag{4.88b}$$

and

$$\delta\bar{x}_{m^+} = \phi_{12}(t_m, t_f)\delta\bar{v}_f \tag{4.89a}$$

$$\delta\bar{v}_{m^+} = \phi_{22}(t_m, t_f)\delta\bar{v}_f \,. \tag{4.89b}$$

So, subtracting (4.88b) from (4.89b) in order to form the difference in the contemporaneous variation in velocity at the instant of the intermediate impulse (*i.e.*, the velocity increment by equation (4.71)),

$$\delta\bar{v}_{m^+} - \delta\bar{v}_{m^-} = \phi_{22}(t_m, t_f)\delta\bar{v}_f - \phi_{22}(t_m, t_0)\delta\bar{v}_0 \,. \tag{4.90}$$

Inverting equations (4.88a) and (4.89a) and noting that position continuity requires that $\delta\bar{x}_{m^-} = \delta\bar{x}_{m^+} = \delta\bar{x}_m$,

$$\delta\bar{v}_0 = \phi_{12}^{-1}(t_m, t_0)\delta\bar{x}_m \tag{4.91a}$$

$$\delta\bar{v}_f = \phi_{12}^{-1}(t_m, t_f)\delta\bar{x}_m \,. \tag{4.91b}$$

Recall that (4.91), which are the expressions for the contemporaneous variations in velocity at the terminal points of the transfer trajectory in terms of the contemporaneous variation in the position of the intermediate impulse, were specified previously in equations (4.67). Equations (4.91) can be substituted into (4.90) to yield

$$\delta\bar{v}_{m^+} - \delta\bar{v}_{m^-} = \left[\phi_{22}(t_m, t_f)\phi_{12}^{-1}(t_m, t_f) - \phi_{22}(t_m, t_0)\phi_{12}^{-1}(t_m, t_0)\right]\delta\bar{x}_m \,. \tag{4.92}$$

Hence,

$$\delta\bar{v}_{m^+} - \delta\bar{v}_{m^-} = A\delta\bar{x}_m \,, \tag{4.93}$$

where

$$A \triangleq \phi_{22}(t_m, t_f)\phi_{12}^{-1}(t_m, t_f) - \phi_{22}(t_m, t_0)\phi_{12}^{-1}(t_m, t_0) \,. \tag{4.94}$$

For the maximum improvement in cost, the velocity increment, $(\delta\bar{v}_{m^+} - \delta\bar{v}_{m^-}) = \kappa\hat{\eta}$, should be aligned with $\bar{p}_m^T$. Therefore, assuming that matrix A is non-singular, choose

$$\delta\bar{x}_m = \kappa A^{-1}\frac{\bar{p}_m}{|\bar{p}_m|} \,; \tag{4.95}$$

also, κ should be selected small enough to ensure that a first order analysis is sufficient.

Jezewski and Rozendaal[54] retain second order terms in the expression for the variation in cost for a two-body problem analysis in order to develop a first estimate for the magnitude of the intermediate impulse. In this formulation of the three-body problem, the state transition matrix for the elliptic restricted three-body problem must be

computed numerically; hence, a higher order approximation for the impulse magnitude holds no distinct advantage over the *exact* (within the limitations of the linear nature of the state transition matrix) numerical computation of κ. The determination of the impulse magnitude that results in the greatest decrease in the cost function requires the iterative solution of an algebraic expression for the cost on Γ' as a function of κ; this expression is developed below. Substituting (4.95) into equations (4.91),

$$\delta\bar{v}_0 = \kappa\phi_{12}^{-1}(t_m, t_0)A^{-1}\frac{\bar{p}_m}{|\bar{p}_m|} \tag{4.96a}$$

$$\delta\bar{v}_f = \kappa\phi_{12}^{-1}(t_m, t_f)A^{-1}\frac{\bar{p}_m}{|\bar{p}_m|}\,. \tag{4.96b}$$

Define the vectors $\bar{\alpha}$ and $\bar{\beta}$ such that

$$\bar{\alpha} \triangleq \phi_{12}^{-1}(t_m, t_0)A^{-1}\frac{\bar{p}_m}{|\bar{p}_m|} \tag{4.97a}$$

$$\bar{\beta} \triangleq \phi_{12}^{-1}(t_m, t_f)A^{-1}\frac{\bar{p}_m}{|\bar{p}_m|}\,; \tag{4.97b}$$

then, equations (4.96) can be expressed as

$$\delta\bar{v}_0 = \kappa\bar{\alpha} \tag{4.98a}$$

$$\delta\bar{v}_f = \kappa\bar{\beta}\,. \tag{4.98b}$$

Next, from the definition of a contemporaneous variation, the impulsive maneuvers at the terminal points of Γ' are

$$\Delta\bar{v}_0' = \Delta\bar{v}_0 + \delta\bar{v}_0$$

$$\Delta\bar{v}_f' = \Delta\bar{v}_f - \delta\bar{v}_f\,,$$

or, in terms of the $\bar{\alpha}$ and $\bar{\beta}$,

$$\Delta\bar{v}_0' = \Delta\bar{v}_0 + \kappa\bar{\alpha} \tag{4.99a}$$

$$\Delta\bar{v}_f' = \Delta\bar{v}_f - \kappa\bar{\beta}\,. \tag{4.99b}$$

The cost on the perturbed trajectory, which was expressed in (4.72), is simply the sum of the magnitudes of the impulsive maneuvers on Γ', or

$$J_{\Gamma'} = |\Delta\bar{v}_0'| + |\Delta\bar{v}_f'| + \kappa\,. \tag{4.100}$$

Thus, substituting equations (4.99) into (4.100) and expressing the magnitudes in (4.100) as the square root of the vector sum squared,

$$J_{\Gamma'} = \left[\Delta\bar{v}_0^T\Delta\bar{v}_0 + 2\kappa\bar{\alpha}^T\Delta\bar{v}_0 + \kappa^2\bar{\alpha}^T\bar{\alpha}\right]^{\frac{1}{2}} + \left[\Delta\bar{v}_f^T\Delta\bar{v}_f - 2\kappa\bar{\beta}^T\Delta\bar{v}_f + \kappa^2\bar{\beta}^T\bar{\beta}\right]^{\frac{1}{2}} + \kappa\,. \tag{4.101}$$

Now, equation (4.101) can be solved iteratively for the value of κ that renders the minimum $J_{\Gamma'}$; also, the position on Γ' at which the intermediate impulse should be applied is given by $\bar{x}_m' = \bar{x}_m + \delta\bar{x}_m$, where $\bar{x}_m$ is the position on Γ where the magnitude of the primer vector attains its maximum value and $\delta\bar{x}_m$ is specified in equation (4.95).

Movement of an Interior Impulse

The inclusion of an additional impulse does not necessarily yield an optimal three-impulse trajectory. The time history of the magnitude of the primer vector for each two-impulse segment of Γ' must be examined in order to determine if each segment satisfies the necessary conditions for an optimal trajectory. A typical non-optimal trajectory is characterized by a cusp at the location of the intermediate impulse. Recall that the derivative of the primer vector must be continuous over the duration of an optimal trajectory; however, since the primer derivative is discontinuous at the cusp, then a neighboring three-impulse trajectory with a lower cost must exist.

Let Γ now denote the reference three-impulse trajectory that contains an interior impulse at $(\bar{x}_m, t_m)$, and let Γ' be considered a perturbed three-impulse trajectory that consists of two trajectory segments connecting the states

$$(\bar{x}_0, t_0) \rightarrow (\bar{x}_m + d\bar{x}_m, t_m + dt_m)$$

$$(\bar{x}_m + d\bar{x}_m, t_m + dt_m) \rightarrow (\bar{x}_f, t_f)\,,$$

so that the interior impulse on Γ' occurs at $(\bar{x}_m', t_m')$. Note that movement of the interior impulse from $(\bar{x}_m, t_m)$ to $(\bar{x}_m', t_m')$ is equivalent to execution of a final coast on that segment prior to the interior impulse combined with execution of an initial coast on that segment following the interior impulse. In other words, the variation in cost of the perturbed three-impulse trajectory can be derived from the transversality conditions for an initial coast and for a final coast by allowing each coast to occur at $t = t_m$. In terms

of cost variations on coast trajectories, the difference in cost between Γ and Γ' is

$$\delta J = \left[\delta J \text{ (Final Coast)}\right]\Big|_{t_{m^-}} + \left[\delta J \text{ (Initial Coast)}\right]\Big|_{t_{m^+}} . \tag{4.102}$$

Evaluating the final coast transversality condition (4.46) at $t = t_{m^-}$ instead of at $t = t_f$,

$$\left[\delta J \text{ (Final Coast)}\right]\Big|_{t_{m^-}} = -\dot{\bar{p}}_{m^-}^T d\bar{x}_m + \left(\dot{\bar{p}}_{m^-}^T \bar{v}_{m^-}\right) dt_m , \tag{4.103a}$$

and evaluating the initial coast transversality condition (4.23) at $t = t_{m^+}$ instead of at $t = t_0$,

$$\left[\delta J \text{ (Initial Coast)}\right]\Big|_{t_{m^+}} = \dot{\bar{p}}_{m^+}^T d\bar{x}_m - \left(\dot{\bar{p}}_{m^+}^T \bar{v}_{m^+}\right) dt_m , \tag{4.103b}$$

and substituting (4.103) into (4.102),

$$\delta J = -\dot{\bar{p}}_{m^-}^T d\bar{x}_m + \left(\dot{\bar{p}}_{m^-}^T \bar{v}_{m^-}\right) dt_m + \dot{\bar{p}}_{m^+}^T d\bar{x}_m - \left(\dot{\bar{p}}_{m^+}^T \bar{v}_{m^+}\right) dt_m . \tag{4.104}$$

Rearranging (4.104),

$$\delta J = \left(\dot{\bar{p}}_{m^+}^T - \dot{\bar{p}}_{m^-}^T\right) d\bar{x}_m + \left[\left(\dot{\bar{p}}_{m^-}^T \bar{v}_{m^-}\right) - \left(\dot{\bar{p}}_{m^+}^T \bar{v}_{m^+}\right)\right] dt_m , \tag{4.105}$$

and the variation in cost is expressed in terms of the noncontemporaneous variations in the position and time of the interior impulse.

Recall that the Hamiltonian on a coastal arc is written

$$H = \bar{p}^T \bar{g} - \left(\dot{\bar{p}}^T + \bar{p}^T G_v\right) \bar{v} .$$

Evaluating the Hamiltonian prior to and subsequent to the intermediate impulse on the reference trajectory and noting that the primer vector is continuous across an impulse (*i.e.*, $\bar{p}_{m^+} = \bar{p}_{m^-}$),

$$\begin{aligned} H_{m^+} - H_{m^-} = \; & \bar{p}_{m^+}^T \bar{g}_{m^+} - \left(\dot{\bar{p}}_{m^+}^T + \bar{p}_{m^+}^T G_{v_{m^+}}\right) \bar{v}_{m^+} - \\ & \left[\bar{p}_{m^-}^T \bar{g}_{m^-} - \left(\dot{\bar{p}}_{m^-}^T + \bar{p}_{m^-}^T G_{v_{m^-}}\right) \bar{v}_{m^-}\right] . \end{aligned} \tag{4.106}$$

Thus, by rearranging (4.106), the expression for the jump in the Hamiltonian at the corner of the reference trajectory is

$$H_{m^+} - H_{m^-} = \bar{p}_m^T \left[\left(\bar{g}_{m^+} - G_{v_{m^+}} \bar{v}_{m^+} \right) - \left(\bar{g}_{m^-} - G_{v_{m^-}} \bar{v}_{m^-} \right) \right] + \dot{\bar{p}}_{m^-}^T \bar{v}_{m^-} - \dot{\bar{p}}_{m^+}^T \bar{v}_{m^+} \quad . \tag{4.107}$$

Recall that the quantity,

$$\bar{g} - G_v \bar{v} = \begin{Bmatrix} \dot{n}y + U_x \\ -\dot{n}x + U_y \\ U_z \end{Bmatrix},$$

was previously determined to be continuous at a corner since the partial derivatives of the pseudo-potential, the position coordinates, and $\dot{n}$ are all continuous at a corner. Hence, the term in brackets in equation (4.107) disappears, and the discontinuity in the Hamiltonian at the instant of the intermediate impulse reduces to

$$H_{m^+} - H_{m^-} = \dot{\bar{p}}_{m^-}^T \bar{v}_{m^-} - \dot{\bar{p}}_{m^+}^T \bar{v}_{m^+} \quad . \tag{4.108}$$

Substituting equation (4.108) into (4.105) allows the variation in cost to be written as

$$\delta J = \left(\dot{\bar{p}}_{m^+}^T - \dot{\bar{p}}_{m^-}^T \right) d\bar{x}_m + \left(H_{m^+} - H_{m^-} \right) dt_m \quad . \tag{4.109}$$

So, equation (4.109) represents the difference in the costs on the reference three-impulse trajectory and a neighboring three-impulse trajectory whose interior impulse is moved by an amount $d\bar{x}_m$ in position and by an amount dt_m in time, where $d\bar{x}_m$ and dt_m are chosen independently.

If the reference trajectory is an optimum, $\delta J = 0$; consequently, the Hamiltonian and the first derivative of the primer vector must both be continuous across the impulse. That is,

$$\dot{\bar{p}}_{m^+} = \dot{\bar{p}}_{m^-} \quad \text{and} \quad H_{m^+} = H_{m^-} \quad .$$

Then, from equation (4.108),

$$H_{m^+} - H_{m^-} = 0 = \dot{\bar{p}}_m^T (\bar{v}_{m^-} - \bar{v}_{m^+}) \; ; \tag{4.110}$$

however, since the primer vector at $t = t_m$ is aligned with the velocity impulse $(\bar{v}_{m^+} - \bar{v}_{m^-})$, the right side of (4.110) simplifies to

$$\dot{\bar{p}}_m^T \bar{p}_m = 0 \, . \tag{4.111}$$

Equation (4.111), equivalent to equation (3.63) evaluated at $t = t_m$, confirms that $\dot{\bar{p}}$ must be zero on an optimal trajectory at the instants of impulsive maneuvers and constitutes an alternate proof of the fourth necessary condition.

If either the derivative of the primer vector or the Hamiltonian is discontinuous, then the reference trajectory is not an optimum, and a neighboring trajectory with a lower cost must exist. Note that equation (4.109) can be written in the form

$$\delta J = \nabla J \cdot d\bar{z}\,, \tag{4.112}$$

where

$$\nabla J = \begin{bmatrix} \dot{\bar{p}}_{m^+} - \dot{\bar{p}}_{m^-} \\ H_{m^+} - H_{m^-} \end{bmatrix}, \tag{4.113}$$

and $\bar{z}$ is a vector comprised of the position vector and time of the intermediate impulse. Thus, the problem of determining an optimal trajectory becomes one of minimizing $J(\bar{z})$ by some multivariable search method. Since the gradients are known analytically in terms of the derivative of the primer vector and the velocity on the reference three-impulse trajectory, a minimizing technique that utilizes the gradient components is indicated. Again, the technique that is employed is the Broydon-Fletcher-Goldfarb-Shanno (BFGS) variable metric method for unconstrained minimization which is available in the ADS package developed by Vanderplaats.[71]

After the four variables (associated with the location and time of the additional impulse) that render the minimum cost are determined, the primer magnitude history of the resultant transfer is examined in order to ascertain whether a second interior impulse would lower fuel expenditure. If the primer magnitude exceeds unity at any time on the optimal three-impulse transfer trajectory, another impulse is implemented, and its time and location are optimized via the above algorithm. Thus, the position and time of each intermediate impulse are optimized prior to evaluation of the need for an additional impulse. If K interior impulses are deemed necessary to yield an optimal transfer trajectory, then the minimization of the cost is accomplished by K successive minimizations of equation (4.112) using a multivariable search technique. Noteworthy is the fact that the methodology applied to transfers in the more traditional two-body problem computes the optimal locations and times of K interior impulses by the minimization of a single function of 4K variables.[54] In contradistinction, a similar approach to multiple-interior-impulse solutions in this formulation of the three-body problem

destroys the integrity of the numerical solutions for the initial and final halo orbits. Hence, the position and time of the k*th* ($1 \le k < K$) interior impulse are unaltered during the optimization of the K*th* impulse; consequently, a very slight cusp may appear in the primer magnitude plot at the instant of the k*th* impulse.

Computation of Analytic Gradients

Although the gradients that appear in equations (4.61) and (4.113) are known analytic functions, the solution for the spacecraft's trajectory in the elliptic restricted three-body problem must be determined numerically; hence, the actual values of the gradients along the trajectory are known only at distinct instants. Consequently, if the values of the gradients are unknown, they must be approximated at the desired time. Only the computation of the gradients arising from consideration of the addition of an interior impulse is presented below; however, the gradients associated with the dual coast cost function can be determined in an analogous manner.

In order to evaluate the gradients at the instant of the interior impulse, the values of the primer derivative and of the Hamiltonian must be known on both the plus- and minus-side of $t = t_m$. If the states $(\bar{x}_m, t_m)$ result from the i*th* integration step, then the derivative of the primer vector and the Hamiltonian on the minus-side of the impulse are just given by their values at the i*th* step. That is,

$$\dot{\bar{p}}_{m^-} = \dot{\bar{p}}_i \tag{4.114}$$

$$H_{m^-} = H_i \, . \tag{4.115}$$

However, the primer derivative and the Hamiltonian on the plus-side of the impulse must be approximated from their values resulting from integration steps beyond the i*th* step. Since the first derivatives of $\dot{\bar{p}}$ and H can be readily computed, a first-order approximation is chosen; additionally, in an effort to increase the accuracy of the approximation, information at both the first and the second steps beyond the impulse are utilized. Consequently, the derivative of the primer vector and the Hamiltonian on the plus-side of the interior impulse are calculated using a two-step, first-order, backward difference approximation.

Suppose f(x) represents an arbitrary, smooth, continuous function. Then, the value of f(x) at $x = x_i$ can be determined from knowledge of the function and its derivative at $x = x_{i+1}$ and at $x = x_{i+2}$ [See Figure 4.12]. Expanding f(x) in a Taylor series about

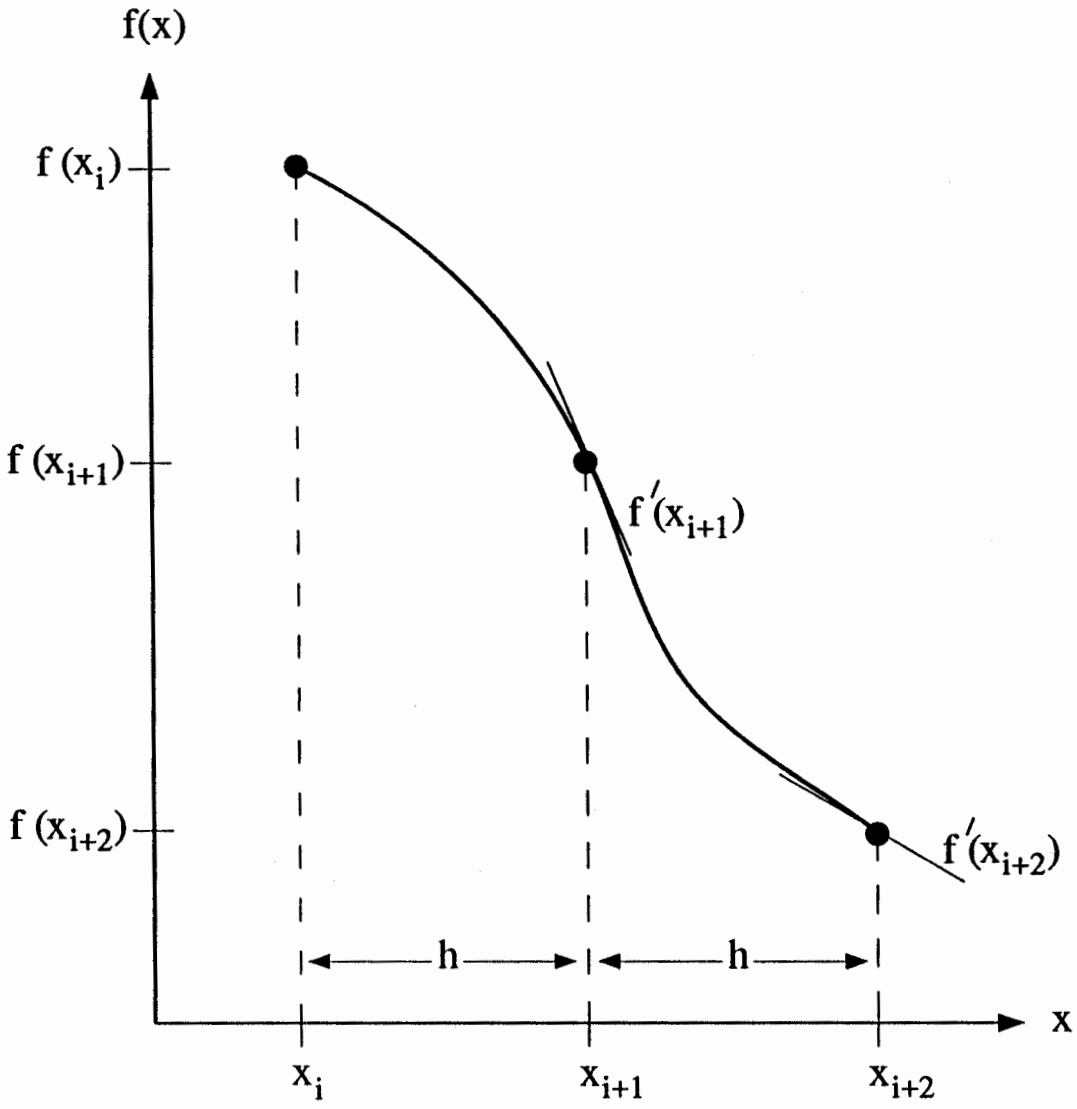

Figure 4.12 Two-Step, First-Order, Backward Difference Approximation to an Arbitrary Function

$x = x_{i+1}$,

$$f(x_i) = f(x_{i+1} - h) = f(x_{i+1}) - hf'(x_{i+1}) + \frac{h^2}{2!}f''(x_{i+1}) - \cdots , \qquad (4.116)$$

where primes denote derivatives with respect to the variable x and h is the small, constant x step size (*i.e.*, $h = \Delta x = x_p - x_{p-1}$; p = i+2, i+1). Similarly, expanding f(x) in a Taylor series about $x = x_{i+2}$,

$$f(x_i) = f(x_{i+2} - 2h) = f(x_{i+2}) - 2hf'(x_{i+2}) + \frac{4h^2}{2!}f''(x_{i+2}) - \cdots . \qquad (4.117)$$

Since the values of the function and its derivative at the i+1 step are deemed to be slightly more representative of the behavior of the function at the i*th* step than the same information at the i+2 step, equation (4.116) is weighted more heavily than (4.117). Obtained by multiplying equation (4.116) by three, subtracting equation (4.117), and neglecting second and higher order terms in h, the value of $f(x_i)$ is approximated as

$$f(x_i) \approx \frac{1}{2}\left\{3f(x_{i+1}) - f(x_{i+2}) + h\left[2f'(x_{i+2}) - 3f'(x_{i+1})\right]\right\}. \qquad (4.118)$$

Thus, equation (4.118) represents a two-step, first-order, backward difference approximation to the value of the function f evaluated at $x = x_i$.

So, from (4.118), the Hamiltonian on the plus-side of the impulse can be approximated as

$$H_{m^+} \approx \frac{1}{2}\left\{3H_{i+1} - H_{i+2} + \Delta t\left[2\dot{H}_{i+2} - 3\dot{H}_{i+1}\right]\right\}, \qquad (4.119)$$

where, again, i is the integration step corresponding to the occurrence of the interior impulse and Δt is the constant integration step size. The derivative of the Hamiltonian at the i+1 and i+2 steps is computed from equation (3.72) evaluated at the instant corresponding to the appropriate integration step. Similarly, by extrapolating the applicability of equation (4.118) to the function of a vector (*i.e.*, let $f = f(\bar{x})$), the primer derivative on the plus-side of the intermediate impulse can be approximated as

$$\dot{\bar{p}}_{m^+} \approx \frac{1}{2}\left\{3\dot{\bar{p}}_{i+1} - \dot{\bar{p}}_{i+2} + \Delta t\left[2\ddot{\bar{p}}_{i+2} - 3\ddot{\bar{p}}_{i+1}\right]\right\}. \qquad (4.120)$$

The second derivative of the primer vector is calculated from equation (3.51). Additionally, the accuracy of approximations (4.119) and (4.120) is substantially increased

if the integration step size is significantly reduced on that portion of the trajectory immediately following the intermediate impulse. Thus, if the primer derivative and the Hamiltonian on the plus-side of the interior impulse are approximated using a two-step, first-order, backward difference, then the gradients of the cost function can be calculated from the differences of equation (4.120) from (4.114) and of equation (4.119) from (4.115).

CHAPTER V

SUPERIOR TRANSFER OPTIMIZATION APPLICATIONS

The nominal transfer trajectory constructed in Chapter II is optimized utilizing the techniques developed in Chapters III and IV. Additionally, reference transfer paths between a variety of other halo orbits are created. These nominal transfers are then optimized employing, first, additional impulses to produce time-fixed solutions and, secondly, coastal arcs to produce time-free solutions. Variances in $|\Delta\bar{v}|$ expenditures, times of flight on the transfer trajectory, and shifts in the departure and arrival locations on the halo orbits are examined as the amplitude of the final halo orbit is varied. Plots of the nominal and optimal trajectories as well as the corresponding primer vector histories are presented.

Optimality of a Nominal Transfer Trajectory

Recall that in the fifth section of Chapter II a nominal transfer trajectory is constructed that moves a spacecraft from an initial L_1 libration-point halo orbit characterized by a z-amplitude of 110,000 km to a final halo orbit, about the same libration point, with a z-amplitude of 160,000 km (Case A). The complete nominal trajectory is illustrated in Figures 2.7-2.9. Now the optimality of this reference two-impulse transfer, which possesses a $|\Delta\bar{v}|$ expenditure of 198.46 m/s, is investigated by examining the magnitude of the primer vector over the duration of the transfer trajectory. Concurrent with numerical integration of the transfer segment of the complete nominal trajectory, the primer vector is computed from equation (3.52). The resulting history of the primer magnitude over the duration of the transfer segment is shown in Figure 5.1. In order for the nominal transfer to be optimal, it must satisfy the four necessary conditions stated in Chapter III; however, upon examination of Figure 5.1, the primer magnitude clearly exceeds unity, and the second necessary condition is violated.

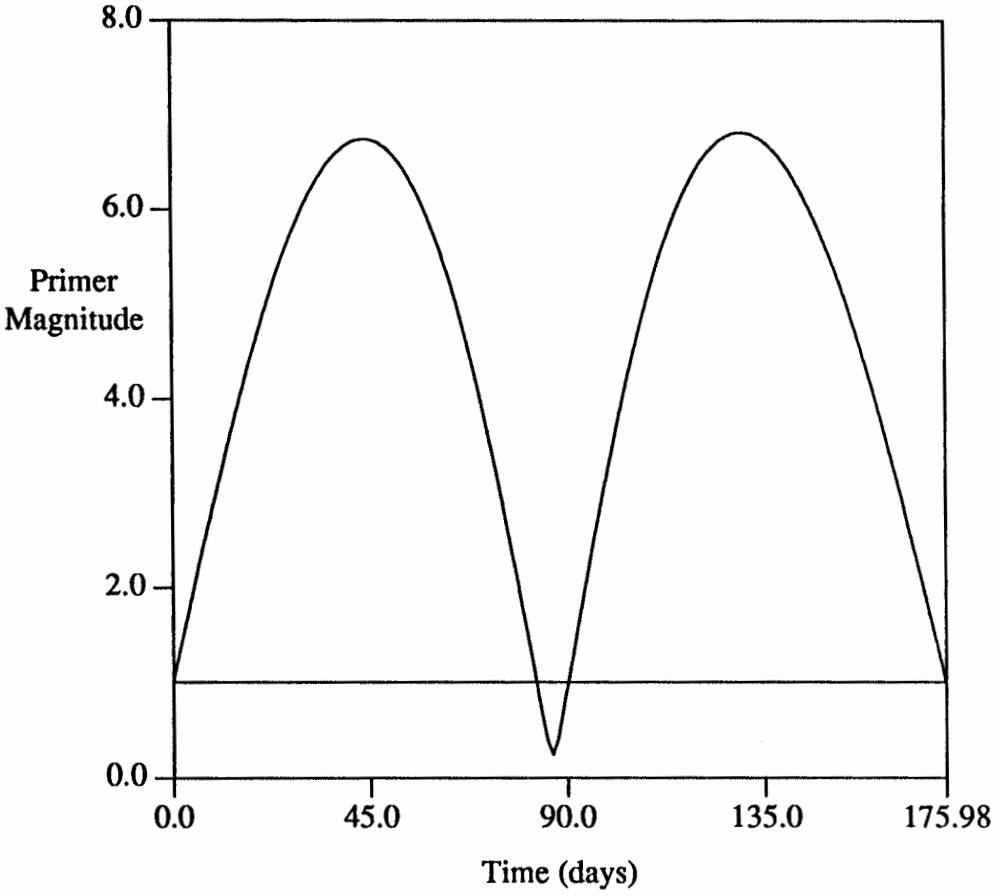

2–Impulse $\Delta\bar{v}$ Expenditure = 198.46 m/s

Figure 5.1 Primer Magnitude History of Two-Impulse Nominal Transfer (Case A)

Consequently, this two-impulse reference transfer is not optimal and can be improved by the time-fixed and time-free optimization techniques developed in Chapter IV.

Optimal Time-Fixed Superior Transfer Trajectories

Figure 5.1 suggests that an improved transfer, for which the time of flight is unaltered, is obtained if an additional impulse is executed interior to the terminal impulses. The location where the primer magnitude attains its maximum value is ascertained, and an intermediate impulse is implemented at this point. The magnitude of the impulse is determined from the iterative solution of equation (4.101) that renders $J_{\Gamma'}$ a minimum; also, the direction of the impulse is specified to be that associated with the primer vector at this point. If this additional impulse is implemented, the resulting primer magnitude plot [See Figure 5.2] exhibits a cusp at the interior impulse location. According to the fourth necessary condition, the slope of the primer magnitude at the location of the interior impulse must be zero. Thus, in order to remove the cusp in Figure 5.2, the timing and placement of the intermediate impulse is optimized employing gradient information in the utilization of the BFGS variable metric method. If the interior impulse is moved -1.39 days and a distance of 101,268.95 km, the resultant three-impulse transfer trajectory possesses a primer magnitude history [See Figure 5.3] that complies with the necessary conditions for an optimal trajectory; additionally, the complete trajectory (initial halo, optimal three-impulse transfer, final halo) [See Figures 5.4-5.6] is accomplished at a cost of only 35.94 m/s (a substantial savings of 162.52 m/s). Because the $\underset{\sim}{y}$-$\underset{\sim}{z}$ projection is, for present considerations, the most illustrative of the three planar projections, subsequent trajectories will be presented only in the $\underset{\sim}{y}$-$\underset{\sim}{z}$ projection.

Digress temporarily and recall that, although the Hamiltonian expressed in terms of rotating coordinates is not constant, a variational expression relating a reference and perturbed trajectory is rendered constant over a coastal arc. Since the adjoint equation (3.91) is used extensively in the development of the time-fixed and time-free optimization strategies presented in Chapter IV, a test of the validity of (3.91) is warranted. Consequently, the two-impulse reference trajectory is compared to the perturbed transfer trajectory to which an interior impulse is added. The left side of (3.91), computed over the duration of the transfer, is plotted in Figure 5.7. The maximum deviations from the mean constants over the first and second coastal arcs, respectively, are 15.66% and 7.23%—satisfactory results given the linear nature of the approximation.

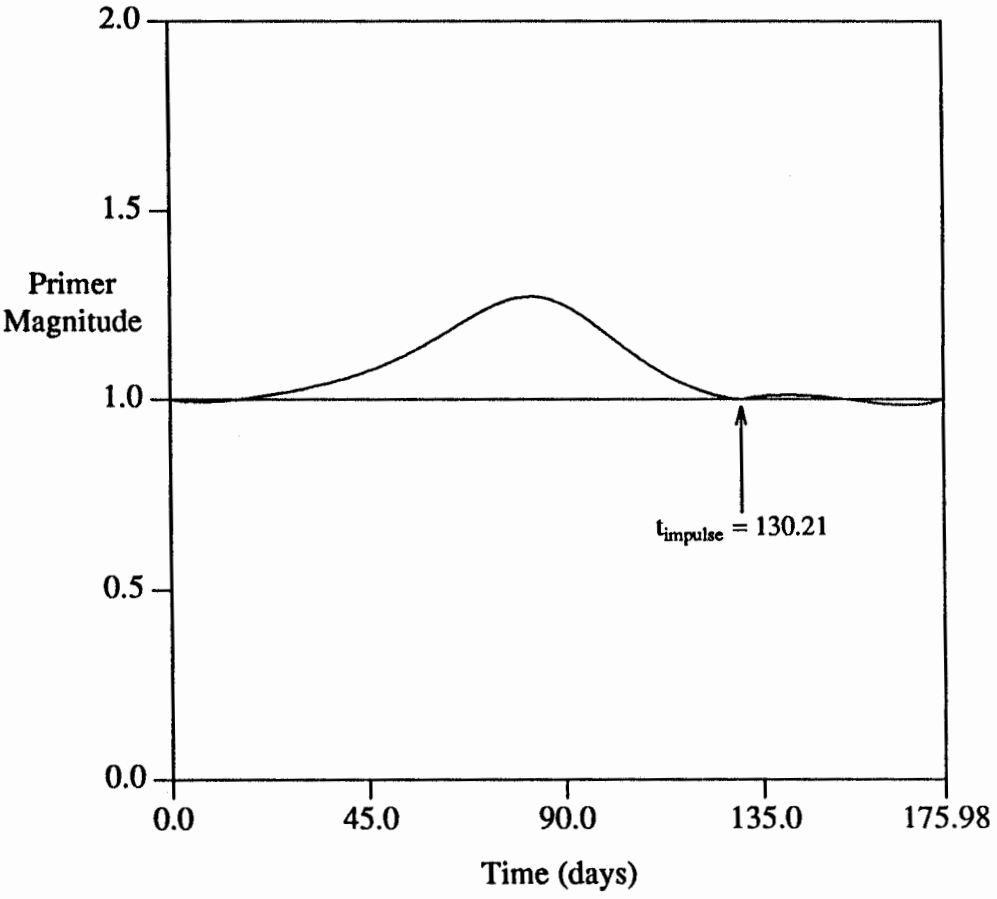

3–Impulse $\Delta\bar{v}$ Expenditure = 88.33 m/s

Figure 5.2 Primer Magnitude History of Time-Fixed Three-Impulse Transfer Exhibiting a Cusp (Case A)

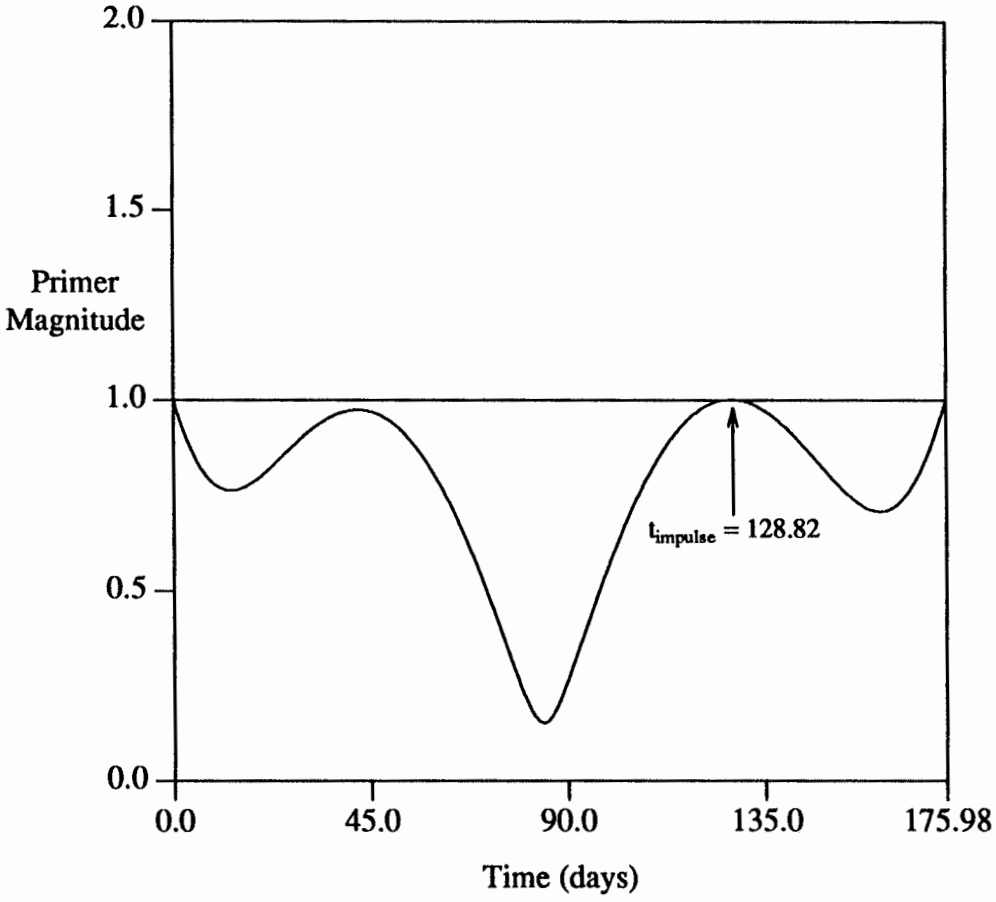

3–Impulse $\Delta\bar{v}$ Expenditure = 35.94 m/s

Figure 5.3 Primer Magnitude History of Optimal Time-Fixed Three-Impulse Transfer (Case A)

Initial Halo: $A_z = 110{,}000$ km

Final Halo: $A_z = 160{,}000$ km

Transfer TOF = 175.98 days

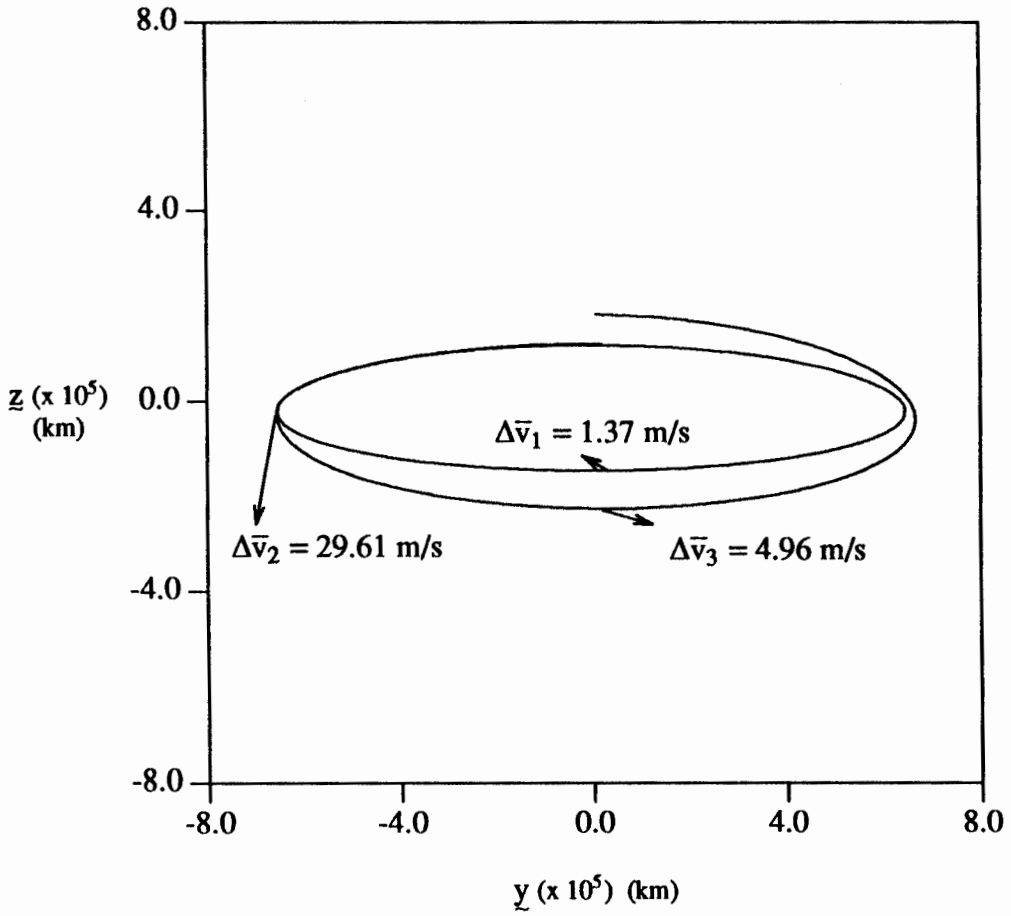

3–Impulse $\Delta\bar{v}$ Expenditure = 35.94 m/s

Figure 5.4 y-z Projection of Optimal Time-Fixed Three-Impulse Transfer (Case A)

Initial Halo: $A_z = 110{,}000$ km

Final Halo: $A_z = 160{,}000$ km

Transfer TOF = 175.98 days

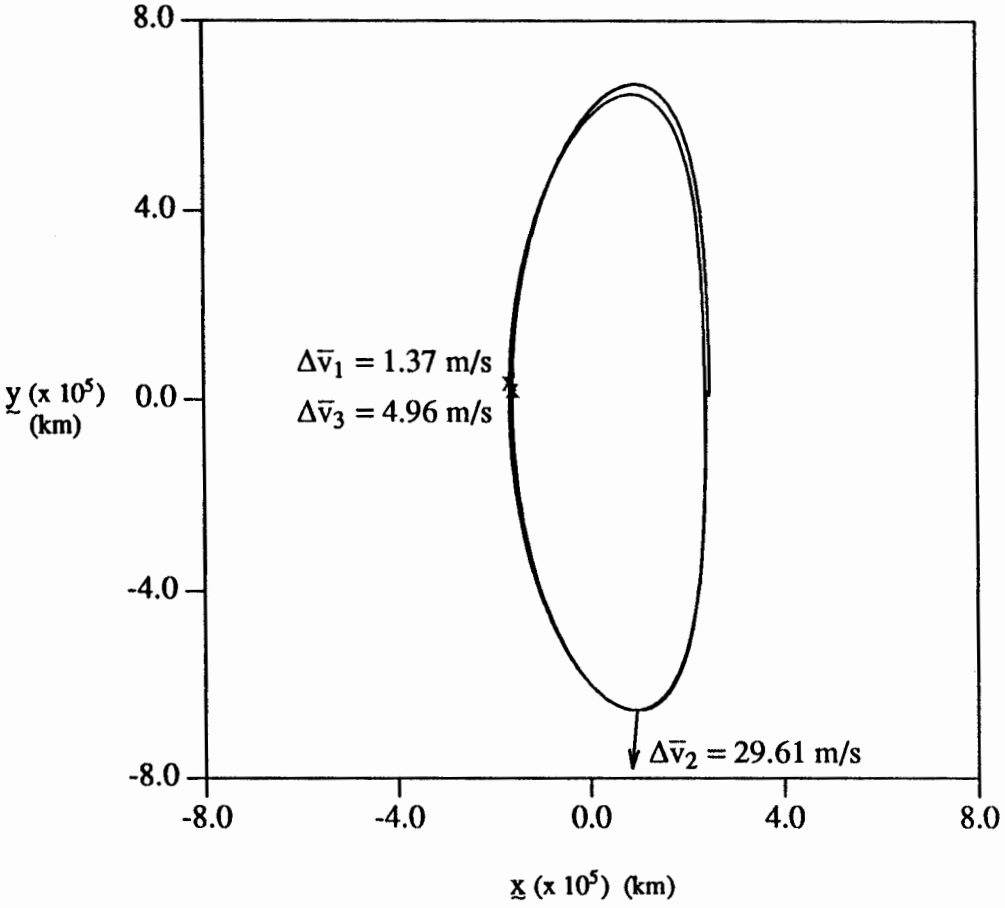

3–Impulse $\Delta\bar{v}$ Expenditure = 35.94 m/s

Figure 5.5 x-y Projection of Optimal Time-Fixed Three-Impulse Transfer (Case A)

Initial Halo: $A_z = 110{,}000$ km

Final Halo: $A_z = 160{,}000$ km

Transfer TOF = 175.98 days

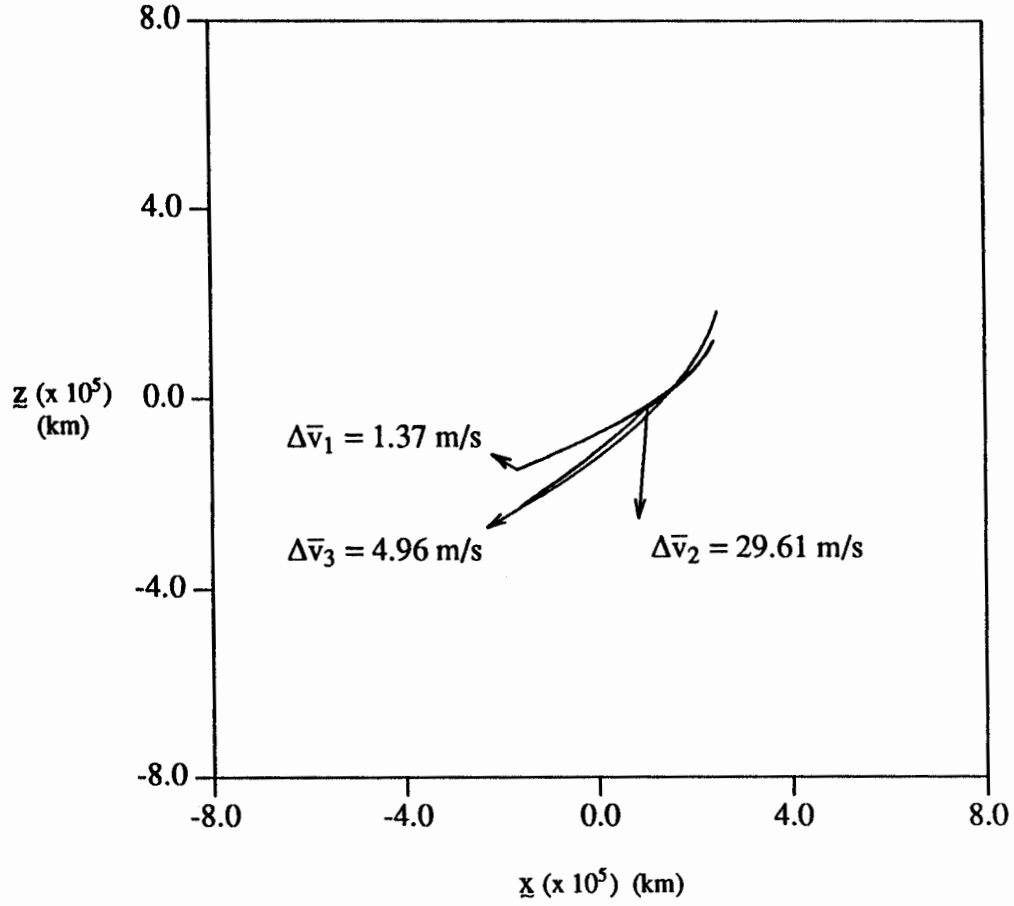

3–Impulse $\Delta\bar{v}$ Expenditure = 35.94 m/s

Figure 5.6 $\underset{\sim}{x}$-$\underset{\sim}{z}$ Projection of Optimal Time-Fixed Three-Impulse Transfer (Case A)

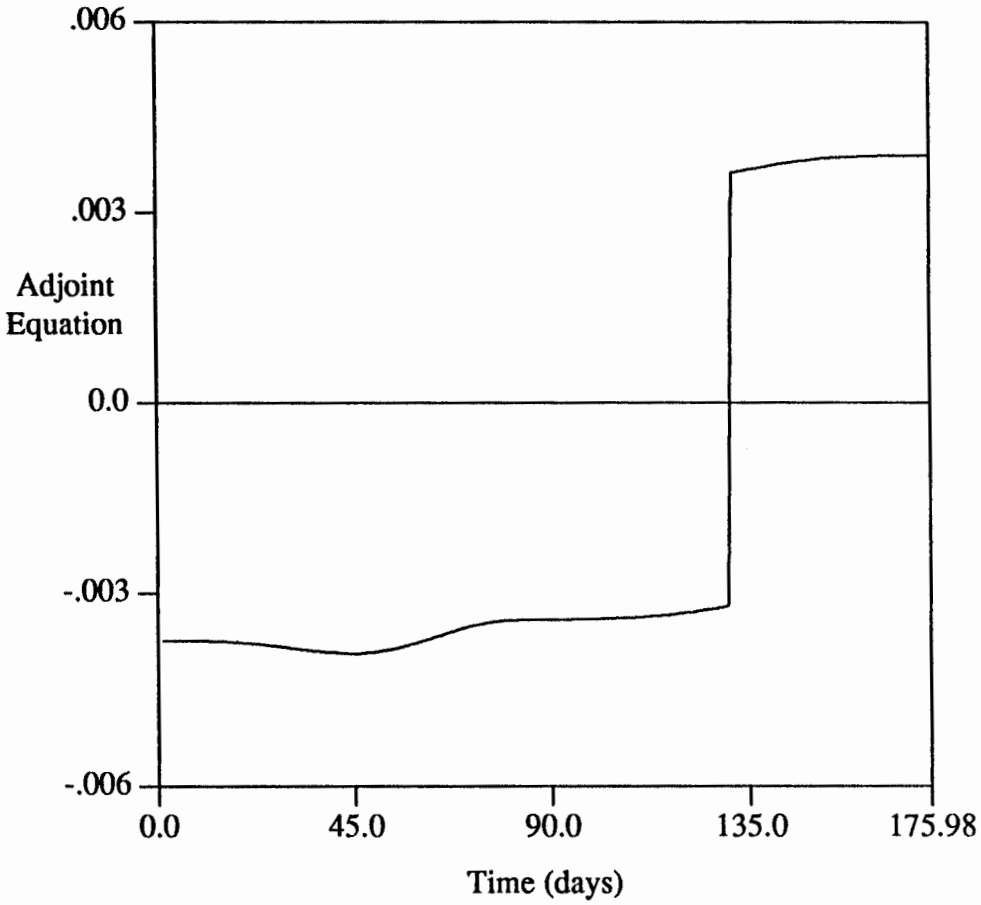

Figure 5.7 Adjoint Equation History (Case A)

Return once again to the construction of transfer paths between halo orbits. In order to determine what effect the size of the final halo orbit has on the optimal trajectory, transfers from the same initial halo orbit to two final halo orbits each of different size, characterized by z-amplitudes of 200,000 km and 240,000 km, are examined. For each of these transfers, the date of injection into the initial halo orbit is unchanged from August 17; moreover, the selection of the minimum $\underset{\sim}{z}$-excursions for the departure and arrival locations on the halo orbits is unaltered. Additionally, the sensitivity of the optimal solution to the original, non-optimal, two-impulse nominal transfer is investigated by considering two different reference transfers to the same final halo orbit having a z-amplitude of 200,000 km. The two-impulse reference trajectory for the first transfer (Case B) is determined in accordance with the algorithm presented in Chapter II; whereas, the nominal trajectory for the second transfer (Case C) is determined by incrementally increasing the components of the velocity maneuvers on the nominal Lissajous transfer in case A until a final halo orbit having a z-amplitude of 200,000 km is attained. The resulting non-optimal two-impulse transfers in cases B and C [See Figures 5.8 and 5.12] differ in $|\Delta\bar{v}|$ expenditure by approximately 14 m/s.

Both of these transfers along with the transfer to a halo orbit characterized by a z-amplitude of 240,000 km (Case D) [See Figure 5.16] exhibit non-optimal primer magnitude plots similar to that in Figure 5.1. (Note that the nominal transfer in case D is constructed in the manner used to determined the nominal transfer in case C.) The cost on each transfer is then reduced by the addition of an impulse at the instant that each of the primer magnitudes attains its maximum. In each of the three cases, the transfer cost can be improved by the implementation of another intermediate impulse such that the optimal time-fixed transfer trajectory contains four impulsive maneuvers. For cases B and C, the best three-impulse primer magnitude plot, the optimal four-impulse primer magnitude plot, and the $\underset{\sim}{y}$-$\underset{\sim}{z}$ projection of the optimal four-impulse trajectory are illustrated in Figures 5.9-5.11 and 5.13-5.15, respectively. Additionally, for case D, the best three-impulse primer magnitude plot, the corresponding $\underset{\sim}{y}$-$\underset{\sim}{z}$ projection, the optimal four-impulse primer magnitude plot, and its corresponding $\underset{\sim}{y}$-$\underset{\sim}{z}$ projection are illustrated in Figures 5.17-5.20, respectively. Observe that very slight cusps appear at the location of the first interior impulse on the primer magnitude histories for the optimal trajectories shown in Figures 5.10, 5.14, and 5.19. Recall, however, that the occurrence of such cusps was predicted in Chapter IV since multi-interior-impulse solutions are obtained by optimization of the position and time of the K*th* interior impulse without

Initial Halo: $A_z = 110{,}000$ km

Final Halo: $A_z = 200{,}000$ km

Transfer TOF = 177.20 days

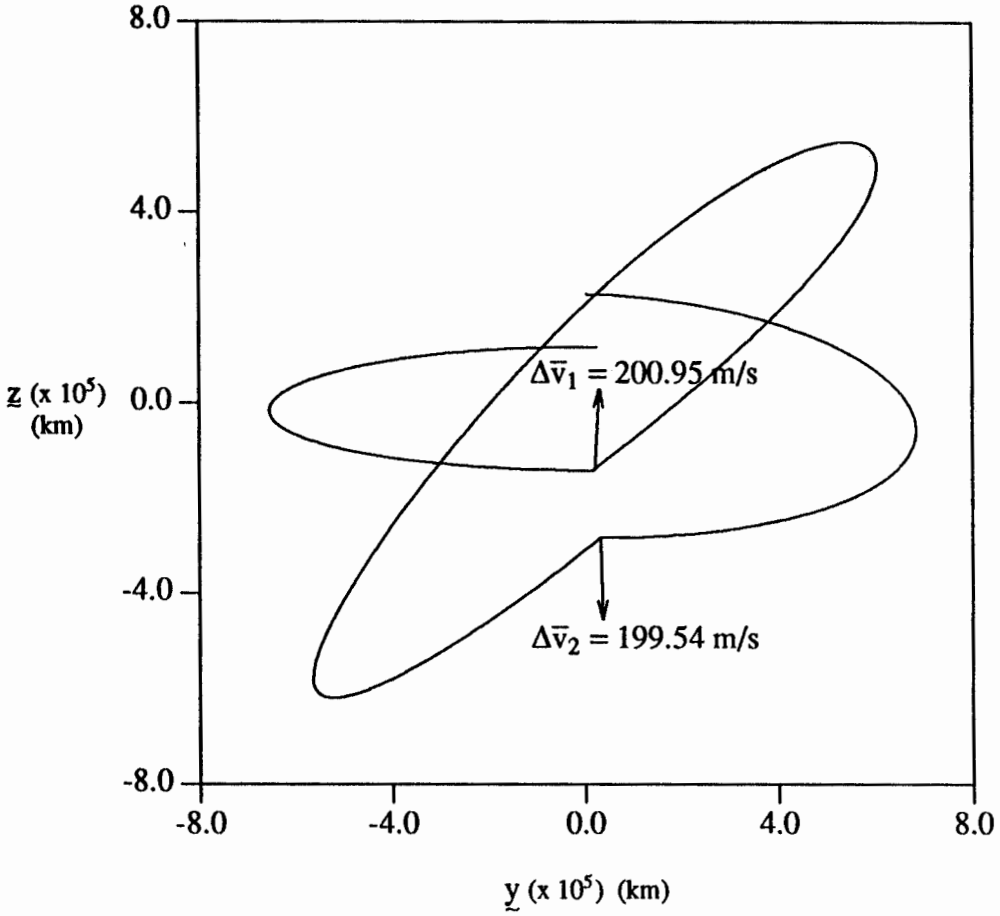

2–Impulse $\Delta\bar{v}$ Expenditure = 400.49 m/s

Figure 5.8 y-z Projection of Two-Impulse Nominal Trajectory (Case B)

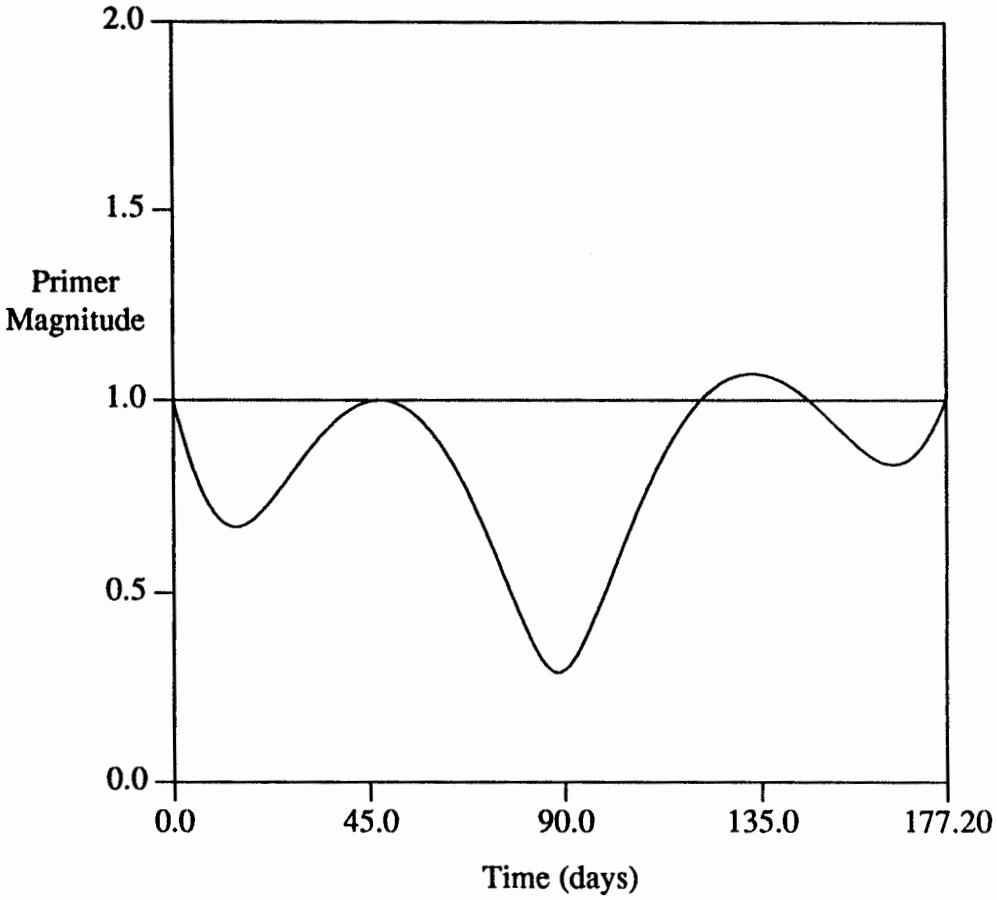

3–Impulse $\Delta\bar{v}$ Expenditure = 125.82 m/s

Figure 5.9 Primer Magnitude History of Best Time-Fixed Three-Impulse Transfer (Case B)

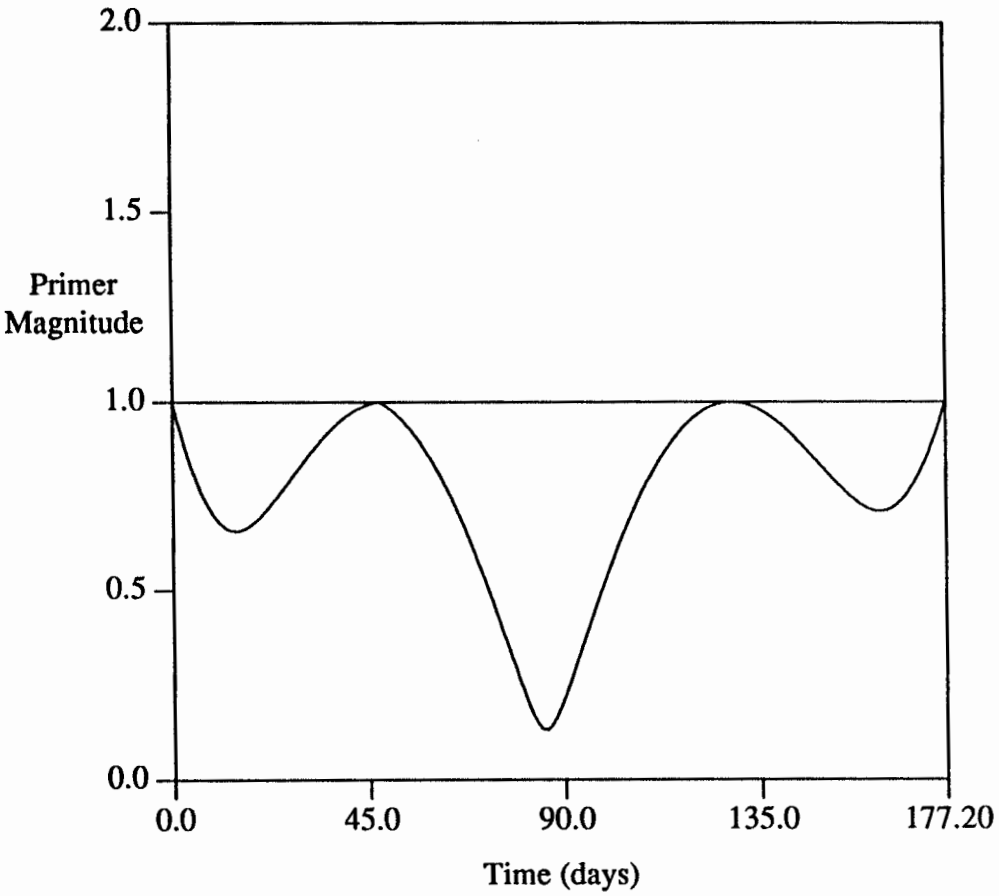

4–Impulse $\Delta\bar{v}$ Expenditure = 124.17 m/s

Figure 5.10 Primer Magnitude History of Optimal Time-Fixed Four-Impulse Transfer (Case B)

Initial Halo: $A_z = 110{,}000$ km

Final Halo: $A_z = 200{,}000$ km

Transfer TOF = 177.20 days

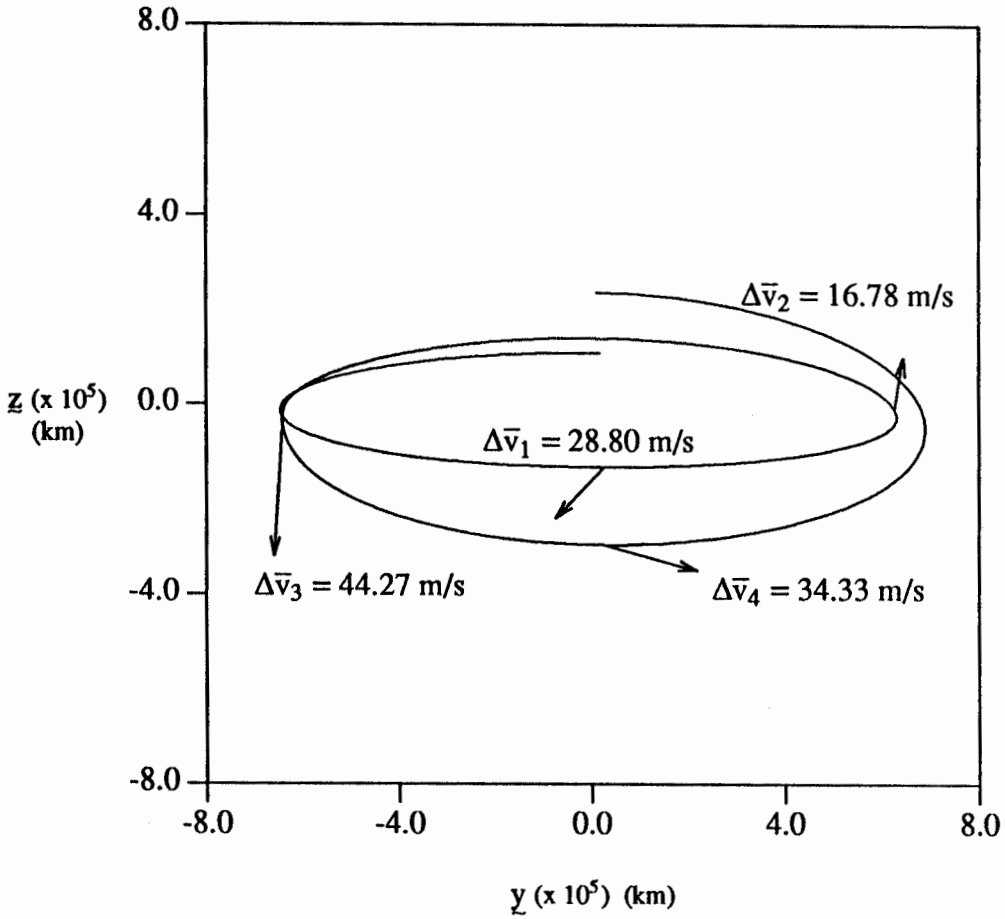

4–Impulse $\Delta\bar{v}$ Expenditure = 124.17 m/s

Figure 5.11 y-z Projection of Optimal Time-Fixed Four-Impulse Transfer (Case B)

Initial Halo: $A_z = 110{,}000$ km

Final Halo: $A_z = 200{,}000$ km

Transfer TOF = 177.20 days

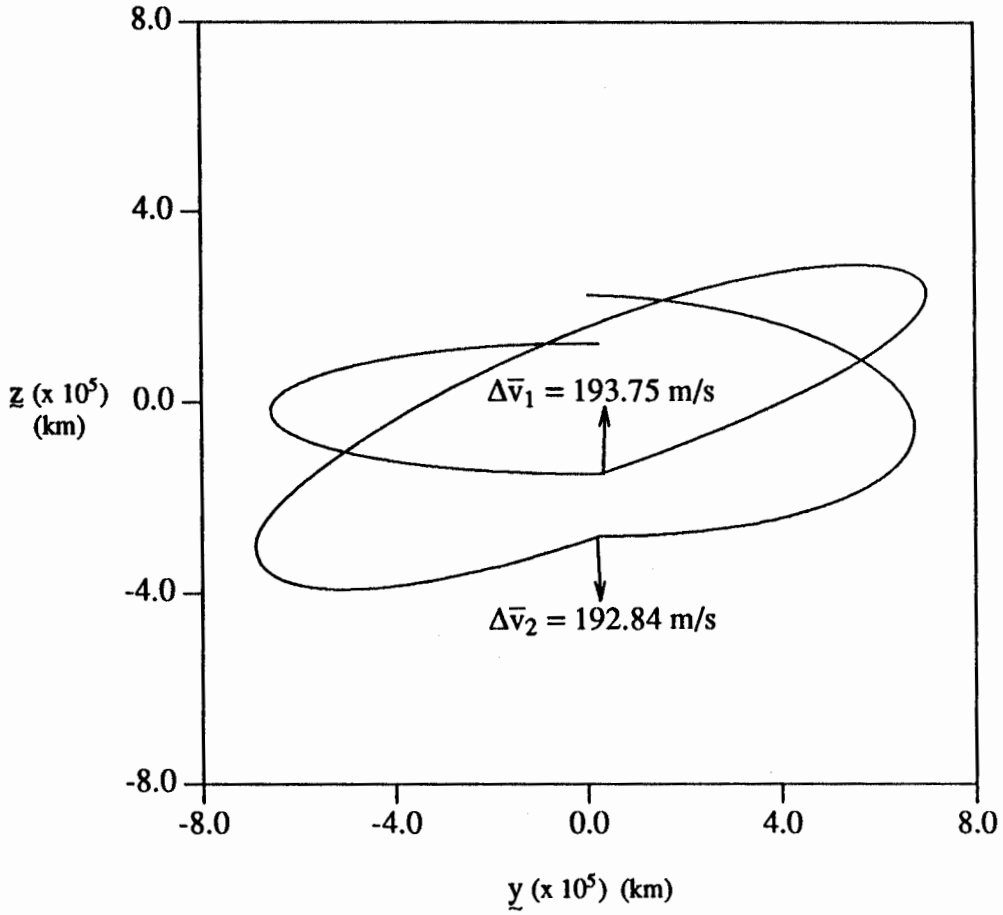

2–Impulse $\Delta\bar{v}$ Expenditure = 386.59 m/s

Figure 5.12 $\underset{\sim}{y}$-$\underset{\sim}{z}$ Projection of Two-Impulse Nominal Trajectory (Case C)

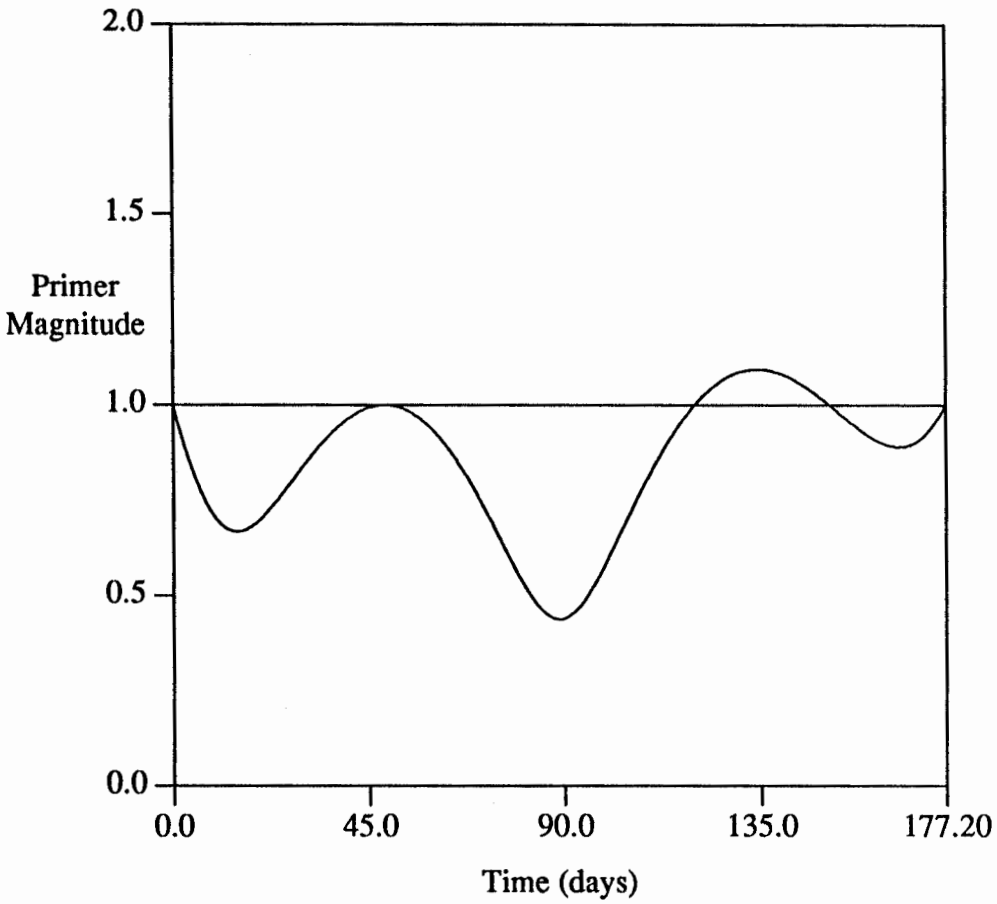

3–Impulse $\Delta\bar{v}$ Expenditure = 93.24 m/s

Figure 5.13 Primer Magnitude History of Best Time-Fixed Three-Impulse Transfer (Case C)

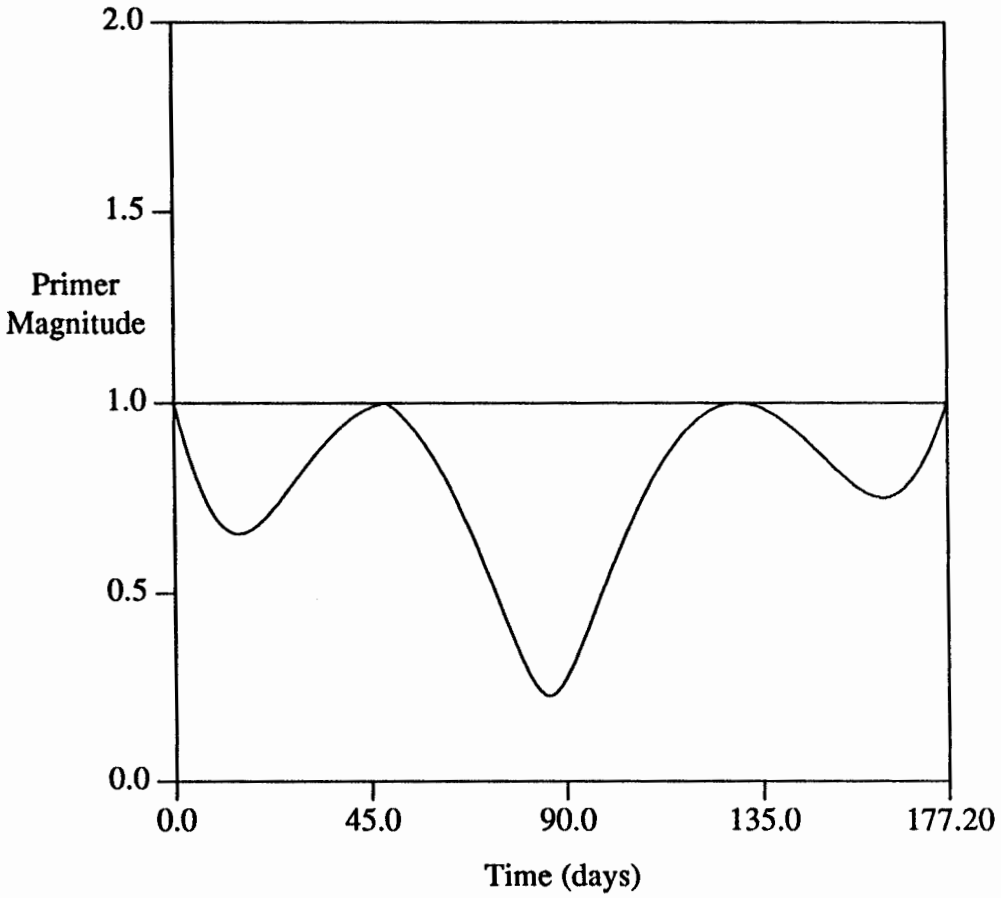

4–Impulse $\Delta\bar{v}$ Expenditure = 91.44 m/s

Figure 5.14 Primer Magnitude History of Optimal Time-Fixed Four-Impulse Transfer (Case C)

Initial Halo: $A_z = 110{,}000$ km

Final Halo: $A_z = 200{,}000$ km

Transfer TOF = 177.20 days

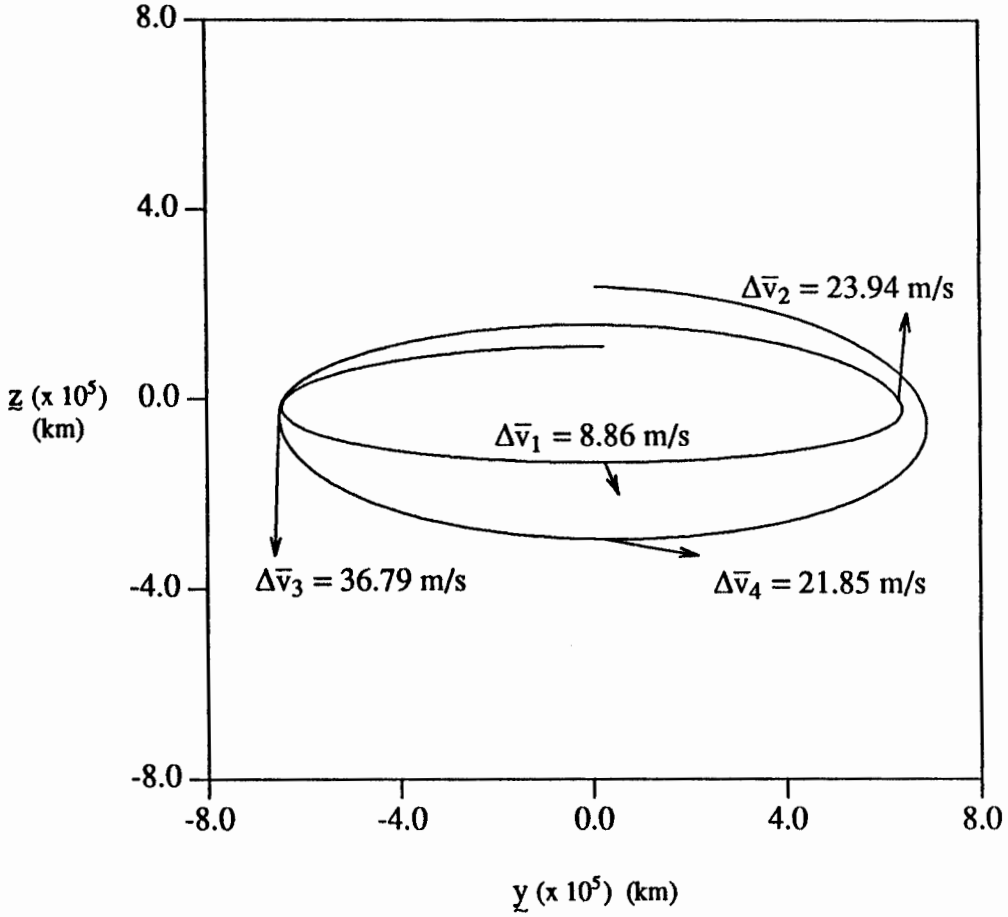

4–Impulse $\Delta\bar{v}$ Expenditure = 91.44 m/s

Figure 5.15 y-z Projection of Optimal Time-Fixed Four-Impulse Transfer (Case C)

Initial Halo: $A_z = 110{,}000$ km

Final Halo: $A_z = 240{,}000$ km

Transfer TOF = 177.20 days

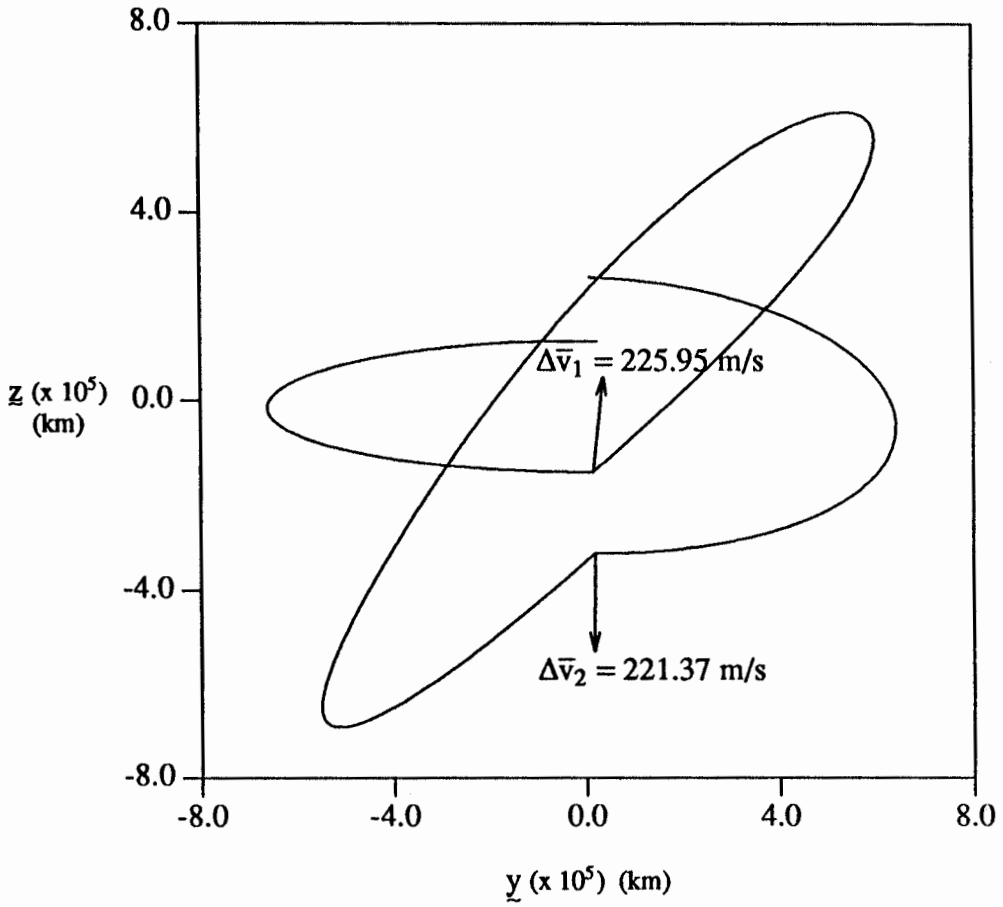

2–Impulse $\Delta\bar{v}$ Expenditure = 447.32 m/s

Figure 5.16 y-z Projection of Two-Impulse Nominal Trajectory (Case D)

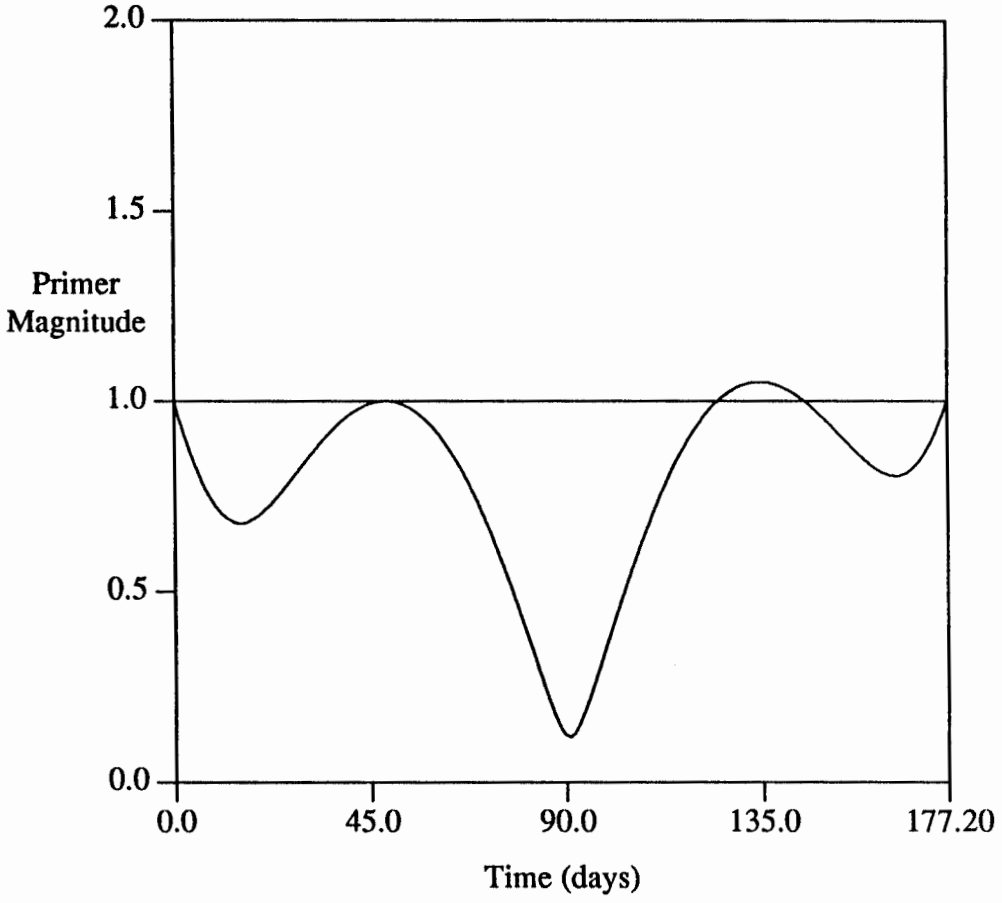

3–Impulse $\Delta\bar{v}$ Expenditure = 123.00 m/s

Figure 5.17 Primer Magnitude History of Best Time-Fixed Three-Impulse Transfer (Case D)

Initial Halo: $A_z = 110{,}000$ km

Final Halo: $A_z = 240{,}000$ km

Transfer TOF = 177.20 days

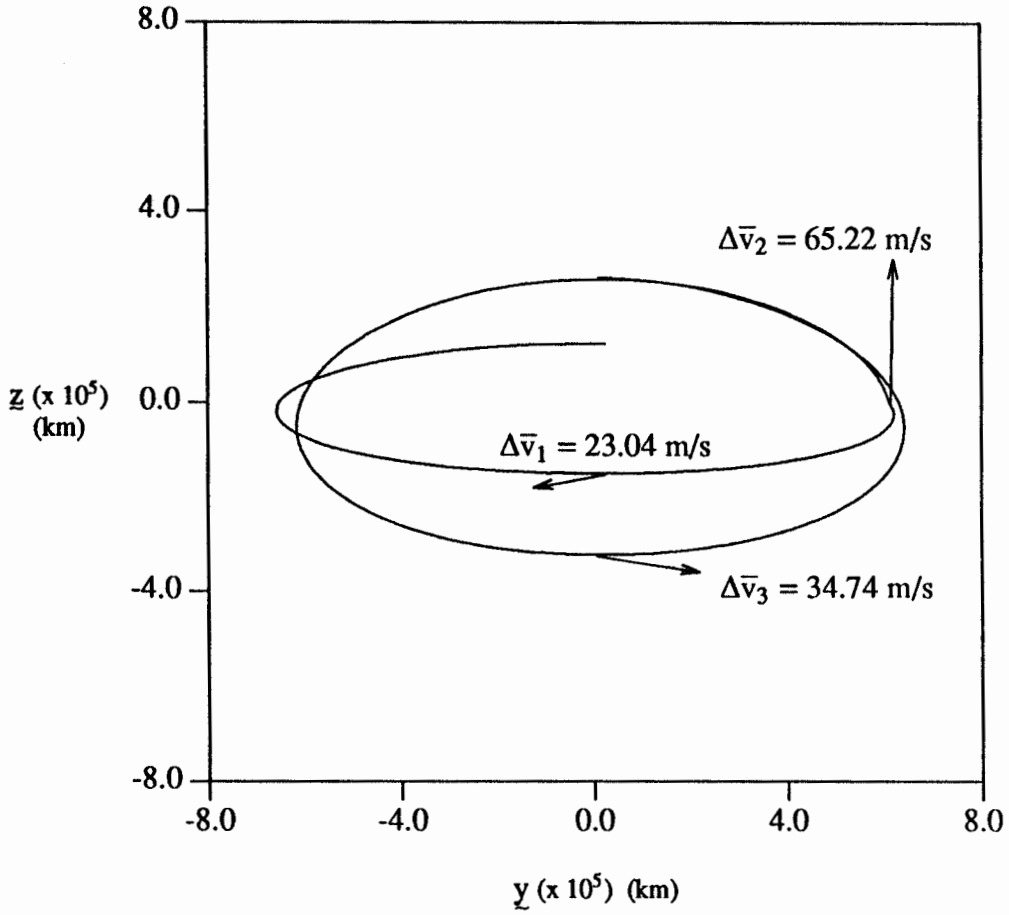

3–Impulse $\Delta\bar{v}$ Expenditure = 123.00 m/s

Figure 5.18 y-z Projection of Best Time-Fixed Three-Impulse Transfer (Case D)

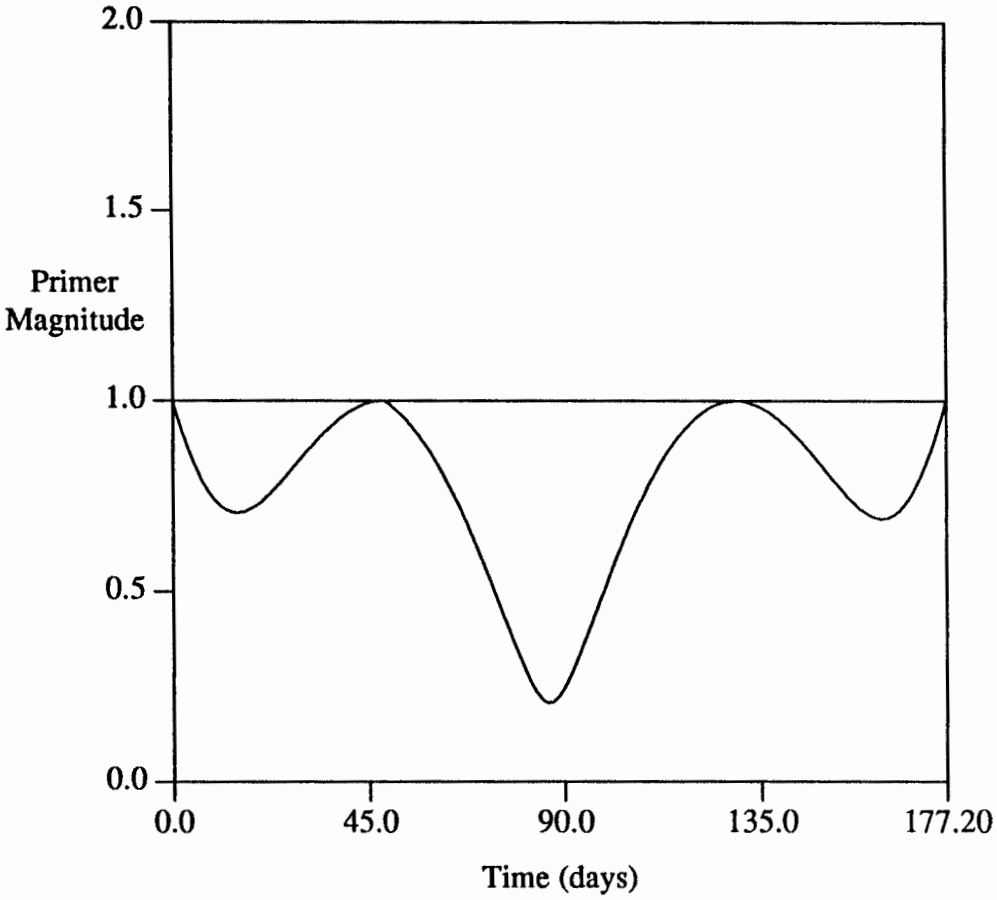

4–Impulse $\Delta\bar{v}$ Expenditure = 121.68 m/s

Figure 5.19 Primer Magnitude History of Optimal Time-Fixed Four-Impulse Transfer (Case D)

Initial Halo: A_z = 110,000 km

Final Halo: A_z = 240,000 km

Transfer TOF = 177.20 days

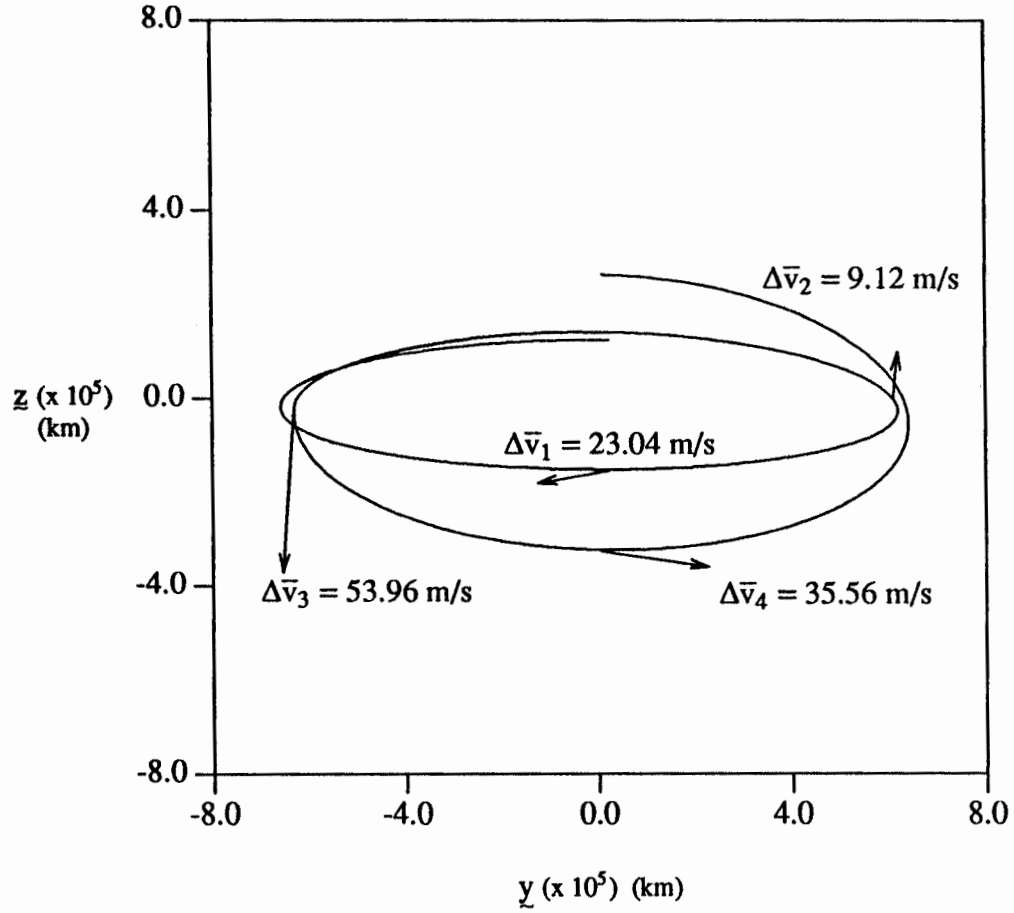

4–Impulse $\Delta\bar{v}$ Expenditure = 121.68 m/s

Figure 5.20 y-z Projection of Optimal Time-Fixed Four-Impulse Transfer (Case D)

Table 5.1 Cost on Time-Fixed Superior Transfers
to a Variety of Final Halo Orbits

(Initial Halo: Z-Amplitude = 110,000 km)

Case	Z-Amplitude of Final Halo (km)	Nominal 2-Impulse Transfer (m/s)	Optimized Time-Fixed Transfers	
			3-Impulse (m/s)	4-Impulse (m/s)
A	160,000	198.4586	35.9410	NA
B	200,000	400.4909	125.8204	124.1742
C	200,000	386.5867	93.2395	91.4449
D	240,000	447.3212	123.0035	121.6799

alteration of the k*th* ($1 \leq k < K$) impulse. The $|\Delta\bar{v}|$ differences between the three- and four-impulse results (1.32 m/s) are very misleading since the trajectories are very different. Notice that the best three-impulse transfer [Figure 5.18] performs the majority of the transition between halo orbits in the first quadrant of the $\underset{\sim}{y}$-$\underset{\sim}{z}$ plane; whereas, the optimal four-impulse trajectory [Figure 5.20] executes the majority of its transition to the final halo in the third quadrant. This phenomenon of quadrant-switching with variation in number of impulses is exhibited in cases B and C as well.

Table 5.1 summarizes the $|\Delta\bar{v}|$ cost for the four cases that are investigated. Excepting case B, the cost on the optimal transfer trajectory increases as the z-amplitude of the final halo orbit increases. Case C, the reference transfer that requires less $|\Delta\bar{v}|$ to reach the final halo orbit with z-amplitude of 200,000 km, results in an optimal four-impulse transfer having a significantly lower cost than its counterpart, case B. Hence, the anomalous behavior of case B apparently results from sensitivity of the cost on the optimal time-fixed transfer to the corresponding nominal two-impulse trajectory from which the optimal transfer is derived.

Optimal Time-Free Superior Transfer Trajectories

Return momentarily to Figure 5.1 in which the slopes of the primer magnitude at the initial and final instants are clearly unequal to zero. Hence, this primer magnitude plot suggests that, if the time of flight on the transfer trajectory is allowed to vary from its nominal value of 175.98 days and if the departure and arrival locations on the initial and final orbits are not constrained, then the cost on the nominal transfer can be improved by the inclusion of coasts on the initial and final halo orbits. Since the slopes of the primer magnitude at the initial and final instants of the reference solution are positive and negative, respectively, an initial coast ($dt_0 > 0$) and a final coast ($dt_f < 0$) are warranted. The coastal periods are optimized employing gradient information in the repeated utilization of the BFGS variable metric method in the ADS package. The resulting coastal periods are $dt_0 = 3.15$ days and $dt_f = -40.11$ days; additionally, the corresponding primer magnitude history, which is plotted relative to the time of flight on the reference transfer in order to illustrate these coastal periods [See Figure 5.21], complies with the necessary conditions for an optimal trajectory within the limitations of the multivariable search routine. Although the primer slope at the initial instant is apparently unequal to zero, the gradient of the cost function (comprised of the primer

slope and the impulse magnitude) is quite small. Since the initial impulse is an order of magnitude smaller than the final impulse, the optimization process has difficulty rendering a solution that possesses primer slopes of comparable magnitude. Execution of the coastal periods $dt_0 = 3.15$ days and $dt_f = -40.11$ days, in effect, moves the arrival on the final halo orbit to a location near its minimum $\underset{\sim}{y}$-excursion while essentially leaving the departure from the initial halo unchanged from its minimum $\underset{\sim}{z}$-excursion point [See Figure 5.22]. This optimized two-impulse transfer trajectory is executed at a cost of 26.92 m/s and is accomplished in 132.72 days.

As noted previously, the two-impulse nominal transfer trajectories for cases B-D exhibit non-optimal primer magnitude plots similar to that in Figure 5.1. The cost on each transfer is then reduced by the execution of coasts in the initial and final halo orbits. The resulting primer magnitude plots for cases B, C, and D are illustrated in Figures 5.23, 5.26, and 5.29, respectively. Notice that the times of flight on the resultant two-impulse time-free transfers are diminished substantially from the reference value of 177.20 days. In each of the three cases, the primer magnitude on the transfer portion of the trajectory lies, in part, above unity; hence, none of these transfers is optimal. However, as outlined in the time-fixed optimization strategy, the total transfer cost can be further improved by the addition of an interior impulse. For case B, the resultant three-impulse transfer is optimal, and the primer magnitude plot as well as the corresponding $\underset{\sim}{y}$-$\underset{\sim}{z}$ projection are illustrated in Figures 5.24 and 5.25.

In contrast, the three-impulse transfer trajectories for cases C and D violate the necessary condition that the primer magnitude not exceed unity [See Figures 5.27 and 5.30]; consequently, these transfers, whose $\underset{\sim}{y}$-$\underset{\sim}{z}$ projections are shown in Figures 5.28 and 5.31, are non-optimal. Thus, another interior impulsive maneuver is implemented such that both transfers contain a total of four impulses, yet the execution of this additional interior impulse produces a minuscule percent variation in cost (-0.00215% for case C and -0.00011% for case D) and still yields a non-optimal solution. Consequently, for cases C and D, no significant gains are realized by the repeated addition of interior impulses in an effort to convergence to the *optimal* transfer trajectories; instead, the *practical* solutions illustrated in Figures 5.28 and 5.31, which accomplish the desired transfers utilizing essentially the same amount of fuel in only three impulses, are chosen to represent the *best* time-free impulsive transfers to their respective final halo orbits.

Notice that for all four optimal or best transfers (cases A-D) the initial impulse as well as the intermediate impulse (if applicable) are small in magnitude and variable in orientation; whereas, the final impulse is quite large and essentially oriented out-of-plane. For each of the transfers considered, the initial and intermediate impulses act to perturb the spacecraft's initial trajectory precisely so that the transfer intersects the final halo orbit near its minimum $\underset{\sim}{y}$-excursion. At this location, a single impulse of significant magnitude is then sufficient to complete the transferal of the spacecraft to the desired final orbit. Hence, these time-free transfers perform the majority of the transition between the halo orbits in the third quadrant of the $\underset{\sim}{y}$-$\underset{\sim}{z}$ plane; remarkably, the optimal multi-impulse time-fixed transfer trajectories constructed in the previous section similarly exhibit this phenomenon of predominantly third-quadrant transferal.

Table 5.2 summarizes the $|\Delta\bar{v}|$ cost for the four cases that are investigated. The time-free transfers demonstrate a dramatic reduction in fuel consumption compared to the non-optimal two-impulse reference solutions. Excepting case B, the cost on the optimal transfer trajectory nearly increases linearly with z-amplitude of the final halo orbit; also, with each successive increase in z-amplitude, the time of flight on the transfer decreases thereby delaying departure from the initial halo orbit and advancing the departure location toward the initial halo's maximum $\underset{\sim}{y}$-excursion. Case C, the nominal transfer that requires less fuel to reach the final halo orbit with z-amplitude of 200,000 km, results in a three-impulse transfer, albeit non-optimal, having a significantly lower cost than its counterpart, case B, although the difference between cases B and C is not quite as dramatic for the time-free transfers as for the time-fixed transfer trajectories. Hence, the relatively anomalous $|\Delta\bar{v}|$ requirements in case B, which is also demonstrated in the corresponding time-fixed transfer, is again explained by the fact that the cost on the optimal time-free transfer is sensitive to the reference two-impulse trajectory from which the optimal transfer is derived. Additionally, increasing the flexibility of the design strategy by relaxing time-of-flight constraints offers some insight into transfer strategies concerning departure and arrival locations and results in time-free transfers possessing lower fuel expenditures than their comparable time-fixed transfers.

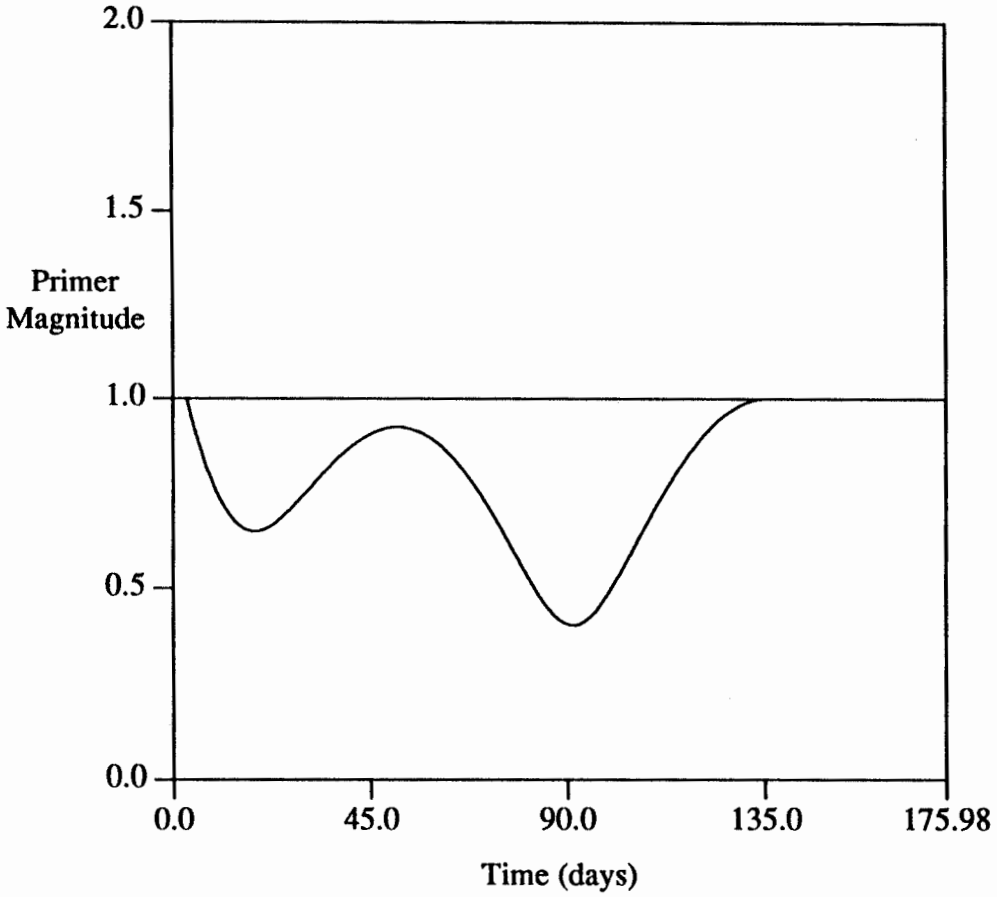

2–Impulse $\Delta\bar{v}$ Expenditure = 26.96 m/s

Transfer TOF = 132.72 days

Figure 5.21 Primer Magnitude History of Optimal Time-Free Two-Impulse Transfer (Case A)

Initial Halo: $A_z = 110{,}000$ km

Final Halo: $A_z = 160{,}000$ km

Transfer TOF = 132.72 days

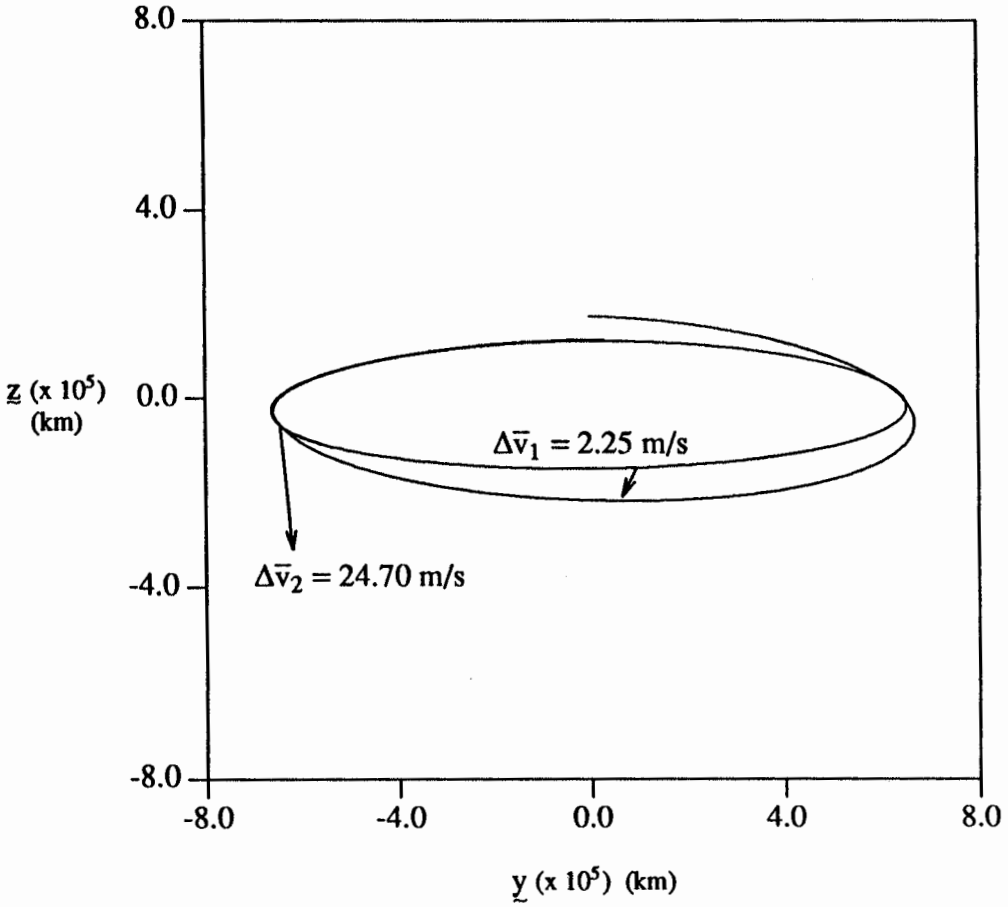

2–Impulse $\Delta\bar{v}$ Expenditure = 26.96 m/s

Figure 5.22 y-z Projection of Optimal Time-Free Two-Impulse Transfer (Case A)

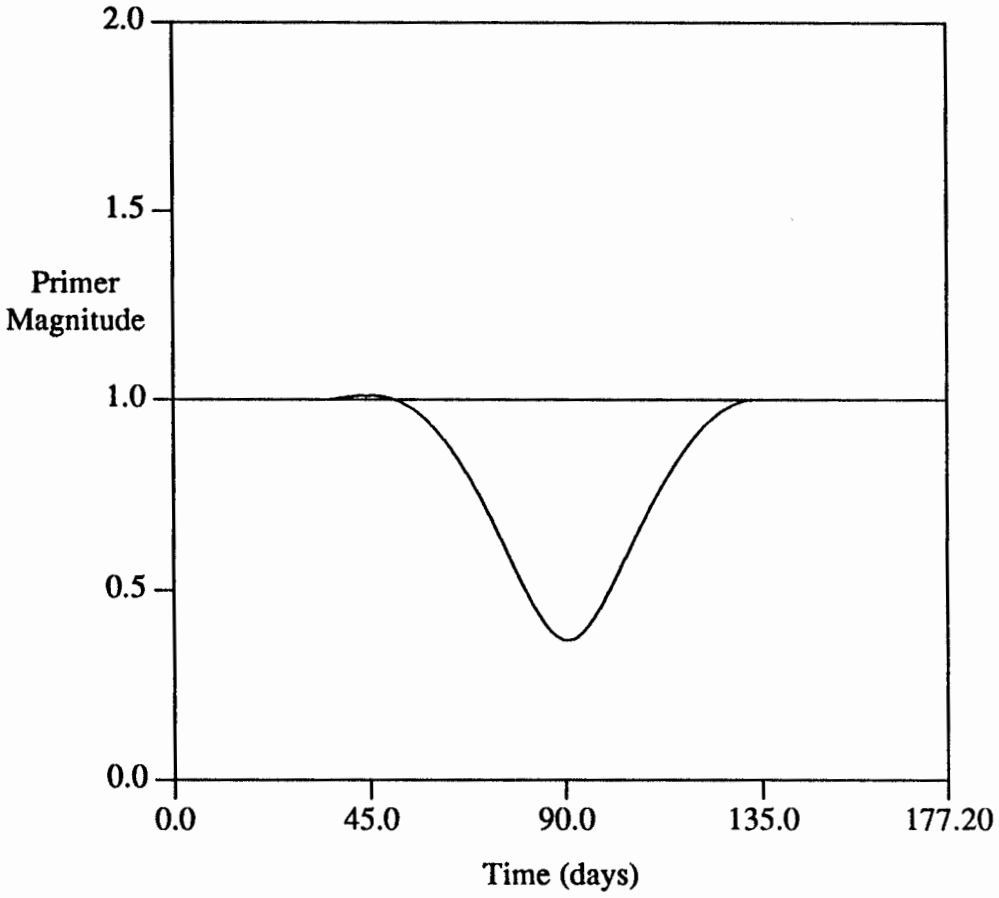

2–Impulse $\Delta\bar{v}$ Expenditure = 40.15 m/s

Transfer TOF = 100.73 days

Figure 5.23 Primer Magnitude History of Best Time-Free Two-Impulse Transfer (Case B)

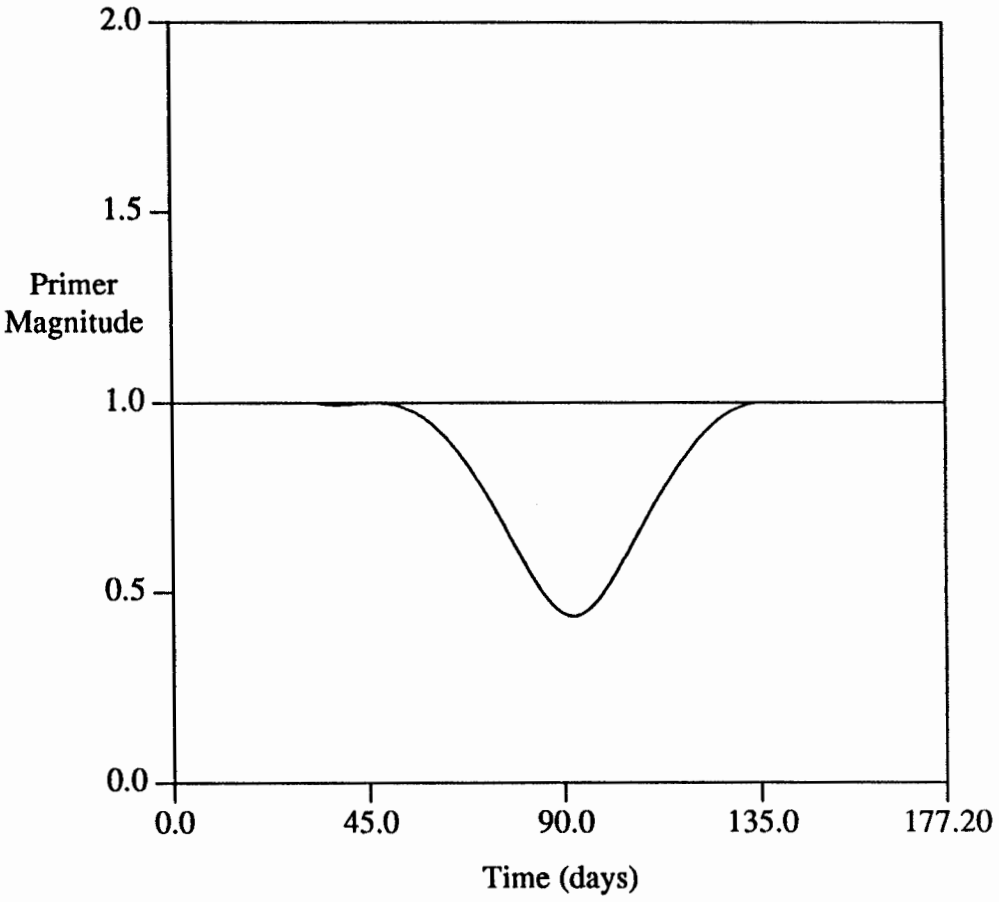

3–Impulse $\Delta\bar{v}$ Expenditure = 40.14 m/s

TOF = 100.73 days

Figure 5.24 Primer Magnitude History of Optimal Time-Free Three-Impulse Transfer (Case B)

Initial Halo: $A_z = 110{,}000$ km

Final Halo: $A_z = 200{,}000$ km

Transfer TOF = 100.73 days

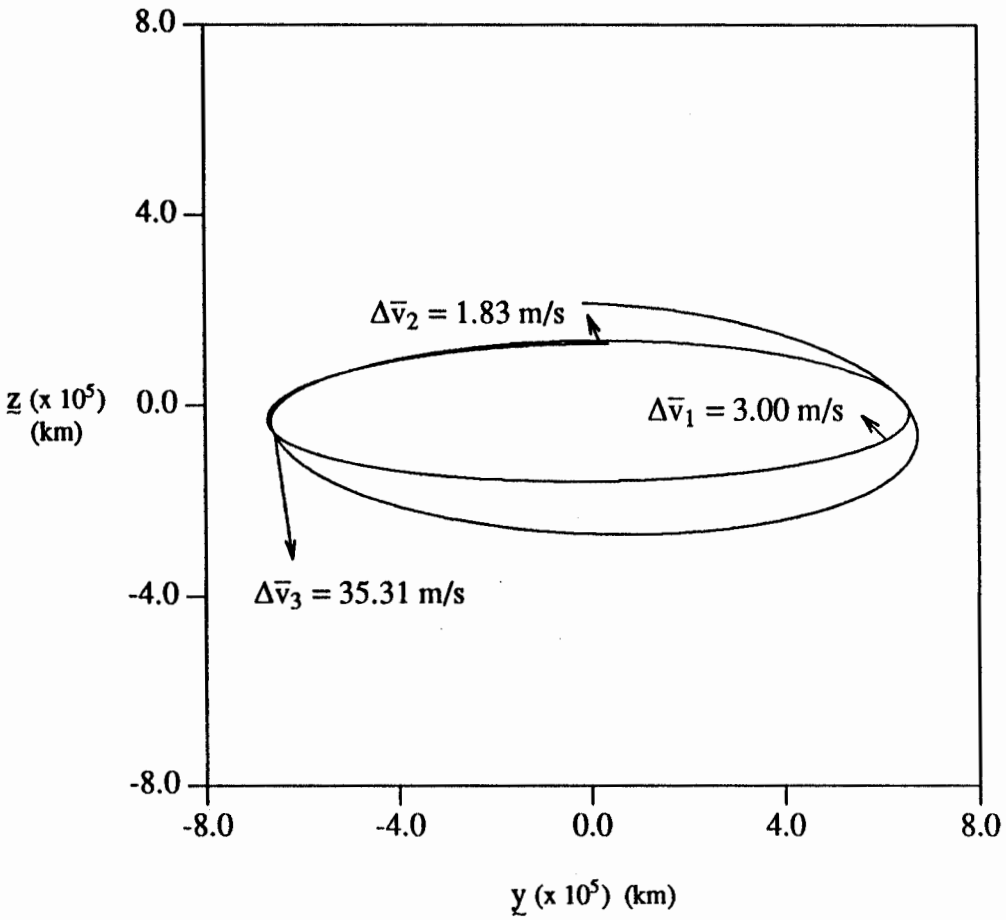

3–Impulse $\Delta\bar{v}$ Expenditure = 40.14 m/s

Figure 5.25 y-z Projection of Optimal Time-Free Three-Impulse Transfer (Case B)

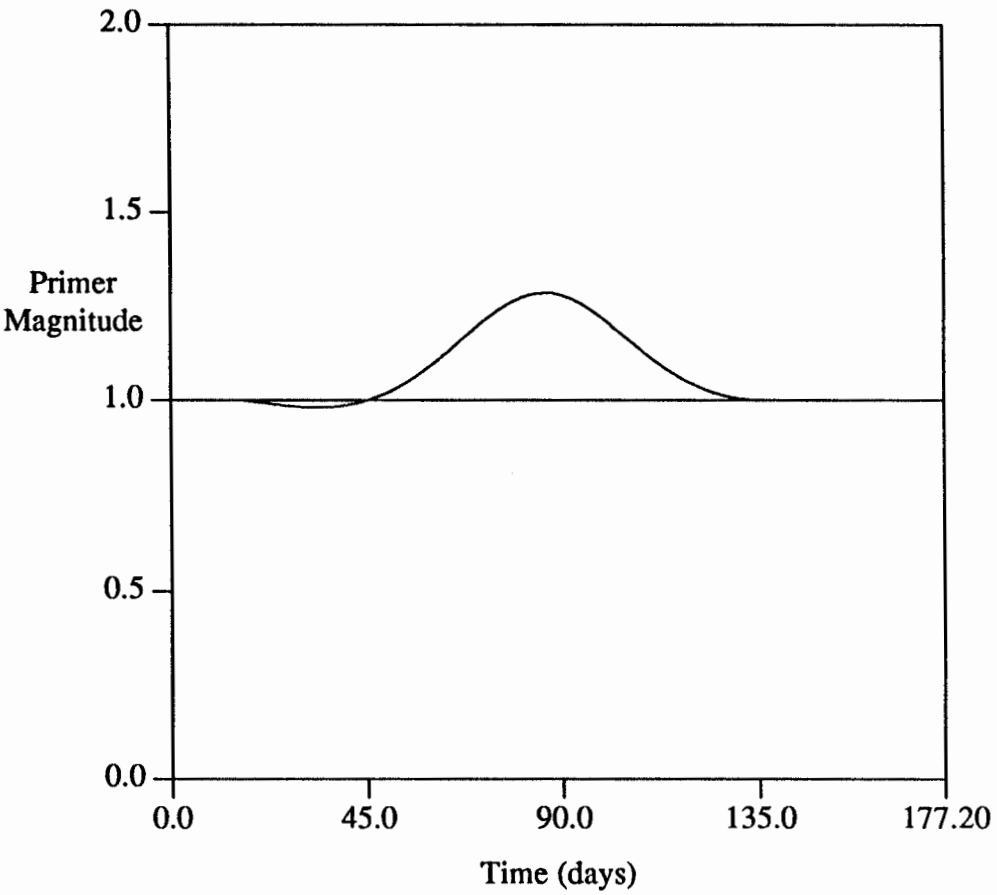

2–Impulse $\Delta\bar{v}$ Expenditure = 37.65 m/s

TOF = 116.86 days

Figure 5.26 Primer Magnitude History of Best Time-Free Two-Impulse Transfer (Case C)

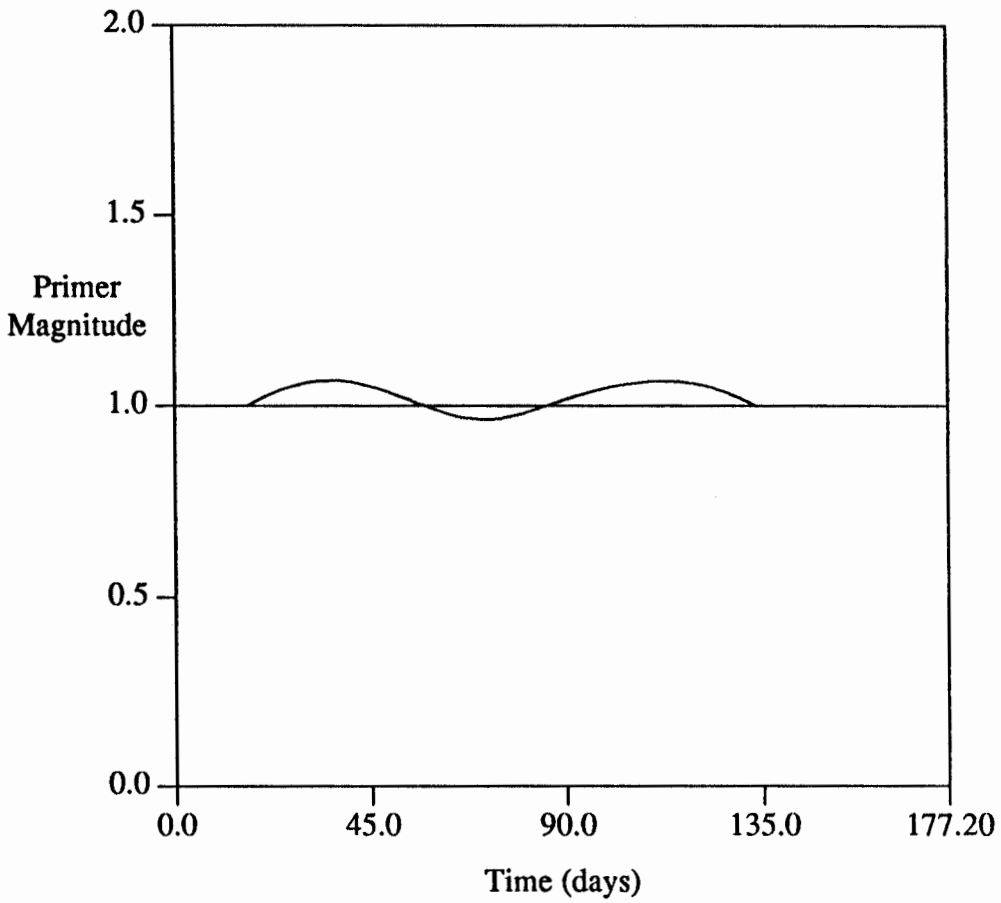

3–Impulse $\Delta\bar{v}$ Expenditure = 37.59 m/s

TOF = 116.86 days

Figure 5.27 Primer Magnitude History of Best Time-Free Three-Impulse Transfer (Case C)

Initial Halo: A_z = 110,000 km

Final Halo: A_z = 200,000 km

Transfer TOF = 116.86 days

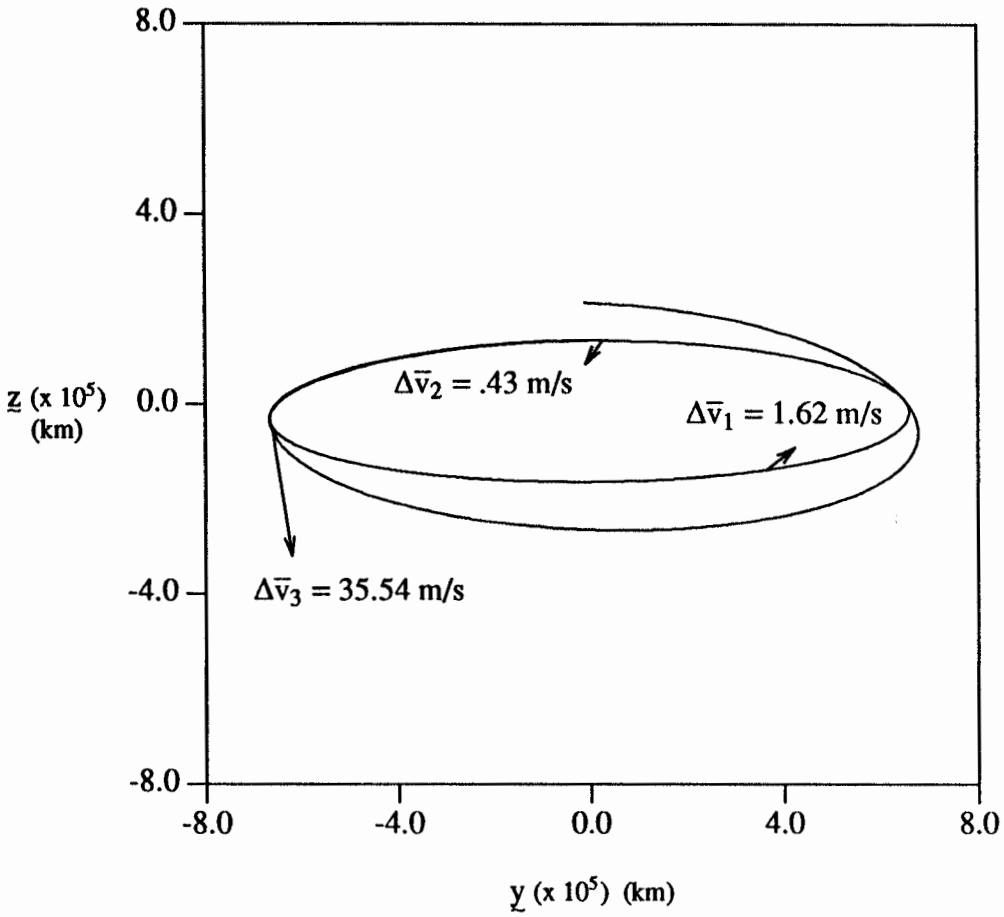

3–Impulse $\Delta\bar{v}$ Expenditure = 37.59 m/s

Figure 5.28 y-z Projection of Best Time-Free Three-Impulse Transfer (Case C)

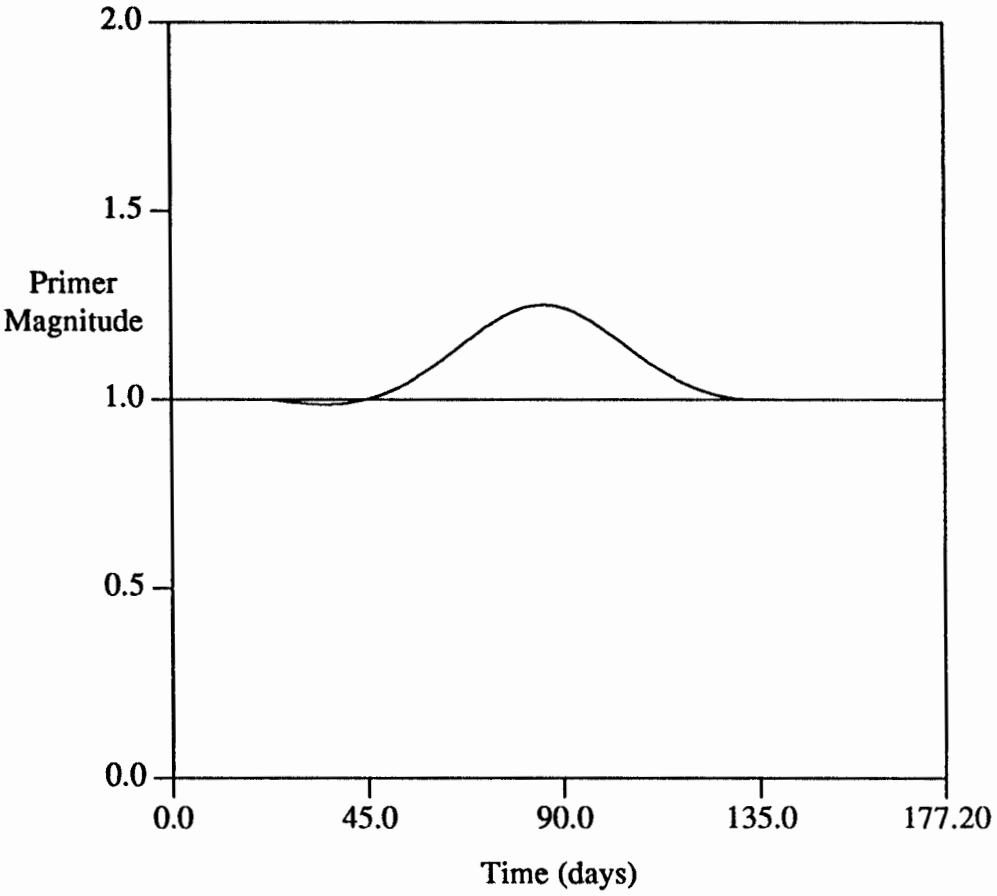

2–Impulse $\Delta\bar{v}$ Expenditure = 49.08 m/s

TOF = 108.95 days

Figure 5.29 Primer Magnitude History of Best Time-Free Two-Impulse Transfer (Case D)

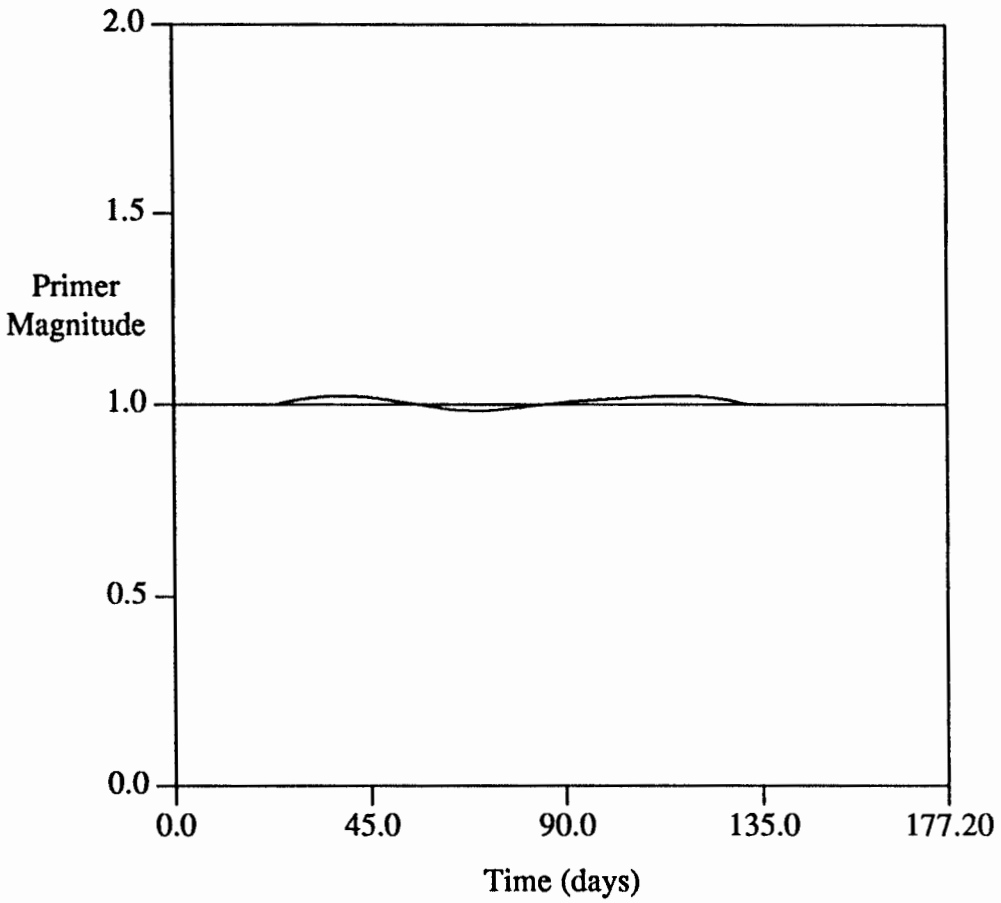

3–Impulse $\Delta\bar{v}$ Expenditure = 49.06 m/s

TOF = 108.95 days

Figure 5.30 Primer Magnitude History of Best Time-Free Three-Impulse Transfer (Case D)

Initial Halo: $A_z = 110{,}000$ km

Final Halo: $A_z = 240{,}000$ km

Transfer TOF = 108.95 days

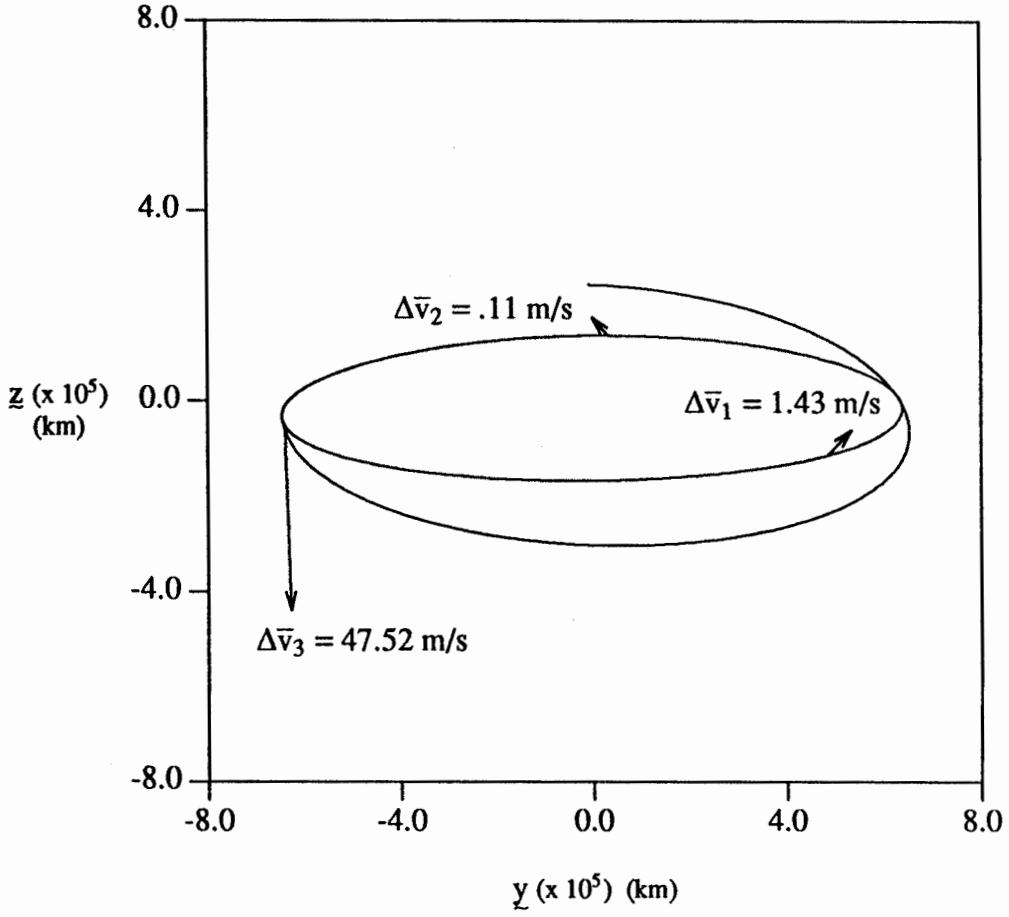

3–Impulse $\Delta\bar{v}$ Expenditure = 49.06 m/s

Figure 5.31 y-z Projection of Best Time-Free Three-Impulse Transfer (Case D)

Table 5.2 Costs on Time-Free Superior Transfers to a Variety of Final Halo Orbits

(Initial Halo: Z–Amplitude = 110,000 km)

Case	Z-Amplitude of Final Halo	Nominal 2-Impulse Transfer		Optimized Time-Free Transfers 2-Impulse		
		3-Impulse				
	(km)	$\lvert\Delta\bar{v}\rvert$ (m/s)	TOF (days)	$\lvert\Delta\bar{v}\rvert$ (m/s)	$\lvert\Delta\bar{v}\rvert$ (m/s)	TOF (days)
A	160,000	198.4586	175.9806	26.9553	NA	132.7199
B	200,000	400.4909	177.2042	40.1532	40.1391	100.7252
C	200,000	386.5867	177.2042	37.6537	37.5868†	116.8598
D	240,000	447.3212	177.2042	49.0800	49.0649†	108.9546

† Resultant trajectory is non-optimal.

CHAPTER VI

AN IMPROVED NOMINAL TRANSFER CONSTRUCTION AND INFERIOR TRANSFER OPTIMIZATION APPLICATIONS

One of the important results of Chapter V is the sensitivity of the cost on an optimal solution to the corresponding nominal solution from which the optimal transfer is derived. Consequently, a reliable and expedient means of producing an economical nominal transfer is desired. An alternative to the nominal transfers constructed using the rather cumbersome methodology presented in Chapter II is developed utilizing a differential corrections procedure in conjunction with a type of continuation algorithm. Observation that optimal transfers are characterized by a much smaller out-of-plane velocity maneuver than the nominal trajectories constructed in Chapter II provides the motivation for the development of this alternative method of transfer construction. This strategy is then utilized to create nominal transfers from large halo orbits to smaller halo orbits, and the resulting inferior transfer trajectories are optimized employing the techniques developed in Chapters III and IV.

A Spiral Method for Target Point Estimation

Suppose that a transfer is desired that moves a spacecraft from the initial halo orbit A, having a z-amplitude A_{z_A}, to the final halo orbit B, having a z-amplitude A_{z_B}. In general, A_{z_B} may be larger or smaller than A_{z_A}. Orbits A and B can be numerically determined as outlined in Chapter II so that $\tilde{\bar{x}}_A$, denoting the position vector at departure from orbit A, and $\tilde{\bar{x}}_B$, symbolizing the position vector at arrival at orbit B, are specified. The construction of a transfer path that connects $\tilde{\bar{x}}_A$ to $\tilde{\bar{x}}_B$ is accomplished using only knowledge of the numerical solutions corresponding to the two halo orbits.

The transfer path construction process employs the numerical algorithm, detailed in Reference [30], for determination of the libration-point orbits. This algorithm

assumes reasonably good approximations for spacecraft position and velocity states at particular points, called *target points*, along the trajectory. Target points are typically spaced at quarter-rev or half-rev intervals, where one revolution is easily ascertained when the trajectory is viewed in either the $\underset{\sim}{y}$-$\underset{\sim}{z}$ or the $\underset{\sim}{x}$-$\underset{\sim}{y}$ projection. Initial estimates for the target points and corresponding velocities on the transfer segment of the trajectory must be provided for input into the numerical algorithm. Assuming that the integration routine implements a quarter-rev patching scheme and that a one-rev transfer is to be constructed, then only the three interior target points on the transfer must be approximated; whereas, the two target points that bound the transfer are simply taken to be the departure and arrival positions and velocities on halo orbits A and B, respectively. The three interior target points are estimated using those target points on orbits A and B which occur near the points of minimum and maximum $\underset{\sim}{y}$- and $\underset{\sim}{z}$-excursion.

For example, if departure from the initial halo occurs near the minimum $\underset{\sim}{z}$-excursion point of orbit A, the first interior target point that must be estimated on a transfer trajectory that proceeds in a counter-clockwise direction in the $\underset{\sim}{y}$-$\underset{\sim}{z}$ projection is located near the maximum $\underset{\sim}{y}$-excursion points of the halo orbits. The second and third interior target points would then lie near the points of maximum $\underset{\sim}{z}$-excursion and minimum $\underset{\sim}{y}$-excursion along the halo orbits, respectively. Estimates for these target points and their corresponding velocities are taken to be weighted averages of the positions and velocities on orbits A and B. For the first interior target point, the position and velocity at the maximum $\underset{\sim}{y}$-excursion point on orbit A are subjectively chosen to be weighted three times more than those on orbit B. For the second interior target point, the maximum $\underset{\sim}{z}$-excursion locations and their corresponding velocities on the two halo orbits are weighted equally; additionally, the position and velocity at the minimum $\underset{\sim}{y}$-excursion on orbit B are weighted three times more than those on orbit A for the third and final interior target point. This method of constructing estimates for the position and velocity states at quarter-rev intervals on the transfer trajectory essentially creates a *spiral* of target points from orbit A to orbit B. Figure 6.1 depicts the locations of the target points, in the $\underset{\sim}{y}$-$\underset{\sim}{z}$ projection, that spiral from orbit A to orbit B to create a superior transfer between the minimum $\underset{\sim}{z}$-excursion points of the halo orbits; likewise, the spiral of target points portrayed in Figure 6.2 is utilized for the construction of an inferior transfer between the maximum $\underset{\sim}{z}$-excursion points of halo orbits A and B.

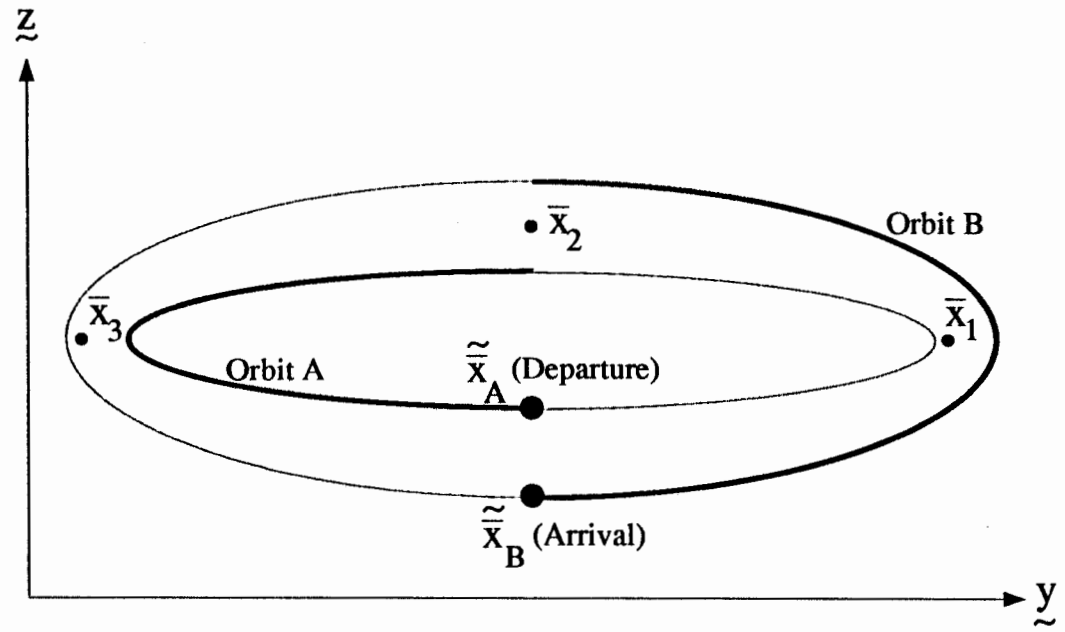

Figure 6.1 Spiral of Target Points for a Superior Transfer Beween Minimum z-Excursion Points on the Halo Orbits

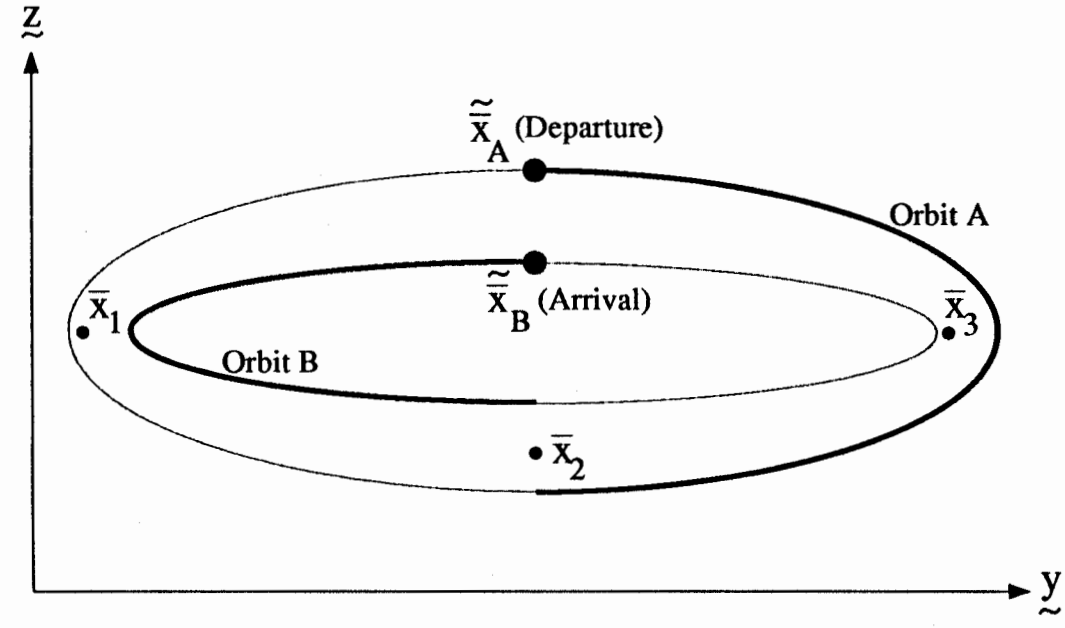

Figure 6.2 Spiral of Target Points for an Inferior Transfer Between Maximum z-Excursion Points on the Halo Orbits

With the target points on the transfer approximated and with those on the halo orbits specified by the results of the original numerical libration-point orbit determination algorithm, the entire trajectory (orbit A, transfer trajectory, orbit B) is input to the same numerical algorithm to produce an integrated solution that is continuous in position. Moreover, since no $\Delta\bar{v}$ maneuvers are imposed at the departure and arrival locations on the halo orbits, the trajectory is continuous in velocity as well. Due to the nature of the integration routine, however, the omission of these impulsive velocity maneuvers results in a solution which diverges from the halo orbits, for no transfer trajectory can be constructed that moves precisely between orbits A and B without the expenditure of fuel. Consequently, the $\Delta\bar{v}$ maneuvers must be specified and inserted along the path to construct a solution that passes through the desired departure and arrival positions.

A Differential Corrections Procedure for Impulsive Maneuvers

Let a quantity be designated with a *tilde* if its *desired* value on the halo orbits is known. So, from the individual numerical simulations of halo orbits A and B, the quantities $\tilde{\bar{x}}_A$, $\tilde{\bar{v}}_A$ and $\tilde{\bar{x}}_B$, $\tilde{\bar{v}}_B$ denote the states at departure from orbit A and at arrival at orbit B, respectively. For a given numerically integrated reference solution for the entire trajectory, assume that the impulsive maneuver $\Delta\bar{v}_0$ is implemented at departure from orbit A, which is located on the transfer trajectory at the point $\bar{x}_0$ at $t = t_0$. (Note that on the initial reference solution $\bar{x}_0 \neq \tilde{\bar{x}}_A$ and $\Delta\bar{v}_0 = 0$.) If the velocity on reference orbit A at $t = t_{0^-}$ is denoted by $\bar{v}_A$, then the velocity on the transfer at $t = t_{0^+}$, denoted by $\bar{v}_0$, can be expressed as

$$\bar{v}_0 = \bar{v}_A + \Delta\bar{v}_0 \,. \tag{6.1}$$

Let a quantity on an improved, or *differentially corrected*, trajectory be denoted with a *prime*. So, the contemporaneous variation in velocity immediately after departure is

$$\delta\bar{v}_{0^+} = \bar{v}_0' - \bar{v}_0 \,. \tag{6.2}$$

Evaluating equation (6.1) on the improved trajectory and substituting the resultant expression as well as equation (6.1) into (6.2),

$$\delta\bar{v}_{0^+} = (\bar{v}_A' + \Delta\bar{v}_0') - (\bar{v}_A + \Delta\bar{v}_0) \,. \tag{6.3}$$

Rearranging equation (6.3),

$$\Delta\bar{v}_0' = \delta\bar{v}_{0^+} + (\bar{v}_A - \tilde{\bar{v}}_A) + \Delta\bar{v}_0 \,, \tag{6.4}$$

where a $\bar{v}_A'$ is replaced by $\tilde{\bar{v}}_A$ because the desired value of this quantity on the differentially corrected solution is known. Thus, equation (6.4) provides an expression for the improved initial impulsive maneuver in terms of the unknown $\delta\bar{v}_{0^+}$, the specified difference in the reference and desired velocities on orbit A, and the reference initial impulsive maneuver. The only unknown quantity on the right side of (6.4) is $\delta\bar{v}_{0^+}$, the computation of which will be addressed shortly.

Next, however, consider impulsive maneuver $\Delta\bar{v}_f$ executed upon arrival at orbit B and located on the transfer trajectory at the point $\bar{x}_f$ at $t = t_f$. (Note that on the initial reference solution $\bar{x}_f \neq \tilde{\bar{x}}_B$ and $\Delta\bar{v}_f = 0$). The final impulsive maneuver on the differentially corrected solution is represented as

$$\Delta\bar{v}_f' = \tilde{\bar{v}}_B - \bar{v}_f' \,, \tag{6.5}$$

where, again, the symbol $\tilde{\bar{v}}_B$ is employed to stress that the desired value of the velocity on orbit B is known; additionally, $\bar{v}_f'$ can be expressed in terms of the contemporaneous variation in velocity at $t = t_{f^-}$ as

$$\bar{v}_f' = \bar{v}_f + \delta\bar{v}_{f^-} \,. \tag{6.6}$$

In a form analogous to equation (6.4) or from substitution of equation (6.6) into (6.5),

$$\Delta\bar{v}_f' = (\tilde{\bar{v}}_B - \bar{v}_B) + \Delta\bar{v}_f - \delta\bar{v}_{f^-} = \tilde{\bar{v}}_B - \bar{v}_f - \delta\bar{v}_{f^-} \,, \tag{6.7}$$

where the second form of (6.7) is used since the value of $\tilde{\bar{v}}_B$ and the reference value of $\bar{v}_f$ are known quantities; however, the computation of $\delta\bar{v}_{f^-}$ remains to be addressed.

In order to evaluate equations (6.4) and (6.7), the contemporaneous variations in velocity subsequent to departure from orbit A and prior to arrival at orbit B must be determined. These two quantities can be computed utilizing the state transition matrix expressed in equation (3.80) and evaluated on the transfer coastal arc $t_0 \leq t \leq t_f$ to yield

$$\begin{bmatrix} \delta\bar{x}_f \\ \delta\bar{v}_{f^-} \end{bmatrix} = \begin{bmatrix} \phi_{11}(t_f,t_0) & \phi_{12}(t_f,t_0) \\ \phi_{21}(t_f,t_0) & \phi_{22}(t_f,t_0) \end{bmatrix} \begin{bmatrix} \delta\bar{x}_0 \\ \delta\bar{v}_{0^+} \end{bmatrix} . \tag{6.8}$$

The quantities $\delta\bar{x}_0$ and $\delta\bar{x}_f$, which simply represent the differences between the desired locations of the impulsive maneuvers and those determined from the numerically integrated reference solution for the entire trajectory, can be expressed as

$$\delta\bar{x}_0 = \tilde{\bar{x}}_A - \bar{x}_0 \tag{6.9a}$$

$$\delta\bar{x}_f = \tilde{\bar{x}}_B - \bar{x}_f \,. \tag{6.9b}$$

The first equation of matrix expression (6.8) is

$$\delta x_f = \phi_{11}(t_f, t_0)\delta\bar{x}_0 + \phi_{12}(t_f, t_0)\delta\bar{v}_{0^+} \,. \tag{6.10}$$

Rearranging equation (6.10),

$$\delta\bar{v}_{0^+} = \phi_{12}^{-1}(t_f, t_0)\left[\delta\bar{x}_f - \phi_{11}(t_f, t_0)\delta\bar{x}_0\right] . \tag{6.11}$$

Additionally, the second equation of matrix expression (6.8) is

$$\delta\bar{v}_{f^-} = \phi_{21}(t_f, t_0)\delta\bar{x}_0 + \phi_{22}(t_f, t_0)\delta\bar{v}_{0^+} \,, \tag{6.12}$$

and substituting equation (6.11) into (6.12) renders

$$\delta\bar{v}_{f^-} = \phi_{21}(t_f, t_0)\delta\bar{x}_0 + \phi_{22}(t_f, t_0)\phi_{12}^{-1}(t_f, t_0)\left[\delta\bar{x}_f - \phi_{11}(t_f, t_0)\delta\bar{x}_0\right] . \tag{6.13}$$

Finally, with expressions (6.11) and (6.13) for the contemporaneous variation in velocity subsequent to the initial impulsive maneuver and prior to the final maneuver, the differentially corrected $\Delta\bar{v}$'s can now be computed. Substituting (6.11) into equation (6.4) yields

$$\Delta\bar{v}_0' = \phi_{12}^{-1}(t_f, t_0)\left[\delta\bar{x}_f - \phi_{11}(t_f, t_0)\delta\bar{x}_0\right] + (\bar{v}_A - \tilde{\bar{v}}_A) + \Delta\bar{v}_0 \,, \tag{6.14}$$

and substituting (6.13) into equation (6.7) yields

$$\Delta\bar{v}_f' = \tilde{\bar{v}}_B - \bar{v}_f - \phi_{21}(t_f, t_0)\delta\bar{x}_0 - \phi_{22}(t_f, t_0)\phi_{12}^{-1}(t_f, t_0)\left[\delta\bar{x}_f - \phi_{11}(t_f, t_0)\delta\bar{x}_0\right] . \tag{6.15}$$

Consequently, the impulsive maneuvers on the numerically determined reference trajectory should be differentially corrected to the values computed in equations (6.14) and (6.15), where $\delta\bar{x}_0$ and $\delta\bar{x}_f$ are computed from (6.9), such that the improved trajectory more closely approximates the desired locations of departure and arrival on the halo orbits. Computation of differentially corrected trajectories continues iteratively until the departure and arrival position on the improved path lie within a selected tolerance region. Provided that the difference in z-amplitudes of the two halo orbits is fairly small, convergence to the desired positions is achieved. The primary benefit of this differential corrections procedure is the refined estimation of the targets points on the transfer trajectory that connects halo orbits A and B.

Although the differential corrections procedure outlined above produces a complete solution that converges to the departure and arrival locations on the respective halo orbits A and B, the other points on the halo orbit segments of the integrated trajectory may diverge from those position coordinates desired on the halo orbits. That is, the differential corrections algorithm only ensures convergence to the last point on orbit A and to the first point on orbit B; all other points representing the portions of the integrated trajectory that correlate to the initial and final halo orbits may remain remote from the affiliated coordinates on the specified halos. The weighting matrix scheme introduced in Chapter II is implemented during each numerical integration in order to lessen the deviation of the solution from the desired halo orbits; however, divergence still occurs. Therefore, the components of the impulsive maneuvers must be further modified to accomplish convergence of the halo orbit segments of the complete integrated trajectory to the desired orbits A and B. This modification is performed manually using a visual comparison of the integrated solution to the desired halo orbits in order to repeatedly adjust the $\Delta\bar{v}$ maneuvers. Despite the subjective nature of this procedure, insight into the appropriate alterations of the velocity components is readily gained, and nominal transfers between two libration-point orbits can be constructed in a straightforward and rapid fashion.

A Continuation Algorithm for Nominal Transfer Construction

If the difference in the z-amplitudes of halo orbits A and B becomes too great (*i.e.*, $|A_{z_A} - A_{z_B}| \geq .20A_{z_A}$), the differential corrections procedure will fail to converge to the desired coordinates of departure and arrival. Hence, the original formulation of the single-path determination of a nominal transfer from halo orbit A to halo orbit B must be recast as the construction of multiple nominal transfers from halo orbit A to a series of intermediate halo orbits that culminates at halo orbit B. Note that the intermediate nominal transfers are not arranged consecutively; rather, each nominal contributes to the construction of the successive transfer such that the outcome of the algorithm is still a one-rev transfer trajectory. Introduce an intermediate halo orbit C that has a z-amplitude

$$A_{z_C} = A_{z_A} + \Delta A_z \, ,$$

where ΔA_z is chosen at the discretion of the trajectory designer. A transfer trajectory passing through the specified points of departure on orbit A and arrival on orbit C is

then constructed utilizing the methodology, developed above, that employs only the integrated solutions for these halo orbits and a differential corrections procedure to determine the impulsive maneuvers necessary to implement the transfer. The resultant complete trajectory (orbit A, transfer trajectory, orbit C) will not necessarily converge to the desired solutions for the halo orbits over the appropriate portion of the path; thus, the components of the impulsive maneuvers are modified manually until the complete numerical solution includes convergence to the prescribed initial and final orbits. A nominal transfer between two halo orbits of z-amplitude A_{z_A} and A_{z_C} results.

However, the ultimate goal is the determination of a nominal transfer to the final halo orbit B possessing a z-amplitude of A_{z_B}. If the difference in z-amplitudes of orbits B and C is greater than the increment ΔA_z, continue the series of intermediate halo orbits with the introduction of another orbit D having z-amplitude A_{z_D} such that

$$A_{z_D} = A_{z_C} + \Delta A_z \, .$$

With the aid of the nominal transfer between orbits A and C, the procedure for construction of a nominal transfer from halo orbit A to halo orbit D is considerably abbreviated from that developed in the previous section. The target points on the nominal $A \rightarrow C$ transfer are taken as approximations to those target points on the transfer from orbit A to orbit D. Consequently, the spiral method of target point estimation is omitted from the algorithm at this step. Often the differential corrections procedure may be omitted as well, and only the manual modification of the impulsive maneuvers is required to produce the desired transfer.

The introduction of intermediate halo orbits and the subsequent construction of nominal transfers from orbit A to the intermediate halos continue until the difference in z-amplitude between the last intermediate halo and the final halo orbit B is less than ΔA_z. Values of ΔA_z on the order of 10,000 km to 50,000 km are appropriate for the transfer trajectories constructed here. The final transfer trajectory constructed in this chain of nominal solutions is the transfer path, desired at the outset, that moves a spacecraft between orbits A and B. The determination of a transfer from halo orbit A to each subsequent intermediate halo, and finally to halo orbit B, employs knowledge of the preceding nominal solution to continue or progress the algorithm; consequently, the sequential routine outlined above is an example of a type of *continuation algorithm.*

This continuation algorithm is applied to the construction of a transfer trajectory from an initial halo orbit characterized by a z-amplitude of $A_{z_A} = 240{,}000$ km to a final

halo orbit with z-amplitude $A_{z_B} = 110{,}000$ km. Two halo orbits C and D that have intermediate z-amplitudes of 200,000 km and 160,000 km, respectively, are introduced such that the product of the sequential determination of the three transfers

Halo A (240,000 km) → Halo C (200,000 km)
Halo A (240,000 km) → Halo D (160,000 km)
Halo A (240,000 km) → Halo B (110,000 km)

is the desired nominal transfer from halo orbit A to halo orbit B. The maximum $\underset{\sim}{z}$-excursions on the halo orbits are selected to be the departure and arrival locations; thus, the three target points estimated by the spiral method are, respectively, the minimum $\underset{\sim}{y}$-excursion, the minimum $\underset{\sim}{z}$-excursion, and the maximum $\underset{\sim}{y}$-excursion points on the A → C transfer trajectory. After differential correction and manual modification of the impulsive maneuvers, the nominal transfer plotted relative to the libration point L_1 and illustrated in the $\underset{\sim}{y}$-$\underset{\sim}{z}$ projection in Figure 6.3 is attained. Then, the target points on this nominal transfer are utilized as estimates for the target points on the path connecting halo orbits A and D. Again, the components of the impulsive maneuvers are varied manually to produce the trajectory shown in Figure 6.4. Next, the third nominal transfer from the initial halo orbit A to the final halo orbit B is constructed using the transfer path of Figure 6.4 as an initial approximation, and the final outcome of the continuation algorithm is the desired nominal transfer depicted in the $\underset{\sim}{y}$-$\underset{\sim}{z}$, $\underset{\sim}{x}$-$\underset{\sim}{y}$, and $\underset{\sim}{x}$-$\underset{\sim}{z}$ projections in Figures 6.5-6.7.

Optimal Time-Free Inferior Transfer Trajectories

In order to determine the effect of declivity and acclivity on the cost of a transfer trajectory between two libration-point orbits, inferior transfers are constructed between halo orbits of z-amplitude gradations equal to those considered for the superior transfers presented in Chapter V. For each of the inferior transfers, the date of injection into the initial halo orbit is unaltered from August 17; however, the selection of the maximum $\underset{\sim}{z}$-excursion points for the departure and arrival locations on the halo orbits differs from the choice of the minimum $\underset{\sim}{z}$-excursion for those transfers constructed in Chapter V. The initial phase angles are chosen such that the spacecraft is injected near the point of maximum $\underset{\sim}{z}$-excursion on the initial halo orbit. The spacecraft then proceeds for approximately one revolution in a counter-clockwise direction in the $\underset{\sim}{y}$-$\underset{\sim}{z}$ projection prior to commencement of the one-rev transfer segment. Arrival at the final

Initial Halo: $A_z = 240{,}000$ km

Final Halo: $A_z = 200{,}000$ km

Transfer TOF = 175.91 days

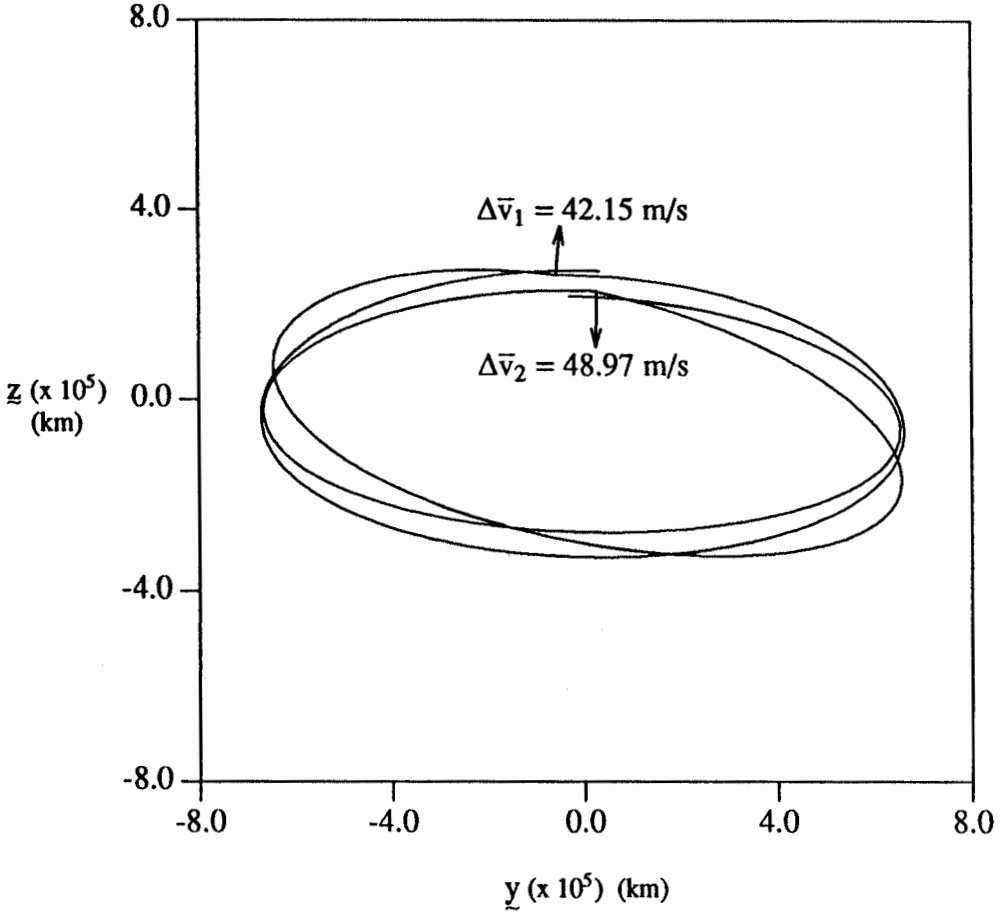

2–Impulse $\Delta\bar{v}$ Expenditure = 91.11 m/s

Figure 6.3 $\underline{y}$-$\underline{z}$ Projection of the Orbit A → Orbit C Nominal Trajectory

Initial Halo: $A_z = 240{,}000$ km

Final Halo: $A_z = 160{,}000$ km

Transfer TOF = 175.91 days

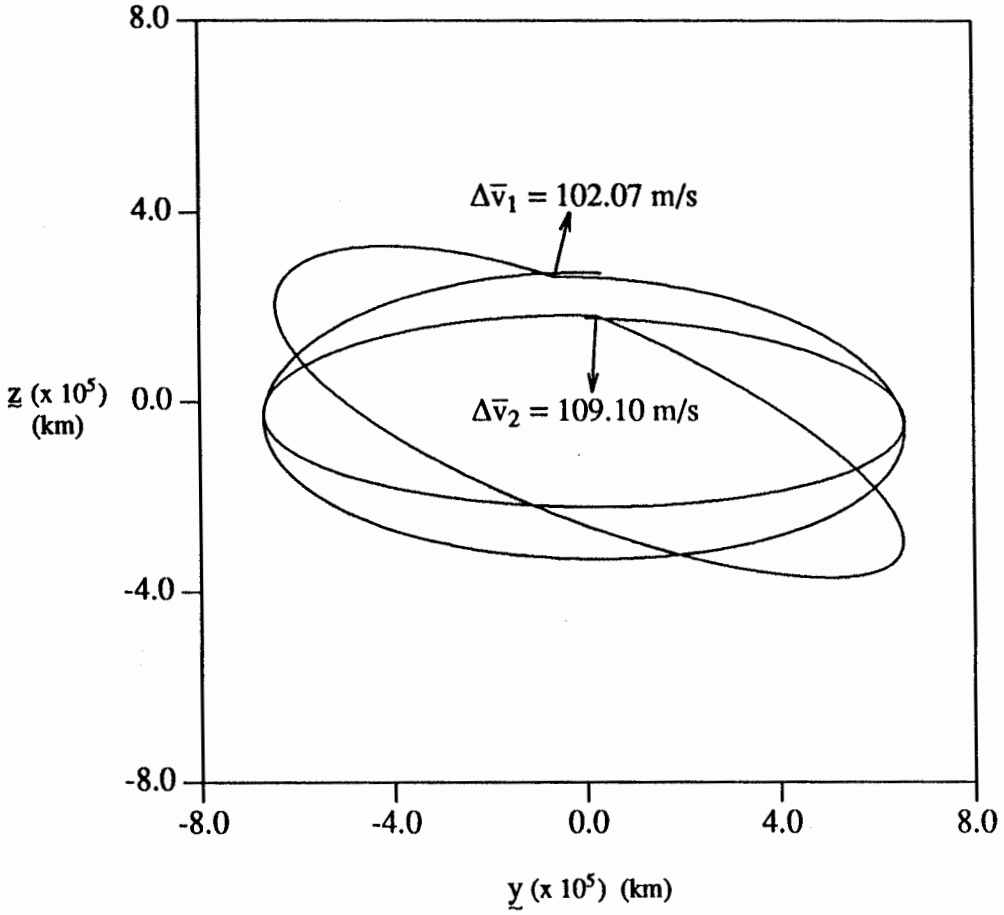

2–Impulse $\Delta\bar{v}$ Expenditure = 211.17 m/s

Figure 6.4 $\underline{y}$-$\underline{z}$ Projection of the Orbit A → Orbit D Nominal Trajectory

Initial Halo: $A_z = 240{,}000$ km

Final Halo: $A_z = 110{,}000$ km

Transfer TOF = 175.91 days

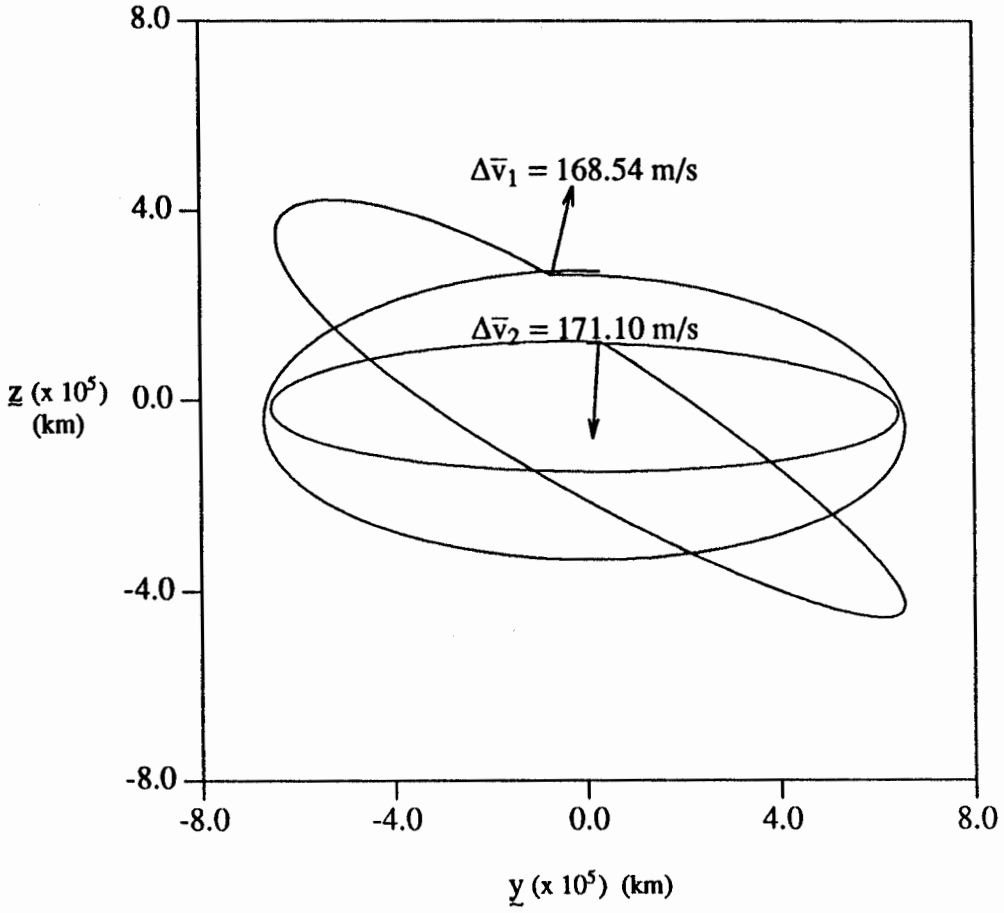

2–Impulse $\Delta\bar{v}$ Expenditure = 339.64 m/s

Figure 6.5 $\underset{\sim}{y}$-$\underset{\sim}{z}$ Projection of the Orbit A → Orbit B Nominal Trajectory

Initial Halo: $A_z = 240{,}000$ km

Final Halo: $A_z = 110{,}000$ km

Transfer TOF = 175.91 days

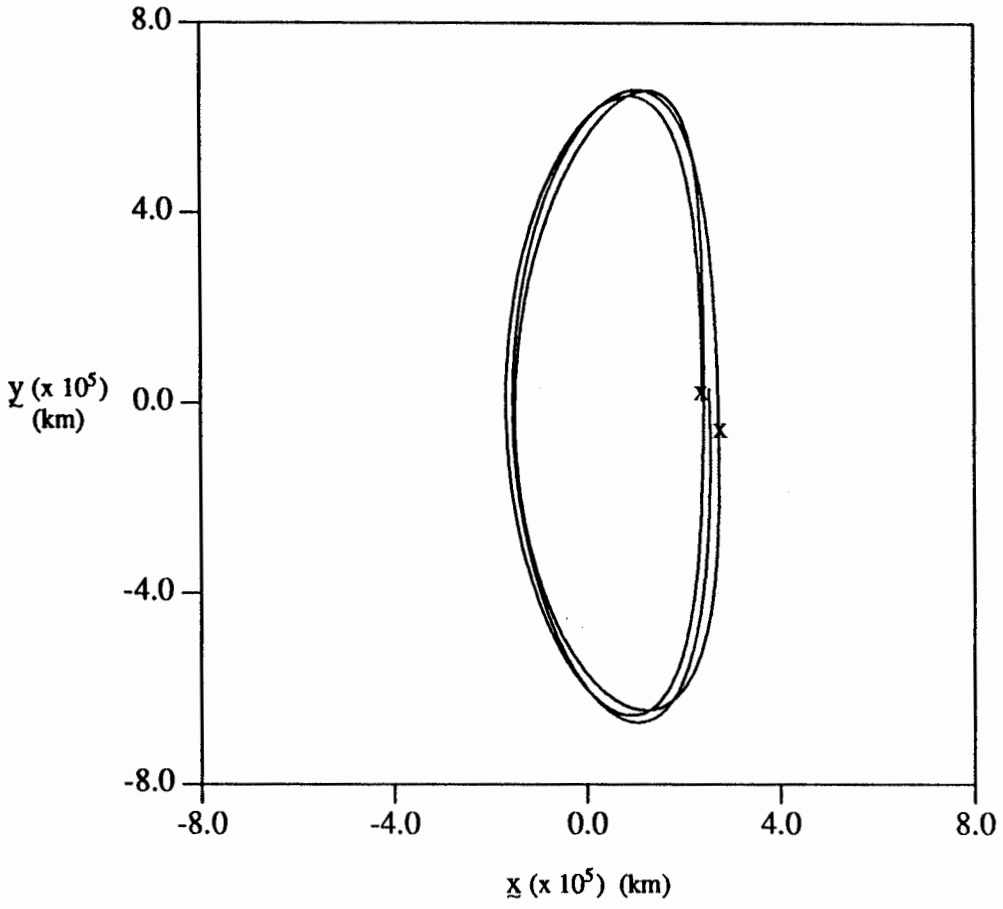

2–Impulse $\Delta\bar{v}$ Expenditure = 339.64 m/s

Figure 6.6 $\underset{\sim}{x}$-$\underset{\sim}{y}$ Projection of the Orbit A → Orbit B Nominal Trajectory

Initial Halo: $A_z = 240{,}000$ km

Final Halo: $A_z = 110{,}000$ km

Transfer TOF = 175.91 days

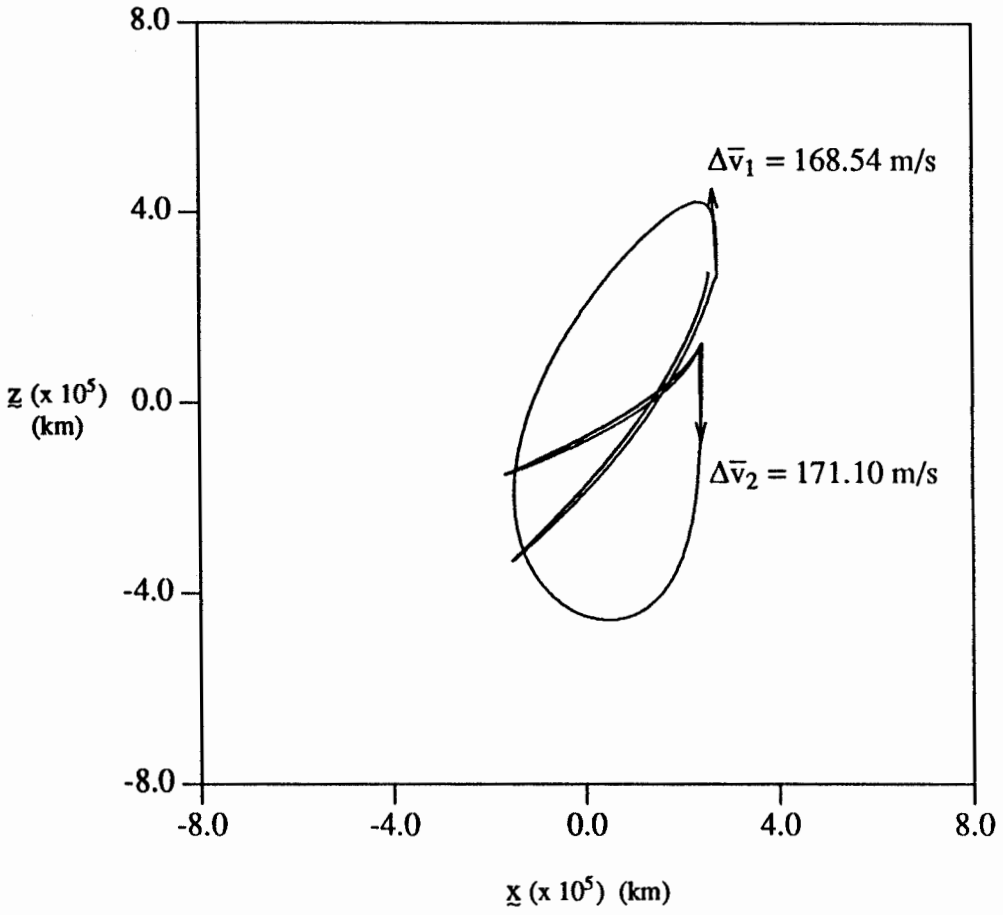

2–Impulse $\Delta\bar{v}$ Expenditure = 339.64 m/s

Figure 6.7 $\underset{\sim}{x}$-$\underset{\sim}{z}$ Projection of the Orbit A → Orbit B Nominal Trajectory

halo orbit occurs near its maximum $\underset{\sim}{z}$-excursion point, and the trajectory concludes with one revolution in the final halo. So, each nominal trajectory contains three complete revolutions in the $\underset{\sim}{y}$-$\underset{\sim}{z}$ plane.

The time-free optimization of the characteristic velocity on each two-impulse nominal transfer is investigated by assessing the slope at the endpoints of a plot of the magnitude of the primer vector over the duration of the transfer. If the slope of the primer magnitude at the terminal points of the transfer segment of the trajectory is non-zero, initial and final coastal segments are implemented, and the coastal periods are optimized employing the BFGS multi-variable search routine. If the magnitude of the primer vector then lies entirely below unity, the resultant transfer trajectory is optimal; however, if any portion of the primer magnitude history exceeds one, the optimization process proceeds with the application of interior impulses. The location and timing of each impulse must be optimized to render an optimal time-free solution.

Three cases are investigated for which inferior transfers are constructed from initial halo orbits characterized by z-amplitudes of 160,000 km (Case E), 200,000 km (Case F), and 240,000 km (Case G). A z-amplitude of A_z = 110,000 km is imposed on the final halo orbit. The nominal transfer trajectories for cases E-G are constructed utilizing the spiral method, the differential corrections procedure, and the continuation algorithm outlined in the preceding sections. The z-amplitude increment ΔA_z is chosen to assume the values 10,000 km and 20,000 km for the creation of the nominal transfer in case E and the values of 40,000 km and 50,000 km for the creation of the nominal transfers in cases F and G.

The $\underset{\sim}{y}$-$\underset{\sim}{z}$ projection of the two-impulse nominal trajectory for case E is illustrated in Figure 6.8. The transfer segment of this trajectory is accomplished in 175.98 days at a cost of 160.60 m/s, and the resulting history of the primer magnitude over this portion of the trajectory is shown in Figure 6.9. Clearly, the slopes of the primer magnitude at the initial and final instant are unequal to zero; thus, the cost on the nominal transfer can be improved by the inclusion of coasts on the initial and final halo orbits. Since the slopes of the primer magnitude at the initial and final instants on the reference solution are positive and negative, respectively, an initial coast ($dt_0 > 0$) and a final coast ($dt_f < 0$) are warranted. The optimized coastal periods are determined to be dt_0 = 22.83 days and dt_f = –24.02 days. In order to illustrate these coastal periods, the corresponding primer magnitude history is plotted relative to the time of flight on the nominal transfer [See Figure 6.10]. Although the slopes of the primer magnitude at the

endpoints of the transfer are zero, the primer magnitude still lies, in part, above unity and indicates that the cost on the resulting trajectory can be improved. Despite being non-optimal, the corresponding trajectory [See Figure 6.11], which is executed at a cost of only 28.16 m/s (a substantial saving of 132.44 m/s over the nominal solution) and which is accomplished in 129.13 days, represents the *best* time-free two-impulse transfer trajectory obtained for case E. A comparison of Figures 6.8 and 6.11 shows that the coastal arcs drive the departure and arrival locations on the halo orbits toward points of minimum and maximum $\underline{y}$-excursion, respectively.

A further reduction in cost can only be achieved by the addition of interior impulses. One, two, and three interior impulses are applied, and the locations and times of each impulse are optimized prior to the application of the next impulse; however, an optimal solution is elusive. Illustrated in Figures 6.12 and 6.13 are the primer magnitude history and the $\underline{y}$-$\underline{z}$ projection of the best complete trajectory that contains one interior impulse. Notice that application of an interior impulse results in non-zero slopes at the endpoints of the primer magnitude history plotted in Figure 6.12. Restoration of these slopes to zero would require the simultaneous optimization of the coastal periods and the timing and location of the interior impulse, but such an approach destroys the integrity of the numerical solutions for the initial and final halo orbits. Thus, the coastal periods are unaltered during the optimization of the interior impulse. The time-free three-impulse transfer illustrated in Figure 6.13 is accomplished at a cost of 26.38 m/s. In addition, the primer magnitude histories for the best time-free four- and five-impulse solutions are shown in Figure 6.14 and 6.15, respectively; however, only a minuscule reduction in cost is achieved by the application of the third interior impulse; therefore, no significant gains are expected by the implementation of additional impulses. Representing a compromise between a practical number of impulsive maneuvers and the greatest reduction in $|\Delta\bar{v}|$, the three-impulse trajectory of Figure 6.13 is considered to be the *best* time-free transfer trajectory for case E that results from this procedure.

The two-impulse nominal solutions and the corresponding primer magnitude histories for cases F and G are displayed in Figures 6.16-6.17 and Figures 6.24-6.25, respectively. Note that the nominal transfer constructed in case G is identical to the one selected to demonstrate the continuation algorithm in section B [See Figures 6.5-6.7]. The time-free optimizations of cases F and G follow the trends established by case E. Figures 6.18-6.19 (case F) and 6.26-6.27 (case G) illustrate the plots of the

primer magnitude over the duration of the best time-free two-impulse transfers and the $\underset{\sim}{y}$-$\underset{\sim}{z}$ projections of the corresponding trajectories. Once again, the coastal periods act to move the departure and arrival locations toward the extreme $\underset{\sim}{y}$-excursion points. Also, the cost on the time-free two-impulse trajectory is reduced substantially from 254.95 m/s to 44.25 m/s in case F and from 339.64 m/s to 65.03 m/s in case G. Interior impulses are applied in an effort to further reduce the cost necessary to implement each transfer. The resulting best time-free three-impulse primer magnitude histories, the corresponding $\underset{\sim}{y}$-$\underset{\sim}{z}$ projections, and the primer magnitude histories of the best time-free four- and five-impulse solutions are illustrated in Figures 6.20-6.23 and Figures 6.28-6.31 for cases F and G, respectively. Again the time-free three-impulse transfer trajectories seen in Figures 6.21 (case F) and 6.29 (case G) are deemed the best compromise between fuel economy and practicality of maneuver occurrences.

In each of the three cases investigated, the best time-free two-impulse transfer trajectory [See Figures 6.11, 6.19, and 6.27] has a duration of approximately three-quarters of a revolution using a fairly small initial impulsive maneuver followed by a final maneuver of significant magnitude. Notice that the bulk of the transition to the final halo orbit by these two-impulse solutions occurs chiefly in the first quadrant of the $\underset{\sim}{y}$-$\underset{\sim}{z}$ plane. The primer magnitude histories [See Figures 6.10, 6.18, and 6.26] corresponding to the best two-impulse transfers are all very similar. After the application and the subsequent optimization of an interior impulse, however, the distribution of $|\Delta\bar{v}|$ expenditure is altered. For case E, the interior impulse applied near the minimum $\underset{\sim}{y}$-excursion becomes the dominant impulsive maneuver; whereas, for cases F and G, the magnitude of the interior impulse is quite small, and the final maneuver maintains its strength. Unlike the transfers in cases F and G which retain the characteristic of predominantly third-quadrant transferal, the preponderance of the transition to the final halo orbit by the transfer in case E switches to the third quadrant. Although this difference in distribution of $|\Delta\bar{v}|$ expenditure is not immediately apparent in a comparison of the primer magnitude histories for the best three-impulse transfers for the cases E-G [See Figures 6.12, 6.20, and 6.28], the primer magnitude histories for the best four- and five-impulse transfers for case E are markedly different from those for cases F and G. The distinction between the time-free optimization of case E and that of cases F and G is also evident in the increased effort required to optimize the placement and timing of each additional impulse applied to the trajectories constructed in case E. The increased primer magnitudes in Figures 6.14 and 6.15 reflect the difficulty

Initial Halo: $A_z = 160{,}000$ km

Final Halo: $A_z = 110{,}000$ km

Transfer TOF = 175.98 days

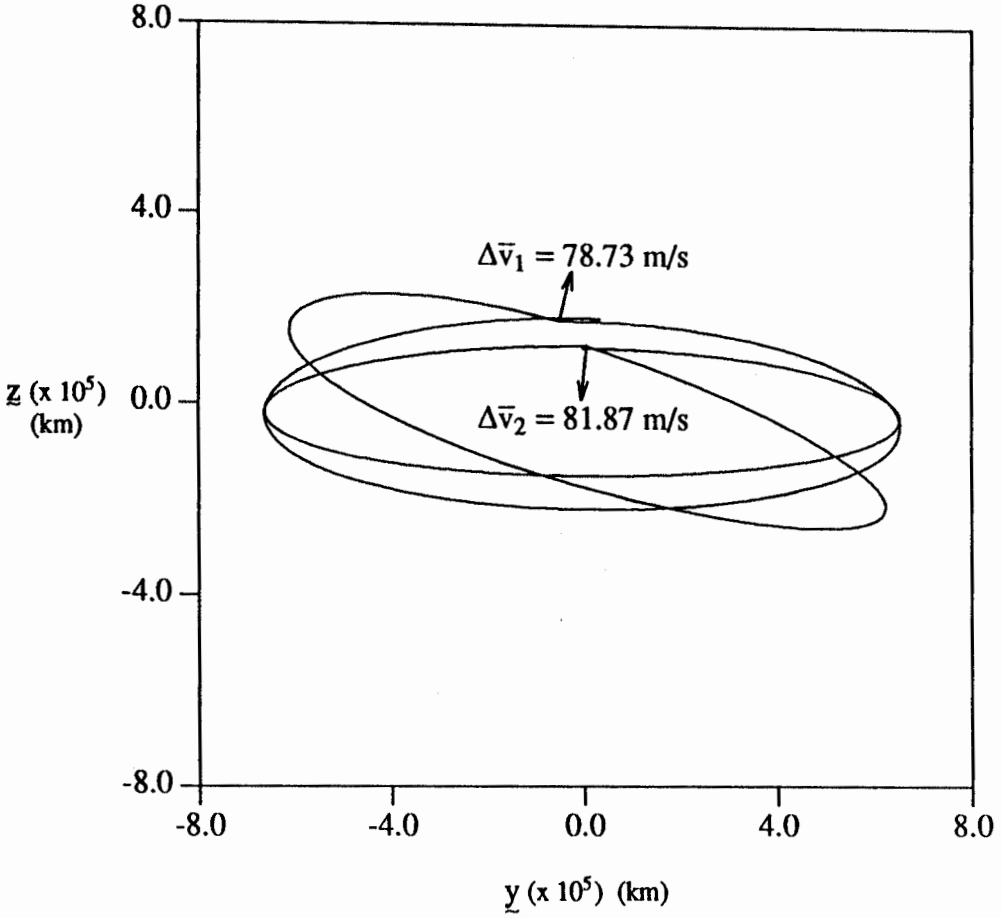

2–Impulse $\Delta\bar{v}$ Expenditure = 160.60 m/s

Figure 6.8 $\underline{y}$-$\underline{z}$ Projection of Two-Impulse Nominal Trajectory (Case E)

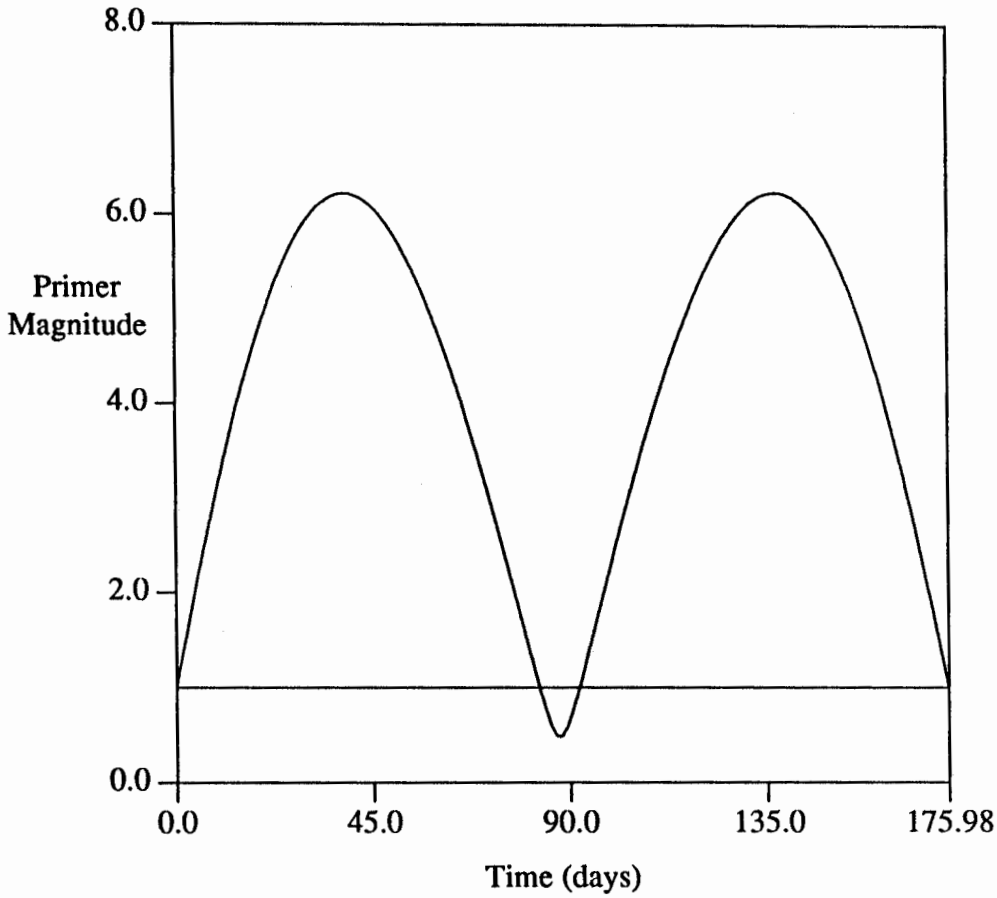

2–Impulse $\Delta\bar{v}$ Expenditure = 160.60 m/s

Transfer TOF = 175.98 days

Figure 6.9 Primer Magnitude History of Two-Impulse Nominal Transfer (Case E)

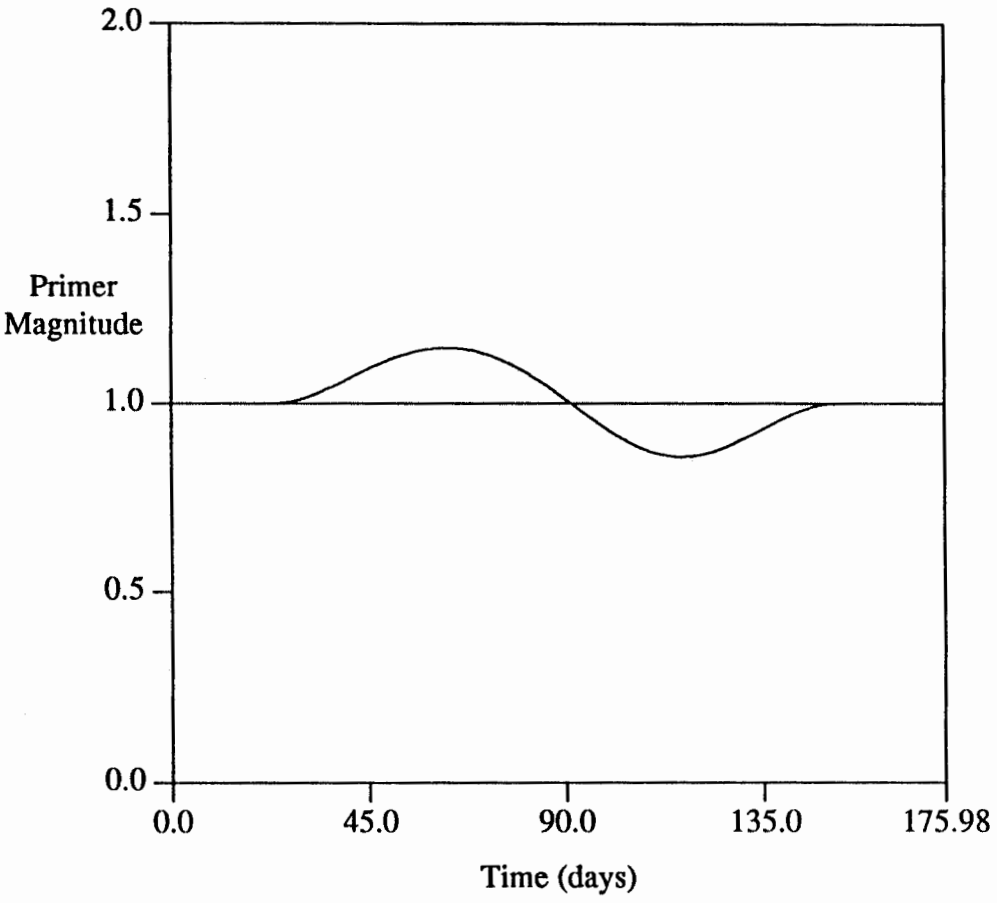

2–Impulse $\Delta\bar{v}$ Expenditure = 28.16 m/s

Transfer TOF = 129.13 days

Figure 6.10 Primer Magnitude History of Best Time-Free Two-Impulse Transfer (Case E)

Initial Halo: $A_z = 160{,}000$ km

Final Halo: $A_z = 110{,}000$ km

Transfer TOF = 129.13 days

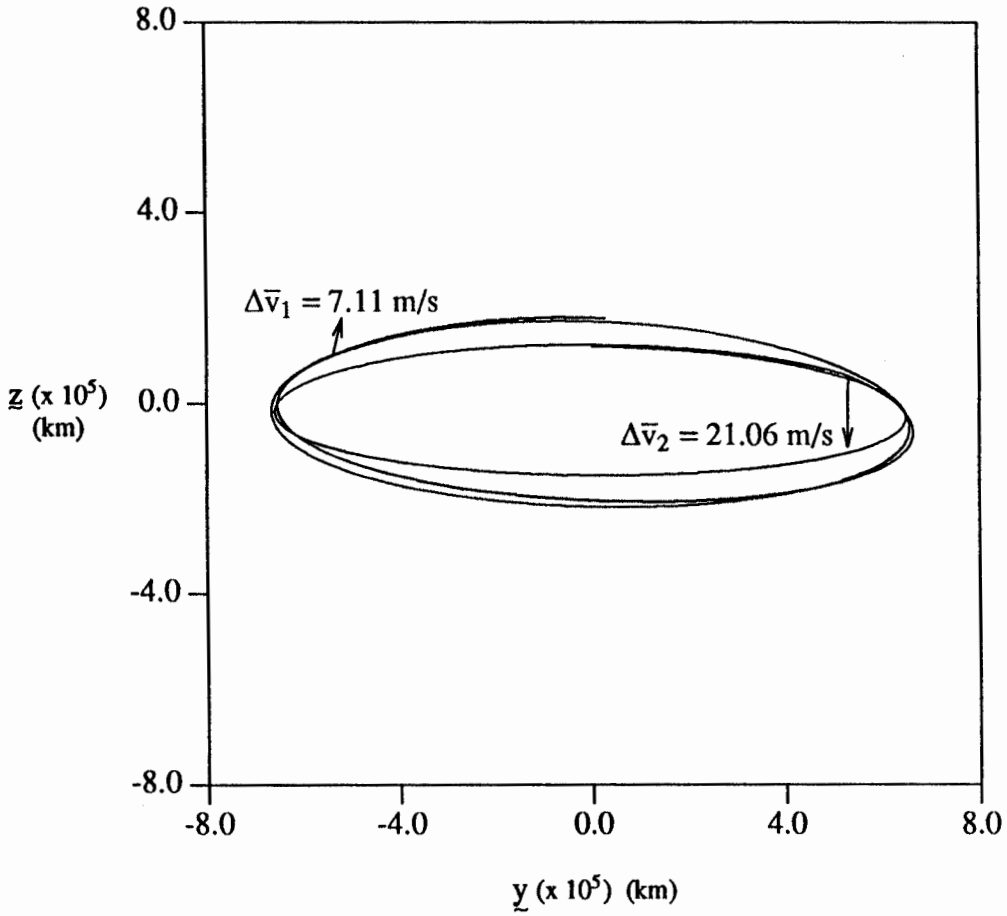

2–Impulse $\Delta\bar{v}$ Expenditure = 28.16 m/s

Figure 6.11 y-$\underline{z}$ Projection of Best Time-Free Two-Impulse Transfer (Case E)

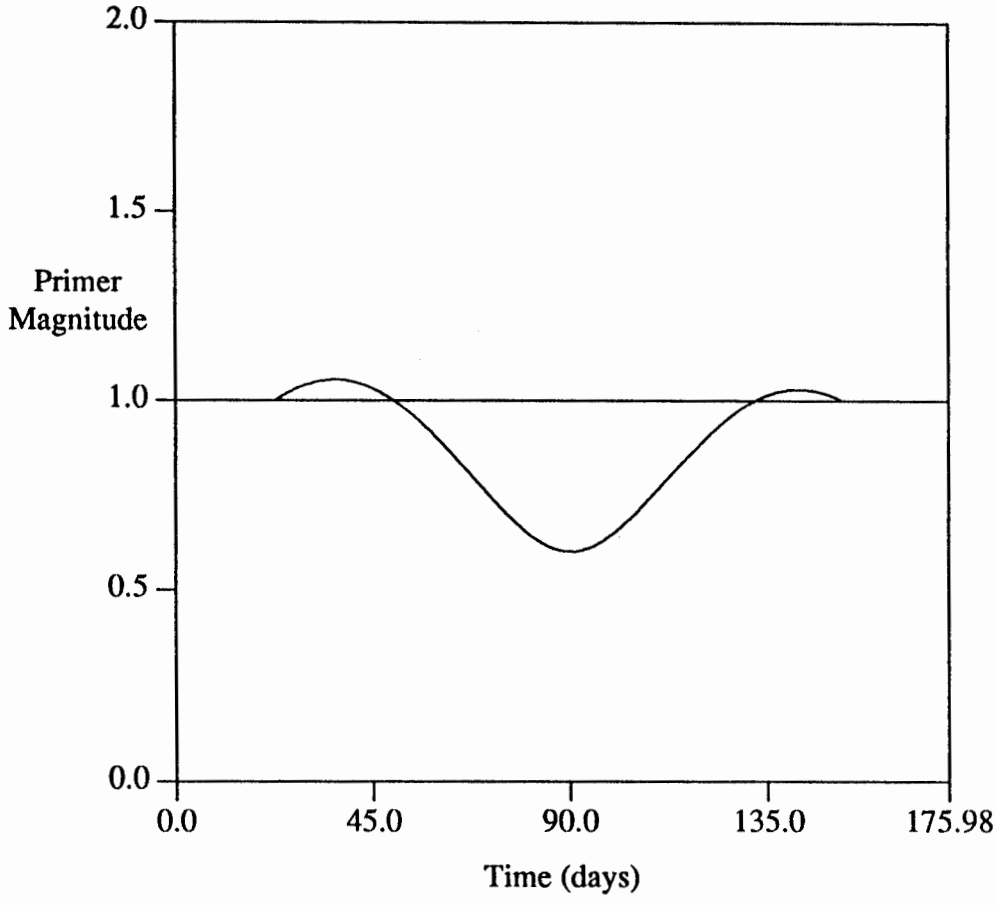

3–Impulse $\Delta\bar{v}$ Expenditure = 26.38 m/s

Transfer TOF = 129.13 days

Figure 6.12 Primer Magnitude History of Best Time-Free Three-Impulse Transfer (Case E)

Initial Halo: A_z = 160,000 km

Final Halo: A_z = 110,000 km

Transfer TOF = 129.13 days

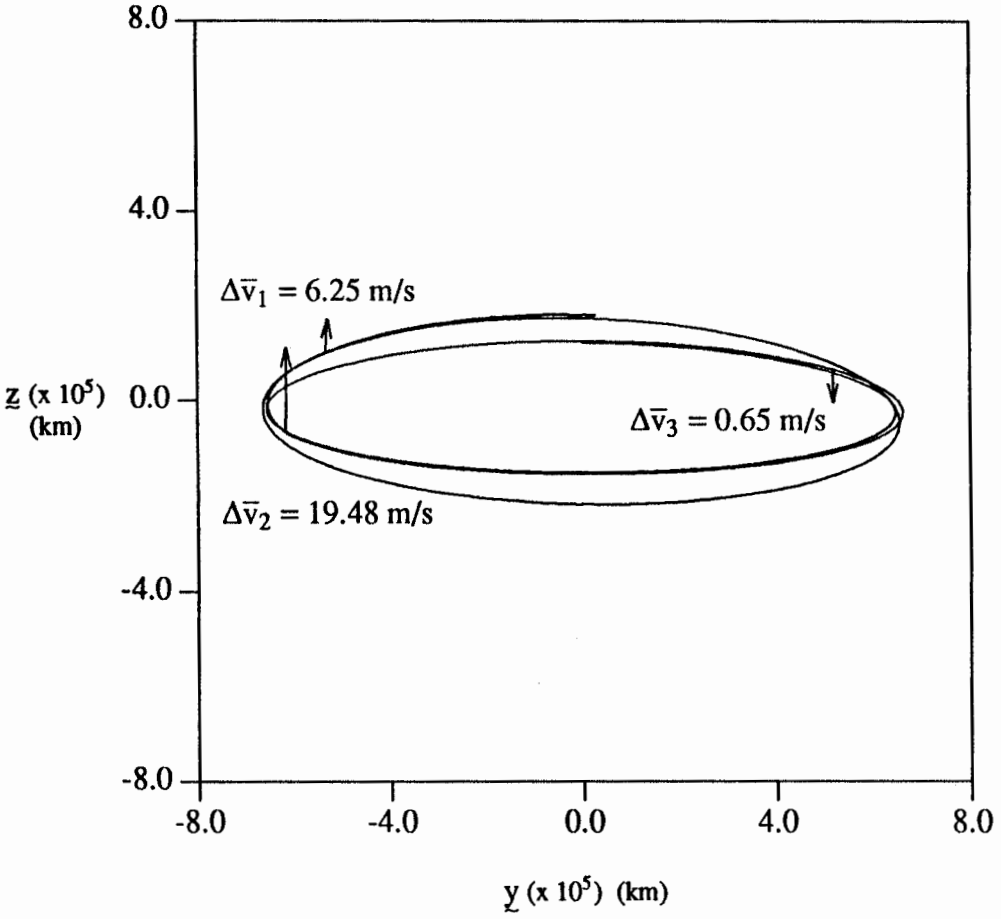

3–Impulse $\Delta\bar{v}$ Expenditure = 26.38 m/s

Figure 6.13 y-z Projection of Best Time-Free Three-Impulse Transfer (Case E)

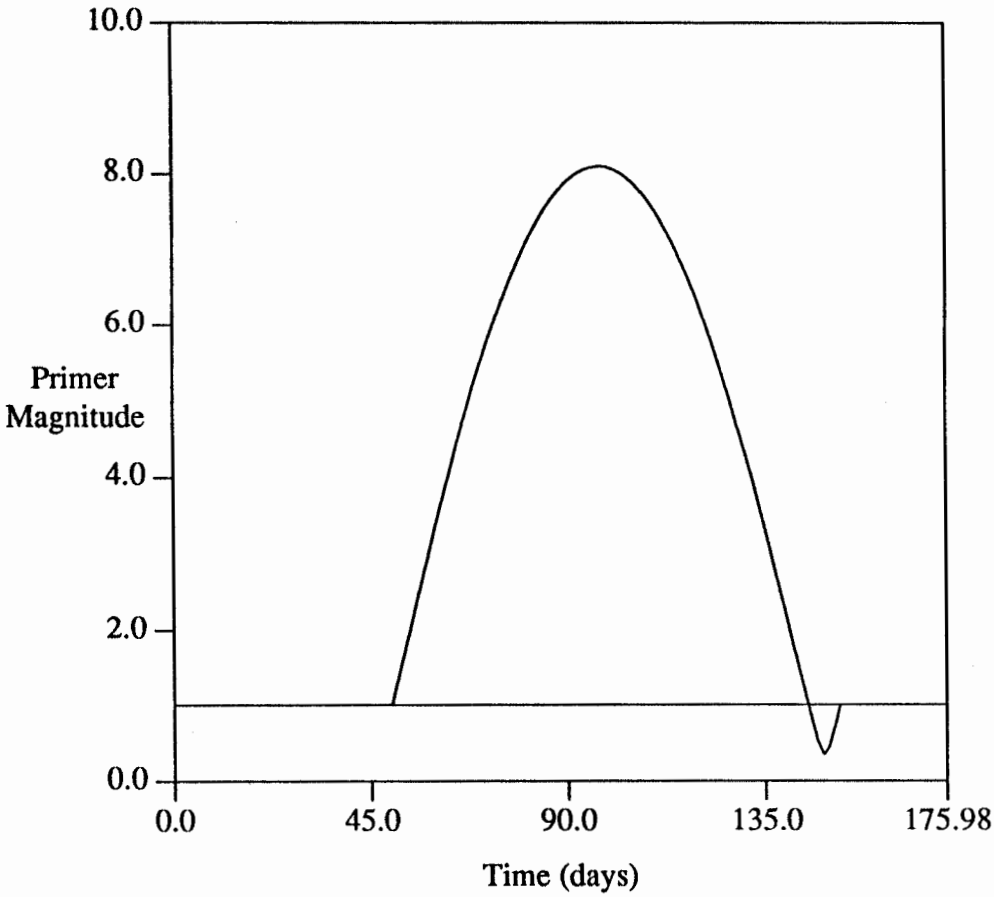

4–Impulse $\Delta\bar{v}$ Expenditure = 26.23 m/s

TOF = 129.13 days

Figure 6.14 Primer Magnitude History of Best Time-Free Four-Impulse Transfer (Case E)

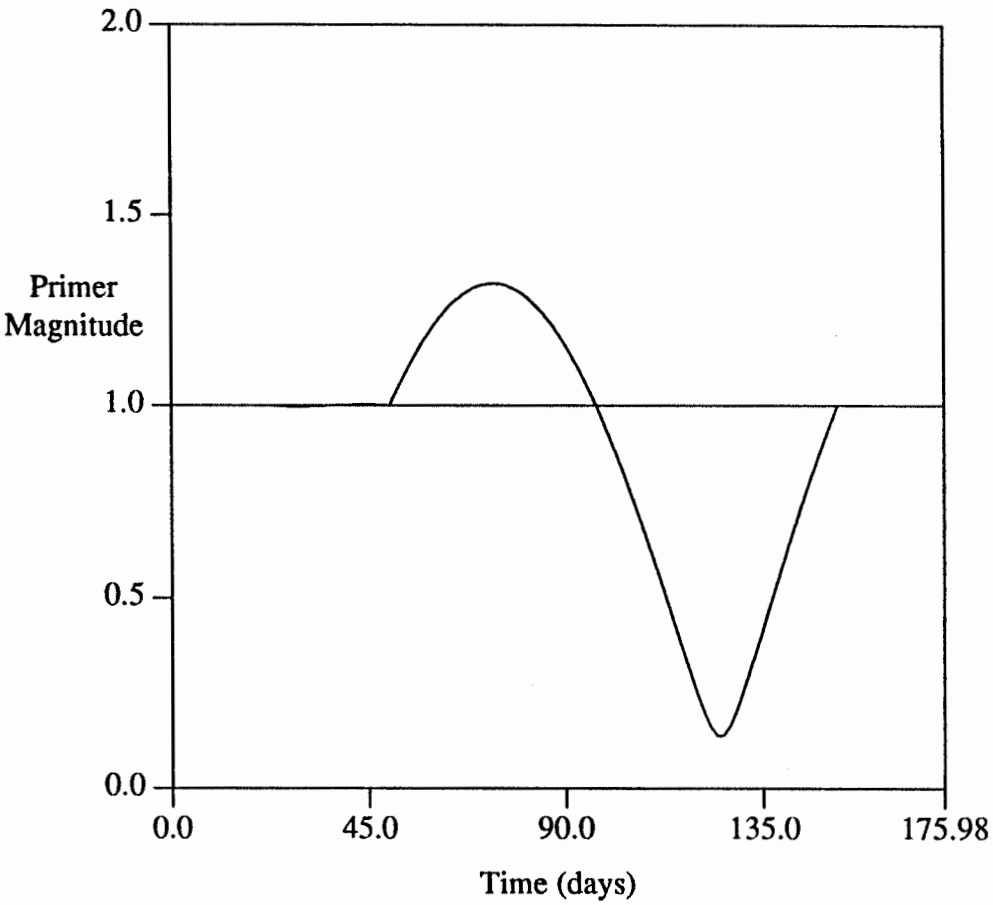

5–Impulse $\Delta\bar{v}$ Expenditure = 26.23 m/s

TOF = 129.13 days

Figure 6.15 Primer Magnitude History of Best Time-Free Five-Impulse Transfer (Case E)

Initial Halo: $A_z = 200{,}000$ km

Final Halo: $A_z = 110{,}000$ km

Transfer TOF = 175.95 days

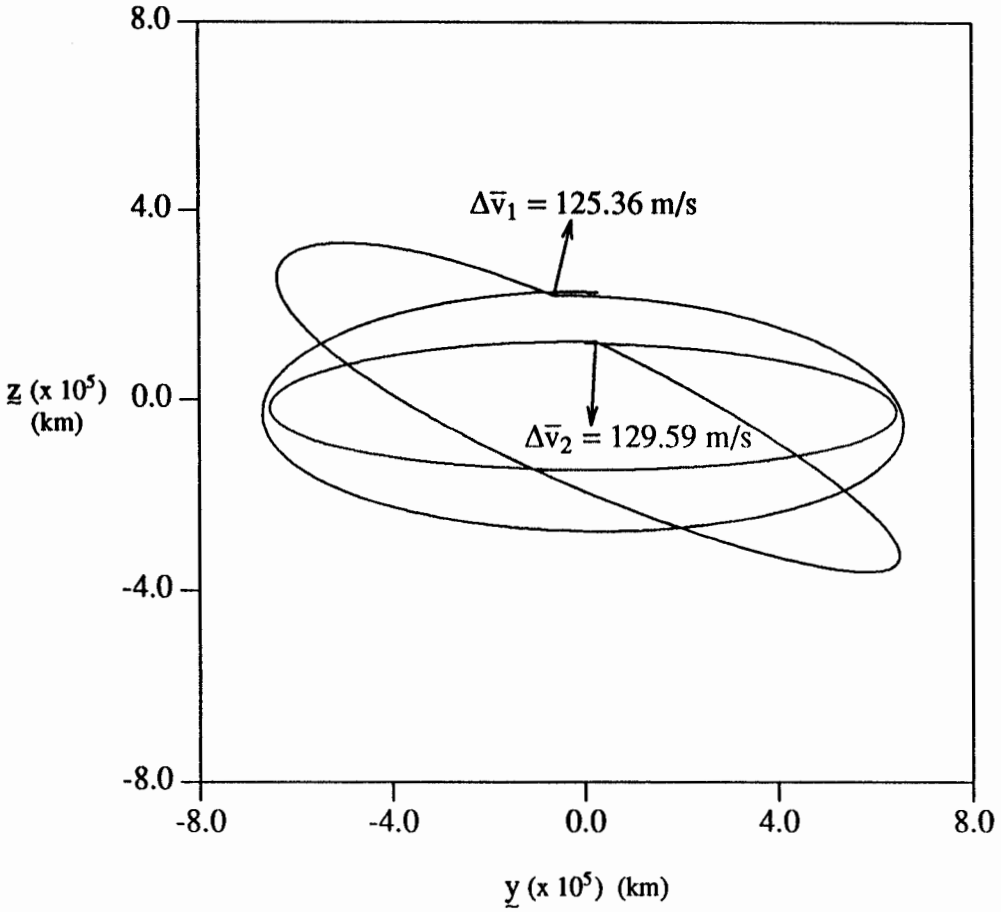

2–Impulse $\Delta\bar{v}$ Expenditure = 254.95 m/s

Figure 6.16 y-z Projection of Two-Impulse Nominal Trajectory (Case F)

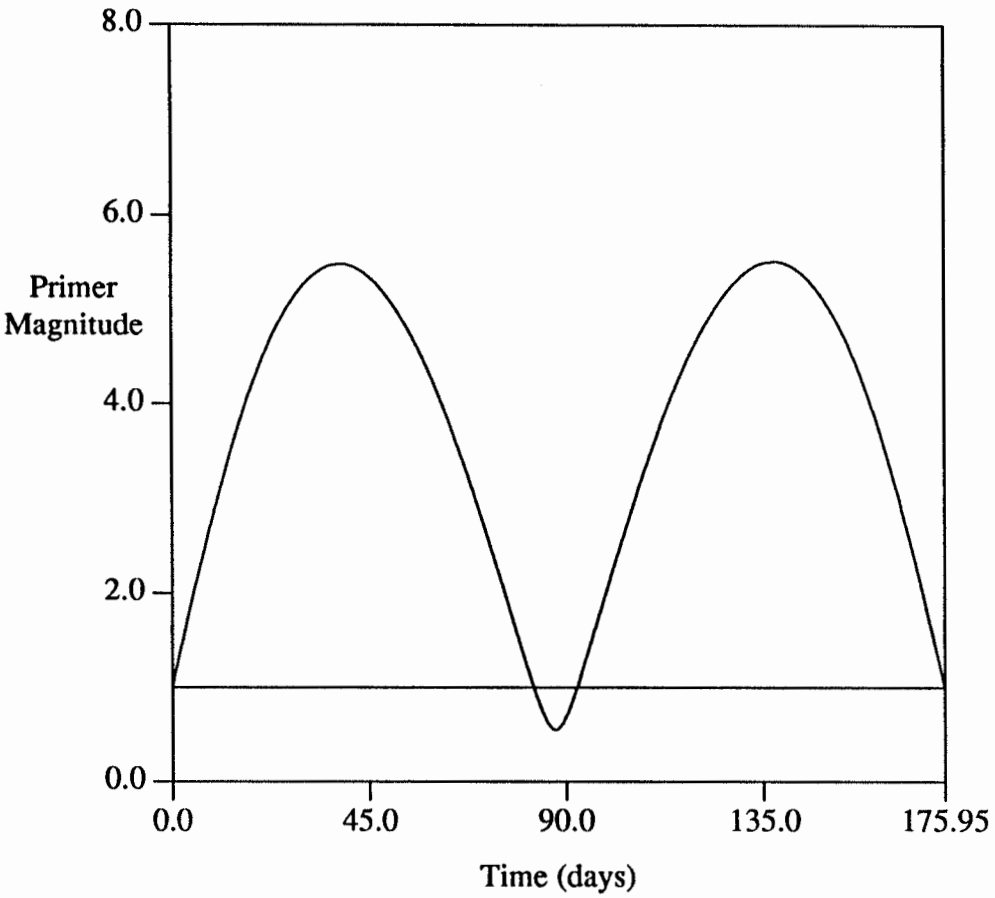

2–Impulse $\Delta\bar{v}$ Expenditure = 254.95 m/s

Transfer TOF = 175.95 days

Figure 6.17 Primer Magnitude History of Two-Impulse Nominal Transfer (Case F)

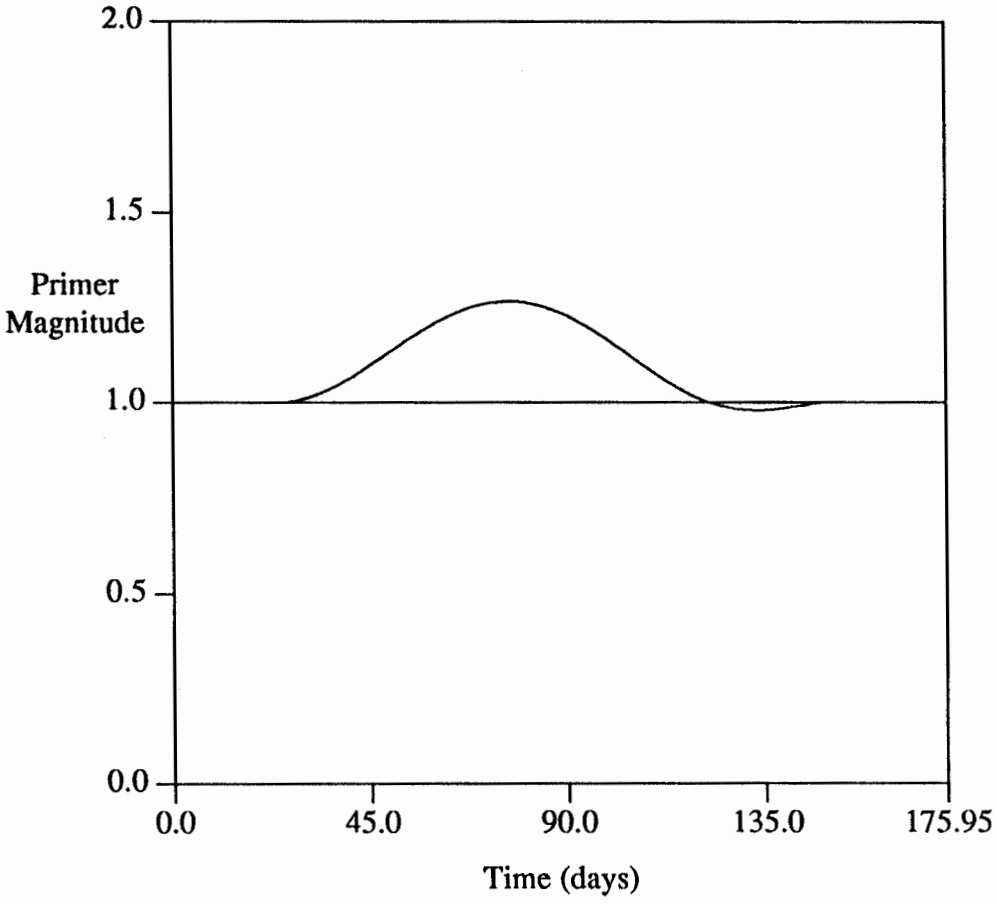

2–Impulse $\Delta\bar{v}$ Expenditure = 44.26 m/s

Transfer TOF = 122.61 days

Figure 6.18 Primer Magnitude History of Best Time-Free Two-Impulse Transfer (Case F)

Initial Halo: $A_z = 200{,}000$ km

Final Halo: $A_z = 110{,}000$ km

Transfer TOF = 122.61 days

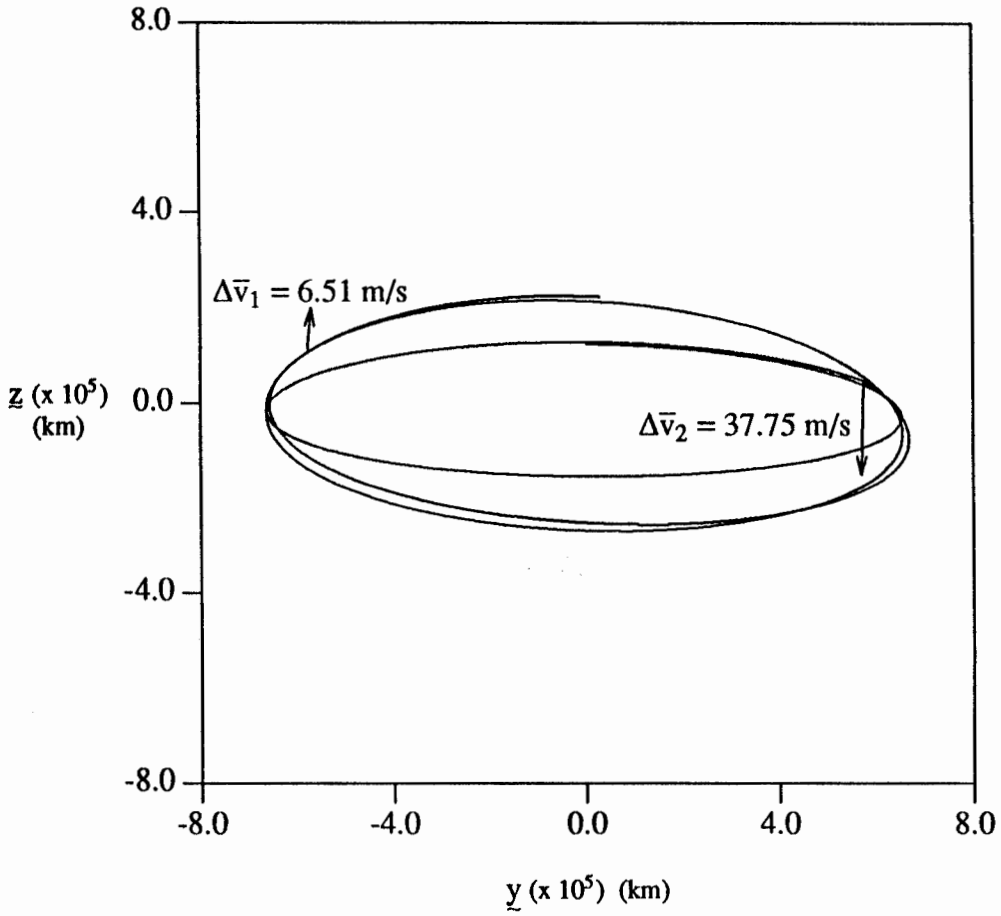

2–Impulse $\Delta\bar{v}$ Expenditure = 44.26 m/s

Figure 6.19 y-$\underset{\sim}{z}$ Projection of Best Time-Free Two-Impulse Transfer (Case F)

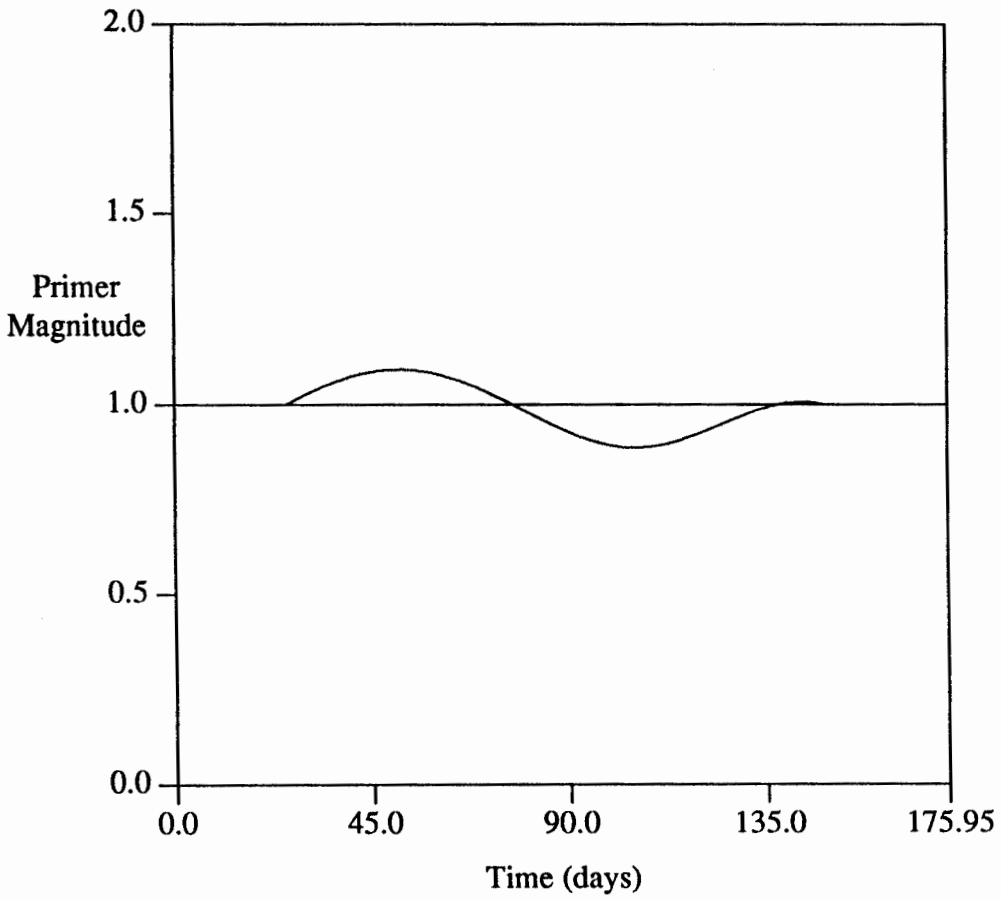

3–Impulse $\Delta\bar{v}$ Expenditure = 44.20 m/s

Transfer TOF = 122.61 days

Figure 6.20 Primer Magnitude History of Best Time-Free Three-Impulse Transfer (Case F)

Initial Halo: $A_z = 200{,}000$ km

Final Halo: $A_z = 110{,}000$ km

Transfer TOF = 122.61 days

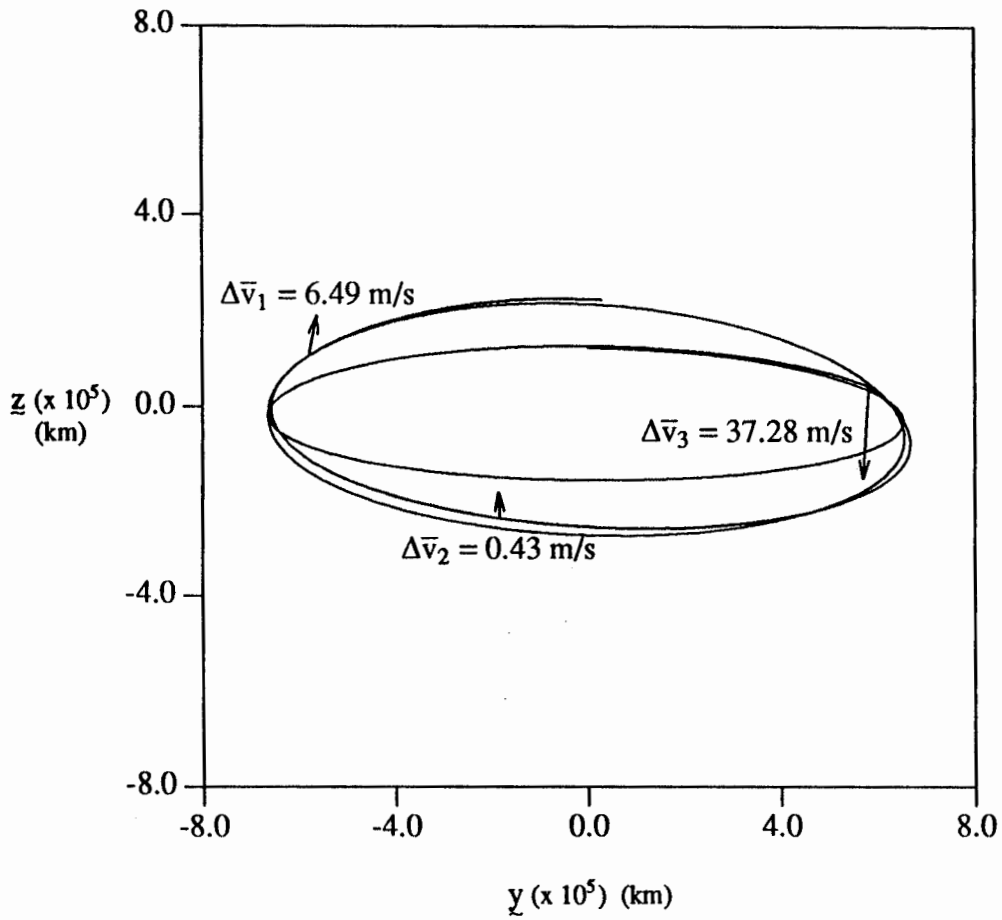

3–Impulse $\Delta\bar{v}$ Expenditure = 44.20 m/s

Figure 6.21 y-z Projection of Best Time-Free Three-Impulse Transfer (Case F)

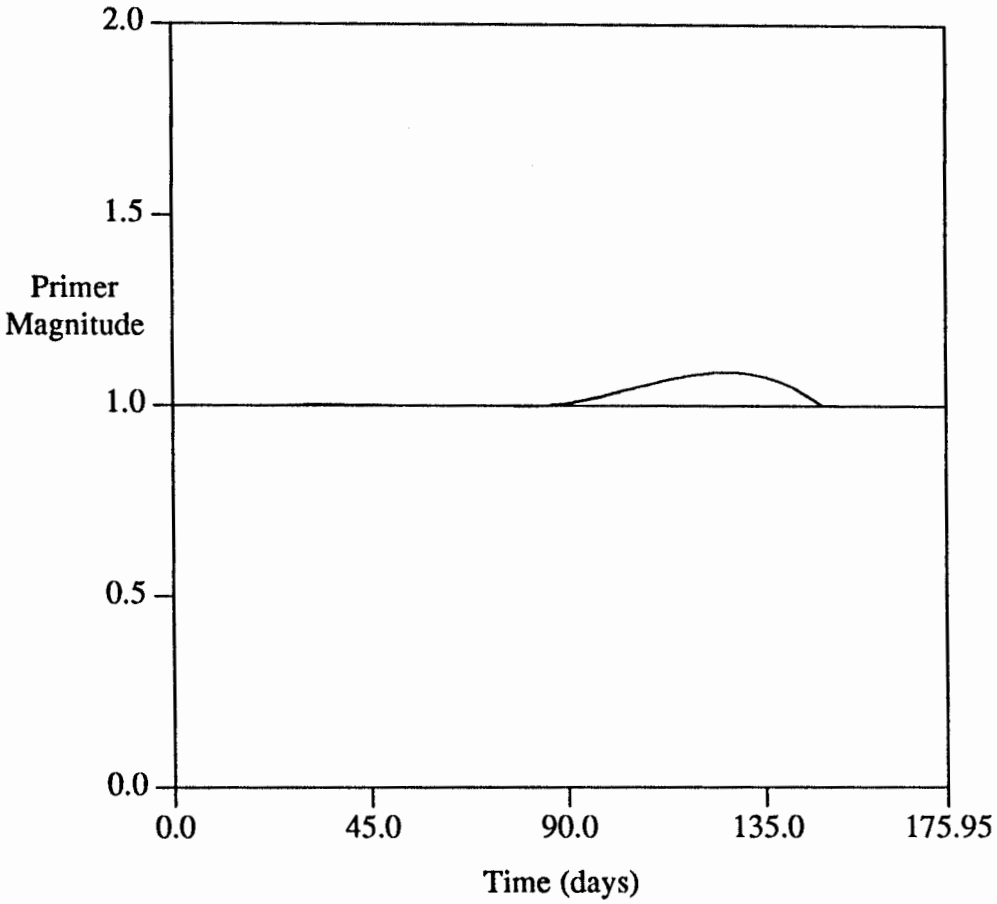

4–Impulse $\Delta\bar{v}$ Expenditure = 44.19 m/s

TOF = 122.61 days

Figure 6.22 Primer Magnitude History of Best Time-Free Four-Impulse Transfer (Case F)

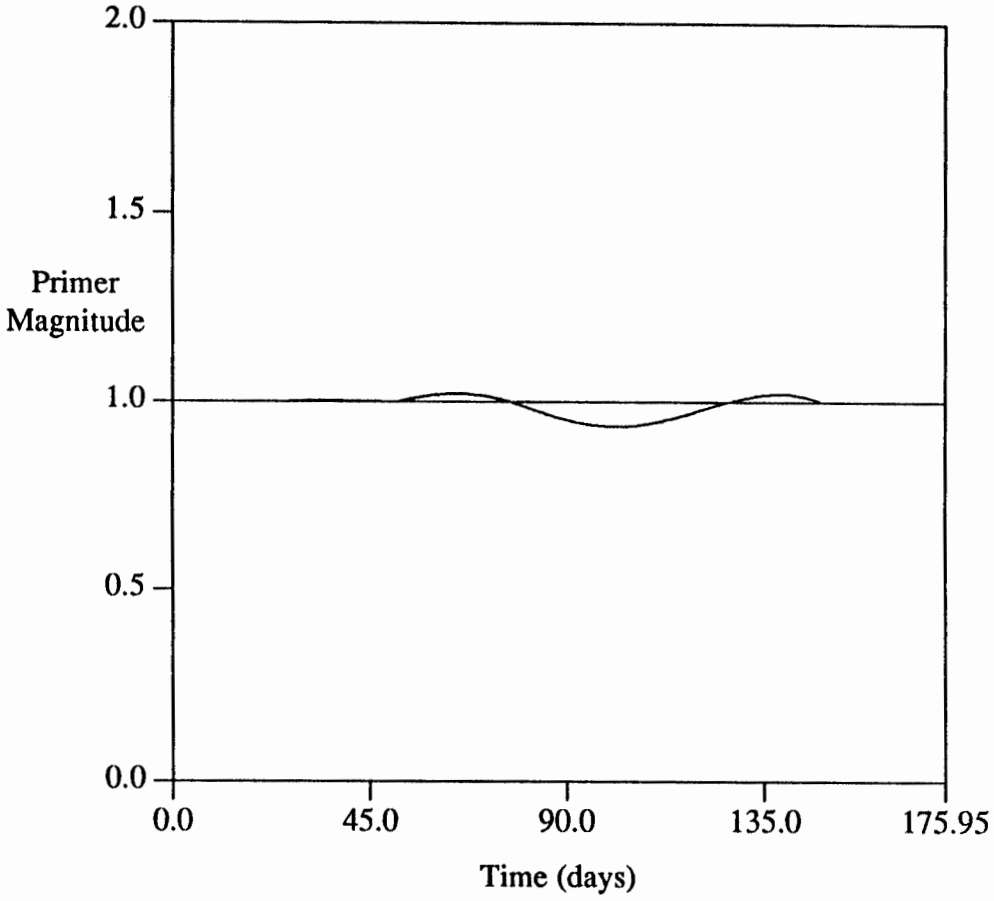

5–Impulse $\Delta\bar{v}$ Expenditure = 44.19 m/s

TOF = 122.61 days

Figure 6.23 Primer Magnitude History of Best Time-Free Five-Impulse Transfer (Case F)

Initial Halo: $A_z = 240{,}000$ km

Final Halo: $A_z = 110{,}000$ km

Transfer TOF = 175.91 days

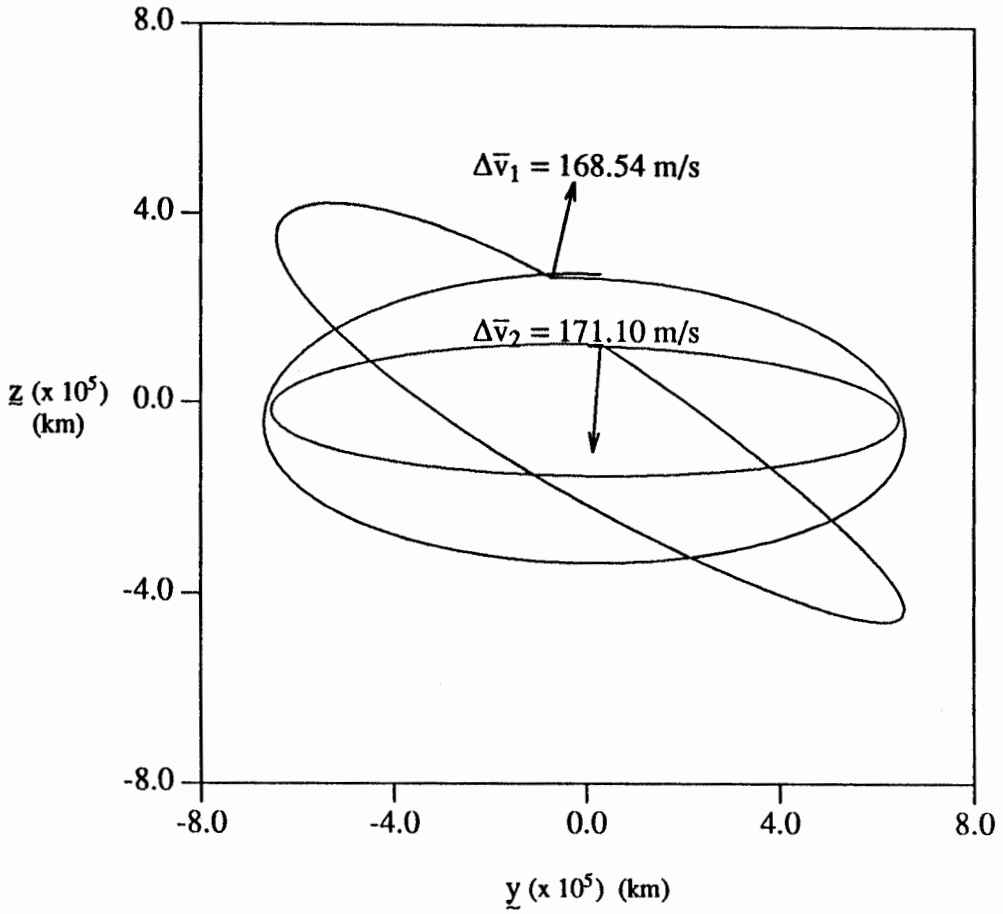

2–Impulse $\Delta\bar{v}$ Expenditure = 339.64 m/s

Figure 6.24 $\underline{y}$-$\underline{z}$ Projection of Two-Impulse Nominal Trajectory (Case G)

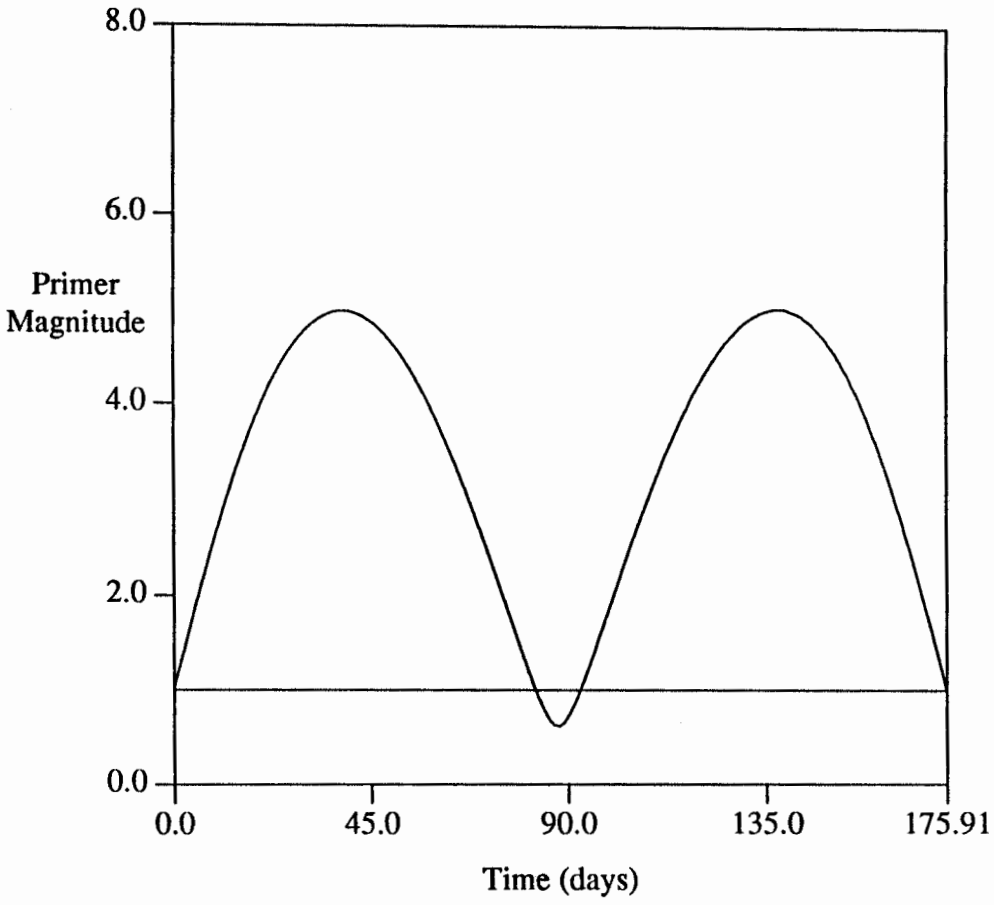

2–Impulse $\Delta\bar{v}$ Expenditure = 339.64 m/s

Transfer TOF = 175.91 days

Figure 6.25 Primer Magnitude History of Two-Impulse Nominal Transfer (Case G)

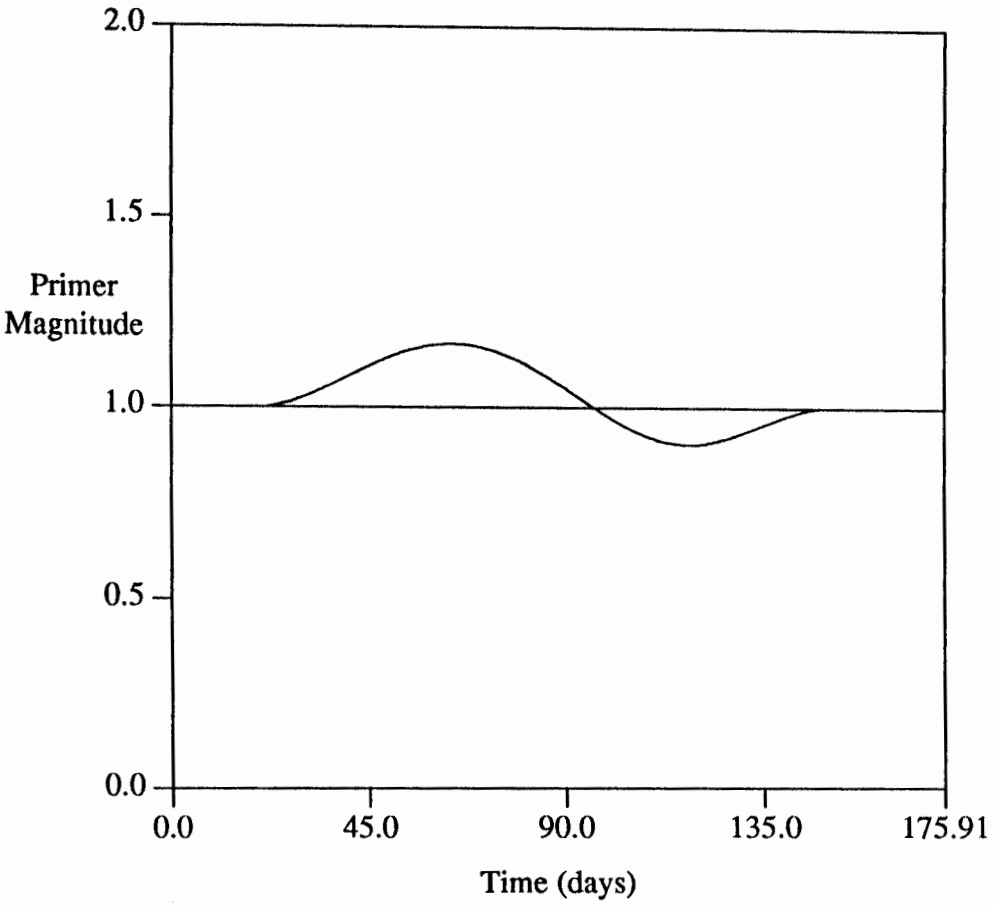

2–Impulse $\Delta\bar{v}$ Expenditure = 65.03 m/s

Transfer TOF = 127.22 days

Figure 6.26 Primer Magnitude History of Best Time-Free Two-Impulse Transfer (Case G)

Initial Halo: $A_z = 240{,}000$ km

Final Halo: $A_z = 110{,}000$ km

Transfer TOF = 127.22 days

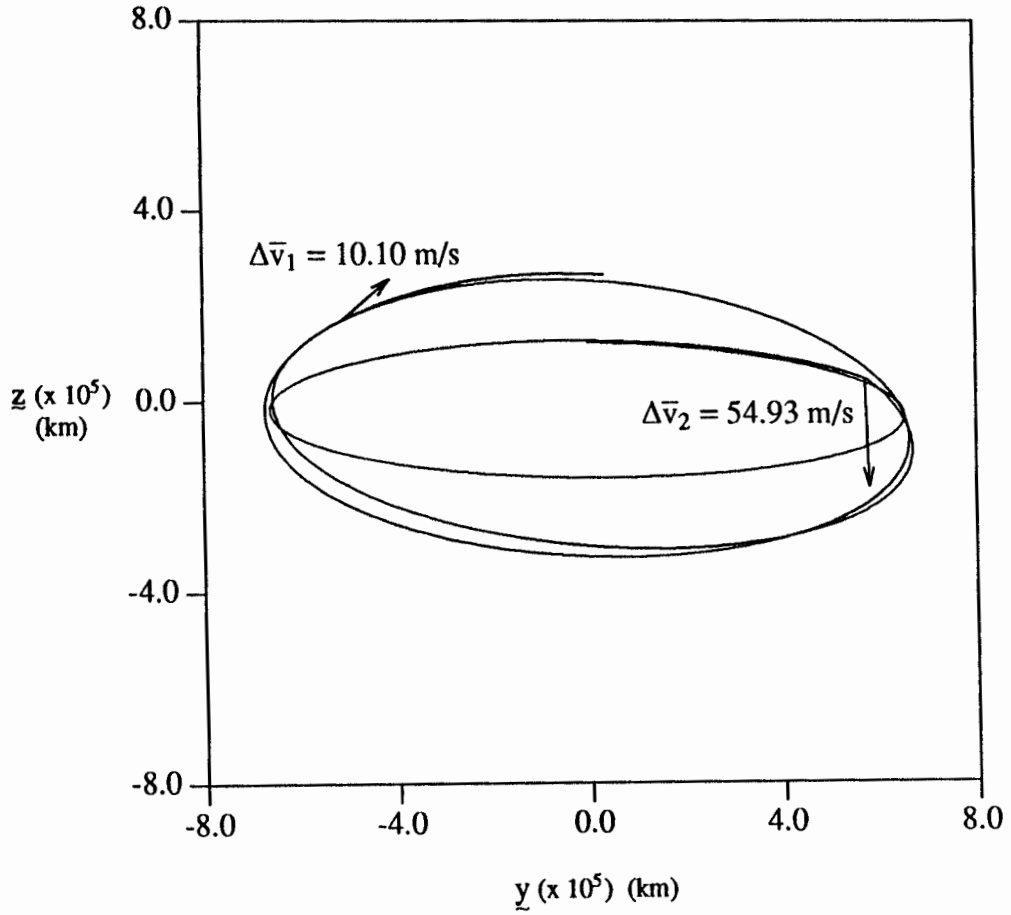

2–Impulse $\Delta\bar{v}$ Expenditure = 65.03 m/s

Figure 6.27 y-$\underset{\sim}{z}$ Projection of Best Time-Free Two-Impulse Transfer (Case G)

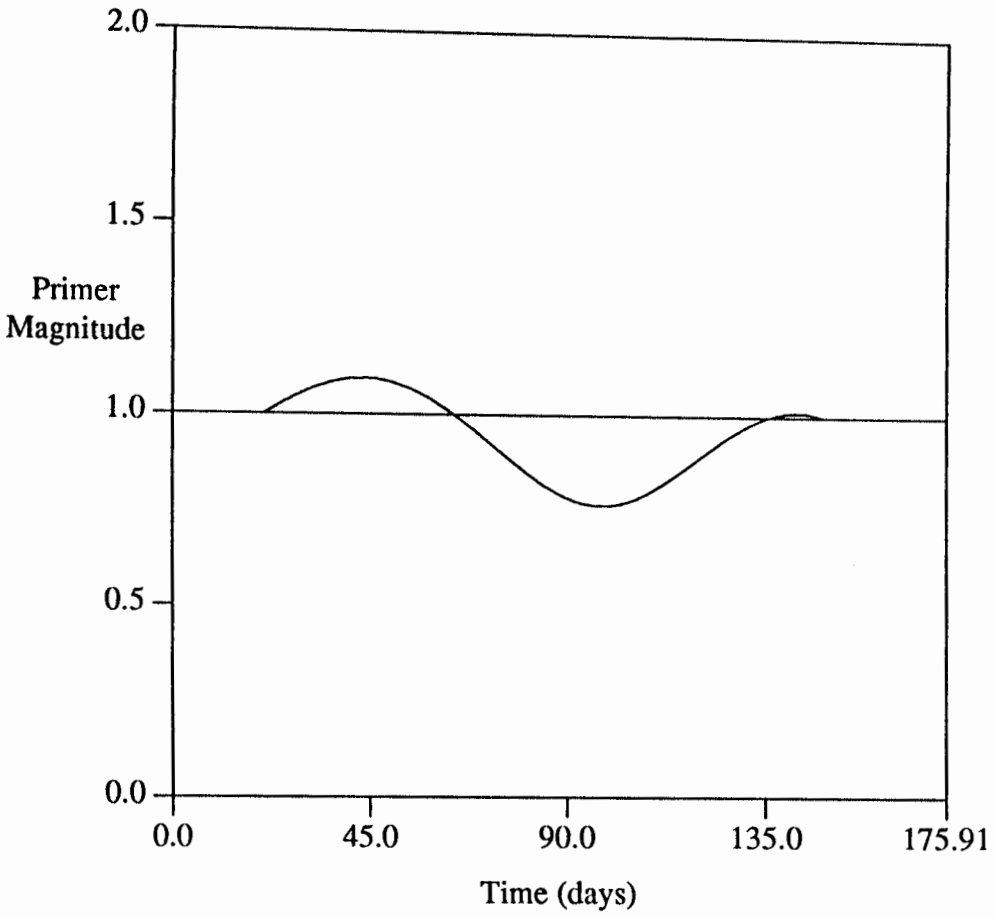

3–Impulse $\Delta\bar{v}$ Expenditure = 64.90 m/s

Transfer TOF = 127.22 days

Figure 6.28 Primer Magnitude History of Best Time-Free Three-Impulse Transfer (Case G)

Initial Halo: $A_z = 240{,}000$ km

Final Halo: $A_z = 110{,}000$ km

Transfer TOF = 127.22 days

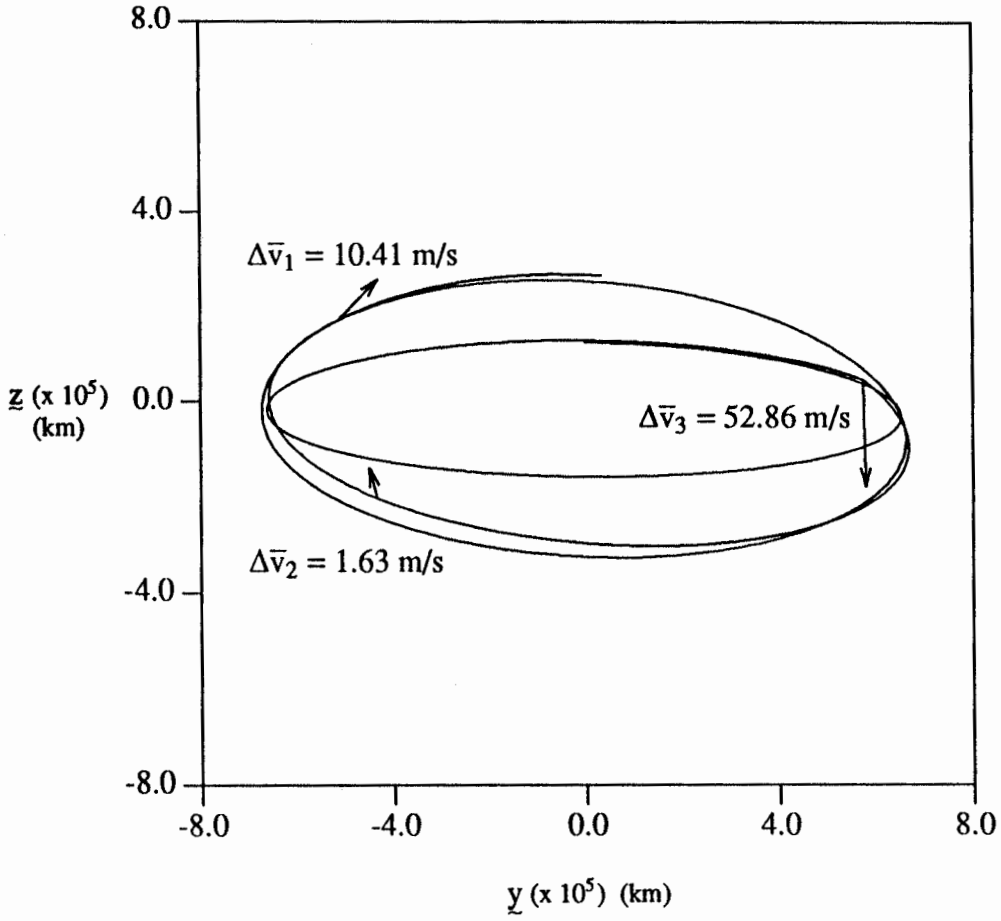

3–Impulse $\Delta\bar{v}$ Expenditure = 64.90 m/s

Figure 6.29 y-z Projection of Best Time-Free Three-Impulse Transfer (Case G)

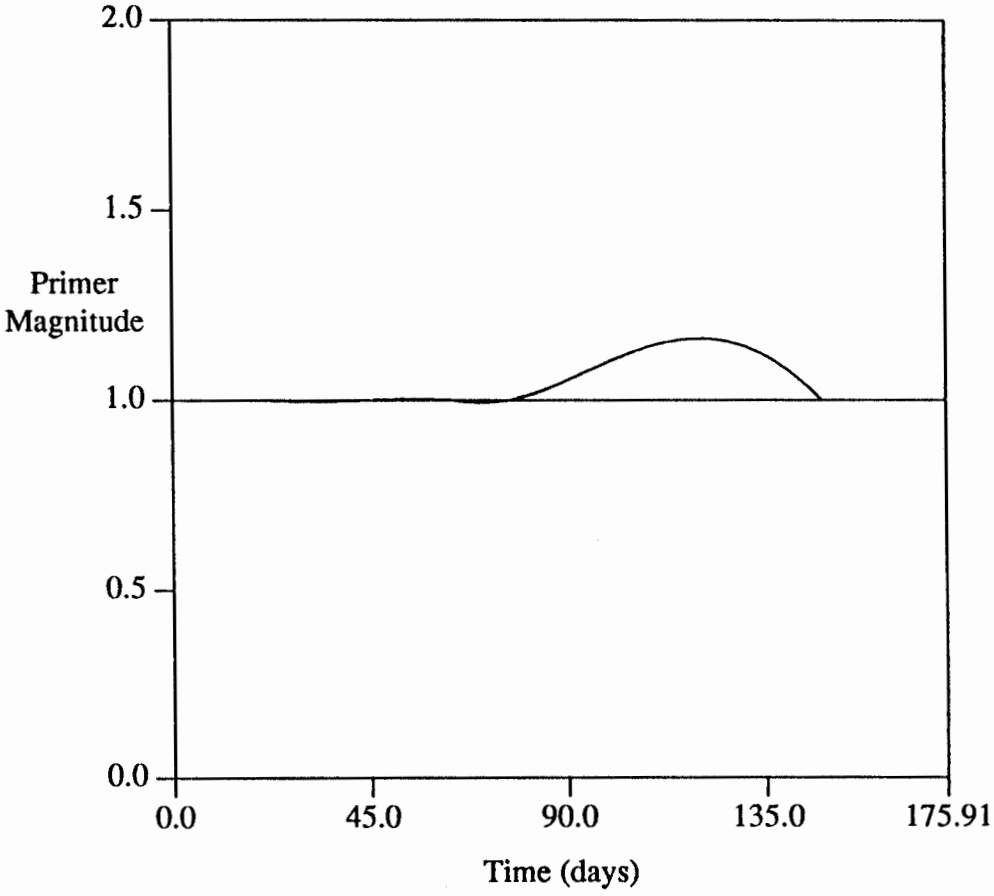

4–Impulse $\Delta\bar{v}$ Expenditure = 64.85 m/s

TOF = 127.22 days

Figure 6.30 Primer Magnitude History of Best Time-Free Four-Impulse Transfer (Case G)

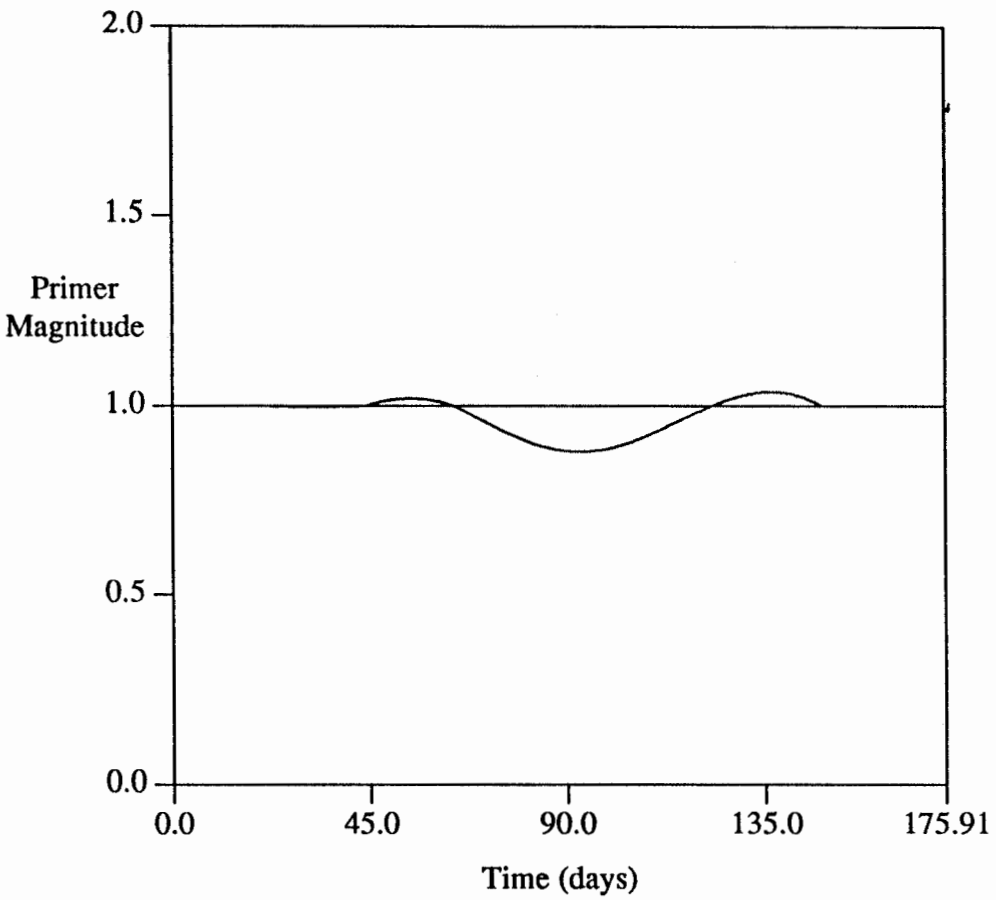

5–Impulse $\Delta\bar{v}$ Expenditure = 64.84 m/s

TOF = 127.22 days

Figure 6.31 Primer Magnitude History of Best Time-Free Five-Impulse Transfer (Case G)

Table 6.1 Costs on Time-Free Inferior Transfers from a Variety of Initial Halo Orbits

(Final Halo: Z–Amplitude = 110,000 km)

Case	Z-Amplitude of Initial Halo	Nominal 2-Impulse Transfer		Improved Time-Free Transfers 2-Impulse	3-Impulse	
	(km)	$\lvert\Delta\bar{v}\rvert$ (m/s)	TOF (days)	$\lvert\Delta\bar{v}\rvert$ (m/s)	$\lvert\Delta\bar{v}\rvert$ (m/s)	TOF (days)
E	160,000	160.60	175.98	28.16	26.38	129.13
F	200,000	254.95	175.95	44.26	44.20	122.61
G	240,000	339.64	175.91	65.03	64.90	127.22

experienced by the optimization procedure. This difficulty results in part from omission of coastal period modification during interior impulse application and subsequent optimization.

Table 6.1 summarizes the $|\Delta\bar{v}|$ cost on the inferior transfers for cases E-G. Although *optimal* solutions are not obtained in any of the three cases examined, the inferior transfers resulting from the time-free optimization process do exhibit a dramatic decrease in characteristic velocity compared to the nominal two-impulse solutions. As demonstrated by the superior time-free transfers constructed in Chapter V, the cost on the best three-impulse transfer trajectory varies nearly linearly with increasing z-amplitude of the initial halo orbit. Additionally, the application of coastal arcs in the initial and final halo orbits tends to drive the departure and arrival locations toward the extreme y-excursion points in each case; however, no clear relationship appears to exist between the time of flight on the transfer and the z-amplitude of the initial orbit.

In order to investigate the effect of declivity and acclivity on the cost of a transfer trajectory between two libration-point orbits, the correlation between the superior time-free transfers summarized in Table 5.2 and the inferior transfers presented in Table 6.1 is explored. Because the methods used to construct the nominal transfers for the superior transfers (cases A, C, and D) and for the inferior transfers (cases E-G) differ, discretion must be exercised to prevent drawing premature conclusions. Transfers between halo orbits of equal z-amplitude gradations are examined; therefore, compare cases A and E, cases C and F, and cases D and G. Notice that the inferior nominal transfers are accomplished using substantially less fuel than that required on analogous superior nominal transfers; however, the optimized inferior trajectories require greater $|\Delta\bar{v}|$ expenditures than do the optimized superior trajectories in order to implement a transfer between halo orbits of similar separation. The fuel expenditures associated with cases A and E are roughly equal, but the solutions are quite different. Whereas an optimal solution in case A is attained with only two impulses and supplementary interior impulses are not necessary for cost reduction, even a five-impulse solution in case E is non-optimal. However, the best three-impulse transfer for case E is comparable in $|\Delta\bar{v}|$ cost and time of flight to the optimal two-impulse transfer trajectory for case A. For the two remaining pairs of cases, optimal solutions are not rendered; thus, the best three-impulse trajectories are compared. The cost on both of the inferior transfers in cases F and G exceed the cost on the superior transfers constructed in cases C and D, and this cost discrepancy appears to increase with separation between

initial and final orbits. Additionally, the decrease in time of flight with increased z-amplitude separation that is characteristic of the superior transfers is not representative of the inferior transfers, for no distinct trend in time-of-flight variation is established in cases E-G.

DENOUEMENT

The aim of this investigation is two-fold. First, a reliable and expedient means must be developed for the construction of an impulsive nominal transfer between two specified libration-point orbits in the elliptic restricted three-body problem. Secondly, a systematic process for reduction of the fuel expenditure on this nominal transfer must be formulated such that the transfer is rendered optimal. The important methodologies and theories that are developed in this research are summarized. The merits of these methods and theories applied to realistic transfer problems are evaluated, and, finally, areas of future research endeavors are recommended.

Summary

Two strategies are presented that detail the construction of a nominal trajectory which transfers a spacecraft between two halo orbits about the L_1 libration point of the Sun/Earth-Moon barycenter system. One procedure is rooted in analytic approximations for the transfer path; whereas, numerical solutions are the core of the other procedure. In the first strategy (outlined in Chapter II), a linear approximation is used initially to characterized the transfer trajectory. This linear approximation is then input to a third-order approximation to render a more accurate estimate of the six parameters that characterize the transfer trajectory. Rarely, however, can a transfer path be determined that converges to the desired departure and arrival coordinates on the specified libration-point orbits. Many manual trial-and-error modifications of the parameters must be attempted in order to produce an approximation adequate for input to the numerical integration algorithm. In the second strategy (outlined in Chapter VI), the transfer path that connects the desired coordinates of departure and arrival is created employing only knowledge of the numerical solutions corresponding to the two halo orbits. Initially, a spiral method is used to estimate the positions and velocities at specific points along the transfer trajectory. Then, a differential corrections procedure

is utilized to determine the $\Delta\bar{v}$ maneuvers that must be inserted along the path in order to construct a solution that passes through the desired departure and arrival locations. Manual alteration of the impulsive maneuvers is generally necessary to accomplish convergence of the halo orbit segments of the complete integrated trajectory to the desired orbits; however, the appropriate modifications are quickly postulated. Finally, if the difference in the out-of-plane amplitude of the halo orbits is great (*i.e.*, more than 20 % of the z-amplitude of the initial halo orbit), a continuation algorithm is implemented; whereby, the desired nominal transfer path is the product of the sequential determination of intermediate transfers.

Next, the four necessary conditions that must be satisfied by an optimal impulsive transfer trajectory in the elliptic restricted three-body problem are developed and expressed entirely in terms of the primer vector and its derivatives. If any of the four conditions is violated, then the fuel expenditure on the path can be improved by the implementation of coastal arcs in the initial and final orbits and/or by the addition of an interior impulse. In contradistinction to the application of additional impulses for which the time of flight on the transfer path is unaltered (time-fixed), the inclusion of coastal arcs on the halo orbits results in a modified transfer time of flight (time-free).

The necessary conditions for the local optimality of a time-fixed transfer trajectory containing additional impulses are satisfied by requiring continuity of the Hamiltonian and the derivative of the primer vector at all interior impulses. The location, orientation, and magnitude of each additional impulse is determined by the unconstrained minimization of a function of four variables by a multivariable search technique. Noteworthy is the fact that the position and timing of an interior impulse is unchanged during the application and optimization of subsequent interior impulses; consequently, given this limitation, absolute compliance with the necessary conditions for an optimal trajectory may be infeasible.

The optimality of a time-free transfer trajectory is surmised by examination of the slopes at the endpoints of a plot of the magnitude of the primer vector over the duration of the transfer path. If the initial and final slopes of the primer magnitude are zero, the time-free path is optimal; otherwise, the execution of coastal arcs in the initial and final orbits is warranted. The direction and length of the coastal arcs are specified by the unconstrained minimization of a function of two variables using a multivariable search technique. If a time-free transfer path results that exhibits zero slopes at the endpoints of the primer magnitude history but that violates the necessary conditions for an

optimal trajectory, additional interior impulses must be applied in order to further reduce the cost. During optimization of the characteristics (*i.e.*, location, orientation, and magnitude) associated with each additional impulse, the duration of the coastal arcs remains unchanged; thus, the slopes at the endpoints of the primer magnitude plot for the resultant transfer may diverge from zero, and strict accordance with optimality conditions may again be hindered by this limitation.

Superior nominal transfers from a given initial halo orbit to a variety of final halo orbits are constructed using the strategy outlined in Chapter II. Both time-fixed and time-free optimization techniques are applied to these reference transfers to reduce fuel expenditure. Additionally, inferior nominal transfer trajectories from a variety of initial halo orbits to the same final orbit are constructed employing the strategy detailed in Chapter VI. Only the time-free optimization of the inferior reference transfers is explored.

Conclusions

Despite fundamentally different approaches, the two nominal transfer construction strategies both demand manual modifications at some stage in the procedures. Because the effect of parameter manipulation on the eventual solution is not immediately apparent in the strategy presented in Chapter II, the construction of nominal paths using this methodology is very cumbersome and tedious. In contrast, the manual alteration of the components of the impulsive maneuvers using a visual comparison of the integrated solution to the desired halo orbits allows for immediate feedback concerning the appropriate modifications; therefore, nominal transfer trajectories can be determined in a straightforward and rapid fashion utilizing the strategy detailed in Chapter VI. Thus, representing a clear improvement over the procedure outlined in Chapter II, the strategy presented in Chapter VI is the procedure recommended for future nominal transfer constructions.

Although *optimal* solutions in some instances are elusive, the time-fixed and time-free optimization techniques prove to be very successful in substantially diminishing $|\Delta\bar{v}|$ expenditures on nominal transfer trajectories. Not surprisingly, an increase in the flexibility of the design strategy by relaxing time-of-flight constraints yields time-free transfers distinguished by lower characteristic velocities than comparable time-fixed transfers. In addition, the cost on the optimal (or best) time-free superior transfer

trajectory increases nearly linearly with z-amplitude of the final halo orbit; similarly, the cost on the best time-free inferior transfer trajectory varies almost linearly with increasing z-amplitude of the initial halo orbit.

A very interesting and unexpected phenomenon of quadrant-switching with variation in number of impulses is observed in the time-fixed superior transfers requiring more than three impulses to render an optimal solution. In each case, the best three-impulse transfer performs the preponderance of the transition between halo orbits in the first quadrant of the y-z plane; whereas, the optimal four-impulse trajectory executes the majority of its transition to the final halo in the third quadrant. Remarkably, time-free superior transfers also exhibit this phenomenon of predominantly third-quadrant transferal; conversely, the bulk of the transition to the final halo orbit by the time-free inferior transfers occurs chiefly in the first quadrant. The inclusion of coastal arcs on the time-free superior transfers, in effect, moves the arrival on the final halo orbit to a location near its minimum y-excursion point. Additionally, with each successive increase in z-amplitude, the time of flight on the transfer decreases thereby delaying departure from the initial halo orbit and advancing the departure location toward the initial halo's maximum y-excursion point. The application of coastal arcs on the time-free inferior transfers tends to drive the departure and arrival locations toward the points of extreme y-excursion; however, no clear relationship appears to exist between time of flight on the transfer and the z-amplitude of the initial orbit.

One of the key results of this investigation is the profound impact that the reference solution has on the product of the optimization process. Due to the local nature of the optimization techniques developed, the solution for an optimal transfer path converges only to a minimum within the same valley as the nominal solution from which the optimal trajectory is derived; hence, other solutions that accomplish the same transfer may exist. Therefore, due to the sensitivity of the cost on the optimal (or best) time-fixed or time-free transfer trajectory to the cost on its corresponding two-impulse nominal trajectory, effort should be made to minimize the cost on the original non-optimal reference path prior to application of the optimization algorithms.

The effect of declivity and acclicity on the cost and time of flight on a transfer between two libration-point orbits is assessed by comparing superior and inferior transfers between halo orbits of equal z-amplitude gradations. Because the methods used to construct the nominal solutions for the superior and the inferior transfers differ, caution against drawing premature conclusions must be exercised. Although the

inferior nominal transfers are accomplished using substantially less $|\Delta\bar{v}|$ than that required on analogous superior transfers, the best inferior trajectories require greater $|\Delta\bar{v}|$ expenditures than do the corresponding optimized superior trajectories. Additionally, the decrease in time of flight with increased z-amplitude separation that is characteristic of the superior transfers is not representative of the inferior transfers.

Evidenced by the existence of cusps at interior impulses on time-fixed transfers and of non-zero primer slopes at the endpoints of time-free transfers, the inability to produce truly *optimal* solutions proves to be the principal shortcoming of both the time-fixed and time-free optimization processes. This difficulty stems from the fact that, in order to preserve the integrity of the halo orbit segments of the integrated trajectory, both the time-fixed and time-free optimization algorithms utilize an unconstrained minimization of one function involving variables characterizing only a single implement of cost improvement (*i.e.*, a coastal arc or an interior impulse). For example, consider a time-free trajectory that requires an interior impulse to reduce fuel expenditure. In determining the optimal location of the interior impulse, the slopes of the primer magnitude at the endpoints of the resulting transfer path diverge from zero, yet the durations of the coastal arcs are unaltered. Hence, without the simultaneous modification of the coastal periods and the characteristics of the interior impulse, the goal of truly *optimal* transfers remains unfulfilled.

Recommendations

Undoubtedly, the most fruitful extension of this investigation would be the development of a means to simultaneously optimize the characteristics associated with multiple cost-improving agents. The cost function that is required to be minimized by such a method can be constructed very quickly using superposition of the cost function associated with a supplementary interior impulse and of that corresponding to a dual coast in the halo orbits. However, employing the BFGS variable metric method for unconstrained minimization results in a numerical solution that diverges completely from the specified libration-points orbits. Thus, the minimization technique in the multivariable search routine that is employed in this research must be supplanted by a constrained optimization process such that the initial and final segments of the integrated path are compelled to match the desired initial and final halo orbits.

The applications presented in this treatise have only begun to explore the possible uses for the optimization algorithms developed for trajectories in the elliptic restricted three-body problem. Thus far, only one-rev nominal transfer trajectories have been examined; hence, a probe into the fluctuations in fuel expenditure and time of flight on optimal transfer paths derived from nominal transfers of modified duration (*e.g.*, half-rev or two-rev duration) could prove to be a very interesting inquiry. The results presented in this study could guide the choice of departure and arrival locations for construction of these variable-revolution nominal transfer trajectories. In addition, only transfers between nearly periodic halo orbits have been surveyed here; therefore, the construction of optimal transfer paths between quasi-periodic Lissajous trajectories could advance the presently limited understanding of optimal libration-point transfers. Finally, the extension of primer vector theory to transfer paths that move a spacecraft between a primary-centered orbit and a libration-point orbit warrants future investigation.

REFERENCES

REFERENCES

[1] R. W. Farquhar, D. P. Muhonen, and D. L. Richardson, "Mission Design for a Halo Orbiter of the Earth," *Journal of Spacecraft*, Vol. 14, No. 3, March 1977, pp. 170-177.

[2] R. W. Farquhar, D. P. Muhonen, C. P. Newman, and H. S. Heuberger, "Trajectories and Orbital Maneuvers for the First Libration-Point Satellite," *Journal of Guidance and Control*, Vol. 3, No. 6, November-December 1980, pp. 549-554.

[3] K. W. Gatland, "Earth Gets a Halo," *Spaceflight*, Vol. 21, No. 5, May 1979, pp. 195-196, 240.

[4] R. W. Farquhar, D. P. Muhonen, and L. C. Church, "Trajectories and Orbital Maneuvers for the ISEE-3/ICE Comet Mission," *The Journal of the Astronautical Sciences*, Vol. 33, No. 3, July-September 1985, pp. 235-254.

[5] D. P. Muhonen, S. Davis, and D. Dunham, "Alternative Gravity-Assist Sequences for the ISEE-3 Escape Trajectory," *The Journal of the Astronautical Sciences*, Vol. 33, No. 3, July-September 1985, pp. 255-273.

[6] L. Efron, D. K. Yeomans, and A. F. Schanzle, "ISEE-3/ICE Navigation Analysis," *The Journal of the Astronautical Sciences*, Vol. 33, No. 3, July-September 1985, pp. 301-323.

[7] F. R. Moulton, *An Introduction to Celestial Mechanics*, The Macmillan Company, New York, Second Edition, 1914, pp. 319-320.

[8] V. G. Szebehely, *Adventures in Celestial Mechanics—A First Course in the Theory of Orbits*, University of Texas Press, Austin, 1989.

[9] G. W. Hill, "Researches in the Lunar Theory," *The American Journal of Mathematics*, Vol. 1, 1878, pp. 5-26, 129-147, 245-260.

[10] G. H. Darwin, "Periodic Orbits," *Acta Mathematica*, Vol. 21, 1897, pp. 99-242.

[11] H. C. Plummer, "On Oscillating Satellites - 1," *Monthly Notices of the Royal Astronomical Society*, Vol. 63, No. 8, June 1903, pp. 436-443.

[12] H. C. Plummer, "On Oscillating Satellites - 2," *Monthly Notices of the Royal Astronomical Society*, Vol. 64, No. 2, December 1903, pp. 98-105.

[13] F. R. Moulton, *Periodic Orbits*, Carnegie Institute of Washington Publications, Washington, DC, No. 161, 1920.

[14] V. Szebehely, *Theory of Orbits: The Restricted Problem of Three Bodies*, Academic Press Inc., Orlando, 1967.

[15] R. W. Farquhar, "The Control and Use of Libration Point Satellites," Ph.D. Dissertation, Department of Aeronautics and Astronautics, Stanford University, Stanford, California, July 1968.

[16] R. W. Farquhar, "The Control and Use of Libration Point Satellites," NASA TR R-346, September 1970.

[17] R. W. Farquhar and A. A. Kamel, "Quasi-Periodic Orbits About the Translunar Libration Point," *Celestial Mechanics*, Vol. 7, 1973, pp. 458-473.

[18] D. L. Richardson, "Analytic Construction of Periodic Orbits About the Collinear Points," *Celestial Mechanics*, Vol. 22, 1980, pp. 241-253.

[19] D. L. Richardson, "Halo Orbit Formulation for the ISEE-3 Mission," *Journal of Guidance and Control*, Vol. 3, No. 6, November-December 1980, pp. 543-548.

[20] C. G. Zagouras and P. G. Kazantzis, "Three Dimensional Periodic Oscillations Generating from Plane Periodic Ones Around the Collinear Lagrange Points," *Astrophysics and Space Science*, Vol. 61, No. 2, April 1979, pp. 389-409.

[21] J. V. Breakwell and J. V. Brown, "The 'Halo' Family of 3-Dimensional Periodic Orbits in the Earth-Moon Restricted 3-Body Problem," *Celestial Mechanics*, Vol. 20, 1979, pp. 389-404.

[22] K. C. Howell, "Three-Dimensional, Periodic Halo Orbits in the Restricted Three-Body Problem," Ph.D. Dissertation, Department of Aeronautics and Astronautics, Stanford University, Stanford, California, March 1983.

[23] K. C. Howell, "Three-Dimensional, Periodic, 'Halo' Orbits," *Celestial Mechanics*, Vol. 32, 1984, pp. 53-71.

[24] K. C. Howell and J. V. Breakwell, "Almost Rectilinear Halo Orbits," *Celestial Mechanics*, Vol. 32, 1984, pp. 29-52.

[25] K. C. Howell and D. B. Spencer, "Periodic Orbits in the Restricted Four-Body Problem," *Acta Astronautica*, Vol. 13, No. 8, 1986, pp. 473-479.

[26] T. A. Heppenheimer, "Out-of-Plane Motion About Libration Points: Nonlinearity and Eccentricity Effects," *Celestial Mechanics*, Vol. 7, 1973, pp. 177-194.

[27] D. L. Richardson and N. D. Cary, "A Uniformly Valid Solution for Motion About the Interior Libration Point of the Perturbed Elliptic-Restricted Problem," AAS/AIAA Astrodynamics Specialist Conference, AAS 75-021, Nassau, Bahamas, July 28-30, 1975.

[28] H. J. Pernicka, "The Numerical Determination of Lissajous Orbits in the Circular Restricted Three-Body Problem," M. S. Thesis, School of Aeronautics and Astronautics, Purdue University, West Lafayette, Indiana, December 1986.

[29] K. C. Howell and H. J. Pernicka, "Numerical Determination of Lissajous Trajectories in the Restricted Three-Body Problem," *Celestial Mechanics*, Vol. 41, 1988, pp. 107-124.

[30] H. J. Pernicka, "The Numerical Determination of Nominal Libration Point Trajectories and Development of a Station-Keeping Strategy," Ph.D. Dissertation, School of Aeronautics and Astronautics, Purdue University, West Lafayette, Indiana, May 1990.

[31] D. J. Bell, "Optimal Space Trajectories--A Review of Published Work," *Aeronautical Journal*, Vol. 72, February 1968, pp. 141-146.

[32] R. F. Hoelker and R. Silber, "The Bi-Elliptic Transfer Between Co-Planar Circular Orbits," Proceedings of the Fourth AFBMD/STL Symposium--Advances in Ballistic Missile and Space Technology, Pergamon Press Inc., Oxford, Vol. 3, 1961, pp. 164-175.

[33] T. N. Edelbaum, "How Many Impulses?" *Astronautics and Aeronautics*, Vol. 5, No. 11, November 1967, pp. 64-69.

[34] F. W. Gobetz and J. R. Doll, "A Survey of Impulsive Trajectories," *AIAA Journal*, Vol. 7, No. 5, May 1969, pp. 801-834.

[35] D. F. Lawden, "Rocket Trajectory Optimization: 1950-1963," *Journal of Guidance, Control, and Dynamics*, Vol. 14, No. 4, July-August 1991, pp. 705-711.

[36] J. P. Carstens and T. N. Edelbaum, "Optimum Maneuvers for Launching Satellites into Circular Orbits of Arbitrary Radius and Inclination," *ARS Journal*, Vol. 31, No. 7, July 1961, pp. 943-949.

[37] T. N. Edelbaum, "Minimum Impulse Transfers in the Near Vicinity of a Circular Orbit," *The Journal of the Astronautical Sciences*, Vol. 14, No. 2, March-April 1967, pp. 66-73.

[38] J. P. Marec, "Rendezvous Impulsionnels, Optimaux, de Longe Durée, Entre Orbites Quasi-Circulaires, Proches, Coplanaires ou Non", Colloquium on Advanced Problems and Methods for Space Flight Optimization, Liège, 1967; also, *Advanced Problems and Methods for Space Flight Optimization*, ed. by B. F. de Veubeke, Pergamon Press, Oxford, 1969.

[39] J. P. Marec, "Transferts Impulsionnels, Economiques, Entre Orbites Quasi-Circulaires, Proches, Non Coplanaires," *Astronautica Acta*, Vol. 14, No. 1, November 1968, pp. 47-55.

[40] J. B. Jones, "Optimal Rendezvous in the Neighborhood of a Circular Orbit," *The Journal of the Astronautical Sciences*, Vol. 24, No. 1, January-March 1976, pp. 55-90.

[41] J. V. Breakwell, "Minimum Impulse Transfer," *Progress in Astronautics and Aeronautics: Celestial Mechanics and Astrodynamics*, Vol. 14, ed. by V. G. Szebehely, Academic Press, New York, 1964.

[42] J. V. Breakwell, "Minimum-Impulse Transfer Between a Circular Orbit and a Nearby Non-Coplanar Elliptic Orbit," Colloquium on Advanced Problems and Methods for Space Flight Optimization, Liège, 1967; also, *Advanced Problems and Methods for Space Flight Optimization*, ed. by B. F. de Veubeke, Pergamon Press, Oxford, 1969.

[43] C. Marchal, "Transferts Optimaux Entre Orbites Elliptiques Coplanaires (Durée Indifférente)," *Astronautica Acta*, Vol. 11, No. 6, November-December 1965, pp. 432-445.

[44] C. Marchal, "Transferts Optimaux Entre Orbites Elliptiques," XVI IAF Congress, Athens, 1965.

[45] F. W. Gobetz, M. Washington, and T. N. Edelbaum, "Minimum-Impulse Time-Free Transfer Between Elliptic Orbits," NASA CR-636, November 1966.

[46] J. P. Marec, "Optimal Transfers Between Close Elliptical Orbits," NASA TT F-554, September 1969.

[47] F. W. Gobetz, "Optimum Transfers Between Hyperbolic Asymptotes," *AIAA Journal*, Vol. 1, No. 9, September 1963, pp. 2034-2041.

[48] C. Marchal, "Transferts Optimaux Entre Orbites Hyperboliques (Rayon Planétaire Non Nul)," XVII IAF Congress, Madrid, 1966.

[49] C. Marchal, "Analytical Comparison of the Successive Planetary Windows in the Study of the Economical Earth-Planet Transfers," XIX IAF Congress, New York, 1968.

[50] J. P. Gravier, C. Marchal, and R. D. Culp, "Optimal Impulsive Transfers Between Real Planetary Orbits," *Journal of Optimization Theory and Applications*, Vol. 15, No. 5, May 1975, pp. 587-604.

[51] C. Marchal, "Synthése des Résultats Analytiques sur les Transferts Optimaux entre Orbites Képlériennes (Durée Indifférente)," Colloquium on Advanced Problems and Methods for Space Flight Optimization, Liège, 1967; also, *Advanced Problems and Methods for Space Flight Optimization*, ed. by B. F. de Veubeke, Pergamon Press, Oxford, 1969.

[52] D. F. Lawden, *Optimal Trajectories for Space Navigation*, Butterworths, London, 1963.

[53] P. M. Lion and M. Handelsman, "Primer Vector on Fixed-Time Impulsive Trajectories," *AIAA Journal*, Vol. 6, No. 1, January 1968, pp. 127-132.

[54] D. J. Jezewski and H. L. Rozendaal, "An Efficient Method for Calculating Optimal Free-Space *N*-Impulse Trajectories," *AIAA Journal*, Vol. 6, No. 11, November 1968, pp. 2160-2165.

[55] D. J. Jezewski and N. L. Faust, "Inequality Constraints in Primer-Optimal, *N*-Impulse Solutions," *AIAA Journal*, Vol. 9, No. 4, April 1971, pp. 760-763.

[56] D. J. Jezewski, "Primer Vector Theory and Applications," NASA TR R-454, November 1975.

[57] D. J. Jezewski, "A Method for Determining Optimal, Fixed-Time, *N*-Impulse Trajectories Between Arbitrarily Inclined Orbits," XIX IAF Congress, New York, 1968.

[58] J. E. Prussing, "Optimal Four-Impulse Fixed-Time Rendezvous in the Vicinity of a Circular Orbit," *AIAA Journal*, Vol. 7, No. 5, May 1969, pp. 928-935.

[59] J. E. Prussing, "Optimal Two- and Three-Impulse Fixed-Time Rendezvous in the Vicinity of a Circular Orbit," *AIAA Journal*, Vol. 8, No. 7, July 1970, pp. 1221-1228.

[60] L. R. Gross and J. E. Prussing, "Optimal Multiple-Impulse Direct Ascent Fixed-Time Rendezvous," *AIAA Journal*, Vol. 12, No. 7, July 1974, pp. 885-889.

[61] J. E. Prussing and J.-H. Chiu, "Optimal Multiple-Impulse Time-Fixed Rendezvous Between Circular Orbits," *Journal of Guidance, Control, and Dynamics*, Vol. 9, No. 1, January-February 1986, pp. 17-22.

[62] J. E. Prussing, L. J. Wellnitz, and W. G. Heckathorn, "Optimal Impulsive Time-Fixed Direct-Ascent Interception," *Journal of Guidance, Control, and Dynamics*, Vol. 12, No. 4, July-August 1989, pp. 487-494.

[63] D.-R. Taur, J. E. Prussing, and V. Coverstone-Carroll, "Optimal Impulsive Time-Fixed Orbital Rendezvous and Interception with Path Constraints," AIAA/AAS Astrodynamics Conference, AIAA-90-2972-CP, Portland, Oregon, August 20-22, 1990.

[64] J. P. Marec, *Optimal Space Trajectories*, Studies in Astronautics, Vol. 1, Elsevier Scientific Publishing Co., Amsterdam, 1979.

[65] L. A. D'Amario, "Minimum Impulse Three-Body Trajectories," Ph.D. Dissertation, Department of Aeronautics and Astronautics, Massachusetts Institute of Technology, Cambridge, Massachusetts, June 1973.

[66] M. Popescu, "The Study of Some Classes of Extremals Concerning the Optimal Transfer from the Equilateral Libration Points by Using the Auxiliary Problem of Bolza Type," IAF-82-313, XXXIII IAF Congress, Paris, 1982.

[67] M. Popescu, "Optimal Transfers from the Lagrangian Points," *Acta Astronautica*, Vol. 12, No. 4, 1985, pp. 225-228.

[68] M. Popescu and T. Popescu, "Optimal Transfers from the Equilateral Libration Points," *Acta Astronautica*, Vol. 15, No. 4, 1987, pp. 209-212.

[69] M. Popescu and T. Popescu, "Functional Analysis Methods in the Study of the Optimal Transfer," *Journal of Guidance, Control, and Dynamics*, Vol. 13, No. 2, March-April 1990, pp. 374-376.

[70] G. Gómez, A. Jorba, J. Masdemont, and C. Simó, "Study Refinement of Semi-Analytical Halo Orbit Theory," European Space Agency Contract No. 8625/89/D/MD(SC), Final Report, April 1991.

[71] G. N. Vanderplaats, *ADS—A Fortran Program for Automated Design Synthesis*, Version 1.10, May 1985.

[72] R. W. Farquhar, "The Moon's Influence on the Location of the Sun-Earth Exterior Libration Point," *Celestial Mechanics*, Vol. 2, 1970, pp. 131-133.

[73] A. H. Nayfeh, *Introduction to Perturbation Techniques*, John Wiley & Sons, Inc., New York, 1981.

[74] F. A. Valentine, *The Problem of Lagrange with Differential Inequalities as Added Side Conditions*, Ph.D. Dissertation, Department of Mathematics, The University of Chicago, Chicago, Illinois, 1937.

[75] I. M. Gelfand and S. V. Fomin, *Calculus of Variations*, Prentice Hall, Inc., Englewood Cliffs, New Jersey, 1963.

VITA

VITA

Lisa Ann Hiday, daughter of Paul and Lurilla Hiday, was born in Indianapolis, Indiana on October 29, 1964. She was educated in the Lawrence Township public school system of Indianapolis and graduated salutatorian of Lawrence North High School in May 1982.

During her undergraduate studies at Purdue University she served as President of the student branch of the American Institute of Aeronautics and Astronautics and as Treasurer of Sigma Gamma Tau (aerospace engineering honor society). She graduated *summa cum laude* with a B. S. degree in Aeronautical and Astronautical Engineering from Purdue University in May 1986. She then attended Stanford University from September 1986 to June 1987 and received an M. S. degree in Aeronautics and Astronautics. Returning to Purdue University, she commenced her doctoral program in Aeronautical and Astronautical Engineering in August 1987.

Throughout her undergraduate and graduate studies, Lisa has performed in numerous modern dance concerts including performances of the Purdue Repertory Dance Company and of the Stanford Contemporary Dance Ensemble; additionally, she has choreographed works for the Purdue Repertory Dance Company. She is also a member of the Order of the Engineer.